

INTERACTIONS OF ANTIOXIDANTS WITH NO_x
AT ELEVATED TEMPERATURES

BERNADETA ANNA POCHOPIEŃ

PhD

2012

Interactions of Antioxidants with NO_x at Elevated Temperatures

by

Bernadeta Anna Pochopiń

A thesis submitted in partial fulfilment of the requirements
for the degree of Doctor of Philosophy

University of York
Department of Chemistry

September 2012

Abstract

Automotive engines contain aggressive environments where lubricants are degraded by exposure to corrosive combustion by-products such as nitrogen oxides (NO₂ and NO), and understanding their interaction is key to the development of long-lived lubricants. Therefore the effect of 1000 ppm of nitrogen oxides on lubricants containing phenolic and aminic antioxidants, individually or in combination, in branched alkane base fluid has been investigated in laboratory reactors at 180 °C, representative of piston conditions.

The reaction of the phenolic antioxidant, octadecyl 3-(3,5-di-*tert*-butyl-4-hydroxyphenyl) propanoate with 1000 ppm NO₂ in N₂ resulted in the formation of a quinone methide product (octadecyl 3-(3,5-di-*tert*-butyl-4-oxo-cyclohexa-2,5-dien-1-ylidene) propanoate), in apparent contradiction to previous studies, which observed at room temperature the formation of nitro-phenols. Therefore a novel reaction mechanism is proposed to account for this change in mechanism with the temperature, with the addition of NO₂ to phenoxy radicals being dominant at low temperatures, but reversible at a higher temperature, at which the dominant reaction becomes an abstraction of a hydrogen atom from the α carbon on the alkyl group at the *para*-position of the phenoxy radical. The thermochemistry of key intermediates for this mechanism was also investigated using ab-initio calculation, allowing the prediction of the ceiling temperature for the addition of NO₂ (1000 ppm) to phenoxy radicals, and hence of the formation of nitrated phenolics, to be approximately 51 ± 57 °C.

The reaction of the aminic antioxidant, 4,4'-dioctyl diphenylamine, with 1000 ppm NO₂ was also investigated, with chemical analysis of the reaction products showing the formation of two monomers and five dimers of the starting antioxidant, and possible reaction mechanisms are based on these results.

The reaction of NO₂ with phenolic and aminic antioxidants when used in conjunction resulted in the identification of two new intermediates formed partially from fragments of aminic and phenolic antioxidants; novel chemical mechanisms for their formation are also suggested.

List of Contents

Title Page	i
Abstract	ii
List of Contents	iii
List of Tables.....	viii
List of Figures	xiv
Abbreviations	xxviii
Acknowledgements	xxx
Author's Declaration.....	xxxii

Chapter 1: Introduction..... 1

1.1 Introduction to the Project	1
1.2 Lubricant Composition	2
1.3 Lubrication in Piston Assembly	5
1.4 Formation of NO _x in Automotive Engines	6
1.5 Chemistry and Reactions with NO _x (NO, NO ₂)	9
1.6 Hydrocarbon Autoxidation in the Liquid Phase	17
1.7 Hydrocarbon Nitration in the Liquid Phase.....	19
1.8 Hydrocarbon Nitro - Oxidation in the Liquid Phase	21
1.9 Inhibition of Lubricant Degradation	22
1.10 Aims of the Project	28

Chapter 2: Experimental 29

2.1 Introduction	29
2.2 Apparatus and Procedures	29
2.2.1 Apparatus Set-up	29
2.2.2 Reactions Procedure.....	30

2.2.3 Reactions Parameters	33
2.2.4 Monitoring of the Reaction	33
2.2.5 Safety Using NO/NO ₂	35
2.2.5.1 Hazards of NO	35
2.2.5.2 Hazards of NO ₂	35
2.2.5.3 Control of Risks from Using NO/NO ₂	36
2.3 Chemical and Physical Analysis	40
2.3.1 Gas Chromatography	40
2.3.2 Gas Chromatography – Mass Spectroscopy	41
2.3.3 UV-Vis Spectroscopy	43
2.3.4 NMR Spectroscopy	43
2.3.5 GPC	44
2.3.6 Comprehensive Two-Dimensional Gas Chromatography	44
2.3.7 FTIR Spectroscopy	46
2.3.8 Kinematic Viscosity	48
2.4 Synthesis	49
2.5 Materials	51
Chapter 3: Autoxidation of Squalane in the Liquid Phase	53
3.1 Introduction	53
3.2 Previous work	54
3.3 Results	66
3.4 Discussion	71
3.5 Conclusion	74

Chapter 4: Reaction of Phenolic Antioxidants with NO₂ at Elevated Temperature 75

4.1 Introduction	75
4.2 Previous Studies on NO ₂ + Phenolics.....	76
4.3 Results and Discussion	79
4.3.1 Product Identification by GC-FID.....	80
4.3.2 Product Identification by High Resolution GC-MS FI and EI.....	81
4.3.3 Product Identification by UV-Vis	84
4.3.4 Product Identification by 1D and 2D proton NMR (COSY, DOSY).....	88
4.3.5 Product Identification by GC x GC NCD	94
4.3.6 Product Identification by ATR/FTIR	95
4.3.7 Summary of Antioxidant Intermediate Identification	97
4.4 Reaction Mechanism	98
4.5 Summary.....	100

Chapter 5: Thermochemical Calculations for Phenolic, Nitroaromatic and Non-Aromatic Compounds using Gaussian Software..... 101

5.1 Introduction	101
5.2 Method Development	105
5.2.1 Testing the Model for the Level Theory	105
5.3 Results	107
5.3.1 Thermochemistry Calculations of Selected Phenoxy-NO ₂ Adducts.....	107
5.3.2 Thermochemistry Calculations of Selected Quinone Methides.....	115
5.4 Discussion.....	119

5.4.1 Potential Energy Diagram for Reactions of Phenolics with NO ₂ ...	119
5.4.2 Ceiling Temperature.....	124
5.4.2.1 Pressure Dependence of Ceiling Temperatures.....	126
5.4.2.2 Ceiling Temperature for NO ₂ Addition.....	129
5.4.2.3 Ceiling Temperature for Quinone Methides Formation	137
5.4.2.4 Summary of T _c calculations.....	139
5.5 Summary.....	143

Chapter 6: Reaction of Aminic Antioxidant with NO₂ at Elevated Temperature 145

6.1 Introduction	145
6.2 Results and discussion	146
6.2.1 Reaction Procedure	146
6.2.2 Product Identification using GC-FID.....	146
6.2.3 Product Identification using High Resolution GC-MS EI	147
6.2.4 Quantitative Analysis using GC-FID.....	161
6.2.5 Summary of Identification	163
6.3 Reaction Mechanism of Aminic Antioxidant with NO ₂	166
6.4 Summary.....	174

Chapter 7: Interactions of Phenolic and Aminic Antioxidant with NO₂ at 180 °C..... 175

7.1 Introduction	175
7.2 Interaction of Phenolic and Aminic Antioxidants during Autoxidation.....	176
7.3 Results and Discussion	178

7.3.1 Quantitative Analysis using GC-FID	178
7.3.2 Identification of Intermediates using High Resolution GC-MS EI	181
7.4 Reaction Mechanisms	188
7.5 Summary	194
Chapter 8: Conclusions and Suggestions for Future Work	195
8.1 Summary and Conclusions	195
8.2 Future Work	199
8.2.1 The Effect of Oxygen Environment on Nitration Lubricants	199
8.2.2 Effect of other Lubricant Additives on Engine Oil Degradation in Bench-Top Reactor	200
8.2.3 The Effect of NO on Engine Lubricant Degradation at 180 °C	200
8.2.4 Monitoring of NO ₂ Consumption	200
8.2.5 Identifying the Nitration Products form Squalane	201
Appendix A	203
Appendix B	216
Appendix C	220
Appendix D	231
Appendix E	242
List of References	251

List of Tables

Table 1.1: API Base Oils Classification.....	3
Table 1.2: Formation of nitrogen monoxide by the Zeldovich mechanism.....	6
Table 1.3: Formation of nitrogen monoxide by the Fenimore mechanism.....	7
Table 1.4: Formation of nitrogen dioxide, reactions [1.6], [1.7] and [1.8]	7
Table 1.5: Examples of NO _x (NO, NO ₂) concentrations in engine cylinder.....	9
Table 1.6: Oxides of nitrogen: formulas, colours and reactivity.....	10
Table 1.7: Solubility of NO in organic solvents	11
Table 1.8: Reactions involved in the liquid-phase oxidation of hydrocarbons initiated by NO ₂ , reactions [1.42],[1.53].....	18
Table 1.9: Reactions of NO ₂ with double bonds.....	18
Table 1.10: Standard mechanism of hydrocarbon oxidation	19
Table 1.11: The mechanism of NO ₂ reaction with n-hexadecane proposed by Johnson.....	21
Table 1.12: Example of common phenolic and aminic antioxidant.....	22
Table 1.13: Inhibition of hydrocarbon oxidation using radical scavengers	22
Table 2.1: Details of the parts used in the apparatus.....	32
Table 2.2: Typical reactions conditions	33
Table 2.3: Chromatographic conditions of GC-FID analysis	40
Table 2.4: Chromatographic conditions for standard GC-MS EI analysis	41
Table 2.5: Chromatographic Conditions for GC-MS EI analysis	42
Table 2.6: GPC conditions details.....	44

Table 2.7: Materials – part 1	51
Table 2.8: Materials – part 2	52
Table 3.1: Autoxidation of pristane – initial reactions.....	57
Table 3.2: Chemical structures and molecular weights of squalane oxidation products.....	66
Table 3.3: GC-MS EI mass spectra matched with NIST Library results (this work).....	67
Table 3.4: Measured FI (this work) and ammonia CI (previous work) mass spectra for squalane oxidation.....	70
Table 3.5: Products formed during the autoxidation of squalane with the carbon initially attacked given	72
Table 3.6: Concentration of alkanes and ketones formed by squalane oxidation at 170 °C in bench-top reactor depended on carbon number	72
Table 4.1: GC-MS EI and FI detail fragmentation patterns of phenolic antioxidant and its intermediate formed from reaction with NO ₂ at 180 °C.....	81
Table 4.2: GC-MS EI detail fragmentation patterns of antioxidant intermediate formed from reaction of EthPh with NO ₂ at 180 °C	83
Table 4.3: GC-MS EI detail fragmentation patterns of synthesised HCIN.....	84
Table 4.4: Summary of an intermediate product identification, from the reaction of antioxidant (OHPP) with NO ₂ at 180 °C	97
Table 5.1: The homolytic bond dissociation enthalpies of C ₆ H ₅ NO ₂ , PhOH, BHT and HONO calculated using different methods and basis sets.	106
Table 5.2: Calculated changes in enthalpy, Gibbs energy and entropy for reaction [5.1], at standard temperature and pressure	108

Table 5.3: Calculated changes in enthalpy, Gibbs free energy and entropy for reaction [5.2], at standard temperature and pressure.....	110
Table 5.4: Calculated changes in enthalpy, Gibbs free energy and entropy for TTBP—NO ₂ at standard temperature and pressure.....	111
Table 5.5: Calculated changes in enthalpy, Gibbs free energy and entropy for reaction [5.4], at standard temperature and pressure.....	113
Table 5.6: Calculated changes in enthalpy, Gibbs free energy and entropy for analogue OHPP—NO ₂ at standard temperature and pressure.....	115
Table 5.7: Calculated changes in enthalpy, Gibbs free energy and entropy for reaction [5.6] at standard temperature and pressure.....	116
Table 5.8: Calculated changes in enthalpy, Gibbs free energy and entropy for QM formation at standard temperature and pressure	118
Table 5.9: Comparison of experimental and calculated bond strengths for phenol O—H, phenoxy & benzyl—NO ₂ adducts and C—H bond strengths for phenoxy radicals	122
Table 5.10: Estimated Ceiling Temperature for reaction $\text{BHT}^\cdot + \text{NO}_2 \rightleftharpoons \text{BHT—NO}_2$ at Different Partial Pressures of NO ₂	127
Table 5.11: Estimated Ceiling Temperature for reaction $\text{BHT}^\cdot + \text{NO}_2 \rightleftharpoons \text{BHT—ONO}$ at Different Partial Pressures of NO ₂	130
Table 5.12: Estimated Ceiling Temperature for reaction $\text{TTBP}^\cdot + \text{NO}_2 \rightleftharpoons \text{TTBP—NO}_2$ at Different Partial Pressures of NO ₂	131
Table 5.13: Estimated Ceiling Temperature for reaction $\text{EthPh}^\cdot + \text{NO}_2 \rightleftharpoons \text{EthPh—NO}_2$ at Different Partial Pressures of NO ₂	134
Table 5.14: Estimated Ceiling Temperature for reaction $\text{OHPP}^\cdot + \text{NO}_2 \rightleftharpoons \text{OHPP—NO}_2$ at Different Partial Pressures of NO ₂	135
Table 5.15: Estimated Ceiling Temperature for reaction $\text{EthPh}^\cdot + \text{NO}_2 \rightleftharpoons \text{QM1} + \text{HONO}$ at Different Partial Pressures of NO ₂	136

Table 5.16: Estimated Ceiling Temperature for reaction $\text{OHPP} \cdot + \text{NO}_2 \rightleftharpoons \text{QM} + \text{HONO}$ at Different Partial Pressures of NO_2	137
Table 6.1: Chemical structures and molecular weights of DODPA and its intermediates (A, B, 1, 2) from the reaction with NO_2	165
Table 6.2: Chemical structures and molecular weights of intermediates (3, 4, 5) formed from the reaction of DODPA with NO_2	166
Table A1: Example of the oxygen uptake calculations from squalane oxidation in bench-top reactor at 180° C (this work results).....	203
Table A2: Carbon constant calculated for standard compounds.....	211
Table A3: Example of 6-methyl-2-heptanone EI and FI fragmentation (this work).....	212
Table A4: Examples of characteristic frequencies of carbonyl functional groups.....	215
Table A5: Examples of characteristic frequencies of nitro, nitroso, N—O functional groups.....	215
Table B1: Products formed during the autoxidation of pristane, the pristoxyl or pristyl radicals from which they are formed by the reactions given	219
Table D1: Computed bond dissociation energies at 298 K with various DFT methods at 6-31G (d,p) basis set. The value in the parenthesis is the deviation from computed BDE for experimental one.....	232
Table D2: Computed bond dissociation energies at 298 K with various DFT methods at 6-31+G (d,p) basis set. The value in the parenthesis is the deviation from computed BDE for experimental one.....	232
Table D3: Computed bond dissociation energies at 298 K with various DFT methods at 6-311G (d,p) basis set. The value in the parenthesis is the deviation from computed BDE for experimental one.....	233

Table D4: Computed bond dissociation energies for H ₂ O, CH ₃ OH and Ph-OH at 298K using B3LYP and (RO)B3LYP methods with 6-311G(d,p) and 6-311++G(2df,2p) basis sets [Ref. ⁸]	233
Table D5: Total energies (a.u.) and energy of dissociation (kcal mol ⁻¹) for HOH→OH +H calculated by using B3LYP Hybrid DFT method and different basis sets [Ref. ⁹]	234
Table D6: Total energies (a.u.) and energy of dissociation (kcal mol ⁻¹) for HOH→OH + H calculated by using 6-31+G(d) basis set and different methods [Ref. ⁹]	234
Table D7: Thermochemical values from Gaussian, calculated for reactants and product for nitrobenzene formation using BPV86/6-311G (d,p) method, units Hartees [This work]	236
Table D8: Conversion factors	237
Table D9: Thermochemical values form Gaussian calculated for reactants and product of BHT–NO ₂ formation, using BPV86/6-311G (d,p) method, units Hartees [This work]	239
Table D10: Thermochemical values form Gaussian calculated for reactants and product for BHT–ONO formation using BPV86/6-311G (d,p) method, units Hartees [This work]	239
Table D11: Thermochemical values form Gaussian calculated for reactants and product for TTBP–NO ₂ formation, using BPV86/6-311G (d,p) method, units Hartees [This work]	240
Table D12: Thermochemical values form Gaussian calculated for reactants and product of EthPh–NO ₂ formation, using BPV86/6-311G (d,p) method, units Hartees [This work]	240
Table D13: Thermochemical values form Gaussian calculated for reactants and product for analogue OHPP–NO ₂ formation, using BPV86/6-311G (d,p) method, units Hartees [This work]	241

Table D14: Thermochemical values form Gaussian calculated for reactants and product of EthPh—QM formation, using BPV86/6-311G (d,p) method, units Hartees [This work].....	241
Table D15: Thermochemical values form Gaussian calculated for reactants and product for ODTBHPP—QM formation, using BPV86/6-311G (d,p) method, units Hartees [This work].....	242
Table D16: O—H Bond Dissociation Energies of different phenolics calculated using BPV86/6-311G (d,p) method [This work]	242

List of Figures

Figure 1.1: Example of linear (top) and branched (bottom) paraffins	3
Figure 1.2: Example of naphthene (left) and aromatic (right) molecules	4
Figure 1.3: Schematic diagram of the piston ring pack with the thin layer of lubricant exposed to blow-by gases	5
Figure 1.4: The dependence of $\ln \text{NO}_2/\text{NO}$ at various temperatures	8
Figure 1.5: State dependency of nitrogen monoxide.....	10
Figure 1.6: Mezoimeric formulas for valence bond description of bonding in NO.....	11
Figure 1.7: Example of the reaction of a carbon radical with nitric oxide.....	12
Figure 1.8: Examples of different elementary reactions with nitrogen monoxide (NO), including: combination [1.10]; homolytic substitution [1.11]; addition [1.12], [1.13]; pericyclic reactions [1.14] and electron transfer [1.15], [1.16]. Where: X = H; Y = (R ₂ N) CH; A [·] -oxidant; and B [·] = reductant	12
Figure 1.9: Example of the reaction mechanism of nitrogen monoxide with alkoxy radicals	13
Figure 1.10: Example of the reaction of nitrogen monoxide with peroxy radicals	13
Figure 1.11: Example of the reaction of substituted phenol with nitrogen monoxide, (SDS – Sodium Dodecyl Sulphate).....	14
Figure 1.12: Mezoimeric formulas of nitrogen dioxide	14
Figure 1.13: Example of the reaction of alkyl radical with nitrogen dioxide	15
Figure 1.14: Reaction of phenoxy radical with nitrogen dioxide	15
Figure 1.15: Hydrogen abstraction from phenolics by nitrogen dioxide	15
Figure 1.16: Reaction of quinone with nitrogen dioxide	16
Figure 1.17: Reaction of benzimidazole with NO_2/O_3	16

Figure 1.18: Reaction of indole with nitrogen dioxide	17
Figure 1.19: Reaction of arylamines with nitrogen dioxide.....	17
Figure 1.20: Conversion of nitroso compounds using nitrogen dioxide.....	17
Figure 1.21: Examples of different BHT reactions: with alkyl radical [1.75]; with peroxy radical [1.76], [1.77]; the interaction of two phenoxy radicals (termination) [1.78] and the decomposition of cyclohexadienone alkyl peroxide at high temperature [1.79].....	23
Figure 1.22: The radical mechanism of octadecyl 3-(3,5-di-tert-butyl-4-hydroxy-phenyl)propanoate proposed by Pospisil	24
Figure 1.23: Reaction mechanism of NO ₂ with 2, 4, 6-tri-tert-butylphenol	25
Figure 1.24: Reaction of aminic antioxidant with radicals	26
Figure 1.16: Reaction of aminic antioxidant with peroxy radicals at high temperature.....	26
Figure 1.17: Reaction of diphenyl amine with NO ₂	27
Figure 2.1: Stainless steel micro-reactor (49.0 cm ³ head space volume).....	29
Figure 2.2: Apparatus set-up for before reaction was undertaken	30
Figure 2.3: Schematic diagram of the apparatus: 1, 2 - gas cylinders; 3, 4, 15 – flowmeters; 5, 6 – non-return valves; 7- micro-reactor; 8- thermocouple; 9 – septum, 10 – pressure gauge; 11 – cold trap; 12, 13 – liquid traps; 14 – particulate filter; 16 – sensor; 17 – data logger and 18 – computer.....	31
Figure 2.4: Example of raw data recorded using thermocouple, pressure gauge and oxygen sensor connected to the data logger/computer. Reaction conditions: 100% (1000 mV) O ₂ at flow rate 100 cm ³ min ⁻¹ , model lubricant squalane, T=180° C, p=1050 mbar	34
Figure 2.5: GC x GC instrument: 1-injector, 1 st Column, 2-Interface, 2 nd Column and 3-detector.....	45

Figure 2.6: An example of FTIR spectrum of used lubricant from an engine, oxidation and nitration products in region 1940-1430 cm^{-1} (BP/Castrol Laboratory in Pangbourne UK, obtain by S. Holliday)	46
Figure 2.7: Set up of universal transmission cell for the analysis of liquids in FTIR	47
Figure 2.8: Cannon-Manning micro-viscometer U-tube 300	48
Figure 2.9: Reaction of synthesis of 6-di- <i>tert</i> -butyl-4-ethylidene-cyclohexa-2,5-dien-1-one (quinone methide, QM1)	49
Figure 2.10: Apparatus for synthesis: 1-thermometer, 2- thermometer adapter with side arm adapter, 3-magnetic stirrer, 4-septum, 5 -(3)-neck flask, 6- magnetic stirrer bar	49
Figure 3.1: Chemical structure of squalane ($\text{C}_{30}\text{H}_{62}$)	53
Figure 3.2: Chemical structure of n-hexadecane ($\text{C}_{16}\text{H}_{34}$), n-decane ($\text{C}_{10}\text{H}_{22}$), n-octane (C_8H_{18})	54
Figure 3.3: Schematic diagram of oxidation of hydrocarbons	55
Figure 3.4: Chemical structure of 2,4,6-trimethylheptane ($\text{C}_{10}\text{H}_{22}$)	56
Figure 3.5: Chemical structure of pristane ($\text{C}_{19}\text{H}_{40}$)	57
Figure 3.6: Chemical mechanism of oxidation of pristane - formation of ketones and carboxylic acids. Product identification in Appendix C	59
Figure 3.7: Lactone formation by Goosen et al	61
Figure 3.8: Lactone formation by Belenkov et al	62
Figure 3.9: Chemical mechanism of alkenes formation	63
Figure 3.10: GC-FID trace of squalane oxidation for 10 minutes at 170 °C in static reactor. Peaks 1: propan-2-one; 2: 2-methylpentane; 3: 6-methylhept-2-one; 4: 2, 6-dimethylnonane; 5: 6,10-dimethylundecan-2-one; 6: 2,6,10-trimethyltetradecane; 7: 7,11,15-trimethylhexadecan-2-one; 8: 2,6,10,15-	

tetramethyloctadecane; 9: 6,11,15,19 – pentamethyleicosan-2-one; 10: 2,6,10,15,19-pentamethyldocosane; and 11: 2,6,10,15,19,23- hexamethyltetracosane (Squalane).....	65
Figure 3.4: Example of GC-MS EI identification of 2,6,10,15- tetramethyloctadecane.....	69
Figure 3.5: Mechanism of ketones and alkanes formation from squalane.....	71
Figure 4.1: Structure of commercial phenolic antioxidant; octadecyl 3-(3,5-di- <i>tert</i> - butyl-4-hydroxy-phenyl) propanoate (OHPP), BASF Irganox [®] L107	75
Figure 4.2: Structure of 2,6-di- <i>tert</i> -butyl-4-ethylphenol (EthPh)	75
Figure 4.3: Brunton’s mechanism for the reaction of phenolics with NO ₂	77
Figure 4.4: Astolfi’s mechanism for the reaction of phenolics with NO ₂	78
Figure 4.5: GC traces 0-240 min. of products formation form reaction OHPP in squalane with NO ₂ at 180 °C	80
Figure 4.6: OHPP and intermediate protecting the base oil from nitration up to 135 min., when both are consumed squalane nitration products form.....	81
Figure 4.7: Possible alternative structures of antioxidant intermediate; quinone methide (QM) and hydroxy cinnamate (HCIN).....	82
Figure 4.8: Characteristic EI fragmentation for QM, OHPP and HCIN	83
Figure 4.9: Colour development in samples 0-240min from reaction OHPP with NO ₂ at 180 °C	85
Figure 4.10: UV-Vis spectra of all samples from reaction of OHPP with NO ₂ at 180 °C	85
Figure 4.11: UV-Vis spectra of synthesised 2,6-di- <i>tert</i> -butyl-4-ethylidene- cyclohexa-2,5-dien-1-one (QM1), reaction mixture with quinone methide intermediate (QM1) and starting material (EthPh)	86
Figure 4.12: UV-Vis spectra of starting material with an antioxidant (OHPP) and	

reaction mixture with intermediate (QM) comparing to model compound hydroxycinnamate (HCIN).....	87
Figure 4.13: High resolution 700 MHz 1D ¹ H NMR spectra of reaction mixture 0 to 15 min. (in CDCl ₃) with identified products from antioxidant depletion: HCIN = Hydroxy Cinnamate and QM = Quinone Methide	88
Figure 4.14: Proton NMR spectrum of Hydroxy Cinnamate (model compound), obtained using Bruker 400 MHz (solvent CDCl ₃), synthesised at University of York by G. Moody	89
Figure 4.15: Comparison of predicted HCIN spectrum, obtained using ACD/I-lab ¹ H NMR Prediction Software, to 5 min. reaction mixture	90
Figure 4.16: Comparison of predicted HCIN spectrum, obtained using ACD/I-lab ¹ H NMR Prediction Software, to 5 min. reaction mixture	90
Figure 4.17: High resolution 700 MHz ¹ H DQF COSY spectrum of 10 minutes sample (in CDCl ₃), shows nearest neighbours diagonal and cross peaks of hydroxy cinnamate, proves that two doublets (~16Hz typical for trans coupling) are the same molecule	92
Figure 4.18: High resolution 700 MHz ¹ H DOSY spectrum of 10 minutes sample (in CDCl ₃), shows diffusion coefficient for Hydroxy Cinnamate and Quinone Methide proves that both molecules are the same size	93
Figure 4.19: 1D and 2D GC NCD chromatograms of 45 min. sample with not detected nitrated products	94
Figure 4.20: FTIR results show no changes up to 135 min. Overlaid spectra of samples: 0 - 135 minutes.....	95
Figure 4.21: Overlaid FTIR spectra of samples: 135 - 240 minutes shows nitrated base oil	95
Figure 4.22: FTIR spectra of starting material and 10 minutes reaction mixture recorded in the thin layer cell (CaF ₂)	96
Figure 4.23: Novel reaction mechanism of phenolic antioxidant (OHPP)	

with NO ₂	99
Figure 5.1: Structures of phenolic antioxidants; octadecyl 3-(3,5-di- <i>tert</i> -butyl-4-hydroxy-phenyl)propanoate (OHPP), 2,6-di- <i>tert</i> -butyl-4-ethylphenol (EthPh), 2,4,6-tri- <i>tert</i> -butylphenol (TTBP), 4-methyl-2,6-di- <i>tert</i> -butylphenol (BHT)	102
Figure 5.2: Reaction [5.1] of NO ₂ addition to phenoxy radical from 4-methyl-2,6-di- <i>tert</i> -butylphenol (BHT).....	107
Figure 5.3: Optimised geometry of BHT—NO ₂ using BPV86/6-311G(d,p) method (Output File).....	108
Figure 5.4: Reaction [5.2] of NO ₂ addition through the oxygen atom to phenoxy radical from 4-methyl-2,6-di- <i>tert</i> -butylphenol (BHT).....	109
Figure 5.5: Optimised geometry of BHT—ONO using BPV86/6-311G(d,p) method (Output File).....	109
Figure 5.6: Reaction [5.3] of NO ₂ addition to phenoxy radical from 2,4,6-tri- <i>tert</i> -butylphenol (TTBP)	110
Figure 5.7: Optimised geometry of TTBP—NO ₂ using BPV86/6-311G(d,p) method (Output File).....	111
Figure 5.8: Reaction [5.4] of NO ₂ addition to phenoxy radical from 2,6-di- <i>tert</i> -butyl-4-ethyl-phenol (EthPh)	112
Figure 5.9: Optimised geometry of EthPh—NO ₂ using BPV86/6-311G(d,p) method (Output File).....	112
Figure 5.10: Reaction [5.5] of NO ₂ addition to phenoxy radical from OHPP analogue	113
Figure 5.11: Optimised geometry of OHPP—NO ₂ using BPV86/6-311G(d,p) method (Output File).....	114
Figure 5.12: Reaction [5.6] of formation of 2,6-di- <i>tert</i> -butyl-4-ethylidene-cyclohexa-2,5-dien-1-one (QM1) from 2,6-di- <i>tert</i> -butyl-4-ethyl-phenol	

(EthPh)	115
Figure 5.13: Optimised geometry of QM1 using BPV86/6-311G(d,p) method (Output File).....	116
Figure 5.14: Reaction [5.7] of formation of octadecyl 3-(3,5-di- <i>tert</i> -butyl-4-oxo- cyclohexa-2,5-dien-1-ylidene) propanoate (QM), from OHPP—peroxyl radical	117
Figure 5.15: Optimised geometry of analogue QM using BPV86/6-311G(d,p) method (Output File).....	118
Figure 5.16: Potential energy diagram of reactions phenolic species with NO ₂ ..	120
Figure 5.17: Arrhenius equation of the dependence of the rate constant $\ln k$ on the temperature $1/T$ for TTBP (previous studies)	121
Figure 5.18: Equilibrium constant vs. temperature. Example of determination of ceiling temperature for reaction 5.1, when $K=1$	124
Figure 5.19: Calculated ceiling temperature for BHT-NO ₂ formation (the line) (this work), compared to the experimental conditions 25 °C and 1 bar NO ₂ used by Brunton (the triangle) (previous studies), which product was nitrated BHT.	128
Figure 5.20: Ceiling Temperatures for BHT—ONO formation	129
Figure 5.21: Ceiling Temperatures for TTBP—NO ₂ formation	132
Figure 5.22: Calculated ceiling temperature for EthPh—NO ₂ formation (line) (this work) compared to the experiment carried out at 180 °C and 0.001 bar NO ₂ (the dot), which produced quinone methide (QM1) product from EthPh (this work). 133	
Figure 5.23: Calculated ceiling temperature for OHPP—NO ₂ formation (line) (this work), compared to the experiment carried out at 180 °C and 0.001 bar NO ₂ (dot), which produced quinone methide (QM) product from OHPP (this work).	135
Figure 5.24: Calculated ceiling temperature for QM and QM1 formation (lines) compared to the experimental conditions (two experiments), which produced QM and QM1.....	137
Figure 5.25: Estimated ceiling temperatures for nitrated BHT, EthPh and	

OHPP.....	138
Figure 5.26: Comparison of previous experimental conditions (25°C and 1 bar NO ₂) product nitrated (BHT), (the triangle) and current (EthPh, OHPP) experimental results (the line).....	139
Figure 5.27: Proposed reaction mechanism based on product identification for the reaction of 0.5% OHPP in squalane with 1000 ppm of NO ₂ at 180 °C	140
Figure 6.1: Structure of commercial aminic antioxidant; 4,4'-Dioctyl Diphenylamine (DODPA), BASF Irganox [®] L01	143
Figure 6.2: GC-FID chromatogram of 60 minutes sample mixture of aminic antioxidant and its products (A, B, 1, 2, 3, 4, 5)	144
Figure 6.3: GC chromatogram of 60 minutes sample with suppressed solvent and squalane peaks. Peaks between 20-40 minutes are squalane impurities.....	145
Figure 6.4: GC/TOF MS (EI) spectrum of aminic antioxidant (DODPA)	146
Figure 6.5: Confirmation of EI mass spectrum of aminic antioxidant (DODPA) (top spectrum) with NIST Library database (bottom spectrum). Analysis by GC Perkin Elmer Clarus 500	147
Figure 6.6: Resonance structures of aminyl radical from DODPA	147
Figure 6.7: GC/TOF MS (EI) spectrum of product A from the reaction of aminic antioxidant (DODPA) with NO ₂ at 180 °C	148
Figure 6.8: Possible structure of product A based on GC/TOF MS (EI) fragmentation	149
Figure 6.9: GC/TOF MS (EI) spectrum of product B from the reaction of aminic antioxidant (DODPA) with NO ₂ at 180 °C	150
Figure 6.10: Mechanism of the H ₂ O elimination from the molecular ion of Product B with formation of characteristic m/z 333 fragment.....	151
Figure 6.11: GC/TOF MS (EI) spectrum of product 1 from the reaction of aminic antioxidant (DODPA) with NO ₂ at 180 °C	152

Figure 6.12: GC/TOF MS (EI) spectrum of product 2 from the reaction of aminic antioxidant (DODPA) with NO ₂ at 180 °C	153
Figure 6.13: Possible dimer structures of products 1 and 2	154
Figure 6.14: GC/TOF MS (EI) spectrum of product 3 from the reaction of aminic antioxidant (DODPA) with NO ₂ at 180 °C	155
Figure 6.15: Possible dimer structures of products 3	156
Figure 6.16: GC/TOF MS (EI) spectrum of product 4 from the reaction of aminic antioxidant (DODPA) with NO ₂ at 180 °C	157
Figure 6.17: GC/TOF MS (EI) spectrum of product 5 from the reaction of aminic antioxidant (DODPA) with NO ₂ at 180° C	158
Figure 6.18: Possible dehydrodimers structures of products 4 and 5	158
Figure 6.19: Aminic antioxidant consumption vs. total of intermediate products formation for the reaction of DODPA with NO ₂ at 180 °C	159
Figure 6.20: Calculated concentrations of intermediates products for the reaction of DODPA with NO ₂ at 180° C	160
Figure 6.21: Reaction mechanism of formation of product 2 (R=C ₈ H ₁₁)	167
Figure 6.22: Mechanism I and II – possible reaction mechanisms of formation of product A. (R=C ₈ H ₁₁)	168
Figure 6.23 Mechanism III – first possible reaction mechanism of formation of product A (R=C ₈ H ₁₁)	169
Figure 6.24 Reaction mechanism of formation of product B (R=C ₈ H ₁₁)	170
Figure 6.25 Reaction mechanism of formation of product 3 (R=C ₈ H ₁₁)	171
Figure 6.26: Reaction mechanism of formation of product 1, 4 and 5 (R=C ₈ H ₁₁).....	172
Figure 6.27: Summarising mechanism of intermediates formed from DODPA in the reaction with NO ₂ (R=C ₈ H ₁₁).....	173

Figure 7.1: Structures of commercial phenolic (OHPP) and aminic (DODPA) antioxidants	175
Figure 7.2: Synergistic mechanism between phenolic and aminic antioxidant in the reaction with peroxy radicals	177
Figure 7.3: Decay of phenolic (0.25% w/w) and aminic (0.25% w/w) antioxidants, and their intermediates formation (products 1, 3 and 4) in the reaction with NO ₂ at 180 °C	178
Figure 7.4: GC chromatogram of 10 minutes reaction mixture containing phenolic and aminic antioxidants and phenolic antioxidant intermediate product (Product 1), other peaks squalane impurities. Analysis using GC-FID, Shimadzu GC, column ZB-5HT, inj. 350 °C, oven 50-350 °C at 5 °C/min, hold for 20 min , FID 350 °C	179
Figure 7.5: GC chromatogram of 60 minutes reaction mixture containing aminic antioxidant and three intermediates (products 2, 3 and 4)	179
Figure 7.6: GC chromatogram of 90 minutes reaction mixture containing aminic antioxidant, products 2, 3, 4 and five new intermediates (zoom Agilent 7890A GC). Analysis using GC-FID, Shimadzu GC, column ZB-5HT, inj. 350 °C, oven 50-350 °C at 5 °C/min, hold for 20 min , FID 350 °C	180
Figure 7.7: GC/TOF MS (EI) spectrum of Product 1 from the reaction of aminic (DODPA) and phenolic (OHPP) antioxidant with NO ₂ at 180 °C	181
Figure 7.8: GC/TOF MS (EI) spectrum of Product 4 from the reaction of aminic (DODPA) and phenolic (OHPP) antioxidant with NO ₂ at 180 °C	182
Figure 7.9: Possible fragment structures of Product 4 from the reaction of aminic (DODPA) and phenolic (OHPP) antioxidant with NO ₂ at 180 °C - Part 1	183
Figure 7.10: Possible fragment structures of Product 4 from the reaction of aminic (DODPA) and phenolic (OHPP) antioxidant with NO ₂ at 180 °C - Part 2	184
Figure 7.11: GC/TOF MS (EI) spectrum of Product 2 from the reaction of aminic (DODPA) and phenolic (OHPP) antioxidant with NO ₂ at 180 °C	185

Figure 7.12: GC/TOF MS (EI) spectrum of Product 3	186
Figure 7.13: Possible fragment structures for Product 3 from the reaction of aminic (DODPA) and phenolic (OHPP) antioxidant with NO ₂ at 180 °C.....	187
Figure 7.14: Mechanism of formation of HCIN, from the experiment studying the reaction of model lubricant containing both aminic and phenolic antioxidants with NO ₂ at 180 °C, (R=C ₁₈ H ₃₇)	188
Figure 7.15: Possible synergistic mechanism between phenolic and aminic antioxidant in the reaction with NO ₂ , similar to mechanism previously studied for peroxy radicals	190
Figure 7.16: Possible mechanism of formation of Product 4 in the reaction of model lubricant (containing both aminic and phenolic antioxidants) with NO ₂ at 180 °C: (R=C ₁₈ H ₃₇ ; R ¹ =C ₈ H ₁₇)	191
Figure 7.17: Possible mechanism of formation of Product 3 from the reaction of model lubricant (containing both aminic and phenolic antioxidants) with NO ₂ at 180 °C. (R ¹ =C ₈ H ₁₇ and R=C ₁₈ H ₃₇)	192
Figure A1: Calculated oxygen uptake for four different oxidation experiments using: 1. – squalane (model base oil); 2. – squalane with OHPP (phenolic antioxidant); 3. – squalane with NO ₂ ; 4. - squalane with OHPP and with NO ₂ . Reaction conditions: 180 ± 1 °C, 1000 mbar, oxygen flow rate 0.1 dm ³ min ⁻¹ , [NO ₂] ~1700 ± 200 ppm, [OHPP] 0.5% w/w	204
Figure A2: Identification of carbonyl functional groups from oxidation squalane in bench-top reactor at 180 °C, overlaid IR spectra of samples from: 0, 5, 10, 15, 20, 15, 25 and 30 minutes	206
Figure A3: Inhibited (phenolic antioxidant) oxidation of squalane in bench-top reactor at 180 °C, overlaid IR spectra of samples from: 0, 5, 10, 15, 20, 25 and 30 minutes	206
Figure A4: Identification of nitrate and nitro functional groups from the nitro-oxidation of squalane in bench-top reactor at 180 °C, samples 0, 5, 10, 15, 20, 23, 25 and 30 minutes	207

Figure A5: Antioxidant effect on nitro-oxidation of squalane in bench-top reactor at 180 °C, overlaid IR spectra of samples from: 0, 5, 10, 15, 20, 15 and 25 minutes.....	208
Figure A6: Kinematic viscosity change reported for oxidation of squalane in bench-top reactor at 180 °C, comparison of the reactions with presence or absence nitrogen dioxide (1700 ± 200 ppm) and with presence or absence of antioxidant OHPP (0.5 %, wt/wt)	210
Figure A7: GC response factors plotted against effective carbon number of various compounds (this work).....	211
Figure A8: Example of chromatogram obtained by suppression solvent and squalane. (this work).....	212
Figure A9: Example of 2D GC chromatogram obtained using FID detector: C – before reaction, D – after reaction. Reaction details: model lubricant (squalane), reactive gas NO ₂ , temp. 180 °C, (this work).....	213
Figure A10: Example of 2D GC chromatograms obtained using NCD detector: A - before reaction, B - after reaction. Reaction details: model lubricant (squalane), reactive gas NO ₂ , temp. 180 °C. (this work).....	214
Figure B1: Comparison of tertiary carbon composition of the different commercial base fluids to squalane and n-hexadecane.....	217
Figure B2: GC-FID traces of commercial base fluid, Yubase 4 (top trace) and model base fluid, Squalane 99% purity (bottom trace). (This work results)	218
Figure B3: Proportion of radical attack at tert-carbons of pristane, and quantified reaction pathways for sec- and tert-pristoxyl radicals.....	220
Figure B4: Fragment ketone products formed during the autoxidation of pristane at 170°C.....	220
Figure B5. Fragment alkane products formed during the autoxidation of pristane at 170°C.....	220
Figure C1: High Resolution GC-MS EI of OHPP Intermediate.....	221

Figure C2: High Resolution GC-MS EI of OHPP	222
Figure C3: High Resolution GC-MS FI of OHPP	222
Figure C4: High Resolution GC-MS FI of OHPP Intermediate	223
Figure C5: GC MS EI Perkin Elmer analysis of 2,6-di-tert-butyl-4-ethyl phenol (EthPh), syntheses 2,6-ditert-butyl-4-ethylidene-cyclohexa-2,5-dien-1-one (QM1) and QM1 product of reaction with NO ₂ at 180 °C.....	224
Figure C6: GC Chromatograms of squalane, squalane with EthPh and reaction mixture cont containing product of reaction EthPh with NO ₂ , the 6-ditert-butyl-4-ethylidene-cyclohexa-2,5-dien-1-one (QM1)	224
Figure C7: GPC chromatogram sample 0 min. (in THF), 0.5 % w/w OHPP in squalane.....	225
Figure C8: GPC chromatogram 10min (in THF), reaction mixture with max. absorption of 305 nm characteristic for QM	226
Figure C9: GPC chromatogram 45min, reaction mixture with max absorption of 310 nm characteristic for HCIN	227
Figure C10: GPC chromatogram of syhtesised HCIN with max absorption of 310 nm.....	228
Figure C11. High resolution 700 MHz 1D proton NMR spectra of reaction mixture 0 to 135 min. (in CDCl ₃), full range. Reaction of OHPP in squalane with NO ₂ at 180°C	229
Figure C12: Comparison of 5 min. reaction mixture with predicted proton NMR of HCIN.....	230
Figure C13: Comparison of 5 min. reaction mixture with predicted proton NMR of QM.....	230
Figure C14: Comparison of 0 min. reaction mixture with predicted H ¹ NMR of OHPP.....	231

Figure C15. 2D GCxGC NCD chromatogram of nitrated squalane	231
Figure D1: Optimised geometry of nitrobenzene $C_6H_5NO_2$ using BPV86/6-311G (d,p) method (Output File)	234
Figure E1: TOF/GC MS (EI) aminic antioxidant (DODPA)	242
Figure E2: TOF/GC MS (EI) Product A	243
Figure E3: TOF/GC MS (EI) Product B	245
Figure E4: Possible structures of product B	244
Figure E5: TOF/GC MS (EI) Product 1	246
Figure E6: TOF/GC MS (EI) Product 2	247
Figure E7: TOF/GC MS (EI) Product 3	248
Figure E8: TOF/GC MS (EI) Product 4 and 5	249

List of Abbreviations

AO	Antioxidant
API	American Petroleum Institute
ATIEL	Association Technique de L'Industrie Europeene Des Lubrifiants (Technical Association of the European Lubricants Industry)
ATR	Attenuated Total Reflection
BDE	Bond Dissociation Energy
BHT	Butylated Hydroxyl Toluene
B3LYP	Becke, Three-parameter, Lee-Yang-Parr
B3PW91	Becke, Three-parameter, Perdew and Wang's 1991
B3P86	Becke, Three-parameter, Perdew 86
BPV86	Becke, Three-parameter, Vosco 86
CI	Chemical Ionisation
HC	Hydrocarbons
CDCl ₃	Deuterated chloroform
CO	Carbon Monoxide
CO ₂	Carbon Dioxide
COSY	Correlation Spectroscopy
DFT	Density functional theory
DOSY	Diffusion Ordered Spectroscopy
DCM	Dichloromethane
DODPA	4,4'-Diocetyl Diphenyl Amine
EthPh	2,6-Di- <i>tert</i> -butyl-4-ethylphenol
EGR	Exhaust Gas Recirculation
EI	Electron Impact
ECN	Effective Carbon Number
FI	Field Ionisation
FID	Flame Ionization Detector
FTIR	Fourier Transform Infrared
GC	Gas Chromatography
GC-FID	Gas Chromatography with Flame Ionisation Detector
GC-MS	Gas Chromatography-Mass Spectroscopy
TOF-MS	Time-of-Flight Mass Spectrometry

GPC	Gel Permeation Chromatography
2D GC	Two-Dimensional Gas Chromatography
HCIN	Hydroxy Cinnamate
IR	Infra-red
KV	Kinematic Viscosity
LTEL	Long Term Exposure Limit
LC	Lethal Concentration
MW	Mass Weight
MS	Mass Spectroscopy
NCD	Nitrogen Chemiluminescence Detector
NMR	Nuclear Magnetic Resonance
NIST	National Institute of Standards and Technology
NO _x	Nitrogen Oxides
N ₂ O	Nitrous Oxide
NO	Nitrogen Monoxide (Nitric Oxide)
NO ₂	Nitrogen Dioxide
N ₂ O ₄	Dinitrogen Tetroxide
HNO ₂	Nitrous Acid
QM	Quinone methide from OHPP
QM1	Quinone methide form EthPh
OHPP	Octadecyl 3-(3,5-di- <i>tert</i> -butyl-4-hydroxyphenyl)propanoate
OIT	Oxidation Induction Time
PAO	Poly Alpha Olefins
PhOH	Phenol
PC	Computer
RPVOT	Standard Test Method for Oxidation Stability of Steam Turbine
SQ	Squalane
SDS	Sodium Dodecyl Sulphate
STEL	Short Term Exposure Level
TTBP	2,4,6-tri- <i>tert</i> -butylphenol
THF	Tetrahydrofuran
T _c	Ceiling Temperature
UV-Vis	Ultraviolet-Visible Spectroscopy
ZDDP	Zinc Dialkyl-Dithio-Phosphate

Acknowledgements

First and foremost I would like to thank Dr Moray Stark and Dr Duncan MacQuarrie for their excellent supervision, encouragement and enthusiasm over last four years, also for their patience when correcting chapters of this thesis.

I would like to thank my industrial supervisors Dr Kevin West and Dr Mattias Hof for their valuable guidance and helpful discussions. I would like to acknowledge all specialists from BP/Castrol and BASF, who attended the project meetings and provided many helpful comments and suggestions. Gratitude also goes to BP's Investigation Analysis Team for support in used oil samples analysis and Oxidation Team. I am indebted to BP/Castrol and BASF for the financial support given for this project.

Thanks also goes to Gareth and Peter, great colleagues, who were so supportive all these years and always made my day. I would like to thank Tom for mentoring me during my first year and for all his support. I would also like to acknowledge all staff and colleagues in Green Chemistry, who always were very friendly, keen to give advice and help in solving everyday problems, especially Paul Elliot and Owain Samuel.

I would like to thank everyone in mechanical and glass workshops for their help when designing my bench-top reactor; Trevor Dransfield and Karl Heaton for taking a vast number of accurate GC-MS analysis; Dr Jacqui Hamilton and Dr Muftafa Ozel for GC x GC NCD analysis and David Williamson for NMR analysis.

Finally I wish to express my love and gratitude to my beloved family, especially to my husband Krzysztof and my mum for endless encouragement, and my mother in law for nursing my little daughter Suzi while finishing my thesis. Without her this work would possibly never have been completed.

Author's declaration

The High Resolution Mass Spectrometry with Field Ionisation and Electron Impact were performed by K. Heaton and T. Dransfield. The High Resolution Proton Nuclear Magnetic Resonance analysis was performed by D. Williamson. Two-dimensional Chromatography with Nitrogen Chemiluminescence Detector was performed by M. Ozel. The Two-dimensional Chromatography with Flame Ionization Detector was performed by T. Lynch BP/Castrol.

The model compound of hydroxy cinnamate was synthesised and analysed by proton NMR by G. Moody at University of York (Figure 4.14 in Chapter 4). The used oil sample, taken from an engine, was analysed using FTIR by S. Holliday BP/Castrol (Figure 2.6 in Chapter 2).

Chapter 3 is a part of the wider collaboration on the topic of the autoxidation of branched alkanes in liquid phase undertaken by M. Stark, J. Wilkinson, J. Lindsay Smith, A. Alfadhil and B. Pochopien. The pristane analysis was performed by J. Wilkinson. The analysis of ketones from the autoxidation of squalane was performed by A. Alfadhil using Mass Spectrometry with Chemical Ionisation and Electron Impact.

Chapter 1: Introduction

1.1 Introduction to the Project

In today's world the development of new automotive engine technologies is driven by emission legislation and demands for better fuel economy.¹ The key challenges are to reduce emissions of internal combustion engines, which affect climate change and have a negative effect on human health, and also to improve energy efficiency.¹⁻³ This has resulted in the introduction of new engine designs, such as smaller engines, increasing engine power or adding new after-treatment systems to reduce emissions.²⁻³

Unfortunately, some of these changes put further challenges on engine lubrication. For instance, increasing the power density of an engine gives a higher combustion temperature, which results in an increase of the formation of nitrogen oxides (NO_x),⁴⁻⁶ these have an adverse effect on lubricants by increasing sludge formation.⁷⁻⁹ Consequently the thickening of lubricant causes engine wear and reduces efficiency, and so increases emission of the greenhouse gases, such as CO₂ to the atmosphere.

Nitrogen oxides (NO_x), mainly NO and NO₂, are formed during combustion and can enter into the lubricant.^{4,7-10} Nitric oxide (NO) forms during fuel combustion and its formation is significantly rising with increasing combustion temperatures.^{4,6,11} Subsequently, nitric oxide is converted to nitrogen dioxide (NO₂) at lower temperatures¹⁰ as the exhaust gases cool.

The first high temperature region, where engine lubricant has a contact with NO_x is the piston assembly and NO₂ is favoured over NO,¹²⁻¹⁴ is described in detail, in section 1.3.

Engine lubricants comprise of a complex mixture of components¹⁵⁻¹⁸ and antioxidants play an important role in improving engine lubricants resistance to oxidation; unfortunately, the effect of nitrogen oxides on lubricant antioxidants at high temperature piston ring pack conditions have not been studied in detail.

This project aims to improve the understanding of lubricant reactions with nitrogen oxides by identifying the products arising from the interactions of components of lubricants, such as phenolic and aminic antioxidants, with NO_x and to propose the chemical mechanisms by which they react. This understanding will be useful in developing future lubricants, which could therefore be more resistant to nitration and that consequently will extend the lubricant lifetime under the extreme conditions in which the lubricants operate.

1.2 Lubricant composition

Lubrication plays a crucial role in the automotive industry and engine piston assembly is one of the most extreme environments which need to be lubricated. The major functions required from the engine oil are to: lubricate moving surfaces; minimise engine friction and wear hence providing maximum efficiency; removing harmful impurities out of the working parts to prevent deposits formation; cooling engine parts which are exposed to the high temperatures and minimising gas and oil leakages.¹⁵

The typical engine lubricant consists of a so-called base fluid (75 to 95 wt. %) and additives (25 to 5 wt. %), which are balanced to provide maximum lifetime and efficiency.¹⁷

The major part of all engine lubricants is the base fluid, which is typically composed of different base stock to obtain the required physical and chemical properties. The chemical composition of the base stocks depends on the crude oil type and the process by which they were obtained. The American Petroleum Institute (API) classification divides different base stocks into groups, depending on their properties such as: the viscosity index, saturates level and sulphur content, Table 1.1.¹⁹ These properties have a great effect on engine lubricant performance: the viscosity index describes how lubricant viscosity changes with temperature, the saturates level indicates how resistance to oxidation and the sulphur content shows its inherent antioxidant's behaviour.²⁰

Table 1.1: API Base Oils Classification.

API Group	Viscosity Index	Saturates	Sulphur	Other
I	80-120	<90%	and/or $\geq 0.03\%$	-
II	80-120	$\geq 90\%$	and <0.03%	-
III	>120	$\geq 90\%$	and <0.03%	-
IV				PAO (Poly Alpha Olefins)
V				Everything (Else)

Groups I, II and III are called mineral base oils (non-synthetics). They consist of a variety of hydrocarbons, such as: paraffinics (linear and branched chain alkanes),

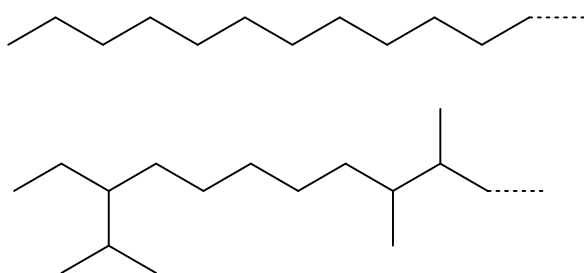


Figure 1.1: Schematic example of linear (top) and branched (bottom) paraffins.

naphthenes (cycloalkanes, five- and six-membered rings) and aromatics (six-membered benzene rings).²¹

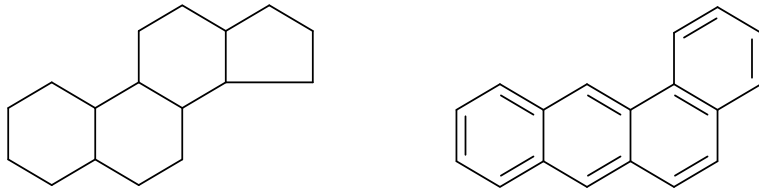


Figure 1.2: Example of naphthene (left) and aromatic (right) molecules.

Each of the API lubricant groups have a characteristic hydrocarbon composition, which influences their oxidation properties: group I is high in naphthene, group II is high in paraffins and group III is highly refined with 95% of paraffins.²² Groups IV and V are synthetic base oils such as PAO (Poly Alpha Olefins).

Lubricant additives are added to the base oil to improve its properties.²¹⁻²⁴ These are typically:

- Detergents
- Dispersants
- Antioxidants
- Antiwear Agents
- Viscosity Modifiers
- Pour Point Depressants
- Friction Modifiers
- Antifoams
- Rust and Corrosion Inhibitors.

These play a variety of different functions²⁴ : dispersants prevent deposits and sludge formation by suspending the insoluble particles in the oil. Viscosity modifiers are

typically large polymeric molecules, which expand as the temperature increases and control the temperature dependence of the oil viscosity. Foam inhibitors prevent foam formation by changing the surface tension. Rust and corrosion inhibitors absorb on the surface to form barrier film against water and aggressive species. Antioxidants are added to lubricants to improve their resistance to oxidation and their effect on NO_x is discussed in more detail in Chapters 4, 5, 6 and 7.

1.3 Lubrication in Piston Assembly

The piston ring pack is one of the main regions where engine lubricants have to work. It is also the most aggressive environment, where lubricants come into contact with harsh combustion products called blow-by gases (including NO_x see Figure 1.3).

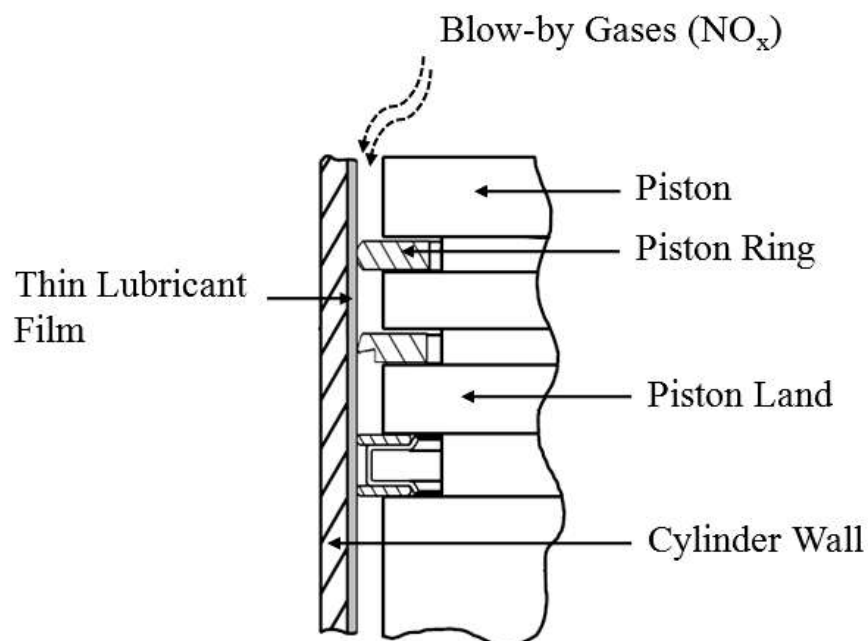


Figure 1.3: Schematic diagram of the piston ring pack^{25,26} with the thin layer of lubricant exposed to blow-by gases.

In the piston environment, a small volume of oil is exposed to high temperatures, which has been reported to have a significant effect on engine lubricant degradation.²⁵⁻²⁷

Previously measured temperatures characteristic for piston ring pack conditions in gasoline engines were 130-180 °C,^{28,29} and for diesel 220-230 °C.^{30,31}

Blow-by gases are a mixture of unburned fuel and oxygen and gaseous combustion products (such as NO_x, CO, CO₂, H₂O, HC, and radicals),¹⁵ which leak past the piston rings into the crankcase. They mix with engine oil during the continuous flow between the piston and sump regions,²⁵ causing lubricant degradation.

Previous studies of interaction of blow-by gases with lubricants suggested formation of highly nitrated products, which were also thought to be precursors for lubricant sludge.³²

1.4 Formation of NO_x in Automotive Engines

Nitrogen oxides (NO_x) are formed during combustion in automotive engines and consist mainly of nitric oxide (NO) and nitrogen dioxide (NO₂), with a negligible amount of nitrous oxide (N₂O) formed.¹¹

The mechanisms which lead to the formation of NO_x in the combustion system are shown below. Primarily, the “thermal” mechanism, also called the Zeldovich mechanism, which includes reactions of atmospheric nitrogen with oxygen, forms from the dissociation of O₂ and N₂ molecules at the high temperature in the flame front,^{4,6,11,33,34} reactions [1.1]-[1.3].³⁵

Table 1.2: Formation of nitrogen monoxide by the Zeldovich mechanism.^{4,6,11,33,34,41}

Reaction	No.
$O_2 \rightleftharpoons 2O$	[1.1]
$O + N_2 \rightleftharpoons NO + N$	[1.2]
$N + O_2 \rightleftharpoons NO + O$	[1.3]

This mechanism is exceedingly dependent on temperature. During combustion, when the temperature rises above 1700 °C, the concentration of NO is comparatively high and because of this depends strongly on the temperature; for instance it almost doubles every 100 °C.^{4,5} However below 1500 °C nitric oxide formation is minor.⁵

The second mechanism of NO formation is the “prompt” type, also called Fenimore,^{36,37} which includes the reaction of hydrocarbon radicals with molecular nitrogen and proceeds rapidly in the combustion flame zone,⁴ reactions [1.4].

Table 1.3: Formation of nitrogen monoxide by the Fenimore mechanism.^{36-38,41}

Reaction	No.
$CH + N_2 \rightleftharpoons HCN + N$	[1.4]
$HCN + O \rightleftharpoons NO + CH$	[1.5]

There can also be the direct reaction of nitrogen containing fuels with molecular oxygen (reactions 1.5).³⁸ However, the contribution of fuel in NO_x formation is negligible, when no or a small amount nitrogen compounds is present in the fuel,^{4,11,33}

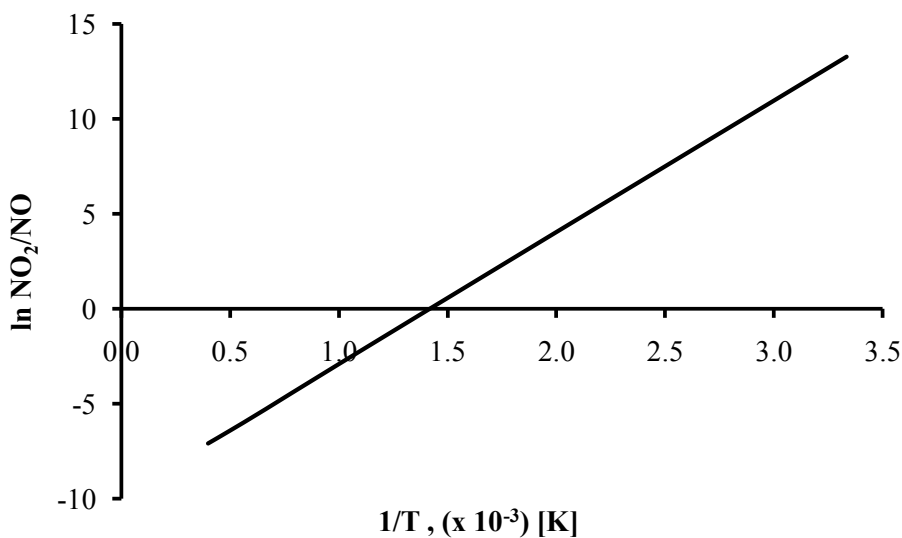
The concentration of NO generated through the Zeldovich mechanism can accounted for 88 % of total NO_x formed during combustion, compared to 7 % formed by the Fenimore mechanism or 1.5 % from N₂O respectively.³⁹

NO formed in the flame zones can be rapidly converted to NO₂ by reaction [1.6] or at lower temperatures is converted to NO₂ by reactions [1.7] or [1.8]:

Table 1.4: Formation of nitrogen dioxide, reactions [1.6], [1.7] and [1.8].^{40,41}

Reaction	No.
$\text{NO} + \text{HO}_2 \rightleftharpoons \text{NO}_2 + \text{OH}$	[1.6]
$\text{NO} + \text{O}_2 \rightleftharpoons \text{NO}_2 + \text{O}$	[1.7]
$2\text{NO} + \text{O}_2 \rightleftharpoons 2\text{NO}_2$	[1.8]

The $\text{NO} \rightleftharpoons \text{NO}_2$ chemical equilibrium indicates that at combustion temperature the NO_2/NO ratios should be negligible. The dependences of $\ln \text{NO}_2/\text{NO}$ at various temperatures are shown in Figure 1.4.⁴²

**Figure 1.4: The dependences of $\ln \text{NO}_2/\text{NO}$ at various temperatures.⁴²**

However the data obtained from the sampling gas collected from the piston region of diesel engine shows NO_2/NO ratios of up to 25 to 50 %.¹⁰ Examples of NO_x (NO , NO_2) concentrations taken during sampling from the cylinder are shown in Table 1.5.

Table 1.5: Examples of NO_x (NO, NO₂) concentrations in engine cylinder.^{35,43-47}

Concentration of NO _x (NO, NO ₂) [ppm]	Engine type	Ref.
[NO _x] 0 - 1550 [NO] 0 - 1100 [NO ₂] 0 - 700	gasoline	43
[NO _x] 1000 - 2000	diesel	44
[NO _x] 0 - 2000	gasoline	45
[NO _x] 200 - 800	diesel	46
[NO] 400 - 2000	gasoline	47
[NO] 500 - 1250	gasoline	35
[NO] 0 - 2500	diesel	15

These results show a maximum NO_x level of 2500 ppm that was measured during sampling in engine cylinders and was dependent on engine type, conditions and type of the fuel. Previous bench tests have been using approximately 1000 ppm of NO₂ concentration in lubricant degradation studies,^{48,49} which is a representative value of that found in real engines.

1.5 Chemistry and Reactions with NO_x (NO, NO₂)

Oxides of nitrogen play an important role in many scientific areas, such as: atmospheric,⁵⁰⁻⁵² medicinal,⁵³⁻⁵⁵ combustional,^{35,43,47} and organic synthesis.⁵⁶⁻⁵⁸

Their chemistry is complex and therefore depending on the environment different oxides play a significant role, Table 1.6.

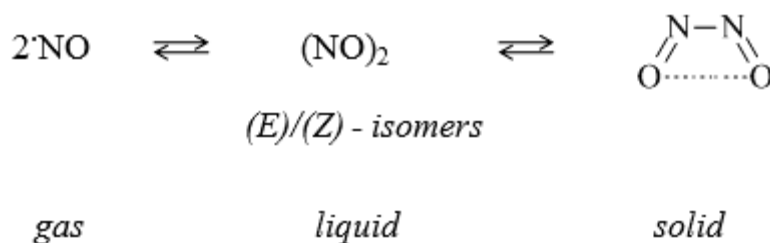
Table 1.6: Oxides of nitrogen: formulas, colours and reactivity.⁵⁹

Formula	Name	Colour	Remarks
N ₂ O	Nitrous oxide	colourless	Rather unreactive
NO	Nitric oxide	colourless	Moderately reactive
NO ₂	Nitrogen dioxide	brown	Rather reactive
N ₂ O ₄	Dinitrogen tetroxide	colourless	Extensively dissociated to NO ₂ as gas and partially as a liquid

This work mainly concentrates on NO and NO₂ as these are important oxides when studying engine piston conditions. N₂O is excluded from the research as it is rather unreactive and its concentration at piston assembly is negligible, Table 1.3.⁵⁹ The other important oxide of nitrogen is N₂O₄, however it is significant only at sump temperatures,^{52,60} where it can be formed from the dimerisation of NO₂. Therefore the chemistry and characteristic reactions for NO and NO₂ are listed below.

Nitrogen Monoxide (NO)

Nitrogen Monoxide, commonly known as nitric oxide, is a paramagnetic gas under standard conditions.^{61,62} Its paramagnetism is decreasing going from the gas phase, through the liquid and to the crystalline,⁶³ Figure 1.5.

**Figure 1.5. State dependency of nitrogen monoxide.**⁶³⁻⁶⁵

NO solubility in oxygen-free water is minor ($1.9 \times 10^{-3} \text{ mol dm}^{-3} \text{ bar}^{-1}$ at 25 °C) and it is independent from pH, because of its low dipole moment of $0.53 \times 10^{-30} \text{ C m}$.⁶⁶ Nitrogen

monoxide is more soluble in organic solvents,⁶⁷ examples of which are summarised in Table 1.7.

Table 1.7: Solubility of NO in organic solvents.⁶⁷

Solvent	Solubility [mol dm ⁻³ bar ⁻¹]
Ethanol	1.1 x 10 ⁻²
C ₆ H ₆	1.3 x 10 ⁻²
CCl ₄	1.4 x 10 ⁻²
CH ₃ CN	1.4 x 10 ⁻²
Ethyl Acetate	1.6 x 10 ⁻²
Cyclohexane	1.9 x 10 ⁻²
Diethyl Ether	2.3 x 10 ⁻²

NO condenses to liquid at -151.8 °C and it almost completely composed of (NO)₂.^{63,68}

The NO in the gas phase gives the characteristic infrared absorption at approximately 1890 cm⁻¹ due to the vibrational stretch mode of (N=O) band.^{69,70}

The NO mesomeric formulas of bonding are illustrated in Figure 16.^{61,62,71}

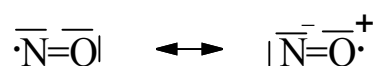


Figure 1.6: Mesomeric formulas for valence bond description of bonding in NO.^{37,61,62,71}

The NO may combine with a second radical to form a diamagnetic product and this property is characteristic for persistent radicals. The example of reaction of a carbon-centred radical and nitric oxide radical is shown below; reaction [1.8] is favoured, [1.9] is disfavoured.⁷²

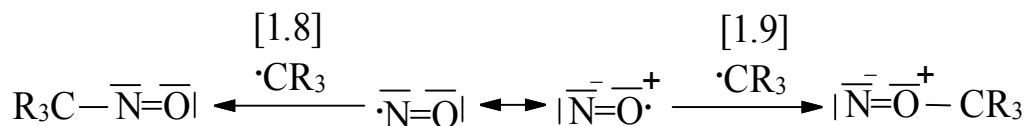


Figure 1.7: Example of the reaction of a carbon radical with nitric oxide.⁷²

The elementary reactions by which NO is known to react with organic compounds are summarised below, [1.10] to [1.16].⁶³

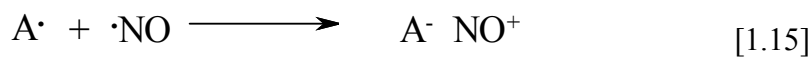
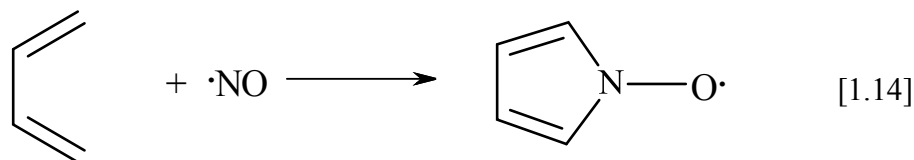
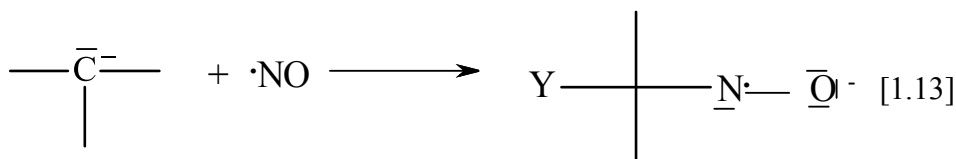
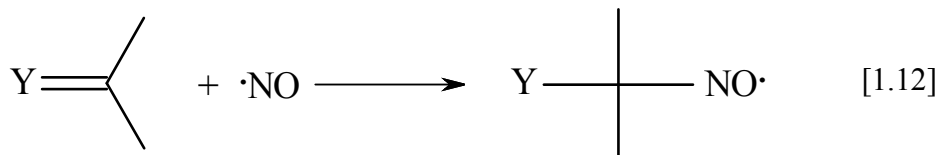
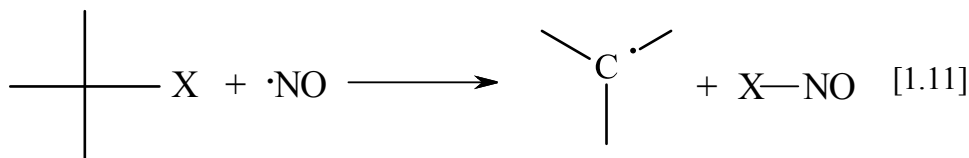
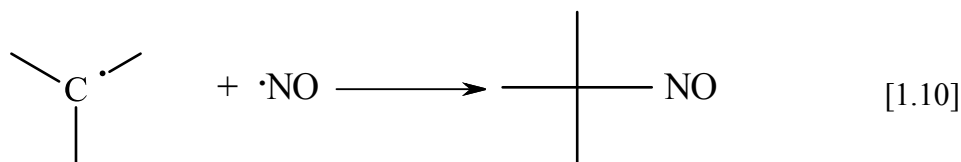


Figure 1.8: Examples of different elementary reactions with nitrogen monoxide (NO), including: combination [1.10]; homolytic substitution [1.11]; addition [1.12], [1.13]; pericyclic reactions [1.14] and electron transfer [1.15], [1.16]. Where: X = H; Y = (R₂N)CH; A[·] = oxidant; and B[·] = reductant.^{37,63}

The mechanisms for the reaction of NO with alkoxy radicals is shown below, reactions [1.17]-[1.20].^{73,74}

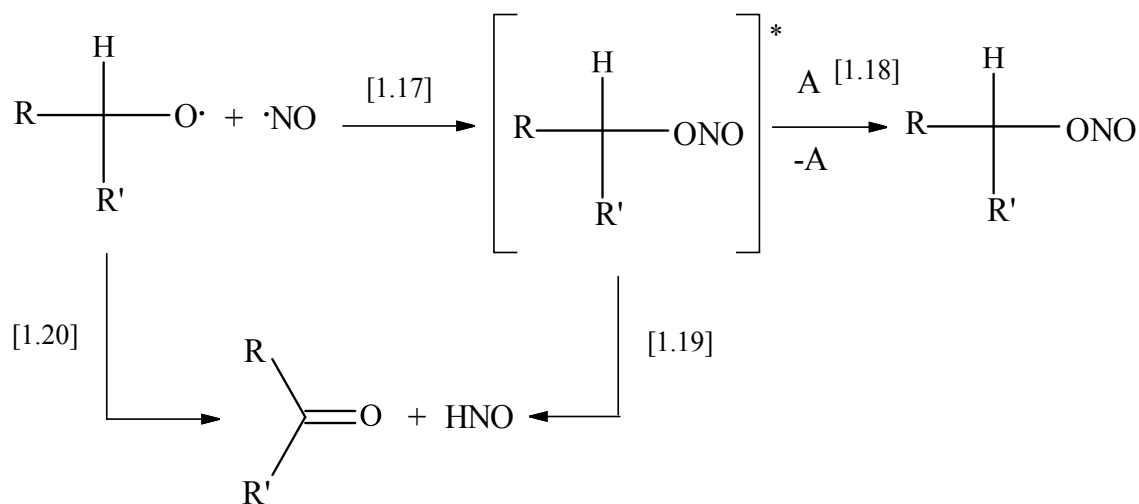


Figure 1.9: Example of the reaction mechanism of nitrogen monoxide with alkoxy radicals.

The other reaction of peroxy radical with nitric oxide radical to form peroxy nitrites is shown in reaction [1.21]-[1.23].^{75,76}

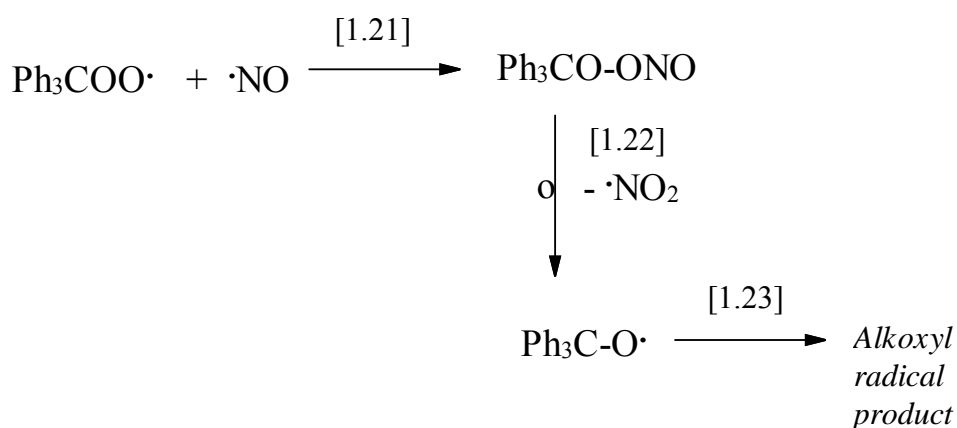


Figure 1.10: Example of the reaction of nitrogen monoxide with peroxy radicals.

The reaction of substituted phenol with nitric oxide radical is shown in [1.24].^{77,78}

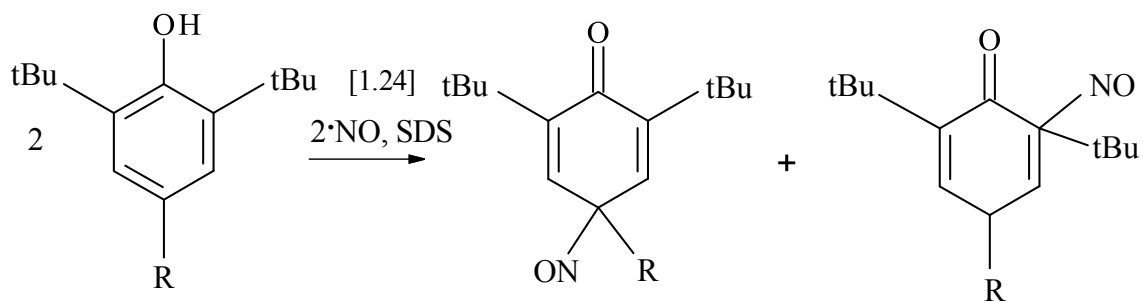


Figure 1.11: Example of the reaction of substituted phenol with nitrogen monoxide, (SDS – Sodium Dodecyl Sulphate).⁷⁷

As a result of reaction [1.24] (*p*- and *o*-) nitroso-substituted cyclohexadienones were identified.

Nitrogen Dioxide (NO₂)

NO₂ have found a wide range of applications in many industries as a powerful reagent in oxidation and nitration.⁵⁸ Similarly to nitrogen monoxide, NO₂ reacts in many different ways, such as: recombination with other radicals,⁷⁹⁻⁸¹ hydrogen abstraction,⁸²⁻⁸⁶ addition,⁸⁷⁻⁸⁹ and electron-transfer.⁹⁰⁻⁹²

NO₂ is a very reactive paramagnetic molecule with unpaired electron, which can be delocalised throughout the molecule, as shown in Figure 1.12.⁹³

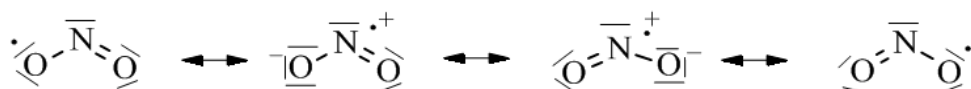


Figure 1.12: Mezomeric formulas of nitrogen dioxide.⁹³

High temperature nitration studies show that the distribution of the unpaired electron of nitrogen dioxide radical can go through the nitrogen or oxygen atom; an example of reactions [1.25, 1.26] with an alkyl radical is shown below.⁹³



Figure 1.13: Example of the reaction of alkyl radical with nitrogen dioxide.⁹³

Substituted phenols react with NO₂ by hydrogen abstraction with the formation of phenoxyl radical, which is stabilised by resonance, as shown in Figure 1.14.

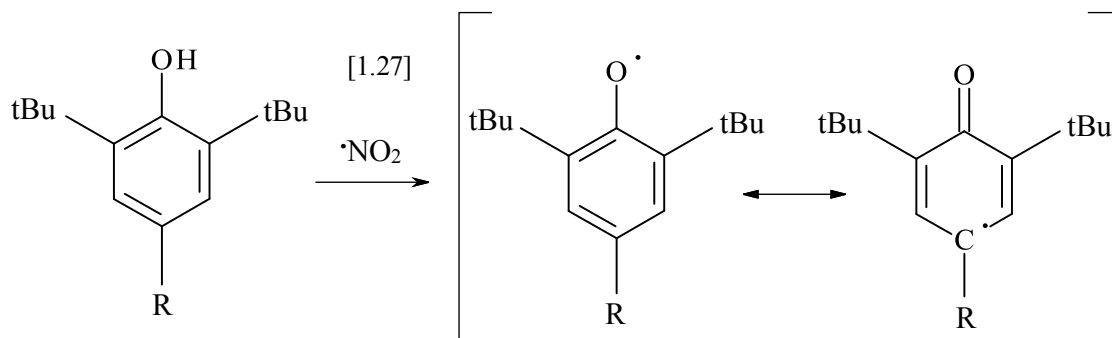


Figure 1.14: Hydrogen abstraction from phenolics by nitrogen dioxide.⁹⁴

The addition of nitrogen dioxide through the oxygen or nitrogen atom was reported also in the reaction with phenoxyl radical, (Figure 1.15).⁹⁴

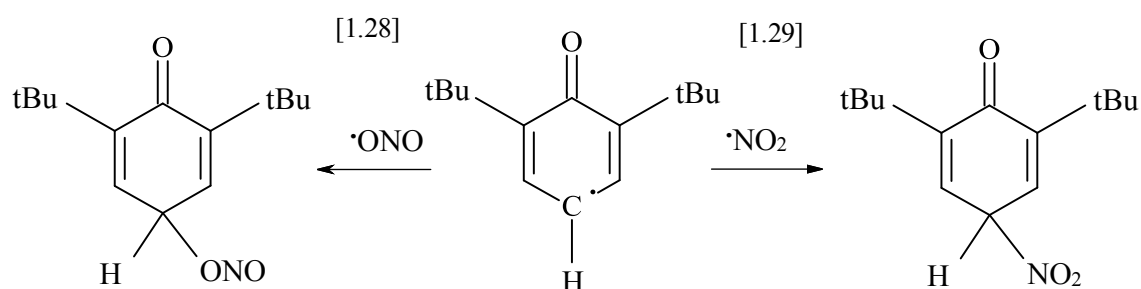


Figure 1.15: Reaction of phenoxyl radical with nitrogen dioxide.⁹⁴

There have also been products other than nitrated observed, in the reaction of phenoxyl radical with NO₂, such as dimers or nitroso compounds, of which the formation was dependent on solvent type.⁹⁴

The reaction of *p*-benzoquinone with nitrogen dioxide results in addition of NO₂ to double bonds of quinone, which then is thermally converted to acyl(alkyl) nitroxyl and iminoxyl radicals, (Figure 1.16).⁹⁴

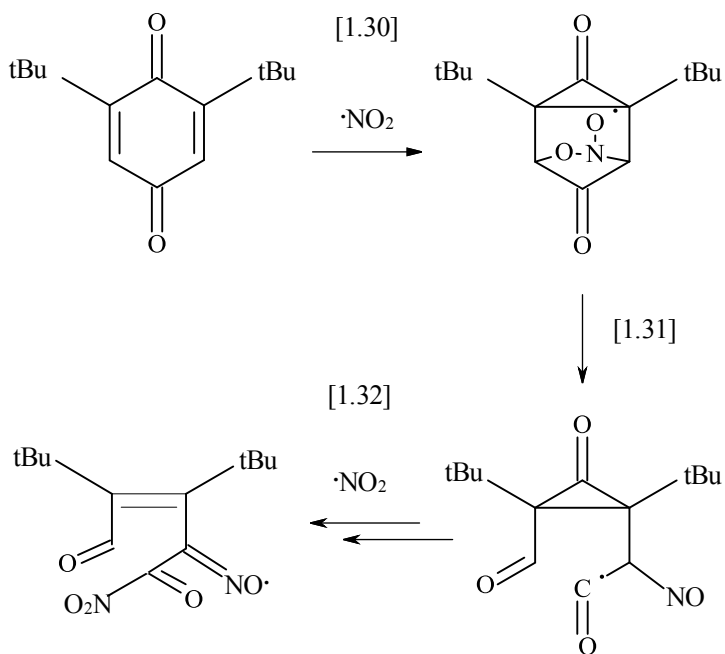


Figure 1.16: Reaction of quinone with nitrogen dioxide.⁹⁴

The reaction of indole with NO₂ effects in 2-(indol-3-yl)-3H-indol-3-one and 2-(indol-3-yl)-3H-indol-3-oxime; however, products concentration might change depending on the conditions, reactions [1.33] or [1.34].⁹⁵

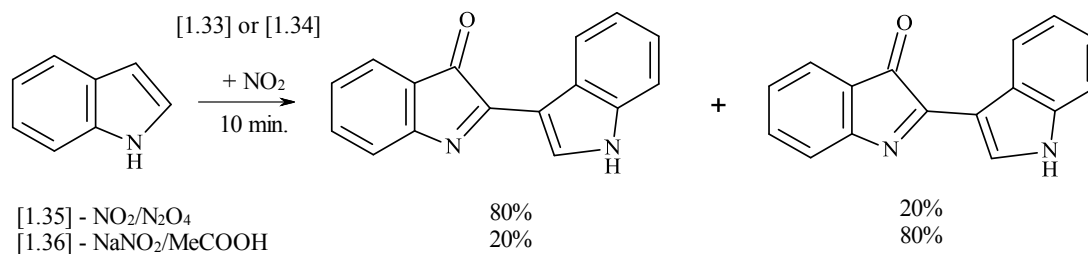


Figure 1.17: Reaction of indole with nitrogen dioxide.⁹⁵

The reaction of diazotisation of arylamines under non-aqueous conditions (in acetonitrile) at -20 °C, gives the final product triazene, Figure 1.18.⁹⁶

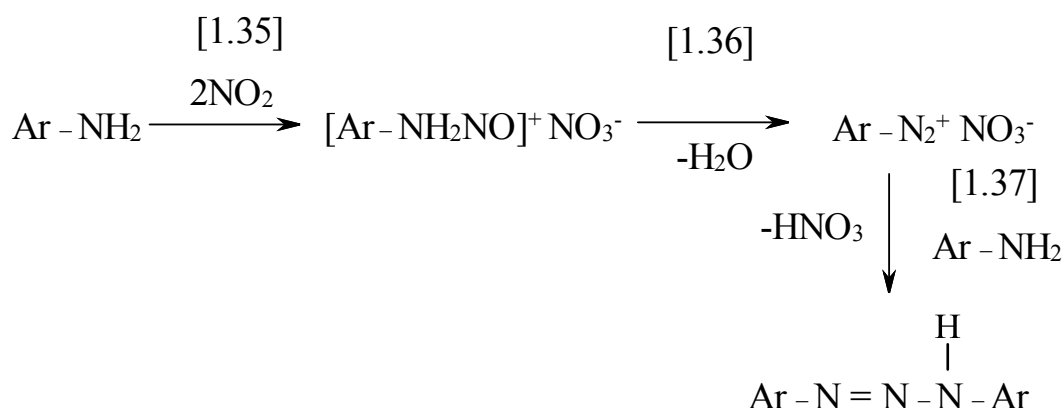


Figure 1.18: Reaction of arylamines with nitrogen dioxide.⁹⁶

There is also the possibility of the conversion of nitroso compounds into nitro compounds when using NO₂, Figure 1.19.^{97,98}

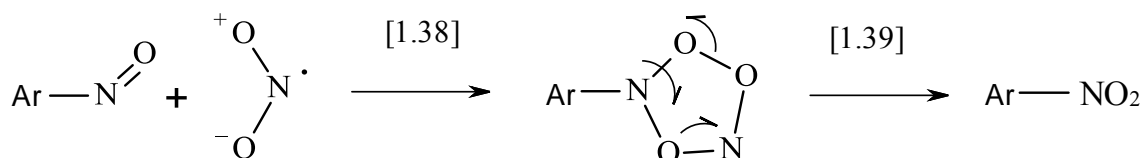


Figure 1.19: Conversion of nitroso compounds using nitrogen dioxide.^{97,98}

1.6 Hydrocarbon Autoxidation in the Liquid Phase

During engine operations the lubricant is exposed to high temperatures, oxygen and aggressive combustion by-products, which lead to lubricant degradation. The main component of lubricant is the base oil, which is a mixture of different size linear, branch and cyclic saturated hydrocarbons, therefore the standard oxidation studies were based on the degradation of hydrocarbons. Previously reported standard oxidation mechanism of n-alkanes is shown in reactions [1.40]-[1.48].²¹

Table 1.8: Standard mechanism of oxidation of hydrocarbon.

	Reaction	No.
Initiation	$\text{RH} + \text{O}_2 \rightarrow \text{R}^\cdot + \text{HOO}^\cdot$	[1.40]
Propagation	$\text{R}^\cdot + \text{O}_2 \rightarrow \text{ROO}^\cdot$	[1.41]
	$\text{ROO}^\cdot + \text{RH} \rightarrow \text{ROOH} + \text{R}^\cdot$	[1.42]
Branching	$\text{ROOH} \rightarrow \text{RO}^\cdot + \text{OH}^\cdot$	[1.43]
	$\text{RO}^\cdot + \text{RH} \rightarrow \text{ROH} + \text{R}^\cdot$	[1.44]
	$\text{HO}^\cdot + \text{RH} \rightarrow \text{H}_2\text{O} + \text{R}^\cdot$	[1.45]
Termination	$\text{R}^\cdot + \text{R}'^\cdot \rightarrow \text{RR}'$	[1.46]
	$\text{R}'\text{CH}_2\text{OO}^\cdot + \text{ROO}^\cdot \rightarrow \text{R}'\text{CHO} + \text{ROH} + \text{O}_2$	[1.47]
	$\text{ROO}^\cdot + \text{R}'\text{O}^\cdot \rightarrow \text{Products}$	[1.48]

This free-radical mechanism consists of four stages: initiation, propagation, chain branching and termination. In the initiation phase the alkyl and hydroperoxy radicals are formed, reaction [1.40]. The oxygen will attack preferentially the weakest C–H bond, therefore for the n-alkanes hydrogen will be abstracted from the secondary carbons.²¹ In general for hydrocarbons the order in hydrogen abstraction will increase as below:



The next step is propagation these reactions are the main source of the alkyl chain carriers and alkylperoxy radicals, reaction [1.41] and [1.42]. The chain branching includes the formation of primary, secondary and tertiary alkoxy radicals, reactions [1.43] to [1.45]. Finally the termination stops the chain reaction and non-radical products are formed by combination of radical species, reactions [1.46] to [1.48].

Previously reported primarily lubricant degradation products were aldehydes, ketones, alcohols and acids, which can undergo polymerisation to form high molecular mass

products visible in engines in the form of sludge or varnishes, which decrease engine performance and could cause breakdown ultimately.⁹⁹

The majority of previous oxidation studies were based on the degradation of smaller *n*-alkanes, which are not representative for real base oils,¹⁰⁰⁻¹⁰² because they are too volatile to study at the high temperatures of engine piston assembly and were lacking in tertiary carbon atoms, which have a significant concentration in real base oils. Therefore Chapter 3 therefore shows the detailed autoxidation studies of branched chain hydrocarbons based on squalane autoxidation, which is more representative as a model lubricant base oil.¹⁰³

1.7 Hydrocarbon Nitration in the Liquid Phase

As the main research of this thesis is the degradation of lubricant due to NO_x, engine lubricant reactions with NO₂ have also been reviewed. The NO₂ effect on model lubricant degradation has been studied previously by Johnson *et al.*⁴⁸ The experiments were undertaken in bench-top reactor at the temperature of 160 °C and *n*-hexadecane was used as a model lubricant. Previous understanding of the free radical chain mechanism of nitration of *n*-alkane was proposed as follows [1.49]-[1.56] to be:

Table 1.9: The mechanism of NO₂ reaction with n-hexadecane proposed by Johnson.⁴⁸

Reaction		No.
RH + NO ₂	→ R· + HONO	[1.49]
HONO	→ NO + HO·	[1.50]
R· + NO ₂	→ RONO	[1.51]
R· + NO ₂	→ RNO ₂	[1.52]
RO ₂ · + NO	→ RO· + NO ₂	[1.53]
RO ₂ · + NO	→ RONO ₂	[1.54]
RO· + NO ₂	→ RONO ₂	[1.55]
RO ₂ · + NO ₂	→ ROONO ₂	[1.56]

NO₂ acts as a free radical, added into the reaction abstracts hydrogen atoms from hydrocarbons with formation of alkyl radical and nitrous acid [1.49]. The nitrous acid decomposes to hydroxyl radical and nitric oxide [1.50]. Nitrogen dioxide and nitric oxide react with alkyl, alkylperoxyl and alkoxy radicals to form nitro [1.52], nitroso compounds, nitrites [1.51], nitrates [1.54], [1.55] and peroxy nitrates [1.56]. Reaction [1.53] between alkylperoxyl radical and nitric oxide regenerate nitrogen dioxide. Unfortunately, the proposed lubricant degradation mechanism was based on previous knowledge on nitration of hydrocarbons,⁸² and there was no evidence on identification of the products to support this mechanism.

1.8 Hydrocarbon Nitro-Oxidation in the Liquid Phase

NO_x are chemically active gases, which can initiate hydrocarbon liquid-phase oxidation by reacting with hydrocarbons and its intermediates and generating free radicals. The well known reaction mechanism by which NO₂ initiates hydrocarbons oxidations was referred as follows [1.57]-[1.68]:

Table 1.10: Reactions involved in the liquid-phase oxidation of hydrocarbons initiated by NO₂, reactions [1.57]-[1.68].¹⁰⁴⁻¹⁰⁶

Reaction	No.
$\text{RH} + \text{NO}_2 \rightarrow \text{R}\cdot + \text{HONO}$	[1.57]
$\text{HONO} \rightarrow \text{NO} + \text{HO}\cdot$	[1.58]
$\text{HO}\cdot + \text{RH} \rightarrow \text{H}_2\text{O} + \text{R}\cdot$	[1.59]
$\text{R}\cdot + \text{O}_2 \rightarrow \text{RO}_2\cdot$	[1.60]
$\text{R}\cdot + \text{NO}_2 \rightarrow \text{RONO}$	[1.61]
$\text{RO}_2 + \text{NO}_2 \rightarrow \text{ROONO}_2$	[1.62]
$\text{RONO} \rightarrow \text{RO}\cdot + \text{NO}$	[1.63]
$\text{RO}_2\cdot + \text{NO} \rightarrow \text{RO}\cdot + \text{NO}_2$	[1.64]
$\text{ROONO}_2 \rightarrow \text{RO}\cdot + \text{NO}_3$	[1.65]
$\text{RO}\cdot + \text{RH} \rightarrow \text{ROH} + \text{R}\cdot$	[1.66]
$\text{NO}_3 + \text{RH} \rightarrow \text{HNO}_3 + \text{R}\cdot$	[1.67]
$\text{ROOH} + \text{ONOH} \rightarrow \text{RO}\cdot + \text{H}_2\text{O} + \text{NO}_2$	[1.68]

The reaction to double bonds was more rapid and reversible,¹⁰⁷ reactions [1.69],[1.70]:

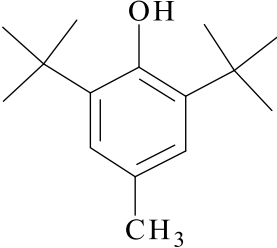
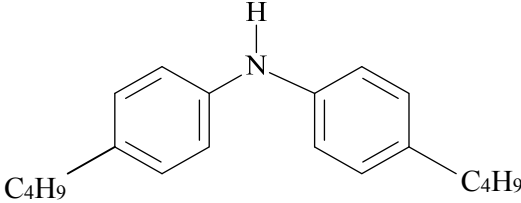
Table 1.11: Reactions of NO₂ with double bonds.¹⁰⁷

Reaction	No.
$\text{NO}_2 + \text{CH}_2=\text{CHR} \rightarrow \text{NO}_2\text{CH}_2\text{C}\cdot\text{HR}$	[1.69]
$\text{O}_2 + \text{NO}_2\text{CH}_2\text{C}\cdot\text{HR} \rightarrow \text{NO}_2\text{CH}_2\text{CH}(\text{O}_2\cdot)\text{R}$	[1.70]

1.9 Inhibition of Lubricant Degradation

The main additives which control lubricant degradation in engines are antioxidants. The most common group of antioxidants are radical scavengers, such as hindered phenols and aromatic amines, with examples shown in Table 1.12.

Table 1.12: Example of common phenolic and aminic antioxidant.

Name	Structure
2,6-di-tert-butyl-4-methylphenol (also known as: 3,5-di-tert-4-butylhydroxytoluene or butylated hydroxy toluene, BHT)	
4-tert-butyl-N-(4-tert-butylphenyl)aniline (Butylated diphenylamine)	

These antioxidants inhibit oxidation by donating the hydrogen atom to peroxy radicals and consequently stopping the chain propagation step, reaction [1.71].

Table 1.13: Inhibition of hydrocarbon oxidation using radical scavengers.^{21,24}

Reaction		No.
Initiation	$\text{RH} + \text{O}_2 \rightarrow \text{R}\cdot + \text{HOO}\cdot$	[1.40]
Propagation	$\text{R}\cdot + \text{O}_2 \rightarrow \text{ROO}\cdot$	[1.41]
Inhibition	$\text{InH} + \text{ROO}\cdot \rightarrow \text{In}\cdot + \text{ROOH}$	[1.71]
	$\text{In}\cdot + \text{ROO}\cdot \rightarrow \text{InOOR}$	[1.72]

Radicals formed from antioxidants (phenoxy and aminyl radicals) are stabilised by the resonance, therefore are very unreactive and so are unable to abstract

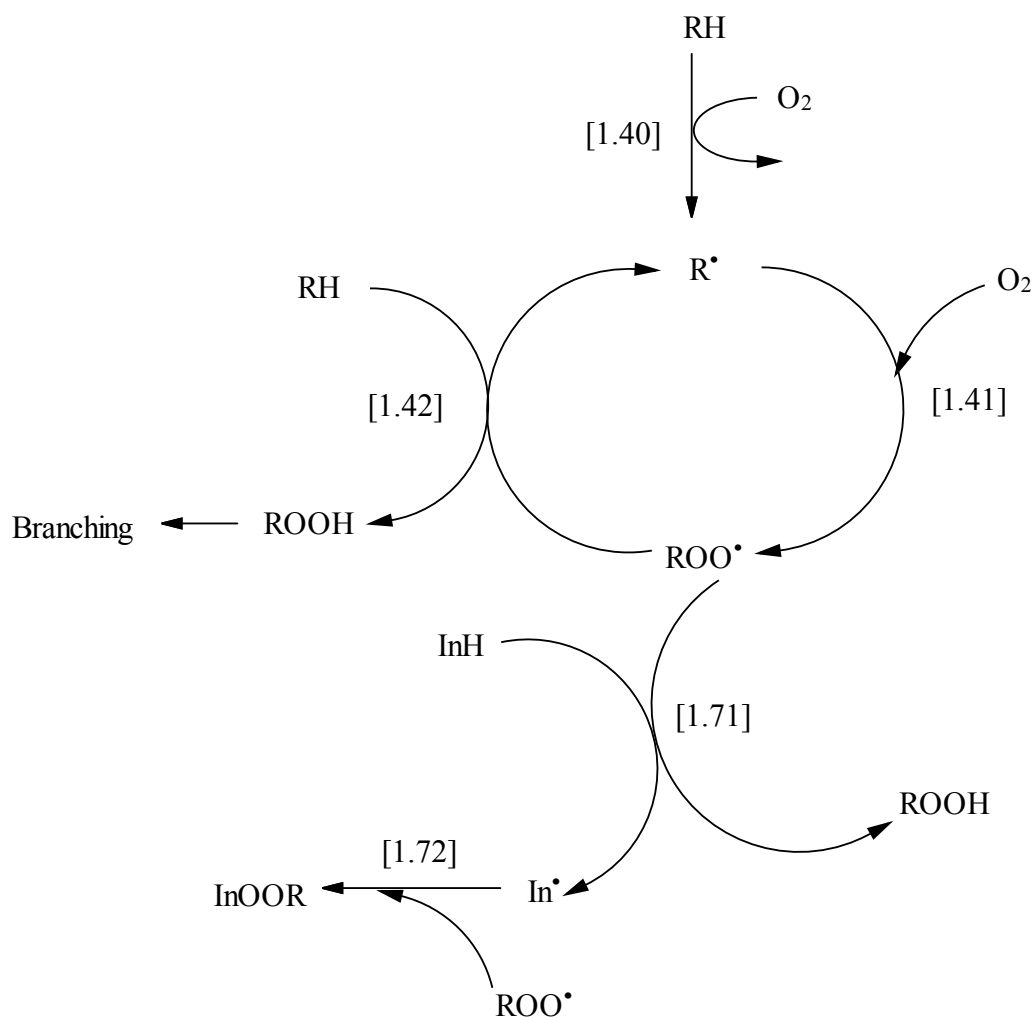


Figure 1.20: Chain cycle mechanism for inhibition of hydrocarbon oxidation by radical scavengers. (R= alkyl group, In=phenoxy radical)

hydrogens from other hydrocarbons and are only capable of reacting with other radical to form stable products, reaction [1.72]. The examples of BHT reactions are shown in Figure 1.21.²⁴

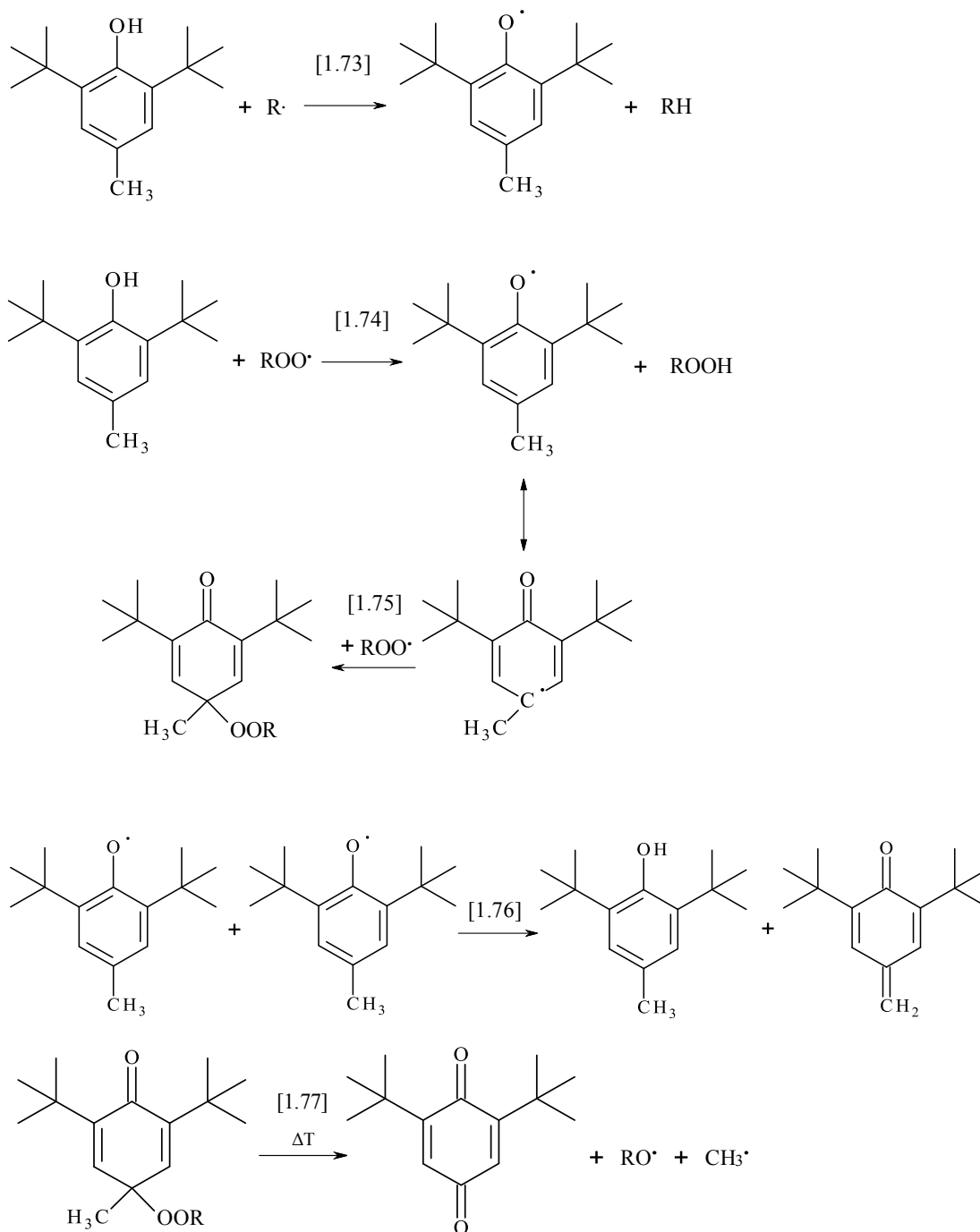


Figure 1.21: Examples of different BHT reactions: with alkyl radical [1.73]; with peroxy radical [1.74],[1.75]; the interaction of two phenoxyl radicals (termination) [1.76] and the decomposition of cyclohexadienone alkyl peroxide at high temperature [1.77].²⁴

Phenolic antioxidants play a crucial role in many industries, including the polymer,¹⁰⁸ food,¹⁰⁹ automotive industries,^{110,111} and also the health sector.¹¹² Therefore one of the phenolic antioxidant inhibition mechanisms of the commercial antioxidant, octadecyl 3-

(3,5-di-tert-butyl-4-hydroxy-phenyl)propanoate, has been proposed by Pospisil *et al.* 2002, in polymer degradation studies, Figure 1.22.¹¹³

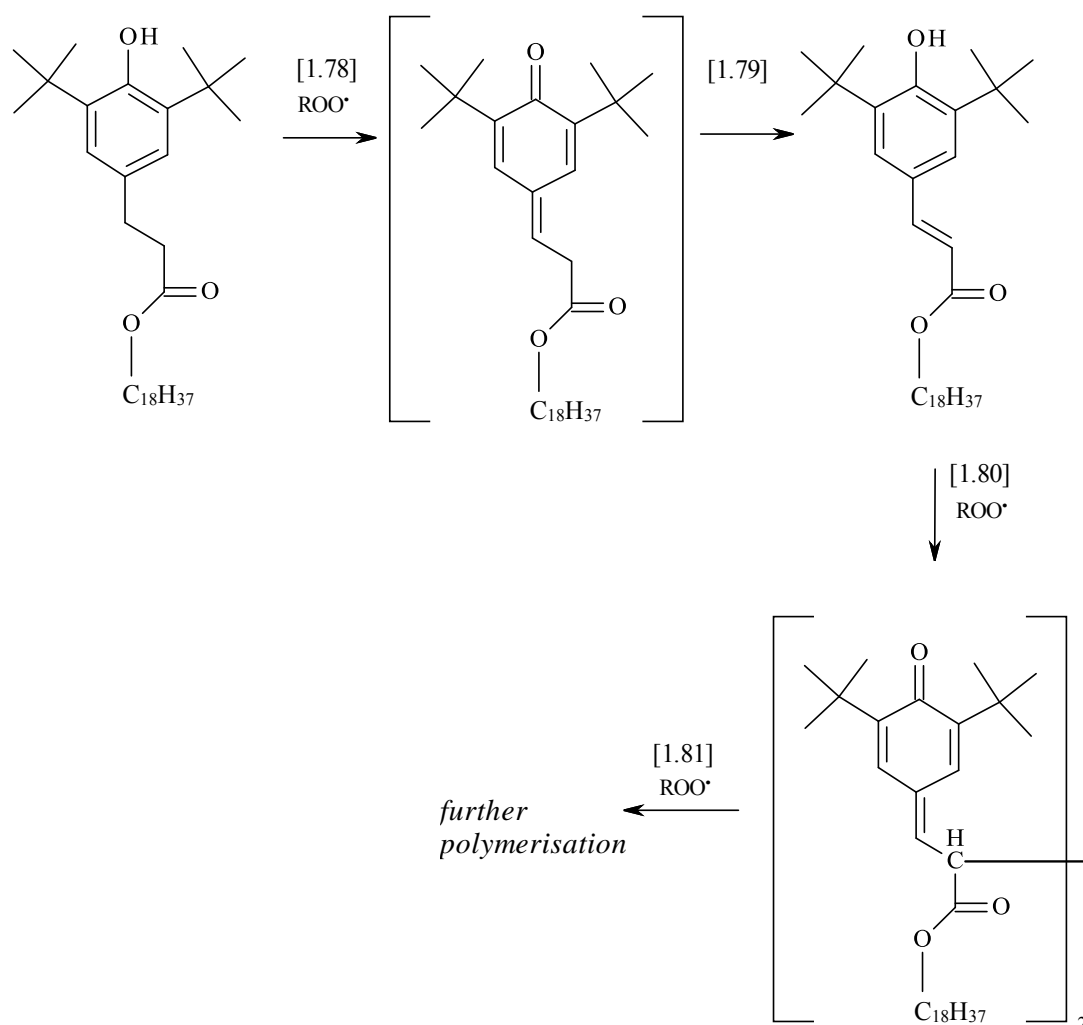


Figure 1.22: The radical mechanism of octadecyl 3-(3,5-di-tert-butyl-4-hydroxy-phenyl)propanoate proposed by Pospisil.¹¹³

The primary products formed from antioxidant were monomeric, however further reaction shows the formation of polymeric products. Interestingly formation of the first product from antioxidant, quinone methide, was suggested, but was not supported by any identification. This reaction mechanism is relevant to this study as octadecyl 3-(3,5-di-tert-butyl-4-hydroxy-phenyl)propanoate is also used as an antioxidant in engine lubricants, as it is sufficiently large to have a high boiling point.

The majority of previous antioxidant studies were based on interaction with radicals, associated with autoxidation, for example: peroxy, alkoxy and alkyl, however reaction with NO_x , have not been explored in as much detail. Previous work, which studied engine lubricant nitration, reported a reaction of 1000 ppm NO_2 with 2, 4, 6-tri-tert-butylphenol in hexadecane solution at 160 °C.⁴⁹ The proposed mechanism of nitration of phenolics, primarily showed the abstraction of phenolic hydrogen by NO_2 and then the addition of nitrogen dioxide this was reported also at low temperatures,⁸³ Figure 1.23. The first addition of NO_2 was to *para*-position and then further addition to *meta*- and *ortho*- positions. Unfortunately product identification in this work was not robust and was based mainly on UV-vis analysis and on other studies at low temperature.¹⁰⁶

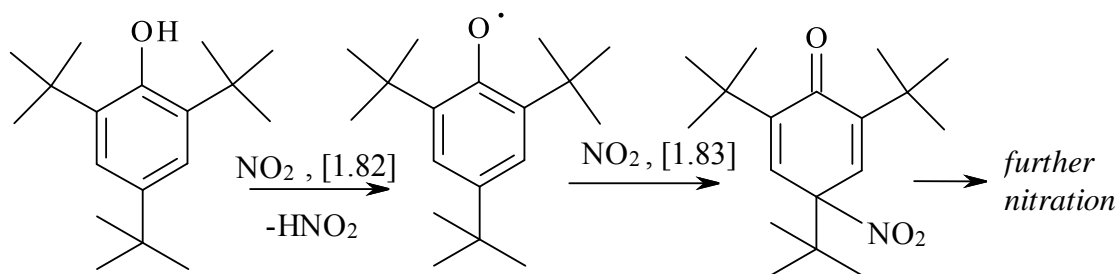


Figure 1.23: Reaction mechanism of NO_2 with 2, 4, 6-tri-tert-butylphenol.¹¹⁴

Other antioxidants, such as aromatic amines, react with radicals in similar way to phenolics, by donating the hydrogen atom to radicals, Figure 1.24.

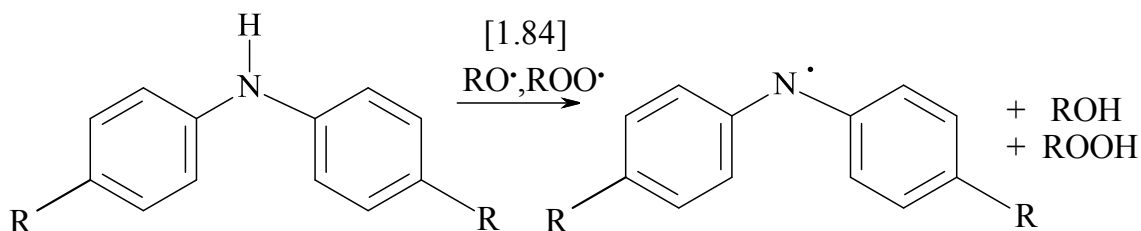


Figure 1.24: Reaction of aminic antioxidant with radicals.²⁴

Previous studies of aminic antioxidant reactions with peroxy radicals at a high temperature (above 120 °C), shown primarily the formation of a nitroxyl radical intermediate, which then might react with a secondary and tertiary alkyl radicals, as the mechanism illustrated below suggested, reactions [1.85]-[1.90].

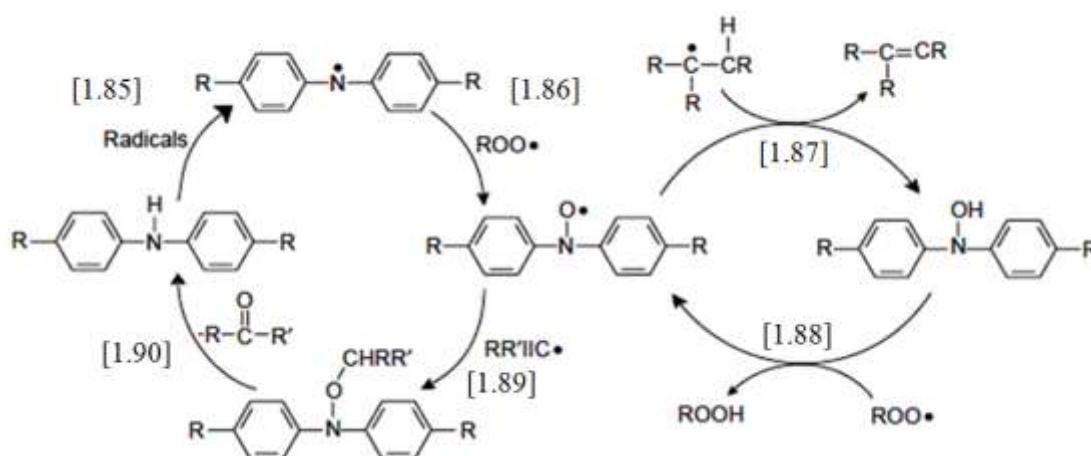


Figure 1.16: Reaction of aminic antioxidant with peroxy radicals at high temperature.²⁴

It was suggested that the alkoxy amine intermediate is thermally unstable and can rearrange to the starting molecule, reaction [1.90].

The reaction of diphenylamine with NO₂ radical, gives the dimer Figure 1.17.¹¹⁴

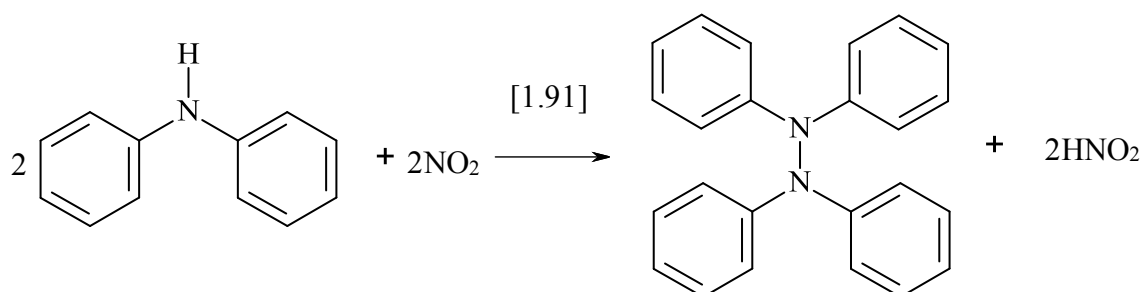


Figure 1.17: Reaction of diphenyl amine with NO₂.¹¹⁴

Primarily the aminic hydrogen is abstracted by nitrogen dioxide and then the termination reaction of two aminyl radicals give a dimer; this reaction was reported to be slow at low temperature.

1.10 Aims of the Project

Engine technology trends have led to an increase of harmful NO_x in the piston assembly of automotive engines.⁴⁻⁶ Nitration of engine oils due to high concentration of NO_x can cause the acidification and thickening of the lubricants and has been implicated in sludge formation.⁷⁻⁹ The aim of this project is to improve the understanding of the reactions of NO_2 with lubricants at the high temperature formed in the piston assembly of automotive engines.

NO_x reacts with hydrocarbons causing engine oil nitration, therefore the importance of this study was to understand the chemical mechanism by which inhibitors react with NO_x , because without antioxidants, oxidation and nitration would quickly decompose the engine oil during use. Therefore the products arising from the interactions of components of lubricant, such as antioxidants with NO_x were identified and the chemical mechanisms by which they react with NO_x were proposed.

The secondary target was also to design and optimise a bench test, where the series of test experiments, such as oxidation, nitration and nitro-oxidation were undertaken. The pre-testing also included the detailed analysis of the model lubricant base oil, squalane.

Chapter 2: Experimental

2.1 Introduction

This chapter describes the details of the apparatus set-up, reaction procedures and analysis techniques used for this project. Additional information includes the details of the synthesis undertaken for standard components.

2.2 Apparatus and Procedures

2.2.1 Apparatus Set-up

Experimental apparatus used in this work included the stainless steel reactor (Figure 2.1), equipped with a system of traps and electronics to monitor the reactions.

An example of this apparatus set-up is shown in Figure 2.2.



Figure 2.1: Stainless steel micro-reactor (49.0 cm³ head space volume).

The stainless steel reactor was made in-house at the Department of Chemistry of the University of York.

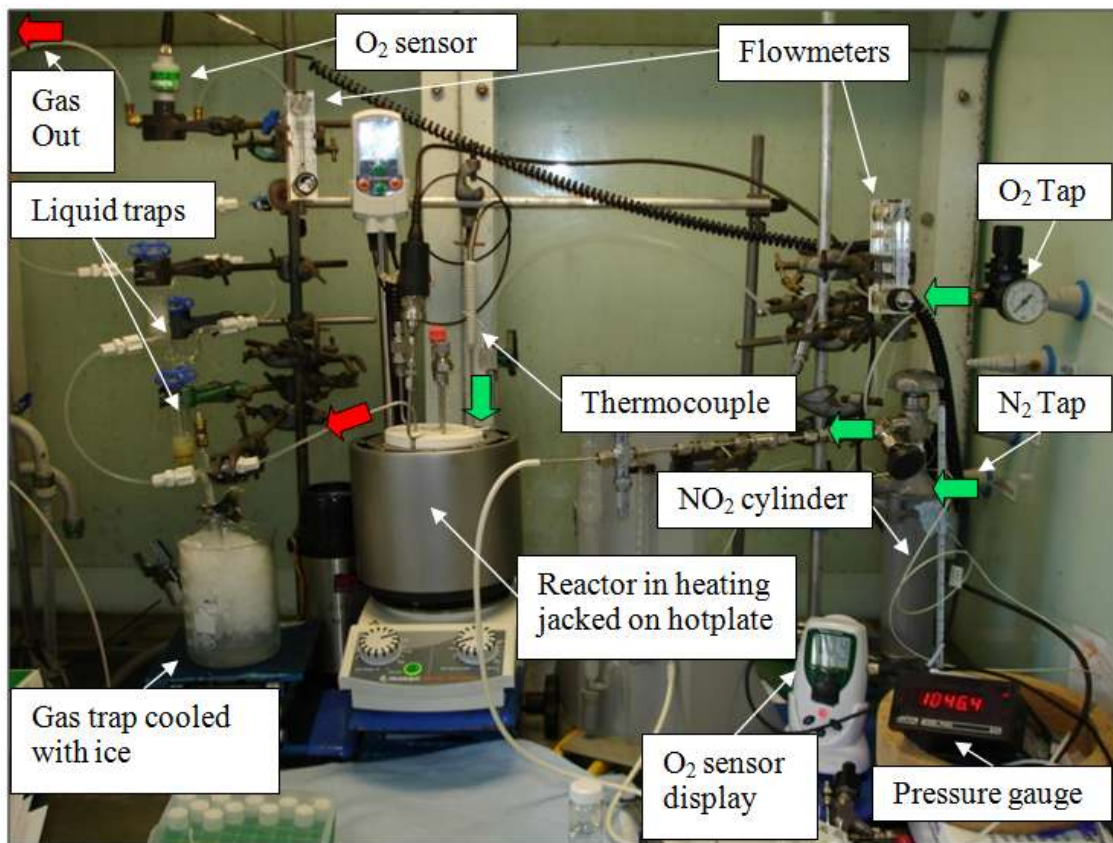


Figure 2.2: Apparatus set-up for before reaction was undertaken.

Using this set-up different types of experiments were performed, including: nitration, oxidation and nitro-oxidation. Most of the reactions were performed using continuous gas flow, however using closed sealed system was also possible.

2.2.2 Reactions Procedure

Reactions were undertaken in a stainless steel micro-reactor that was sealed with a stirring bar inside and placed into the heating jacket on the hotplate. All components of the apparatus were connected together and the system was filled with nitrogen, as shown in Figure 2.2 and schematically in Figure 2.3. The pressure gauge and flowmeters (in and out of the reactor) were checked for any leaks or blockages, then the reactor was heated to the desired temperature, e.g. 180 °C, controlled using a stainless steel (BS316) coated K-type thermocouple placed inside. When

the temperature was stable, the nitrogen gas was swapped to the reactive gas (O₂, NO₂ or NO) allowing the calibration of the relevant sensor afterwards the desired gas flow rate was set up to a constant value, e.g. $100 \pm 1 \text{ cm}^3 \text{ min}^{-1}$. The lubricant sample ($7.0 \pm 0.1 \text{ cm}^3$) was injected into the reactor and stirring was started at 600 rpm this was used to define the start of the reaction. The parameters controlled and monitored during the reaction were the temperature and the pressure inside the reactor and the reactive gas concentration in the reactor exhaust. Samples of used lubricant were taken periodically (typically every few minutes) through the septum using a cannula needle and syringe, and then put in the freezer until analysed with different analytical techniques. The volatile products were trapped in the cold trap and then analysed.

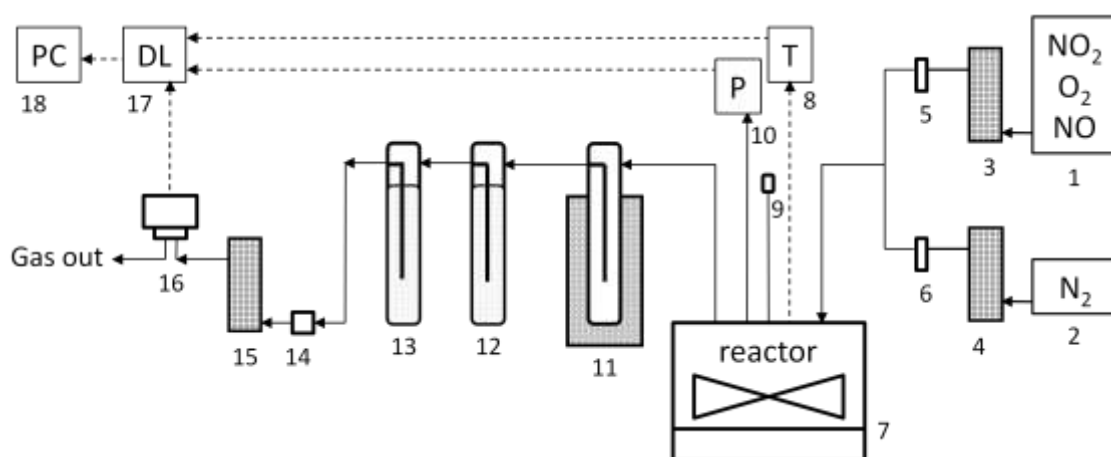


Figure 2.3: Schematic diagram of the apparatus: 1, 2 - gas cylinders; 3, 4, 15 – flowmeters; 5, 6 – non-return valves; 7- micro-reactor; 8- thermocouple; 9 – septum, 10 – pressure gauge; 11 – cold trap; 12, 13 – liquid traps; 14 – particulate filter; 16 – sensor; 17 – data logger and 18 – computer.

The schematic diagram (Figure 2.3) shows an example of the set up for any type of reaction using oxygen, nitrogen dioxide or nitrogen monoxide as a reaction gas and N₂ gas used in calibration; the details of all apparatus parts are described in Table 2.1.

Table 2.1: Details of the parts used in the apparatus.

Part	Details	Supplier	
1, 2	Gas cylinders:		
	Nitrogen Dioxide (NO ₂)	Gas mixture of 1000 ppm of NO ₂ in nitrogen*	BOC
		Concentrated NO ₂ gas (≥ 99.5%)	Sigma-Aldrich
	Nitrogen Monoxide (NO)	Gas mixture of 1000 ppm of NO in nitrogen*	BOC
	Oxygen (O ₂)	High purity oxygen gas (≥ 99.5%)	BOC
Nitrogen (N ₂)	High purity nitrogen gas (≥ 99.5%)	BOC	
3, 4, 15	Flowmeters ranges: 0.02 - 0.5 l/min	Cole-Parmer	
5, 6	Non-return valves, 1/3PSI, H400SSL1/8	Ham-Let	
7	Stainless steel (BS304) reactor, 49.0 cm ³ head space volume with Heating jacket Hotplate, MR Hei-Standard with temperature controller, EKT Spinplus, PTFE-coated, magnetic, stirring bar, size 1 1/2in.	University of York Heidolph Sigma-Aldrich	
8	Stainless steel, 0.5 mm, K-type thermocouple	Fluka	
10	Pressure gauge range 0 - 2 bar absolute, model P400	Digitron Instruments	
11	Gas trap, capacity of 5.6 cm ³ , cooled with ice bath	University of York	
12,13	Solvent traps, capacity of 25.0 cm ³	University of York	
14	Particulate filter, unit 5µm	Minisart	
16	Automotive NO ₂ sensor, NO2/S-5000 or Automotive NO sensor, NO/F-5000 or Automotive O ₂ sensor, class R-17A	Membrapor Teledyne Analytical Instruments	
17	High resolution data logger	Piko Technology	
18	Computer	Vilgen	

All experiments (oxidation, nitration and nitro-oxidation) used the same apparatus set-up, but with connection to different gases and equipped with the appropriate sensors (O₂, NO₂ or NO). The results from the preliminary oxidation, nitration and nitro-oxidation experiments are summarised in pre-testing section, in Appendix A, Figures A1-A6.

2.2.3 Reaction parameters

The typical reaction parameters are presented in Table 2.2.

Table 2.2: Typical reactions conditions.

Parameters	Values	Units
Temperature	180 ± 1	°C
Model lubricants:	Base oil	
	Base oil with phenolic antioxidant	
	Base oil with aminic antioxidant	
	Base oil with phenolic + aminic antioxidants	
Initial oil volume	7.0 ± 0.1	cm ³
Pressure	1050 ± 10	mbar
Gas Mixtures:	100 % O ₂	
	1000 ppm of NO ₂ in N ₂	
	1000 ppm of NO in N ₂	
	100 % O ₂ + 1700 ± 200 ppm of NO ₂	
Sampling volume	0.50 ± 0.01	cm ³
Stirring speed	600	rpm
Flow rate	50 ± 2	cm ³ min ⁻¹
	100 ± 1	

2.2.4 Monitoring of the reaction

The monitored data were:

- Pressure inside reactor (purple line)
- Concentration of O₂/NO/NO₂ in post-reaction gases (blue line)
- Temperature of lubricant (green line)
- Sampling time and start of the reaction (red line)

An example of recorded data for oxidation reaction is shown in Figure 2.4.; recording frequency was set up to one sample every two seconds.

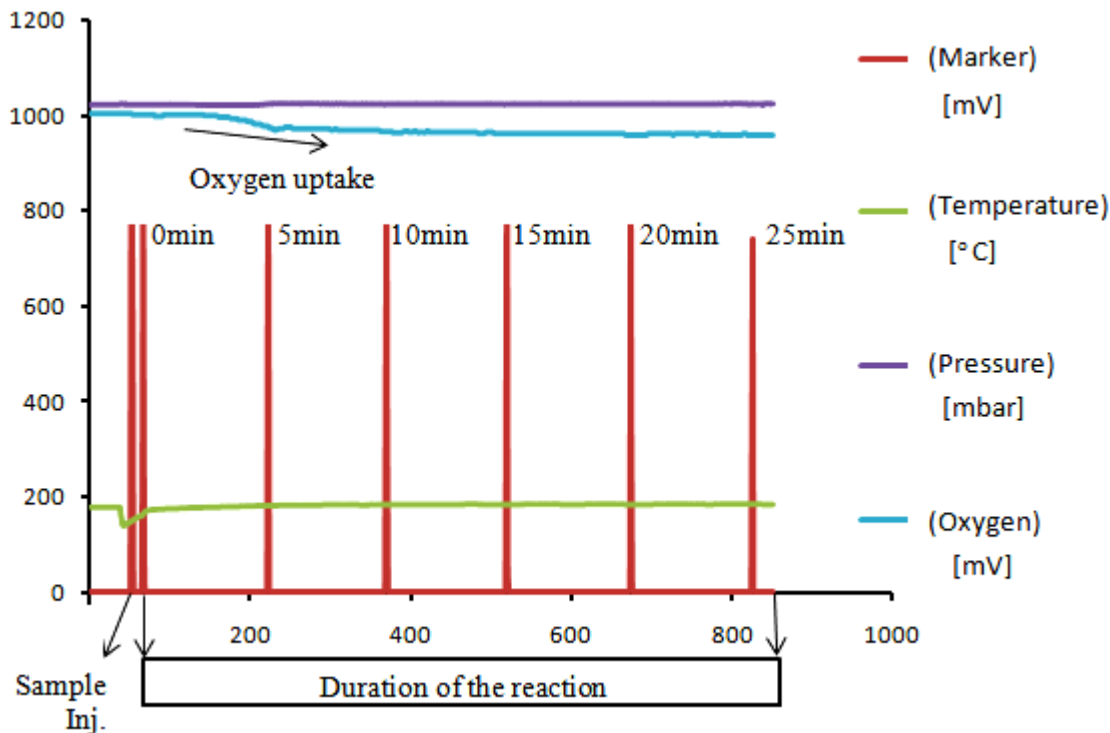


Figure 2.4: Example of raw data recorded using the thermocouple, pressure gauge and oxygen sensor connected to the data logger/computer. Reaction conditions: 100% (1000 mV) O_2 at flow rate $100 \text{ cm}^3 \text{ min}^{-1}$, model lubricant squalane, $T=180^\circ \text{ C}$, $p=1050 \text{ mbar}$.

From the raw data of oxygen consumption in [mV], the oxygen uptake in [mol min^{-1}] was calculated using the ideal gas law equation and then converted to [mol dm^{-3}] as shown in Appendix A, Table A1, as previously described by Alfadhil 2008.¹¹⁵

Early studies included comparisons of oxygen uptake for different experiments, such as: with and without antioxidant and with and without nitrogen dioxide, shown in Appendix A, Figure A1.

This work's experimental set-up (low pressure) was also compared to commercially available oxidation test (high pressure), which shows the effect of the pressure on degradation of model lubricants, in Appendix A.

Calculation of oxygen uptake has also been used also in detailed autoxidation studies of the model base oil in Chapter 3.

2.2.5 Safety using NO/NO₂

The main experiments involved reactions of model lubricants with very aggressive NO/NO₂ gases at the high temperature (180 °C), therefore the safety of using NO/NO₂ is reviewed in this section and hazards from using NO and NO₂ are summarised below.^{116,117}

2.2.5.1 Hazards of NO

The most significant risk from NO is that it is classed as a highly toxic gas (R26). The full list of hazards are as follows:

- R8 Contact with combustible material may cause fire
- R26 Very toxic by inhalation
- R34 Causes burns

Mixture containing 1000 ppm of nitric oxide {O;R8|T+;R26|C;R34} in N₂ is classified as (Xn) harmful:

- R20 Harmful by inhalation

Critical NO concentrations for a mixture of 1000 ppm NO in N₂ are given below:

- Occupational Exposure Limit (UK) - LTEL 25 ppm
- Occupational Exposure Limit (UK) - STEL 35 ppm
- LC50 115ppm

The safety phrases for NO are:

S9 Keep container in a well-ventilated place.

S23 Do not breathe the gas.

2.2.5.2 Hazards of NO₂

The most significant risk from NO₂ is that it is classed as a highly toxic gas (R26).

The full list of hazards below are as follows:

- R26 Very toxic by inhalation
- R34 Causes burns

Mixture containing 1000 ppm of nitrogen dioxide {T+;R26|C;R34} in N₂ are classified as (Xn) harmful:

- R20 Harmful by inhalation

Critical NO₂ concentrations for mixture of 1000 ppm NO₂ in N₂ are given below:

- Occupational Exposure Limit (UK) - LTEL 3 ppm
- Occupational Exposure Limit (UK) - STEL 5 ppm
- LC₅₀ 115 ppm

The safety phrases for NO₂ are:

S9 Keep container in a well-ventilated place.

S23 Do not breathe the gas.

The risks from the work with NO/NO₂ were covered by experiment risk assessments completed before each experiment, as well as annual risk assessments.

2.2.5.3 Control of Risks from Using NO/NO₂

Control of risk from NO/NO₂ to those in laboratory

Each experiment procedure using NO/NO₂ was confirmed by the detailed risk assessment, and also

- Had individual risk assessment checked and countersigned in advance by either of the project supervisors.

- At least one of the supervisors would be in the Chemistry Department during an experiment.
- Two members of the breathing apparatus team who are also first aid trained are to be informed in advance and be available during the experiment.
- The safety officer is to be made aware of the experiment start time, location and duration before it starts.
- The head technician for Green Chemistry is to be made aware of the experiment start time, location and duration before it starts.

Operation of Experiment

To minimise the risks from using NO/NO₂, the following restrictions had to be in place:

- If the cylinder is to be removed from the fumehood then while in the fumehood it will be turned off at the main tap and a blank fitted. Storage when not in the fumehood will be in the well-ventilated cylinder cage.
- The entire experiment, including the NO/NO₂ cylinder is to take place within a fumehood. No other experiments are to take place in the fumehood.
- The lab air outside the fumehood will be monitored for NO/NO₂ with a lower alarm level of 25ppm/3 ppm. The monitoring is done by a BW Technologies Gas Alert Extreme (Honeywell) NO and NO₂ gas detectors.
- Experiments can only be undertaken during normal working hours.
- Experiments cannot be left unattended for more than few minutes the sensor should stay by the fumehood and another member of the group nominated to monitor the experiment and sensor.
- The fume cupboard flow rate and sash high alarm should be checked each day before experiments start.
- The experiment exhaust pipe is to be secured to the back of the fume cupboard.

Control of risk from NO/NO₂ to those on roof of building

There was a conceivable risk to anyone on the roof, who is in the vicinity of the fume cupboard stack during the normal operation of this experiment. This was addressed by:

- Access to the roof controlled by a permit to work system.
- Work using high risk chemicals should stop when informed that people are on the roof in the vicinity of the fumehood stacks.
- The reactor exhaust gas is passed through two traps containing NaOH, which is intended to convert the NO₂ to NaNO₃.
- Even if the scrubbers do not work, and someone was adjacent to the fumehood stack, the concentration NO₂ in the fumehood exhaust stack can be estimated as ca. 6ppb, which is $\times 10^4$ lower than the Long Term Occupational Exposure Limit of 25 ppm for NO (16 ppb, which is $\times 10^3$ lower than the Long Term Occupational Exposure Limit of 3 ppm for NO₂).

Details of concentration calculations

Concentration of NO

Volume flow rate of 1000 ppm NO in nitrogen- $0.1 \text{ dm}^3 \text{ min}^{-1}$

Volume flow rate of NO – $0.1 \text{ cm}^3 \text{ min}^{-1}$ or $1 \times 10^{-7} \text{ m}^3 \text{ min}^{-1}$

Volume flow rate in the fumehood exhaust (assuming only one fumehood feeds the stack and the velocity at 0.5 m sash height is 0.5 m s^{-1} and width 1 m) – $0.25 \text{ m}^3 \text{ s}^{-1}$ or $15 \text{ m}^3 \text{ min}^{-1}$. Thus the concentration estimate in the fumehood exhaust: $= 1 \times 10^{-7} \text{ m}^3 \text{ min}^{-1} / 15 \text{ m}^3 \text{ min}^{-1}$ or ca. 6 ppb, which is $\times 10^4$ lower than the Long Term Occupational Exposure Limit of 25 ppm.

Concentration of NO₂

Volume flow rate of 1000 ppm NO₂ in nitrogen - $0.1 \text{ dm}^3 \text{ min}^{-1}$

Volume flow rate of NO₂ – 0.1 cm³ min⁻¹ or 1x10⁻⁷ m³ min⁻¹

Volume flow rate in the fumehood exhaust (assuming only one fumehood feeds the stack and the velocity at 0.2 m sash height is 0.5 m s⁻¹ and width 1 m) is – 0.1 m³ s⁻¹ or 6 m³ min⁻¹. Thus the concentration estimate in the fumehood exhaust: = 1 x 10⁻⁷ m³ min⁻¹ / 6 m³ min⁻¹ or ca. 16_ppb, which is x 10³ lower than the Long Term Occupational Exposure Limit of 3_ppm.

In case of accidental release

Possible scenarios for the accidental release of NO/NO₂ into the lab air could be envisioned:

Fume cupboard extract failure during normal running of experiment

If the fume cupboard fails during an experiment then the fume cupboard alarm will sound. The main tap on the cylinder of NO/ NO₂ should be shut immediately and the NO/NO₂ monitor checked for its concentration in lab air.

During the experiment, the volume flow rate of NO/NO₂ is 1 x 10⁻⁷ m³ min⁻¹, so if the fumehood failed completely, the time taken to fill the fumehood (assuming a volume of 1 m³) to a concentration of 25ppm/3 ppm (the LTEL) would be approximately 250 minutes for NO/ 30 minutes for NO₂.

Fumehood extract and fumehood alarm failure during normal running of experiment

If both the fumehood extracts and fumehood alarm fail during an experiment then a hazard warning occurs on the NO/NO₂ monitor, which is sampling the air in the lab. If the alarm sounds (at 25 ppm/ 3 ppm) the main valve on the cylinder should be shut off immediately. If it is found from the monitor that the NO/NO₂ concentration has gone noticeably above 25 ppm/3 ppm (the LTEL) the lab shall be evacuated immediately as

a precaution. From the above calculation it may take at least 4h 20 min. for the concentration of NO to build up to the 25 ppm alarm level and half an hour for the concentration of NO₂ to build up to the 3 ppm alarm level.

2.3 Chemical and Physical Analysis

2.3.1 Gas Chromatography

Samples from reactions in the micro-reactor were routinely analysed using GC-FID. The GC consisted of a Shimadzu GC17 gas chromatograph, equipped with a 5% phenoxyl capillary column (Zebron ZB-5HT, Phenomenex, film thickness 0.25 μm x internal diameter 0.25 mm x length 30 m) and flame ionisation detector (FID); chromatographic conditions are shown in Table 2.3.

Table 2.3: Chromatographic conditions of GC-FID analysis.

GC Conditions	
Inlet temperature	360° C
Inlet type	Split
Split ratio	10:1
Detector temperature	360° C
Programmed temperature	50-350° C at 5° C/min
Final temperature	350° C for 20 min
Carrier gas	Helium
Helium flow rate	2.0 mL/min

Samples were prepared by diluting 1:3 by mass in n-hexane; 1 μL of each sample was injected into the GC.

Quantitative Analysis

Quantitative analysis was undertaken using GC-FID results together with the effective carbon number (ECN) method,¹¹⁸ because appropriate GC calibration standards were not always available, details in Appendix A (Figure A7, Table A2).

2.3.2 Gas Chromatography – Mass Spectroscopy (GC-MS)

Standard GC-MS EI

The qualitative analyses were primarily undertaken using a Perkin Elmer Clarus 500 Gas Chromatograph with ZB-5HT column and equipped with electron impact (EI) mass spectrometer (Perkin Elmer Clarus 560S), the chromatographic conditions are shown in Table 2.4.

Table 2.4: Chromatographic conditions for standard GC-MS EI analysis.

GC Conditions	
Inlet temperature	300° C
Inlet type	Split
Split ratio	50:1
Initial temperature	60° C for 1 min
Programmed temperature	8° C/min
Final temperature	360° C for 20 min
Carrier gas	Helium
Helium flow rate	1.0 mL/min
MS Detector	
Interface temperature	300° C
Ionisation energy	70eV

This standard GC-MS EI analysis was good enough for screening of complex samples. To acquire more accurate product identification the high resolution GC-MS EI and FI were employed.

High Resolution Accurate Mass GC-MS EI and FI

To identify reaction products, accurate GC-MS with electron ionisation technique (EI) or field ionisation (FI) were used. The EI and FI mass spectra are complementary methods; the EI contains information about fragment ions and was used to identify the structures, whereas the FI contains more reliable information on molecular mass ion,¹¹⁹ particularly for species that fragment easily under electron impact. The analysis used an Agilent 7890A GC with ZB-5HT column coupled to a Waters GCT Premier Micromass TOF EI/FI MS, and chromatographic conditions shown in Table 2.5. To obtain a better spectrum of the products a solvent suppression method was used, which minimised large hexane and squalane peaks, e.g. Appendix A, Figure A8.

Table 2.5: Chromatographic Conditions for GC-MS EI analysis

GC Conditions	
Inlet temperature	300° C
Inlet type	Splitless
Initial temperature	60° C for 1 min
Programmed temperature	5° C/min
Final temperature	350° C for 16 min
Carrier gas	Helium
Helium flow rate	1.0 mL/min
MS Detector	
Interface temperature	300° C
Ionisation energy	70eV

The example of identification of one of the oxidation products the 6-methyl-2-heptanone, using the GC-MS EI and FI methods is shown in Appendix A, Table A3. The characteristic fragment ions, such as: m/z 43, 58, 71 and 85 were obtained in the EI mass spectrum, where only one, the parent peak of m/z 128 (M^+) without any fragment ions was observed in the FI mass spectrum.

2.3.3 UV-Vis Spectroscopy

UV-Vis spectroscopy was an additional method to help identify lubricant degradation products which absorb UV-Vis light, such as transformation products of phenolic antioxidants. The analysis was undertaken using Jasco V-550 Spectrophotometer with quartz cuvettes 0.5 mm path length (100 µl max. sample volume, 20 dilution factor). Samples were prepared by diluting in dichloromethane (DCM) in ratio approximately 1 to 100.

2.3.4 NMR Spectroscopy

Standard ¹H NMR

¹H NMR using a Bruker Ultra Shield 400 MHz spectrometer was routinely used in structural analysis of organic species. Samples were prepared by diluting 1:4 w/w in deuterated chloroform (CDCl₃).

High Resolution ¹H NMR (COSY, DOSY)

Analysis of reaction products was carried out using a Bruker Ultra Shield 700 MHz spectrometer. The 1D proton NMR was measured with solvent suppression of the squalane using the excitation sculpting suppression method.¹²⁰ The 2D proton NMR, standard COSY (Correlation Spectroscopy) sequence with the addition of squalane suppression method and DOSY (Diffusion Ordered Spectroscopy) sequence used stimulated gradient echoes with bipolar pulsed field gradients for the diffusion measurements and the same excitation sculpting method to suppress the squalane.

2.3.5 GPC

The GPC analysis used HP Series 1090 Liquid Chromatograph, equipped with Gel Permeation Column (Phenomenex Phenogel, styrene-divinylbenzene copolymer packing material, narrow bore 5 μm x diameter 4.6 mm x length 300 mm) with 50 Angstrom pore size (allowed molecular separation range 100-10000 g mol^{-1}); the operating conditions are given in Table 2.6.

Table 2.6: GPC conditions details.

GPC Conditions	
Column temperature	40 \pm 1 $^{\circ}\text{C}$
Mobile phase flow rate	0.35 $\text{cm}^3 \text{min}^{-1}$
Run time	20 min
Mobile Phase	Tetrahydrofuran (THF)
Photodiode array (PDA) Detector	
Spectrum range	280-560 nm
Channels acquisition	8
Main wavelengths set up	260, 280, 305, 310, 315

In GPC, separation of components is obtained by effective molecular size or hydrodynamic volume, therefore the large molecules elute first and small molecules elute last. The retention time depends on the hydrodynamic volume / size. Separation of components with a size difference greater than 10% could be achieved.¹²¹

2.3.6 Comprehensive two-dimensional gas chromatography (GCxGC)

Comprehensive two-dimensional gas chromatography combines two GC columns with different separation polarities. This allows for the problem of two eluants eluting simultaneously, as the likelihood of this happening on two different columns is reduced

enormously and the technique also provides higher sensitivity and selectivity than conventional GC, Figure 2.5.¹²²

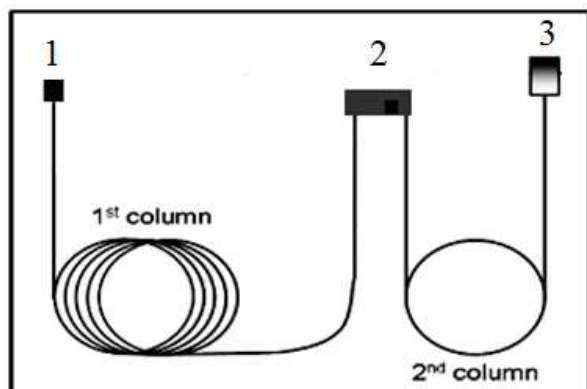


Figure 2.5: GCxGC instrument: 1-injector, 1st Column, 2-Interface, 2nd Column and 3-detector.

GCxGC with FID

The oxidised and nitrated samples were screened using GCxGC system with FID detector. The analysis was undertaken using an Agilent 5975 gas chromatograph equipped with 1st column ZB5-HT (non-polar) oven programmed 40-260° C, rate 8° C min⁻¹ and 2nd column HP-INNOWax (high polarity), oven 40-270° C, rate 8° C min⁻¹, example of 2D chromatogram in Appendix A, Figure A9.

GCxGC with NCD

The determination of nitrated products was undertaken using a GCxGC system consisting of an Agilent 6890 gas chromatograph with the first column DB5-HT (non-polar) oven programmed 55-335° C, rate 5 °C min⁻¹ and the second column SGE BPX50 (moderately polar), oven 70-350° C, 5 °C min⁻¹ connected to a nitrogen chemiluminescence detector (NCD), example chromatogram in Appendix A, Figure A10.

2.3.7 FTIR /ATR Spectroscopy

Fourier-transform infrared (FTIR) spectroscopy is widely used to monitor increase in oxidation and nitration products in used lubricants,¹²³⁻¹²⁴ an example in Figure 2.6.

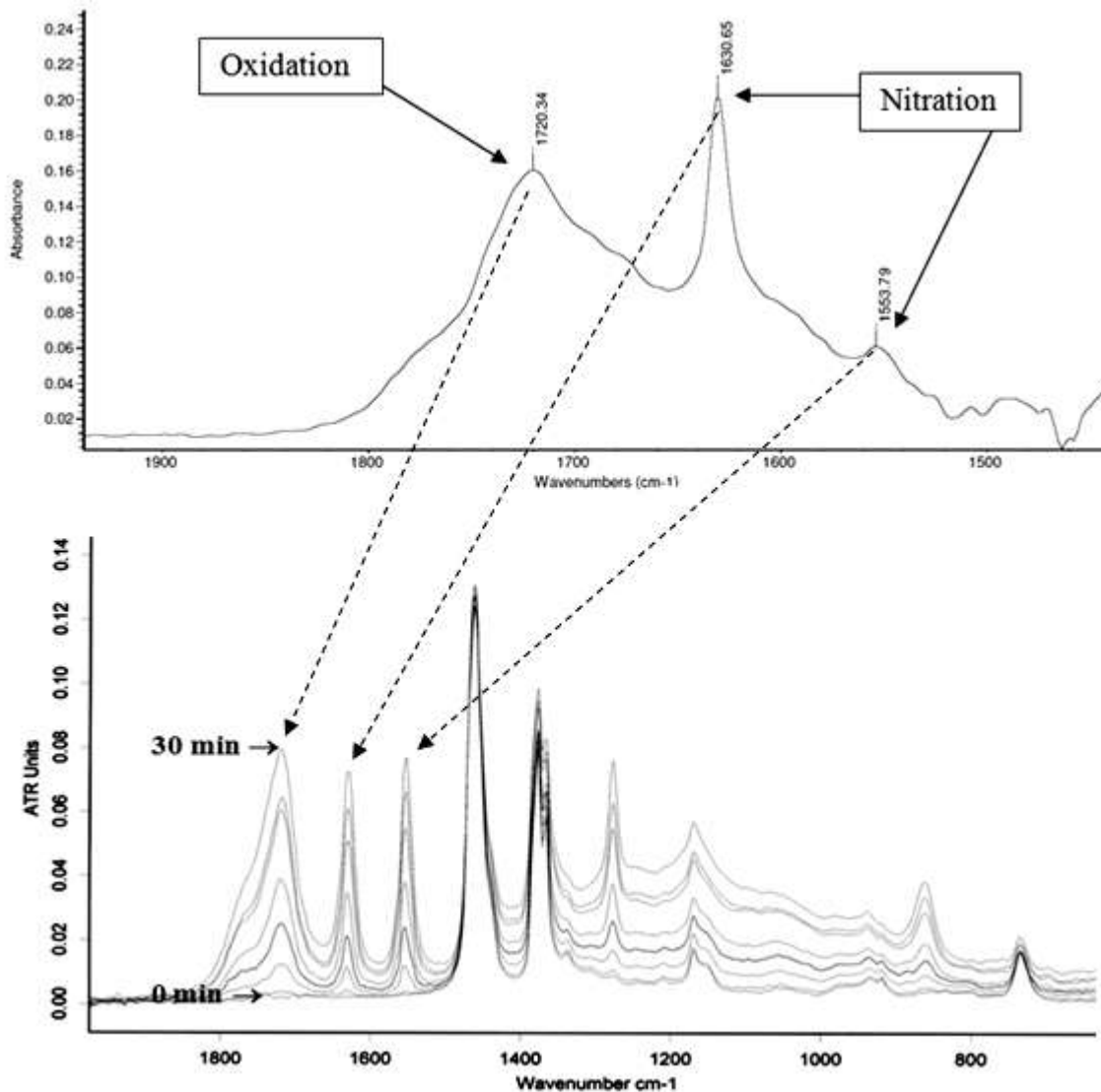


Figure 2.6: An example of FTIR spectrum of used lubricant from an engine showing oxidation and nitration products in region $1940\text{-}1430\text{ cm}^{-1}$ (BP/Castrol Laboratory in Pangbourne UK, obtain by S. Holliday), (Top spectrum). Identification of functional groups from the nitro-oxidation of squalane in the bench-top reactor at $180\text{ }^{\circ}\text{C}$ (this work), samples 0, 5, 10, 15, 20, 23, 25 and 30 minutes (bottom spectrum).

The examples of the characteristic frequencies for carbonyl, nitro, nitroso and $\text{N}=\text{O}$ functional groups from the literature are shown in Appendix B, Table B3-B4.¹²⁵

The primary analysis of neat reaction mixtures were undertaken using Bruker FTIR Vertex 70 with resolution of 4 cm⁻¹ at 64 scans, spectra recorded from 4000 to 600 cm⁻¹ and collected using IR Opus 5.5 Software, examples in Appendix B, Figures A2 to A5. Attenuated Total Reflectance (ATR) spectroscopy has been used for screening samples from the experiments. However to analyse small concentration of the products the Specac Omni-Cell System was used, Figure 2.7.

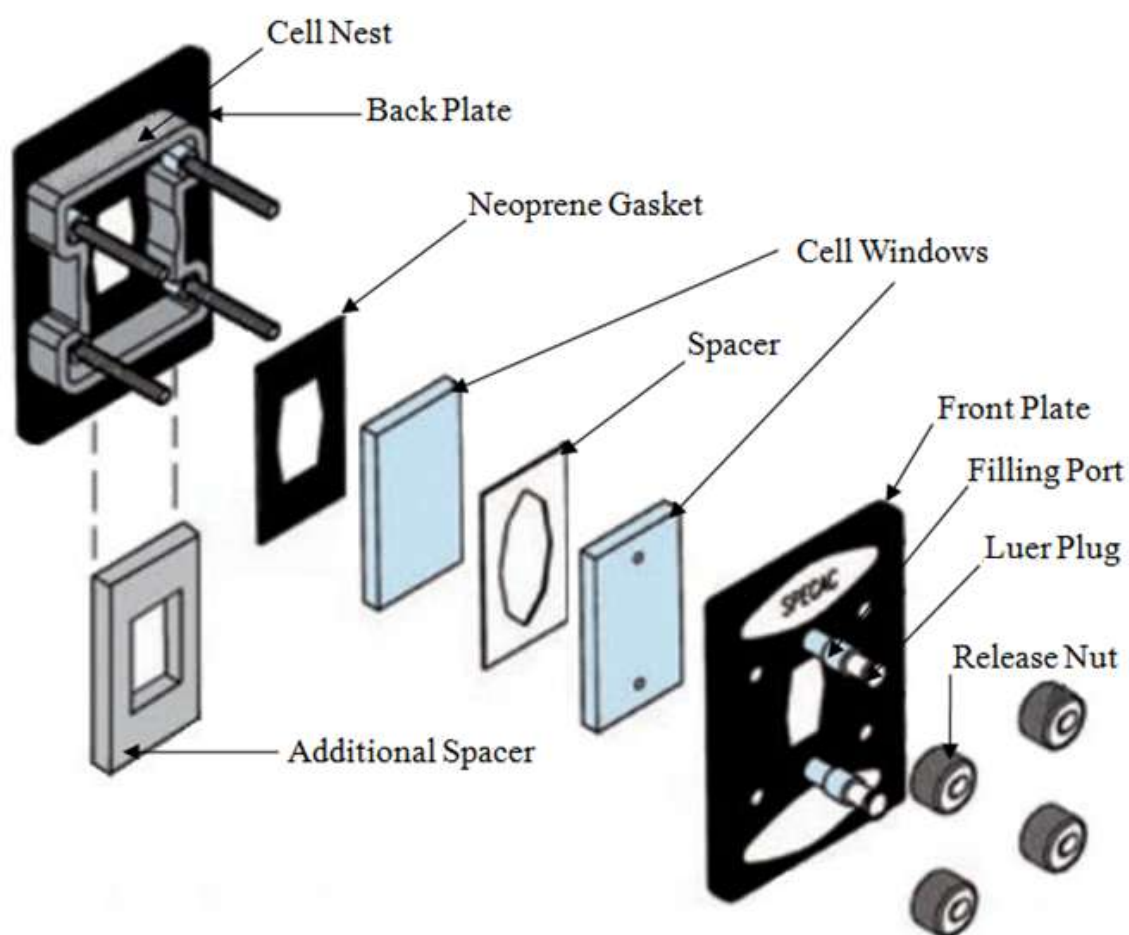


Figure 2.7: Set up of universal transmission cell for the analysis of liquids in FTIR.

Specac Omni-Cell System is a universal transmission cell for the analysis of liquids in FTIR. The samples were analysed neat in the thin film sandwich between two CaF₂ windows (4 mm thick) in a liquid cell and using 0.5 mm teflon spacer.

2.3.8 Kinematic Viscosity

Viscosity is a very important engine oil property, which measures its resistance to flow. In this work, kinematic viscosities at $40.0 \pm 0.1^\circ \text{C}$ were taken using Cannon-Manning micro-viscometer U-tube 300, Figure 2.8. The temperature of the water bath was $40.0 \pm 0.1^\circ \text{C}$. The sample of the oil was drawn into the viscometer tube, then the tube was left for ten minutes in the heating bath to stabilise. The efflux time taken for the level of the liquid to pass between marks A to B was proportional to the kinematic viscosity. Kinematic viscosity was calculated by multiplying efflux time by viscometer tube constant.

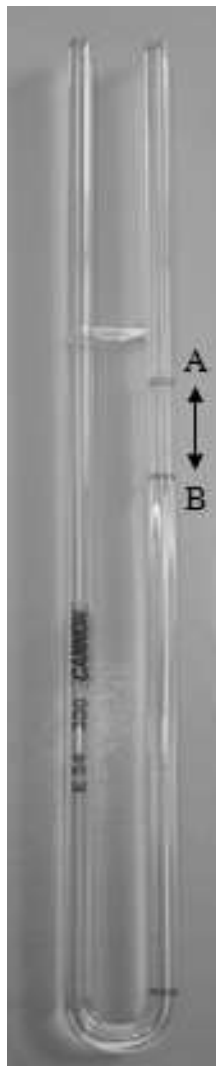


Figure 2.8: Cannon-Manning micro-viscometer U-tube 300.

2.4 Synthesis

The 2,6-di-*tert*-butyl-4-ethylidene-cyclohexa-2,5-dien-1-one (quinone methide, QM1) was synthesised from 2,6-di-*tert*-butyl-4-ethylphenol using a similar procedure to Cook *et al.* 1958,¹²⁶ reaction 2.1. This product was used as a reference during product analysis in Chapter 4.

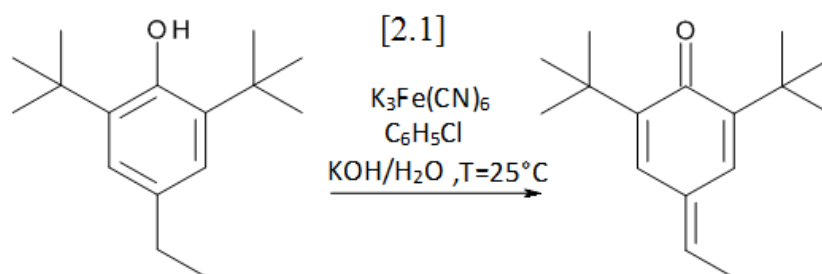


Figure 2.9: Reaction of synthesis of 6-di-*tert*-butyl-4-ethylidene-cyclohexa-2,5-dien-1-one (quinone methide, QM1).

A solution of 1g 2,6-di-*tert*-butyl-4-ethylphenol in 2.5ml of chlorobenzene was stirred with 3g potassium ferricyanide (III), $\text{K}_3\text{Fe}(\text{CN})_6$, in an excess of alkaline solution (6 ml, 0.2 M KOH solution) under an inert (N_2) atmosphere at room temperature. The alkaline solution was added to the starting solution by syringe, until the blue colour disappeared. Synthesis set-up is shown in Figure 2.10.

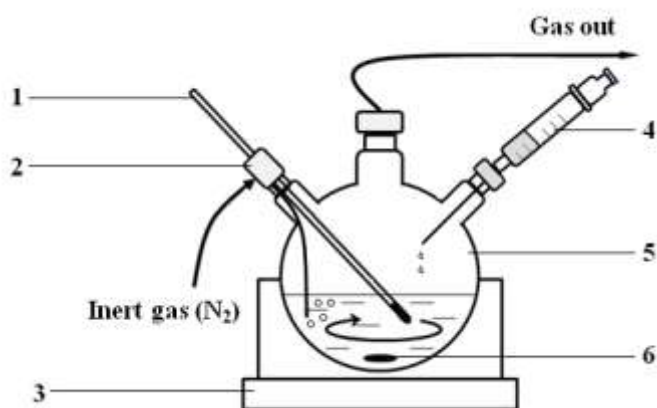


Figure 2.10: Apparatus for synthesis: 1-thermometer, 2- thermometer adapter with side arm adapter, 3-magnetic stirrer, 4-septum, 5 -(3)-neck flask, 6- magnetic stirrer bar.

The crude product was filtered, washed with n-hexane and recrystallised, the yield obtained was approximately 80%. Product was analysed using: ^1H NMR, GC-MS EI, UV-Vis and GPC details below.

Product: 2,6-ditert-butyl-4-ethylidene-cyclohexa-2,5-dien-1-one

^1H NMR (CDCl_3): δ (ppm); 1.29 (s, 18 H), 2.05 (dd, $^3J = 7.5$ Hz, 3 H), 5.65 (q, $^3J = 7.5$ Hz, 1 H), 6.95 (m, 1 H), 7.35 (m, 1 H)

Predicted ^1H NMR (ACD/I-lab): δ (ppm); 1.28 (s, 18 H), 1.96 (dd, $^3J = 7.5$ Hz, 3 H), 5.92 (q, $^3J = 7.5$ Hz, 1 H), 6.96 (m, 1 H), 7.36 (m, 1 H)

MS (EI): m/z (relative intensity) 57.172 (50), 128.337 (27), 133.435 (30), 175.115 (70), 189.129 (65), 217.159 (100), 232.184 (25)

UV-Vis (DCM): $\lambda_{\text{max}} = 304$ nm

GPC (THF): $\lambda_{\text{max}} = 305$ nm

Some figures from QM1 analysis could be found in Chapter 4, where it is compared to other quinone methide product.

2.5 Materials

All commercially available materials used in this experimental work are given in Tables 2.7 and 2.8.

Table 2.7: Materials – part 1.

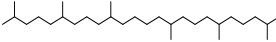
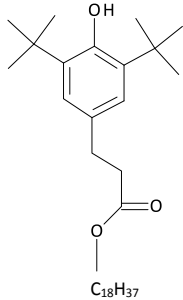
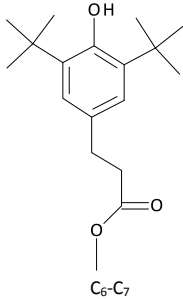
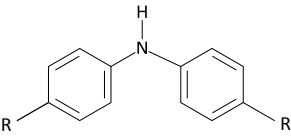
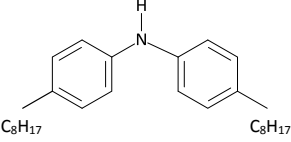
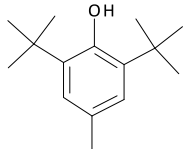
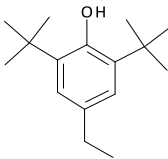
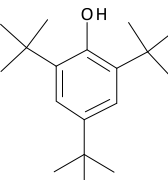
Common name (abbreviation in thesis) /Formula/ Molecular weight	IUPAC name	Structure	CAS No.	Purity/ Supplier
Squalane (SQ) C ₃₀ H ₆₂ 422.81 g/mol	2,6,10,15,19,23-Hexamethyl tetracosane		111-01-3	99% Sigma-Aldrich
Irganox L107® (OHPP) C ₃₅ H ₆₂ O ₃ 530.86 g/mol	Octadecyl 3-(3,5-di- <i>tert</i> -butyl-4-hydroxyphenyl)propanoate		2082-79-3	99.9% BASF
IrganoxL135® C7-C9 branched alkyl esters	3-(3,5-di- <i>tert</i> -butyl-4-hydroxyphenyl)propanoate		128-39-2	BASF
Irganox L57® Butylated/Octylated diphenylamine	4- <i>tert</i> -butyl-N-[4-(1,1,2,2-tetramethylpropyl)phenyl]aniline		6683-19-8	99.9% BASF
Irganox L01®, 4,4'-Dioctyl Diphenyl amine (DODPA) C ₂₈ H ₄₃ N 393.34 g/mol	4-(1,1,3,3-tetramethylbutyl)-N-[4-(1,1,3,3-tetramethylbutyl)phenyl]aniline		23128-74-7	99.9% BASF
3,5-Di- <i>tert</i> -4-butylhydroxytoluene (BHT) C ₁₅ H ₂₄ O 220.35 g/mol	2,6-Di- <i>tert</i> -butyl-4-methylphenol		128-37-0	99% Sigma-Aldrich

Table 2.8: Materials – part 2.

Common name (abbreviation in thesis) /Formula/ Molecular weight	IUPAC name	Structure	CAS No.	Purity/ Supplier
(EthPh) C ₁₆ H ₂₆ O 234.38 g/mol	2,6-Di- <i>tert</i> -butyl-4-ethylphenol		4130-42-1	99% Sigma-Aldrich
TTBP C ₁₈ H ₃₀ O 262.43 g/mol	2,4,6-Tri- <i>tert</i> -butylphenol		732-26-3	98% Sigma-Aldrich
K ₃ Fe(CN) ₆ 329.25 g/mol	Potassium ferricyanide (III)	-	13746-66-2	99% Sigma-Aldrich
C ₆ H ₅ Cl 112.56 g/mol	Chlorobenzene	-	108-90-7	99% Sigma-Aldrich
KOH	Potassium hydroxide	-	71769-53-4	Fisher

Chapter 3: Autoxidation of Squalane in the Liquid Phase

3.1 Introduction

Commercial base fluids typically consist of branched alkenes derived from highly refined crude oil, which consequently have a large variety of masses and structures. It is therefore very difficult to analyse for numerous degradation products when using commercial base fluid and even more difficult to link an individual product with a starting base fluid molecule. However, the analysis of the base fluid degradation products could be simplified, when using a single hydrocarbon as a model base oil. The example of the GC-FID trace of the commercial base oil (Yubase 4) compared to model base oil squalane is shown in Figure B2, Appendix B.

Previous work used linear alkanes to study engine lubricant degradation,^{103-106,111,127} which are not very representative as model base oils due to their lacking tertiary hydrogens, which will be abstracted more readily by radicals than primary or secondary hydrogens.²¹ Another disadvantage was that the hydrocarbons studied were too volatile to be easily used at the high temperature found in piston assemblies.

Therefore, squalane (2,6,10,15,19,23-hexamethyltetracosane), Figure 3.1, has been used in this work as a representative chemical model of lubricant base fluid to investigate engine lubricant degradation at piston ring pack conditions.

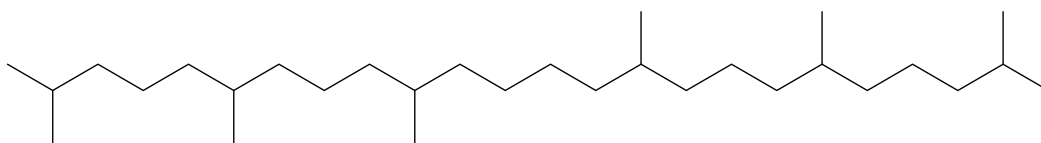


Figure 3.1: Chemical structure of squalane (C₃₀H₆₂).

Autoxidation of squalane has been studied in the liquid phase at 170 °C with products identified by GC-MS EI and FI and quantified by GC-FID, and the chemical mechanisms for their formation were compared to previous work on pristane, a smaller branched hydrocarbon.¹⁰⁷

Squalane has been used as a model lubricant as it contains a comparable percentage of tertiary carbon atoms to the range of commercially available base fluids,^{22,128} shown in figure B1, Appendix B, which influences its thermal oxidative resistance due to the weaker tertiary bond strength.²¹ Another advantage of using squalane as a model base oil is its low volatility at high temperatures with the flash point (closed cup) of 218 °C,¹²⁹ which is important when studying the liquid phase at high temperatures of piston assembly.

Understanding the chemical mechanism underlying lubricant base fluid oxidation is very important, because it determines the useful lifetime of lubricants and squalane is used as a model base fluid in further antioxidant degradation studies, in chapters 4 to 7.

3.2 Previous work

Most of previous work on the autoxidation of alkanes in the liquid phase and hence on lubricant base fluid degradation have been based on linear alkanes (used as a chemical models), such as n-hexadecane, n-decane and n-octane.^{103-106,111,127}

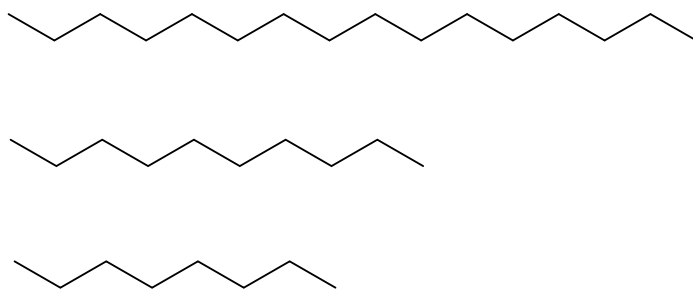


Figure 3.2: Chemical structure of n-hexadecane (C₁₆H₃₄), n-decane (C₁₀H₂₂), n-octane (C₈H₁₈).

The standard, generic hydrocarbon oxidation mechanism was explained above in Table 1.10, Chapter 1. It consisted of four stages: initiation, propagation, chain branching and termination. The diagram of the propagation phase, in which the dominant chain carriers are alkyl and alkylperoxy radicals, is shown in figure 3.3.

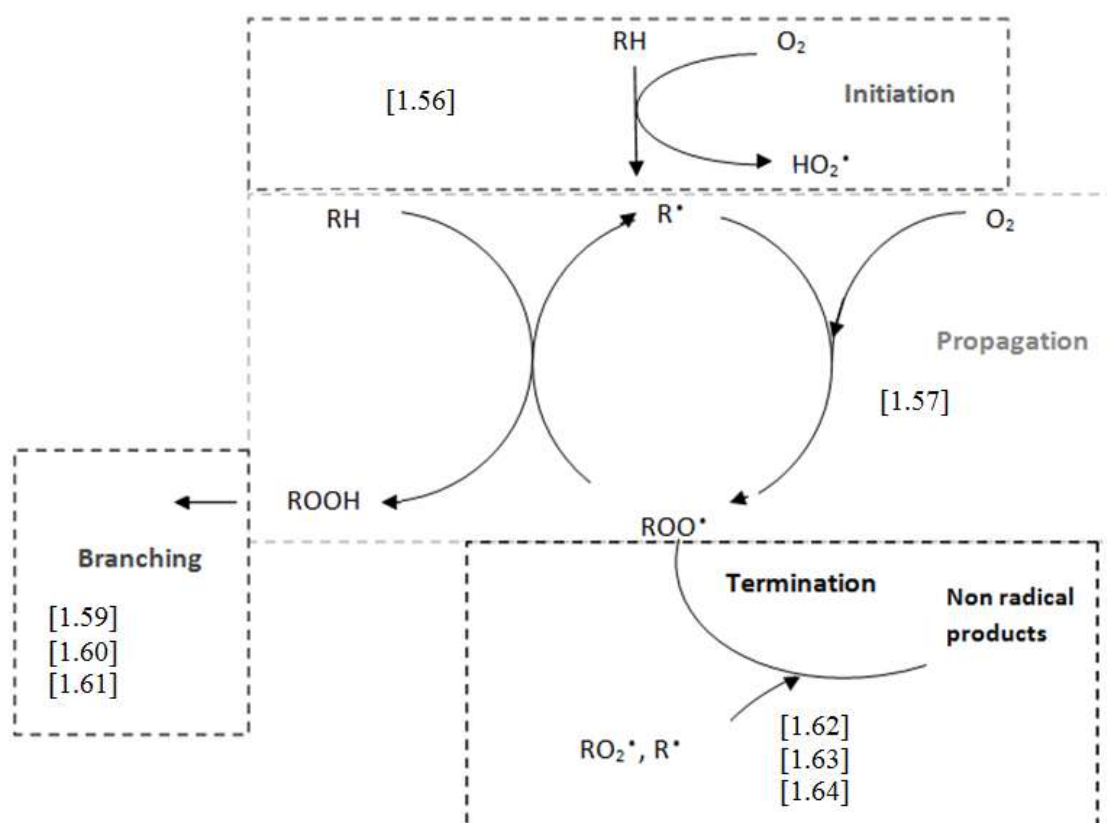


Figure 3.3: Schematic diagram of oxidation of hydrocarbons.^{130,131}

Unfortunately *n*-alkanes are not very representative as model lubricants, because commercial base fluids contain a substantial percentage of the branched alkanes,¹²⁸ which are more likely attacked by the radicals, therefore branched alkanes were reviewed.

Early work on oxidation of branched alkanes in the liquid phase, such as 2,4,6-trimethylheptane, Figure 3.4, reported the formation of di- and tritertiary hydroperoxides and was studied at 80 to 120 °C.¹³²

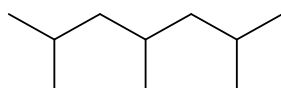


Figure 3.4: Chemical structure of 2,4,6-trimethylheptane (C₁₀H₂₂).

Unfortunately, this hydrocarbon is too volatile to study engine lubricant degradation at piston ring pack conditions, therefore it is not a very good lubricant model. Another disadvantage is that it contains tertiary hydrogen atoms separated by just one carbon this allows internal hydrogen abstraction by a tertiary alkylperoxyl radical via a sterically favourable six-membered cyclic transition state. The separation of tertiary hydrogen in base fluids will normally be greater than for 2,4,6-trimethylheptane and therefore intra-molecular abstraction therefore less likely in a lubricant base fluid.

The longer branched hydrocarbon, squalane, has been investigated as a chemical model of polyolefin degradation in photo-oxidation studies.¹³³ However the oxidation was undertaken at low temperatures 40 to 60 °C not representative for engine piston assembly. The analysis was also limited to FTIR technique and the chemical mechanism was based on the identification of the functional groups.

Squalane has also been recently investigated as a chemical model for base fluid oxidation,¹³⁴ as it is a branched alkane that can remain liquid up to at least 200 °C. Products resulting from the oxidation of squalane and also lighter than squalane were analysed using GC-MS, however with the limited reporting of the mass spectra justifying the assignments or mechanistic explanations for the origins of the products identified.

The next branched hydrocarbon, pristane (2,6,10,14-tetramethylpentadecane), Figure 3.5, has been reported previously in autoxidation studies at 170 °C.¹³⁵

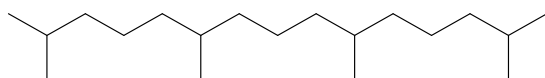


Figure 3.5: Chemical structure of pristane (C₁₉H₄₀).

Pristane was used due to its simpler structure and smaller size. The twenty-three pristane oxidation products were identified, including: alkanes, alkenes, ketones, alcohols, acids and lactones and analysed using various analytical techniques, details in Table B1, Appendix B. Products have been quantified and formation mechanisms proposed.

The initial product formed during the oxidation of alkanes, including pristane is the hydroperoxide. It is formed by the standard hydrocarbon oxidation mechanism by abstraction of a hydrogen atom by a peroxy radical as shown in reactions [3.1] and [3.2], Table 3.1 (R, R' and R'' are alkyl chains and early in the reaction RH is pristane). Hydroperoxides from pristane were not detected, due to the difficulty in detecting them directly by GC, and wet techniques were not used due to the very limited amount of sample available for analysis. Previous work has; however, shown that hydroperoxides are abundant at lower temperatures (e.g. 90 °C), but are more minor products at 170 °C,

as they decompose rapidly to form an alkoxy and a hydroxyl radical, reaction [3.3].^{104,105}

Table 3.1: Autoxidation of pristane – initial reactions.

Reactions	No.
$\text{ROO}^\bullet + \text{RH} \rightarrow \text{ROOH} + \text{R}^\bullet$	[3.1]
$\text{R}^\bullet + \text{O}_2 \rightarrow \text{ROO}^\bullet$	[3.2]
$\text{ROOH} \rightarrow \text{RO}^\bullet + \text{OH}^\bullet$	[3.3]
$\text{RO}^\bullet + \text{RH} \rightarrow \text{ROH} + \text{R}^\bullet$	[3.4]
$\text{R}'\text{R}''\text{C}(\text{H})\text{O}^\bullet + \text{O}_2 \rightarrow \text{R}'\text{R}''\text{C}=\text{O} + \text{HOO}^\bullet$	[3.5]

During the oxidation of pristane, large quantities of pristanols (particularly tertiary), were formed, accounting for (45 ± 6) % of the pristane, reacting in the early reaction, they formed by the abstraction of a hydrogen atom by an alkoxy radical, reaction [3.4]. Formation of the secondary pristanols could be from the secondary alkoxy radicals via hydrogen abstraction, but they could also react with molecular oxygen to form pristanones, reaction [3.5]. The proportion of the secondary alkoxy radicals reacting with oxygen to form pristanones instead of abstracting a hydrogen atom to form pristanols was found to be (42 ± 5) % , it was observed in the early stage of the reaction, when still significant quantities of oxygen were present, as seen in Figure B3, in Appendix B.

However the majority of the products identified from the autoxidation of pristane were smaller and more volatile than pristane itself (19 out of 23), which products could be associated with the decomposition via beta-scission of the two tertiary alkoxy radicals (2-pristoxyl and 6-pristoxyl). Early in the reaction the decomposition of tertiary alkoxy radicals accounts for (53 ± 3) % of the reacting pristane. This decomposition to form a fragment methyl ketone and a primary alkyl radical for the example of the 6-pristoxyl

radical cleaving between carbons 5 and 6 is shown in Figure 3.6, reaction [3.6]. A significant proportion (27 ± 2 %), of these primary alkyl radicals do not add oxygen (e.g. reaction [3.7]), but abstract a hydrogen to form fragment alkanes instead.

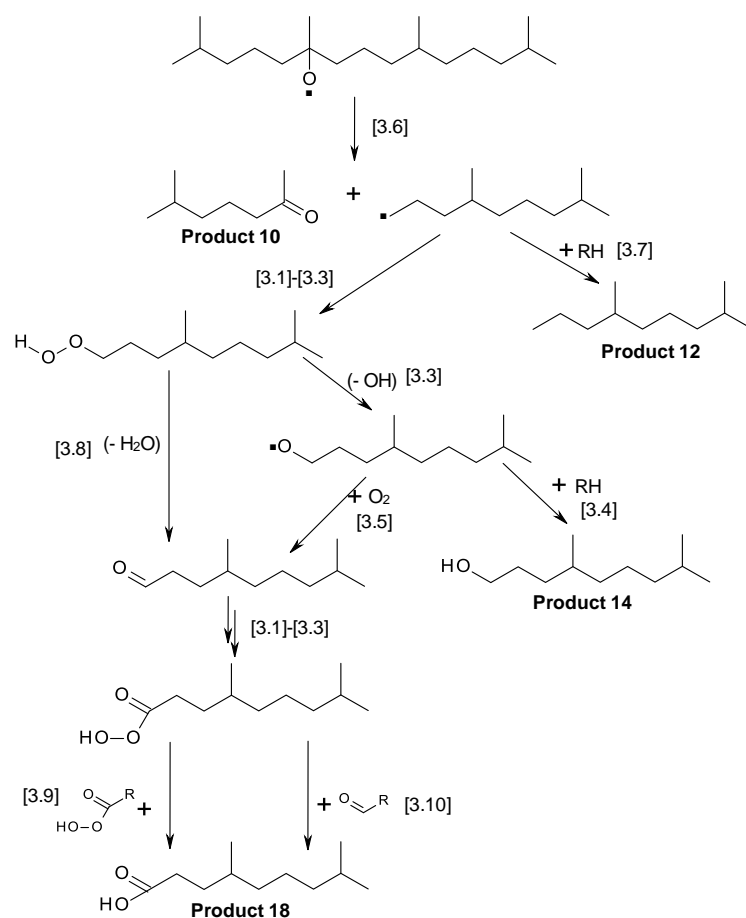


Figure 3.6: Chemical mechanism of oxidation of pristane - formation of ketones and carboxylic acids. Product identification in Appendix B.

The latter part of the reaction showed a noticeable decrease in formation of the most volatile products, such as propanone and 2-methylpentane (Figures B4 and B5 in Appendix B). This loss is possibly associated with condensation of these volatile products in the tubes of the reactor and not due to reacting further, as they are comparatively unreactive species.

There were three carboxylic acids identified from the oxidation of pristane, 4,8-dimethylnonanoic, 3-methylbutanoic acid and ethanoic acid. The example of a possible reaction mechanism of the formation of carboxylic acids, which is based on the formation of 4,8-dimethylnonanoic acid (product 18) is shown in Figure 3.6.

In the second mechanism, the primary hydroperoxide (4,8-dimethylnonyl-1-hydroperoxide) is formed, which can decompose to form a primary alkoxy radical. The alkoxy radical can either abstract a hydrogen atom (reaction [3.4]) to form a fragment primary alcohol (product 14) or react with oxygen to form an aldehyde, reaction [3.5]. Reaction [3.8] shows a direct dehydration of hydroperoxides to the aldehyde.

This work did not detect any aldehydes, possibly they are likely to be attacked far faster than either the substrate or other oxidation products, due to their exceedingly labile hydrogen atoms and react away rapidly (giving a low, steady state concentration throughout the reaction). However the equivalent of peracid is formed (via reactions [3.1], [3.2] and [3.3]), which will readily react with any aldehyde present via reaction [3.10], the Baeyer - Villiger reaction,¹³⁶⁻¹³⁸ or with another peracid molecule, reaction [3.9], to form 4,8-dimethylnonanoic acid (product 18).¹³⁹

Evidence for the formation of aldehydes was primarily supported in the formation of both pristanol (e.g. detected 4,8-dimethyl-1-nonanol) and pristanone, from the attack on the secondary hydrogen atoms, which supports the notion that the equivalent aldehyde must also have been formed.

Secondly, the fraction of tertiary pristoxyl radicals decomposing decreases as the reaction proceeds. The decomposition rate constant will not vary throughout the reaction this implies that the rate of the competing reaction, hydrogen abstraction,

increases throughout the reaction. In the initial stages of the reaction abstraction can only be from pristane; the increase in rate must arise from products with exceedingly labile hydrogen atoms, consistent with aldehyde formation.

The third evidence for the formation of aldehydes was the detection of large quantities of carbon monoxide, which was detected at relatively low temperatures during this study, by the reaction of decarbonylation of the aldehyde following hydrogen abstraction.

Smaller acids such as 3-methylbutanoic acid can form in a related fashion, due to elimination of carbon monoxide or carbon dioxide by acyl or acylperoxy radicals the result of this process is that an alkyl radical is produced with one less carbon atom than its parent. These smaller carboxylic acids can possibly also form by the attack on secondary C-H bonds and the decomposition of the resulting alkoxy radical.

Formation of lactones during autoxidation of hydrocarbons in the liquid phase is the well known mechanism^{103-106,127,140} and in this study two lactones were detected. Previously proposed reaction mechanism for the formation of lactones from secondary peroxy radicals, by Goosen (Figure 3.7),¹⁴⁰ involved the multiple internal abstractions by alkoxy radicals resulting in a hydroxyl substituted carboxylic acid, which then undergoes an internal esterification to give a lactone.

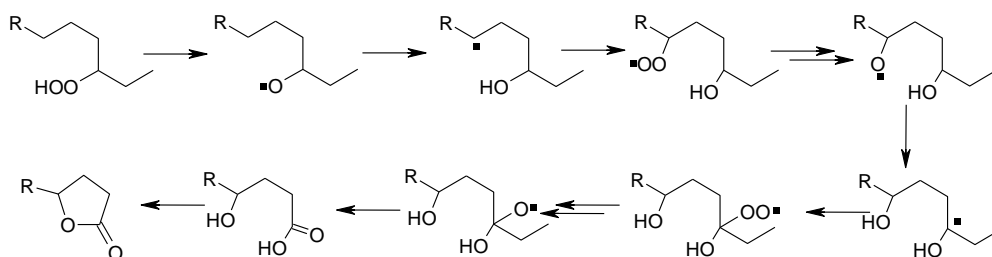


Figure 3.7: Lactone formation by Goosen et al.¹⁴⁰

Goosen's mechanism for lactone formation, however requires two hydrogen abstractions from one carbon atom, and therefore it cannot be applicable here since the lactones detected here result from the abstraction of two tertiary hydrogen atoms.

An alternative to Goosen's mechanism is suggested in Figure 3.8, which provides a competing route for the primary peroxy radical (4,8-dimethylnonyl-1-peroxy radical) from Figure 3.6.

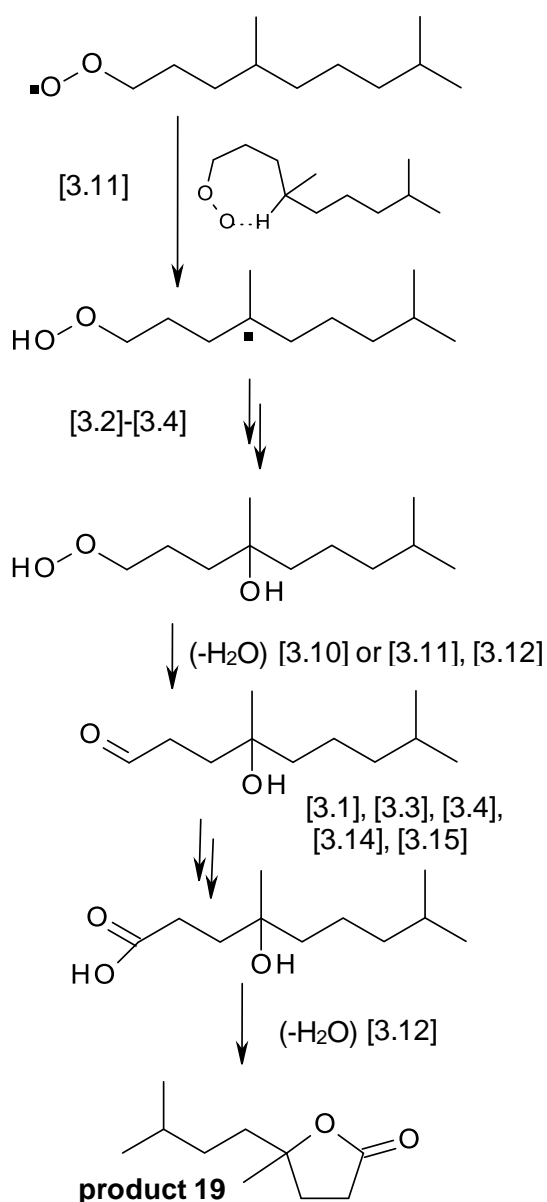


Figure 3.8: Lactone formation by Belenkov et al.¹⁴¹

This can undergo an internal hydrogen abstraction reaction of the tertiary hydrogen next along the chain, which involves a 7-membered transition state, to form a hydroperoxyl-alkyl radical.

The alcohol is formed from the carbon-centred radical reactions [3.2], [3.3] and [3.4] and then possibly dehydrates of hydroperoxide to form an aldehyde, which is via either the single step or multi-step process and the aldehyde group would very likely rapidly be oxidised to a carboxylic acid group. As suggested by Goosen, the hydroxy-carboxylic acid can then undergo an internal esterification to form the lactone.

An alternative mechanism for the formation of γ -lactones suggested by Belenkov involved the further oxidation of a tetrahydrofuran product.¹⁴¹ In this study the trace amounts of 2,2-dimethyltetrahydrofuran were detected; despite the fact that the ratio of lactone to the tetrahydrofuran was very large. This mechanism therefore is unlikely to be significant.

There were two 1-alkenes (2,6-dimethylhept-1-ene, product 7, and 2,6,10-trimethylundec-1-ene, product 16) detected and quantified, which have not been reported previously during autoxidation of alkanes at 170 °C, and have only been observed at temperatures above 300 °C (in dodecane oxidation at high pressure), with the suggested mechanism of their formation being the decomposition of alkyl radicals.¹⁴² The decomposition of the 6-pristyl radical to form two 1-alkenes is illustrated in Figure 3.9. There are formed in two ways, the firstly by the abstraction of the hydrogen atom by primary alkyl radicals, or by oxidation to form a primary alcohol. The 3.7 ± 0.4 % of pristyl radicals decompose to form a 1-alkene, this was examined

by the ratio of 1-alkenes to products formed from the pristoxyl radical, with the rest of pristyl radicals adding oxygen.

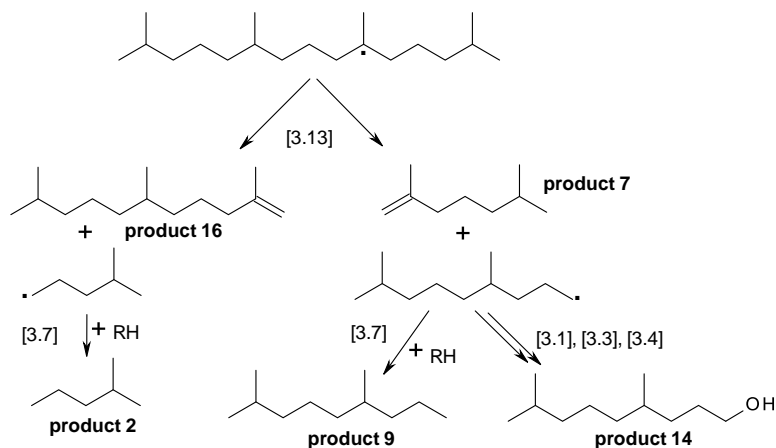


Figure 3.9: Chemical mechanism of alkenes formation.¹⁰⁷

The rate at which lubricants are lost from the automotive engine are known as the useful lifetime of lubricants; this can be determined by so-called volatile oxidative loss.¹⁰⁵ During autoxidation hydrocarbon molecules of the lubricant base fluid are broken to form smaller hydrocarbon molecules, which are sufficiently volatile to be lost from the engine. A previous study of the chemical mechanism for the volatile loss is given as a direct cleavage of the carbon-carbon backbone of the base fluid molecule; however, this is unlikely at the temperatures used in the study or to the temperatures which lubricants are exposed to in gasoline engines. However in this work the oxidative loss of lubricant actually results from cleavage of tertiary alkoxy radicals to form smaller, more volatile fragments.

The well known lubricant science could explain that a base fluid is more susceptible to oxidation the higher the proportion of tertiary hydrogen atoms it contains, as these have weaker bond strengths than secondary or primary C–H bonds this work allows this

understanding to be quantified. The 77 ± 2 % of radical attack occurs at tertiary hydrogen atoms during the autoxidation of pristane at 170 °C with the remaining 23 % due to attack at secondary hydrogen atoms (Figure B3 in Appendix B). As there are only four tertiary hydrogen atoms per molecule, compared with 18 secondary hydrogen atoms, this is equivalent to tertiary hydrogen atoms being 15 ± 1 times more reactive than secondary hydrogen atoms during autoxidation at 170 °C.

An initial oxygen pressure of 1000 mbar pressure used in these studies was different than in automotive engines, where the oxygen pressure is noticeably lower than the ambient 210 mbar; therefore the relative importance of competing reactions of secondary alkoxy radicals to give either ketones or alcohols will be different during lubricant oxidation in engines. The proportion of secondary alkoxy radicals reacting with oxygen to form a ketone during lubricant oxidation, instead of abstracting a hydrogen atom to form secondary alcohol is expected to be considerably lower than the (42 ± 5) % found for pristane oxidation in these experiments, probably in the range of 5 – 10 %.

In other work from these labs, ketones from squalane oxidation were analysed using GC-MS EI and CI, and comparison to NIST library database of MS-EI results was made, details Appendix B.¹¹⁶

Consequently, the following sections give some extended information on squalane degradation and the autoxidation of squalane will be examined to establish whether similar oxidation mechanisms occur with larger alkane compared to smaller ones, such as pristane.

3.3 Results

The GC-FID trace of oxidised squalane at 170 °C in the bench-top reactor is shown in Figure 3.10.

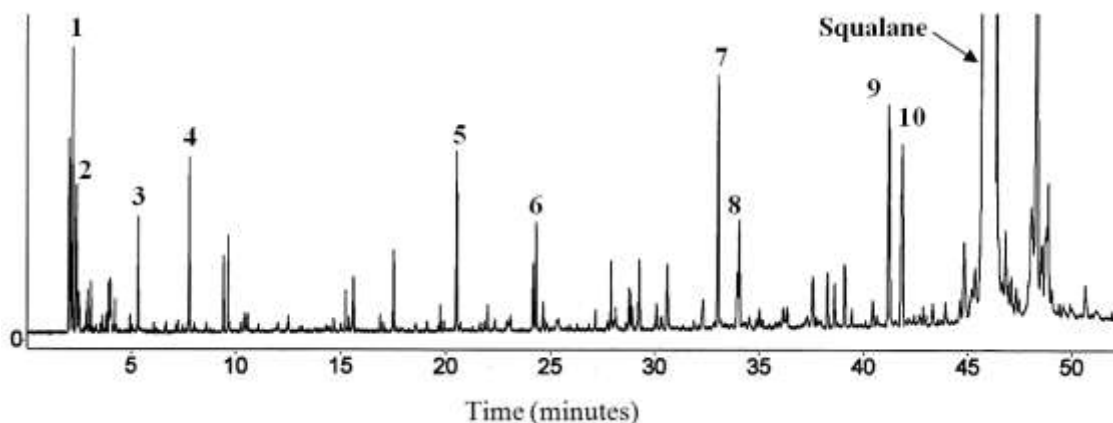
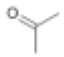
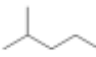
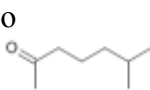
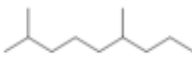
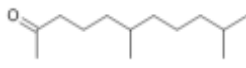
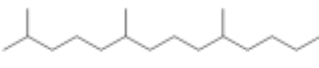

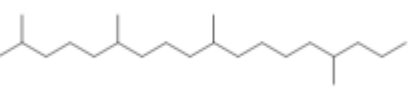
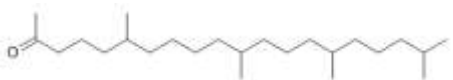
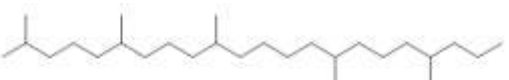


Figure 3.10: GC-FID trace of squalane oxidation for 10 minutes at 170 °C in the static reactor. Peaks 1: propan-2-one; 2: 2-methylpentane; 3: 6-methylhept-2-one; 4: 2, 6-dimethylnonane; 5: 6,10-dimethylundecan-2-one; 6: 2,6,10-trimethyltetradecane; 7: 7,11,15-trimethylhexadecan-2-one; 8: 2,6,10,15-tetramethyloctadecane; 9: 6,11,15,19-pentamethyleicosan-2-one; 10: 2,6,10,15,19-pentamethyldocosane; and 11: 2,6,10,15,19,23-hexamethyltetracosane (Squalane).

This work focuses mainly on the identification of alkanes, which are the second significant peaks numbered: 2, 4, 6, 8 and 10 on the GC trace in Figure 3.10. Five large peaks of ketones were previously identified by Alfadhl, using GC-MS electron ionisation and ammonia chemical ionisation,¹¹⁶ numbered: 1, 3, 5, 7 and 9, and their analysis is confirmed here adding field ionisation (FI) technique. The structures and relative molar masses of identified alkanes and ketones are shown in Table 3.2.

Identification of alkanes (this work) included two complementary analyses the GC-MS FI and the EI. The FI was useful in obtaining information about the molecular mass ion, where the EI gave the characteristic fragmentation patterns, allowing to suggest the appropriate structures.

Table 3.2: Chemical structures and molecular weights of squalane oxidation products.

 <p>1 Name: propanone (acetone) Mr: 58</p>	 <p>2 Name: 2-methyl-pentane Mr: 86</p>
 <p>3 Name: 6-methyl-2-heptanone Mr: 128</p>	 <p>4 Name: 2,6-dimethyl-nonane Mr: 156</p>
 <p>5 Name: 6,10-dimethylundecan-2-one Mr: 198</p>	 <p>6 Name: 2,6,10-trimethyltetradecane Mr: 240</p>
 <p>7 Name: 7,11,15-trimethylhexadecan-2-one Mr: 282</p>	 <p>8 Name: 2,6,10,15-tetramethyloctadecane Mr: 310</p>
 <p>9 Name: 6,11,15,19-tetramethyleicosan-2-one Mr: 352</p>	 <p>10 Name: 2,6,10,15,19-pentamethyldocosane Mr: 380</p>

GC-MS EI results were also compared with EI data from NIST database and confirmations of the characteristic mass ion fragments for smaller alkanes were possible. The similarity indices were not included as for the structural similarity the library matches were not always reliable. Comparison of the GC-MS EI spectra with the library EI data from NIST database are presented in Table 3.3. Where suitable library matches were not available, assignments were made using mass spectrum data, GC retention times and the similarity of this spectrum to that of the previously identified for

smaller molecules the example of identification of 2,6,10,15-tetramethyloctadecane is shown in Figure 3.4

Table 3.3: GC-MS EI mass spectra matched with NIST Library results (this work).

No	Assignment	EI-MS m/z (relative intensity)	NIST Library EI-MS m/z
1	propanone	43 (100) 58 (35)	43 (100) 58 (64)
2	2-methylpentane	41 (31) 42 (42) 43 (100) 57 (10) 71 (32) 86 (18)	41 (29) 42 (54) 43 (100) 57 (10) 71 (27) 86 (3)
3	6-methylhept-2-one	43 (90) 58 (100) 71 (18) 85 (12) 95 (21) 110 (24) 128 (6)	43 (100) 58 (73) 71 (12) 85 (7) 95 (10) 110 (8) 128 (3)
4	2,6-dimethyl nonane	43 (69) 57 (78) 71 (100) 85 (15) 97 (1) 113 (22) 126 (1) 127 (2) 141 (3) 156 (2)	43 (98) 57 (77) 71 (75) 85 (8) 97 (2) 113 (6) 126 (1) 141 (2) 156 (1)
5	2,10-dimethylundecan-2-one	43 (60) 58 (100) 71 (29) 85 (18) 95 (19) 109 (22) 123 (6) 140 (7) 180 (11) 198 (0.1)	43 (98) 58 (100) 71 (32) 85 (16) 109 (11) 123 (4) 140 (6) 180 (8) 198 (1)
6	2,6,10-trimethyltetradecane	43 (52) 57 (100) 71 (80) 85 (63) 99 (21) 113 (21) 127 (8) 155 (17) 183 (5) 197 (0.9) 211 (1) 225 (2) 240 (0.5)	43 (78) 57 (100) 71 (64) 85 (50) 99 (9) 113 (13) 127 (4) 155 (13) 183 (6) 197 (1) 211 (1) 225 (1) 240 (1)
7	7,11,15-trimethylhexadecan-2-one	43 (62) 58 (100) 71 (40) 85 (23) 95 (24) 109 (48) 123 (17) 137 (24) 151 (4) 179 (9) 193 (3) 222 (29) 249 (1) 264 (7) 282 (0.1)	No data available
8	2,6,10,15-tetramethyloctadecane	43 (46) 57 (100) 71 (96) 85 (62) 99 (28) 113 (27) 127 (21) 141 (8) 155 (12) 183 (7) 197 (2) 211 (3) 227 (2) 239 (1) 252 (0.3) 267 (0.5) 281 (0.5) 295 (0.1)	No data available
9	6,11,15,19 – pentamethyleicosan-2-one	43 (59) 58 (100) 71 (44) 83 (34) 85 (30) 95 (46) 109 (62) 123 (23) 138 (22) 151 (5) 179 (2) 193 (6) 222 (8) 249 (1) 264 (1) 282 (2) 334 (40) 352 (0.1)	No data available
10	2,6,10,15,19-pentamethyldocosane	43 (43) 57 (100) 71 (96) 85 (72) 99 (32) 113 (31) 127 (22) 141 (23) 155 (13) 183 (14) 197 (9) 211 (1) 225 (2) 239 (1) 253 (0.3) 267 (0.4) 281 (0.2) 295 (0.4) 336 (0.2) 350 (0.1) 365 (0.1)	No data available
11	2,6,10,15,19,23-hexamethyltetracosane (squalane)	43 (25) 57 (85) 71 (100) 85 (95) 99 (70) 113 (85) 127 (70) 141 (50) 155 (45) 169 (40) 183 (55) 197 (25) 211 (20) 225 (5) 239 (20) 253 (1) 267 (6) 281 (1) 295 (1) 309 (1) 336 (1)	43 (45) 57 (100) 71 (76) 85 (48) 99 (30) 113 (40) 127 (28) 141 (15) 155 (14) 169 (12) 183 (30) 197 (6) 211 (5) 225 (3) 239 (28) 253 (1) 267 (7) 281 (1) 295 (1) 309 (1) 323 (1) 336 (1) 337 (1) 350 (1)

Peak 8: 2,6,10,15-tetramethyloctadecane**Mass Spectrum**

43 (46) 57 (100) 71 (96) 85 (62) 99 (28) 113 (27) 127 (21) 141 (8) 155 (12) 183 (7) 197 (2) 211 (1) 225 (2) 239 (1) 253 (1) 267 (1) 281 (1) 295 (1)

Assignment

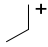
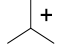
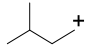
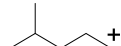
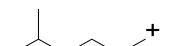


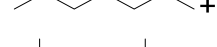
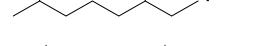
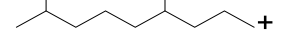
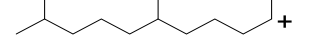
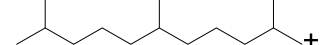
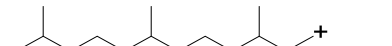


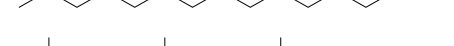
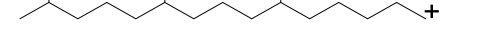
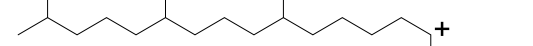
43 (C ₃ H ₇)	
57 (C ₄ H ₉)	
71 (C ₅ H ₁₅)	
85 (C ₆ H ₁₃)	
99 (C ₇ H ₁₅)	
113 (C ₈ H ₁₇)	
127 (C ₉ H ₁₉)	
141 (C ₁₀ H ₂₁)	
155 (C ₁₁ H ₂₃)	
183 (C ₁₃ H ₂₇)	
197 (C ₁₄ H ₂₉)	
211 (C ₁₅ H ₃₁)	
225 (C ₁₆ H ₃₃)	
239 (C ₁₇ H ₃₅)	
253 (C ₁₈ H ₃₇)	
267 (C ₁₉ H ₃₉)	
281 (C ₂₀ H ₄₁)	
295 (C ₂₁ H ₄₃)	

Figure 3.4: Example of GC-MS EI identification of 2,6,10,15-tetramethyloctadecane.

The GC-MS FI results are summarised in Table 3.4 together with ammonia CI data, (which gives fragment [M+18]) from previous work,¹¹⁶ which were added here as supporting data.

Table 3.4: Measured FI (this work) and ammonia CI (previous work) mass spectra for squalane oxidation.

No	Assignment	FI-MS m/z	CI-MS m/z ^a
1	propanone	No data available	No data available
2	2-methylpentane	No data available	No data available
3	6-methylhept-2-one	110 (15) [M-18], 128 (100) [M], 129 (12) [M+1]	58 (78) 71 (25) 85 (32) 95 (40) 110 (100) [M-18], 128 (15) [M], 129 (25) [M+1], 134 (7) 146 (89) [M+18]
4	2,6-dimethyl nonane	156 (100) [M], 157 (12) [M+1]	No data available
5	2,10-dimethylundecan-2-one	43 (8) 180 (42) [M-18], 198 (100) [M], 199 (21) [M+1]	58 (32) 69 (14) 85 (24) 95 (22) 109 (30) 140 (11) 180 (41) [M-18], 198 (8) [M], 199 (13) [M+1], 216 (100) [M+18]
6	2,6,10-trimethyltetradecane	240 (100) [M], 241 (20) [M+1]	No data available
7	7,11,15-trimethylhexadecan-2-one	222 (7) 264 (31) [M-18], 282 (100) [M], 283 (29) [M+1]	58 (23) 82 (15) 95 (17) 109 (30) 123 (10) 137 (16) 151 (5) 179 (6) 222 (25) 264 (14) [M-18], 282 (8) [M], 300 (100) [M+18]
8	2,6,10,15-tetramethyloctadecane	43 (11) 239 (12) 308 (10) 310 (100) [M], 311 (23) [M+1]	No data available
9	6,11,15,19 – pentamethyleicosan-2-one	43 (7) 334 (60) [M-18] 352 (100) [M]	No data available
10	2,6,10,15,19-pentamethyldocosane	43 (15) 380 (100) [M]	No data available
	2,6,10,15,19,23-hexamethyltetracosane (squalane)	43 (18) 422 (100) [M]	No data available

^aRef. 116

The EI and FI (and previous work CI) techniques are used here as complementary methods.

3.4 Discussion

This work reports results from the autoxidation of squalane. A significant number of the products identified from squalane autoxidation are ketones and alkanes, which are smaller and more volatile than squalane itself. These products are associated with the decomposition via beta-scission of the tertiary alkoxy radicals (2-squaloxyl, 6-squaloxyl and 10-squaloxyl) in a similar way to pristane. An example of the 6-squaloxyl radical cleaving between carbons 5 and 6 is shown in Figure 3.5, reaction [3.6], this decomposition forms a fragment methyl ketone and a primary alkyl radical.

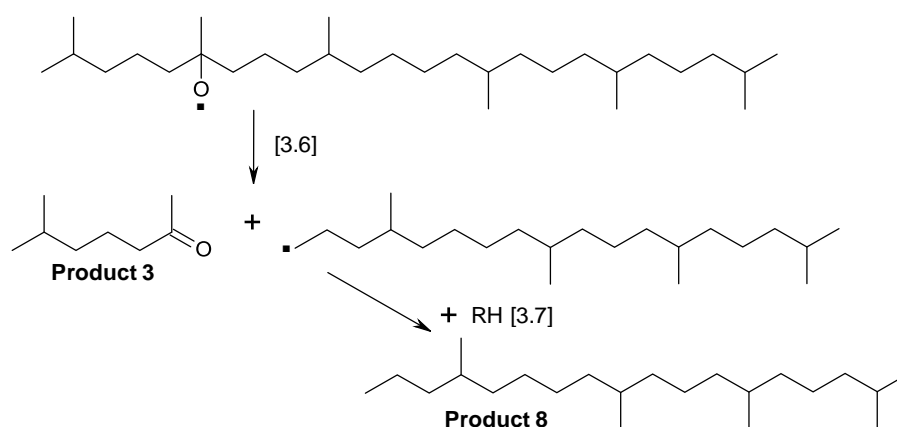


Figure 3.5: Mechanism of ketones and alkanes formation from squalane.

Similarly, as for a pristane study, the significant proportion of these primary alkyl radicals does not add oxygen, but abstract the hydrogen to form fragment alkanes instead. (See, for example, reaction [3.7]).

The summary of initial radical attacks, by which all these squalane autoxidation products are formed are shown in Table 3.5.

Table 3.5: Products formed during the autoxidation of squalane with the carbon initially attacked given.

Peak No.	Product	Squaloxyl radical	Reactions
1	Propanone	2-squaloxyl	[3.6]
2	2-methylpentane	6-squaloxyl	[3.6], [3.7]
3	6-methylhept-2-one	6-squaloxyl	[3.6]
4	2,6-dimethylnonane	6-squaloxyl	[3.6], [3.7]
5	6,10-dimethylundecan-2-one	6-squaloxyl	[3.6]
6	2,6,10-trimethyltetradecane	10-squaloxyl	[3.6], [3.7]
7	7,11,15-trimethylhexadecan-2-one	10-squaloxyl	[3.6]
8	2,6,10,15-tetramethyloctadecane	6-squaloxyl	[3.6], [3.7]
9	6,11,15,19-tetramethyleicosan-2-one	6-squaloxyl	[3.6]
10	2,6,10,15,19-pentamethyldocosane	2-squaloxyl	[3.6], [3.7]

The reference oxidation products were quantified using an effective carbon number technique,¹¹⁷ (described in Appendix A) and all results of which are summarised in Table 3.6. Comparing concentrations of fragment alkanes and ketones formed at 170 °C the ratio was approximately 1:5 for 2-squaloxyl, 1:1 for 6-squaloxyl and 1:2 for 10-squaloxyl site attack.

Table 3.6: Concentration of alkanes and ketones formed by squalane oxidation at 170 °C (for ca. 10 min.) in the bench-top reactor depended on carbon number.

Peak No.	Carbon number	Concentration (mol dm ⁻³)	Peak No.	Carbon number	Concentration (mol dm ⁻³)
1	C ₃ – ketone	1.12E-02	6	C ₁₇ - alkane	1.37E-03
2	C ₆ – alkane	4.12E-03	7	C ₁₉ - ketone	3.38E-03
3	C ₈ – ketone	1.80E-03	8	C ₂₂ - alkane	1.87E-03
4	C ₁₁ – alkane	2.28E-03	9	C ₂₄ - ketone	2.69E-03
5	C ₁₃ – ketone	2.41E-03	10	C ₂₇ - alkane	2.30E-03

Squalane has fragmentation products clearly formed in a similar manner to pristane. As it is less volatile than pristane it is also a more useful as a chemical model of lubricant base fluids, thus allowing oxidation at higher temperatures than pristane. Furthermore, the larger oxidation products, such as 6,11,15,19-tetramethyleicosan-2-one and 2,6,10,15,19-pentamethyldocosane, are easily identifiable by GC and are relatively unreactive and involatile, thus are useful markers for identifying the early stages during the oxidation of squalane, for instance when inhibited by antioxidants.

Analysis of ketones and alkanes from the autoxidation of squalane shows a similarity of products formation when compared with the previously studied smaller branched alkane, pristane. Therefore, other products which form from the autoxidation of squalane, such as: alkenes, alcohols, acids and lactones, which have not been identified in this work, possibly form in the similar way as for pristane. The GC-FID trace of oxidised squalane (Figure 3.10) also showed some significant peaks after the squalane, which are possibly the tertiary alcohols from squalane. However those were difficult to analyse by GC MS EI, and future work should possibly use softer CI analysis to identify squalane alcohols, as this technique was successfully used in the pristanols identification.

3.5 Conclusion

Understanding the liquid phase oxidation of squalane is crucial in future lubricant degradation studies and investigating its oxidation products is a very sensitive way of monitoring degradation of the parent molecule.

Squalane products have been identified (Table 3.5) and quantified (Table 3.6) and the reaction mechanism for their formation compared to previous work on pristane (Figure 3.5).¹⁰⁷ The concentration of ketones and alkanes was monitored; this information can be used to calculate the rate of oil degradation and give the indication of how much base fluid is reactive.

In previous work on the autoxidation in the liquid phase of pristane,¹³⁵ (a branch chain alkane smaller than squalane) Wilkinson also proposed a chemical mechanism for the formation of fragments (other than ketones and alkenes) such as: alkenes, alcohols, acids and lactones, these reactions can also explain the autoxidation of squalane.¹⁰⁷

Ketones, significant products of squalane oxidation, identified previously using GC-MS CI by Alfadhil,¹¹⁶ were also used in this study to explain the mechanism of alkanes formation.

The large fragment ketones and alkanes identified can be used as very sensitive markers for the onset of breakdown due to autoxidation of squalane.

Chapter 4: Reaction of Phenolic Antioxidants with NO₂ at Elevated Temperature

4.1 Introduction

In this chapter the reaction of a phenolic antioxidant, octadecyl 3-(3,5-di-*tert*-butyl-4-hydroxy-phenyl) propanoate (abbreviated here to OHPP), (BASF, Irganox® L107) , Figure 4.1, with 1000 ppm NO₂ in N₂ has been investigated at 180 °C, a temperature representative for engine piston ring pack conditions.

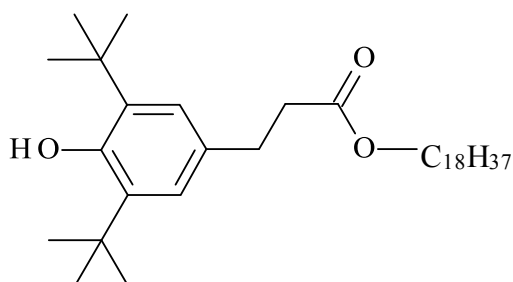


Figure 4.1: Structure of the commercial phenolic antioxidant octadecyl 3-(3,5-di-*tert*-butyl-4-hydroxy-phenyl) propanoate (OHPP), BASF Irganox® L107.

To support the analysis of products formed from OHPP, an additional phenolic compound was investigated, 2,6-di-*tert*-butyl-4-ethylphenol (EthPh), shown in Figure 4.2.

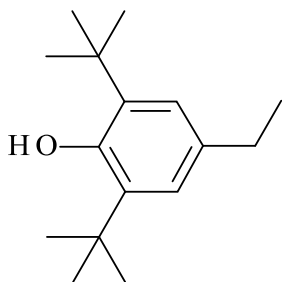


Figure 4.2: Structure of 2,6-di-*tert*-butyl-4-ethylphenol (EthPh).

4.2 Previous Studies on NO₂ + Phenolics

Engine lubricants are comprised of complex mixture of components,¹⁴³⁻¹⁴⁵ and commercial phenolic antioxidants, such as octadecyl 3-(3,5-di-*tert*-butyl-4-hydroxyphenyl)propanoate (OHPP), play an important role in improving the oxidative resistance of engine lubricants.

Previous work on the liquid-phase reactions of substituted phenols with NO₂ identified nitrophenols and nitrocyclohexadienones as the major products of reaction^{83,94,146-148}

However different reaction conditions were studied, for example: polar solvents or low temperatures; therefore these studies are not ideally representative of engine conditions, where lubricants are non-polar and the temperatures in the piston assembly can reach 180 °C. Therefore more work needs to be carried out to understand the behaviour of phenolic antioxidants in lubricant base fluids with NO₂ at piston ring pack conditions.

In fact, there have been a number of nitration mechanisms proposed; unfortunately, most of these lack detailed chemical analysis to support the proposed mechanisms and refer to an early detailed study, by Brunton *et al.* in 1979,⁸³ of the reaction of 4-methyl-2,6-di-*tert*-butylphenol (BHT) with 1 bar of NO₂ under oxygen free, room temperature conditions, Figure 4.3. The initial product of this mechanism was 4-nitro-4-methyl-2,6-di-*tert*-butyl cyclohexadienone, formed from NO₂ addition to the 4-methyl-2,6-di-*tert*-butylphenoxy radical, itself formed by the abstraction of the phenolic hydrogen atom by NO₂, reactions [4.1] and [4.2]. Subsequently, further reactions included the addition of NO₂ to double bonds which occurred with the formation of nitro-nitrite and nitro-alcohol compounds.

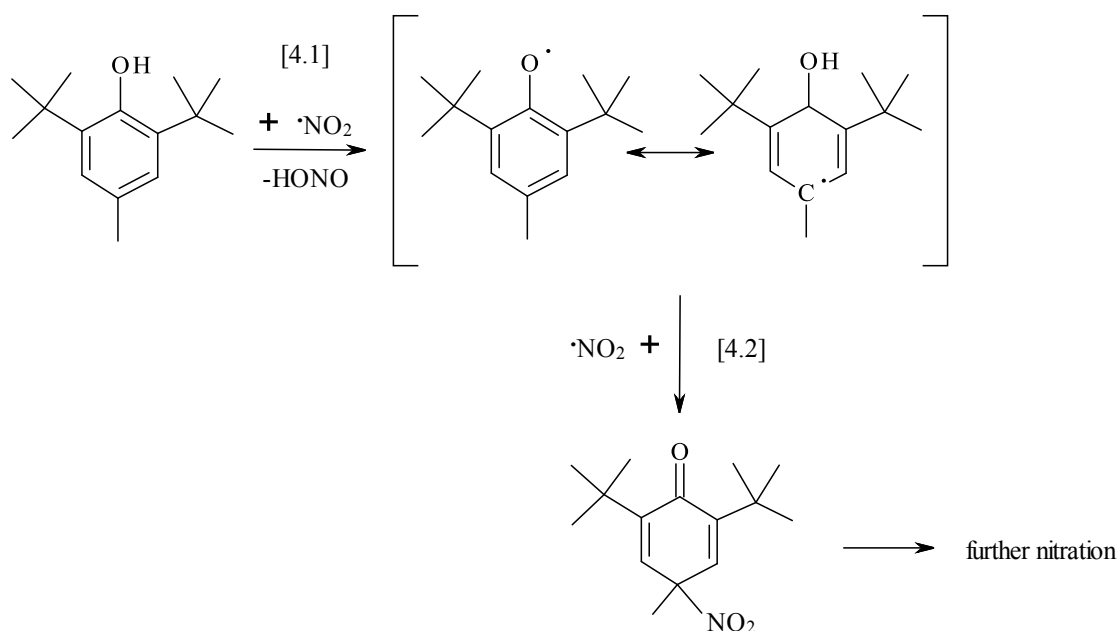


Figure 4.3: Brunton's mechanism for the reaction of phenolics with NO₂.⁸³

More recently, engine lubricant degradation studies based on the reaction of nitrogen dioxide in the air with a phenolic antioxidant by Johnson *et al.* in 1991,¹⁴⁶ proposed similar chemical mechanisms for the reaction of a phenolic antioxidant (2,6-di-*tert*-butyl-4-methylphenol) with NO₂, Figure 4.3, despite the experimental conditions being noticeably different to Brunton's studies (for example the reaction was carried out in presence of oxygen, at the higher temperature of 160 °C and in the non-polar solvent of n-hexadecane) and a lack of chemical analysis of the products formed from the reaction.

Astolfi *et al.* in 2005,⁹⁴ studied the effect of solvents on the reaction of nitrogen dioxide with substituted phenols (R = hydrogen or *tert*-butyl group in Figure 4.4) at room temperature and proposed a more complex mechanism than Brunton *et al.*, and which was based on the effects of solvents, such as: benzene, methanol and dimethyl sulfoxide (DMSO), and NO₂ mesomeric structures.⁸² Despite different solvents being used, the dominant reaction was nitration of phenolics with NO₂. The other reactions

observed were oxidation, dimerisation and nitrosation. The reaction mechanism reported by Astolfi *et al.*⁹⁴ is summarised in Figure 4.4. The initiation step is the same as for Brunton's mechanism, but further reactions show a variety of possibilities. In reactions [4.3] and [4.4], the authors proposed the addition of NO₂ to the phenoxyl radical in two different ways, due to the NO₂ mesomeric structures effect, described in Chapter 1. The predominant route suggested was the coupling of phenoxyl radical with nitrogen atom of NO₂ with the formation of 4-nitrocyclohexa-2,5-dienone, which then rearranges to nitrophenol, reaction [4.3]; with a secondary pathway involving coupling with the oxygen atom of NO₂, reaction [4.4], which then rearranges to quinone in

in polar solvents (reaction [4.5]).

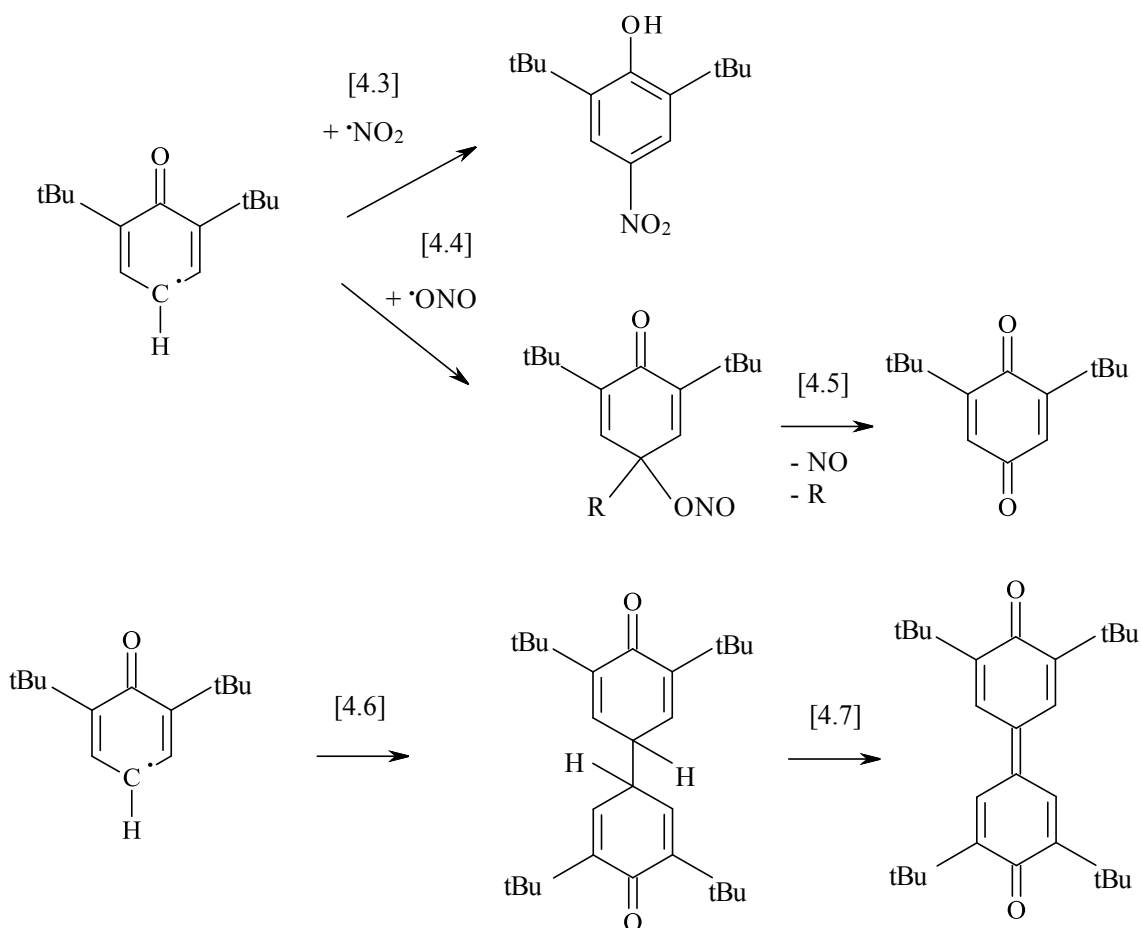


Figure 4.4: Astolfi's mechanism for the reaction of phenolics with NO₂.⁹⁴

In reactions [4.6] and [4.7], the diphenoquinone formation was proposed by the

dimerisation of phenoxy radicals obtained from di-*tert*-butylphenol (R = hydrogen).

Previous studies were not ideally representative of engine conditions, where lubricants are non-polar and the temperatures in the piston assembly can reach 180 °C,^{83,94,146-148} therefore more work needs to be carried out in order to understand the behaviour of phenolic antioxidants in the lubricant base fluids at piston temperatures. Consequently, a study of phenolic antioxidants (mainly commercial, octadecyl 3-(3,5-di-*tert*-butyl-4-hydroxy-phenyl)propanoate) with NO₂ was undertaken at 180 °C and a detailed qualitative and quantitative products analysis was performed.

4.3 Results and Discussion

The reaction of the commercial antioxidant (OHPP) with NO₂ was undertaken in a reactor as described in the experimental chapter. The initial oil volume was 7.0 ± 0.1 cm³, with a starting antioxidant concentration of 8.0×10^{-3} mol dm⁻³, 0.5% (w/w), which was representative of real engine lubricant formulations. The base oil was squalane (SQ) [99 % purity], which has chemical and physical properties similar to commercial base oils, but was easier to analyse, details in Chapter 3.¹⁰ The reaction temperature was 180 ± 1 °C and the pressure 1050 ± 10 mbar. The reaction gas contained 1000 ± 40 ppm of NO₂ in nitrogen and the flow rate was set up to approximately 50 ± 2 cm³ min⁻¹. NO₂ gas was dissolved in the model lubricant by stirring at 600 rpm using a magnetic stirring bar. Liquid samples (~ 0.5 cm³) were extracted during the reaction and analysed.

4.3.1 Product Identification by GC-FID

Samples taken during the reaction were analysed by GC-FID; results are shown in Figure 4.5. During the reaction, the antioxidant (OHPP) and an intermediate formed from it protected the base oil (SQ) from nitration. When both were consumed, base oil nitration products started to form, as described in the following sections.

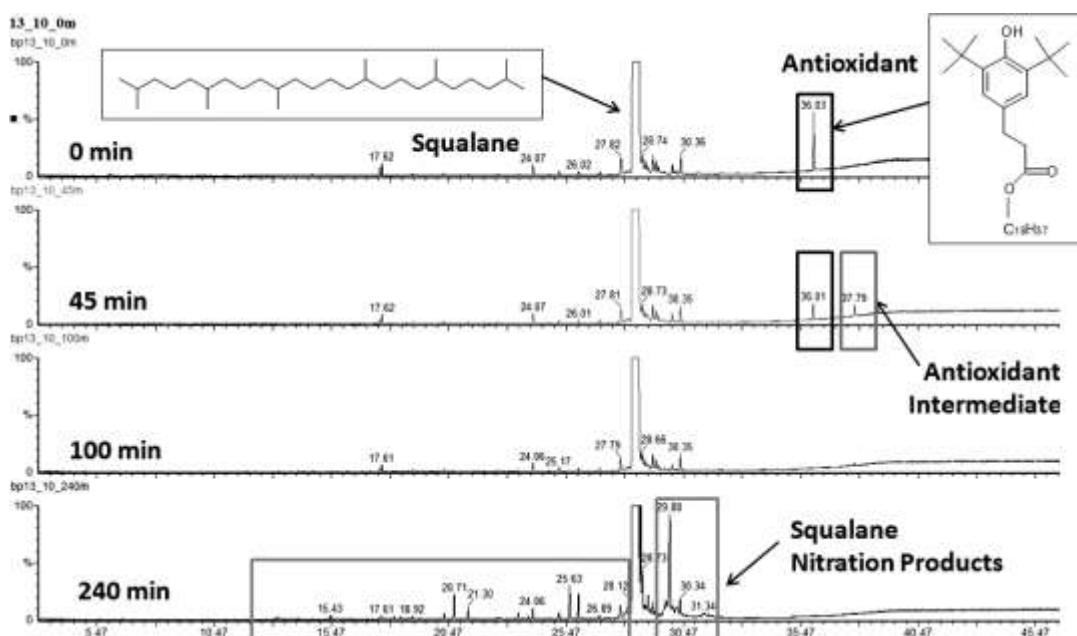


Figure 4.5: GC traces 0-240 min. of products formation from the reaction of OHPP in squalane with NO₂ at 180 °C.

Antioxidant depletion and the formation of an intermediate formed from the antioxidant were plotted as a function of concentration and reaction time, Figure 4.6.

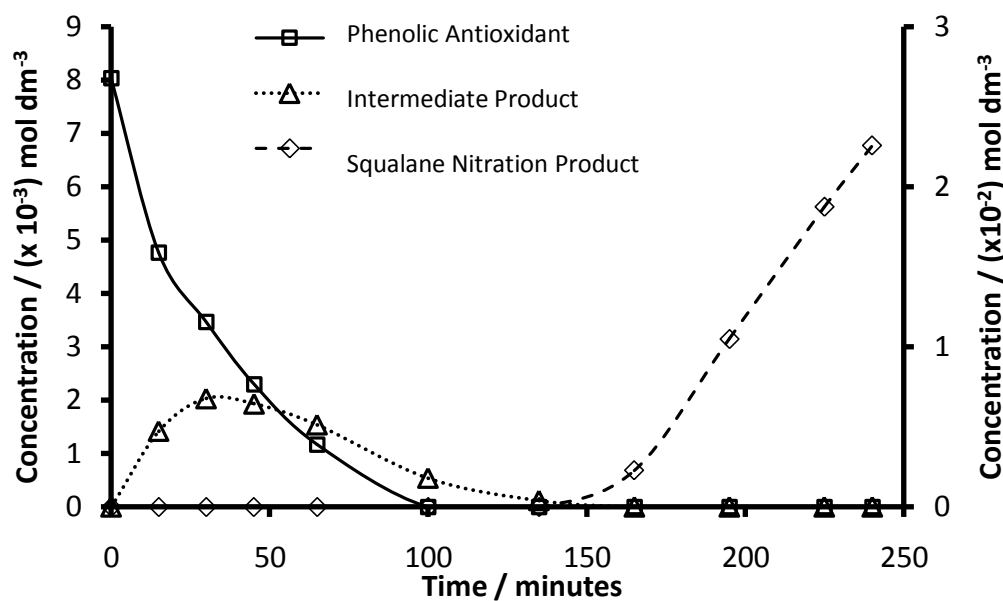


Figure 4.6: OHPP and intermediate (left hand axis) protecting the base oil from nitration up to 135 minutes. When both are consumed squalane nitration products form (right hand axis).

The GC quantified results show that approximately 40 % of OHPP had reacted by 15 minutes, with approximately 50 % of the reacted antioxidant accounted for by the formation of the intermediate, which demonstrates that the reaction of the antioxidant with NO₂ to this antioxidant intermediate was significant.

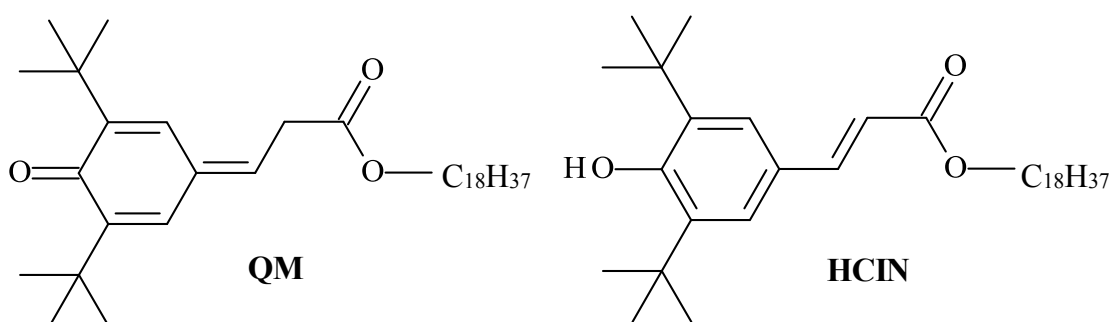
4.3.2 Product Identification by High Resolution GC-MS FI and EI

The intermediate product was analysed by GC-MS FI and EI the detailed fragmentation patterns of the antioxidant and its intermediate are shown in Table 4.1 (EI and FI spectra in Figures C1-C4, Appendix C).

Table 4.1: The accurate GC-MS EI and FI detail fragmentation patterns of phenolic antioxidant and its intermediate formed from reaction with NO₂ at 180 °C.

Peak Assignment	EI-MS m/z (<i>relative intensity</i>)(<i>this work</i>)	FI-MS m/z
OHPP	57.062 (34), 68.988 (6), 219.175 (30), 220.179 (6), 515.491 (90), 530.515 (100), 531.517 (36), 532.520 (8)	530.475 (100) [M], 531.487 (40) [M+1], 532.480 (7) [M+2]
Intermediate Product	57.062 (49), 69.063 (30), 83.079 (23), 97.095 (19), 130.987 (10), 217.158 (8), 259.173 (12) 261.155 (25), 276.180 (9), 513.474 (40), 528.497 (100), 529.500 (39), 530.502(7)	528.458 (100) [M], 529.461 (30) [M+1], 532.463 (4) [M+4]

The accurate GC-MS FI analysis provided evidence for an antioxidant intermediate with the formula ¹²C₃₅¹H₆₀¹⁶O₃ (the calculated molecular mass ion was 528.454; measured 528.458 ± 0.005), which is two Daltons lower than the antioxidant (OHPP) molecular mass ion (calculated m/z for ¹²C₃₅¹H₆₂¹⁶O₃ 530.470; found 530.475 ± 0.005). Two possible structures are immediately suggested for the antioxidant intermediate; the first octadecyl 3-(3,5-di-*tert*-butyl-4-oxo-cyclohexa-2,5-dien-1-ylidene)propanoate, quinone methide (QM) and the second octadecyl-3-(3,5-di-*tert*-butyl-4-hydroxy-phenyl)prop-2-enoate, hydroxy cinnamate (HCIN), which was identified previously as the oxidation product of OHPP,¹¹³⁻¹⁴⁹ structures Figure 4.7.

**Figure 4.7: Possible alternative structures of antioxidant intermediate; quinone methide (QM) and hydroxy cinnamate (HCIN).**

Various analytical techniques were used to help establish which of these two structures was more likely to be the intermediate identified by GC.

Fragment mass ions were obtained from the high resolution GC-MS EI mass spectra.

The characteristic mass ion fragment (Figure 4.8), of formula $^{12}\text{C}_{15}^{1}\text{H}_{21}^{16}\text{O}^+$ (calculated m/z 217.159; measured m/z 217.158 ± 0.005) suggests that the structure of the antioxidant intermediate is the QM. This can be compared to the equivalent cleavage in the parent antioxidant OHPP mass ion fragment, $^{12}\text{C}_{15}^1\text{H}_{23}^{16}\text{O}^+$ (calculated m/z 219.175; measured m/z 219.175 ± 0.005) and it can also be compared with the equivalent (unlikely) fragmentation for HCIN of $^{12}\text{C}_{15}^1\text{H}_{22}^{16}\text{O}^+$ for which the calculated mass of m/z 218.167 was not observed; this result supports the identification of the antioxidant intermediate as the quinone methide, Figure 4.8.

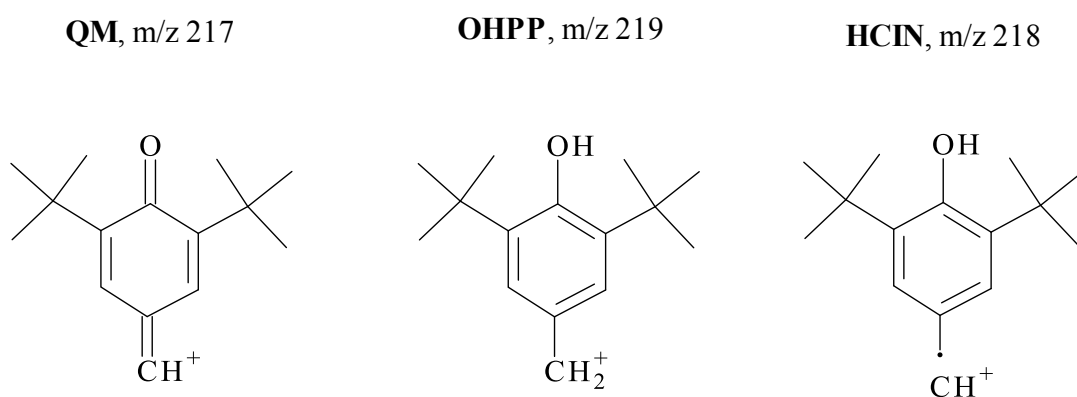
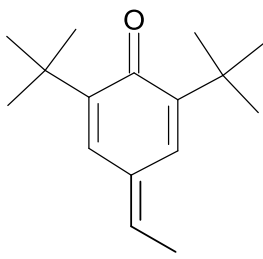


Figure 4.8: Characteristic EI fragmentation for QM, OHPP and HCIN.

To help with confirmation of the structure of the antioxidant intermediate another quinone methide compound was synthesised: 2,6-di-*tert*-butyl-4-ethylidene-cyclohexa-2,5-dien-1-one (QM1), (synthesis details in Chapter 2). This was also identified in the reaction mixture of EthPh with NO₂ the detailed fragmentation patterns are in Table 4.2, (chromatogram and EI mass spectra in Figures C5 and C6, Appendix C). As can be seen from Table 4.2, $m/z = 217$ is the most intense peak, and m/z 218 and m/z 219 are absent.

Table 4.2: GC-MS EI detail fragmentation patterns of antioxidant intermediate formed from the reaction of EthPh with NO₂ at 180 °C.

Peak Assignment	EI-MS m/z (<i>relative intensity</i>)(<i>this work</i>)
	57.172. (49), 67.891 (10), 77.978 (23), 87.233 (15), 91.034 (23), 115.332 (20), 128.337 (26), 133.435 (30), 147.194 (18), 161.089 (21), 175.115 (80), 189.129 (75), 203.151 (21), 217.159 (100), 232.184 (30), 233.265 (10)

Other supporting information was based on comparison to the synthesised hydroxy cinnamate (synthesised at University of York by G. Moody), detailed fragmentation patterns in table 4.3.

Table 4.3: GC-MS EI detail fragmentation patterns of synthesised HCIN.

Peak Assignment	EI-MS m/z (<i>relative intensity</i>)(<i>this work</i>)
HCIN	57.171 (92), 68.991 (72), 83.222 (12), 99.037 (10), 130.334 (48), 147.193 (10), 166.174 (20), 187.246 (21), 219.173 (93), 232.434 (10), 259.171 (45), 261.150 (15), 276.171 (30), 513.435 (87), 528.460 (100), 529.465 (90), 530.468 (8)

The accurate GC-MS EI fragmentation of synthesised HCIN shows fragment m/z 219.026 ± 0.005 ,¹⁵⁰ there was no m/z 218 possible fragmentation of HCIN, earlier suggested in Figure 4.8. This proves that m/z 218 cannot be used as an indication of the presence or absence of HCIN.

There was also no indication of m/z 217 fragment in the mass spectrum of HCIN, which was observed for QM1 (Table 4.2) and OHPP intermediate (Table 4.1), supporting the idea that the product of the reaction of OHPP with NO₂ is quinine methide, rather than hydroxy cinnamate.

4.3.3 Product Identification by UV-Vis

Colour development in samples taken during the reaction of phenolic antioxidant with NO₂ was partially attributed to the formation of reaction products of OHPP, Figure 4.9. The colour of the samples between 15-135 minutes of reaction changed from bright yellow to orange; at this time the reaction product from OHPP (observed by GC) was formed as a result of trapping the NO₂ radicals to prevent degradation of squalane. At 165 minutes, when all of the antioxidant and its intermediate were consumed, there is a distinct change in colour, with the bright yellow colour being attributed to squalane nitration products.

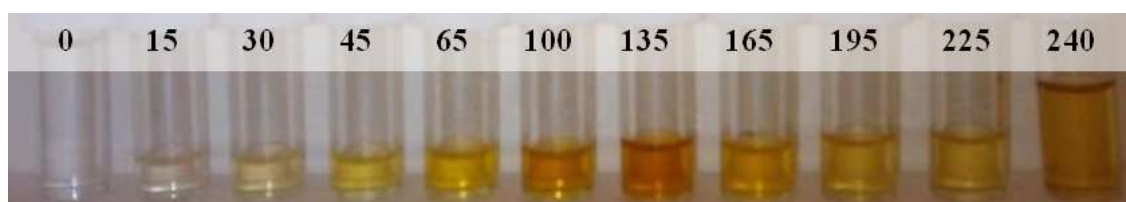


Figure 4.9: Colour development in samples 0-240min from reaction OHPP with NO₂ at 180 °C.

As the phenolic antioxidant, and also the intermediates formed from it, were found to be UV-Vis sensitive, the UV-Vis absorption spectra of several reaction mixtures were determined, Figure 4.10.

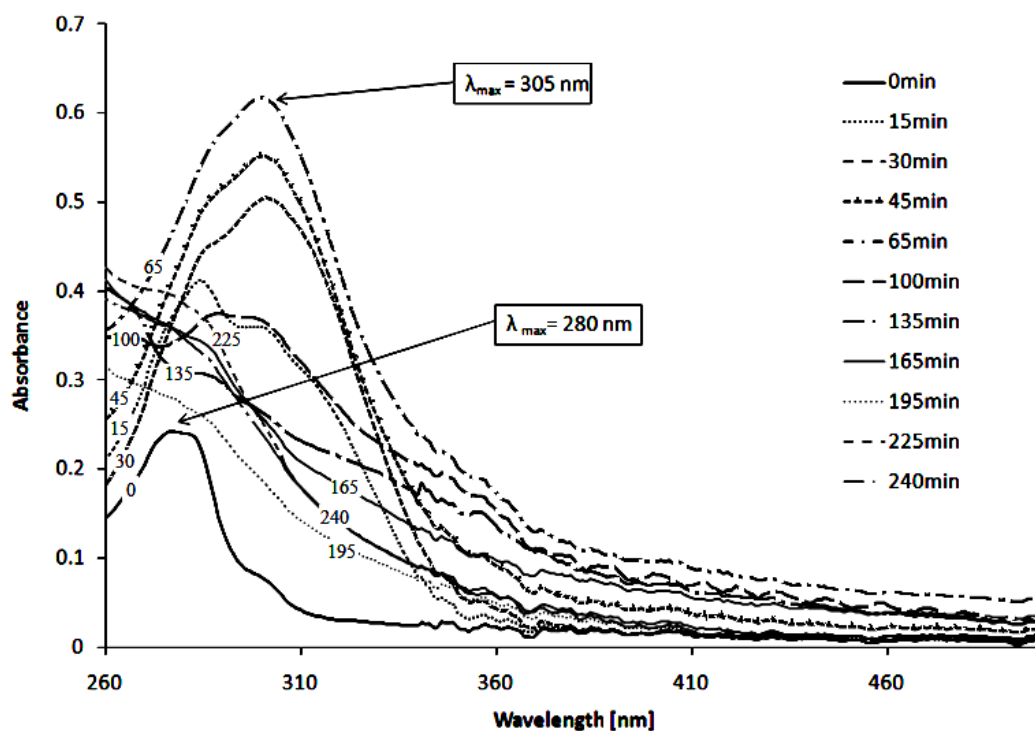


Figure 4.10: UV-Vis spectra of all samples from reaction of OHPP with NO₂ at 180 °C.

The starting material absorption showed a maximum at approximately $\lambda_{max} = 280 \text{ nm}$, characteristic for the phenolic antioxidant (OHPP), analysed previously by Klemchuk *et al.* 1991.¹⁴⁹ Samples extracted during the reaction containing intermediate product (as demonstrated by GC) showed strong absorption at approximately $\lambda_{max} = 305 \text{ nm}$, which was characteristic for quinone methide, compared with previous literature data.^{113,149,151}

QM has been previously mentioned in oxidation studies as a transient intermediate in the production of HCIN, but was not identified in previous studies and it was suggested that it would be highly unstable,¹¹ which is in contradiction to this work, where quinone methide was identified as the main product obtained by the reaction of the antioxidant with NO₂ (quantification by GC). Therefore, more investigation was undertaken using UV-Vis, and the spectrum of a similar synthesised quinone methide, the 2,6-di-*tert*-butyl-4-ethylidene-cyclohexa-2,5-dien-1-one (QM1), was obtained. The synthesised QM1 (synthesis details in chapter 2)¹²⁶ showed the maximum absorption to be at

approximately $\lambda_{\max} = 305$ nm, while the mixture from the reaction of EthPh with NO₂, containing 2,6-di-*tert*-butyl-4-ethylidene-cyclohexa-2,5-dien-1-one, showed also a similar absorption at approximately $\lambda_{\max} = 304$ nm, Figure 4.11.

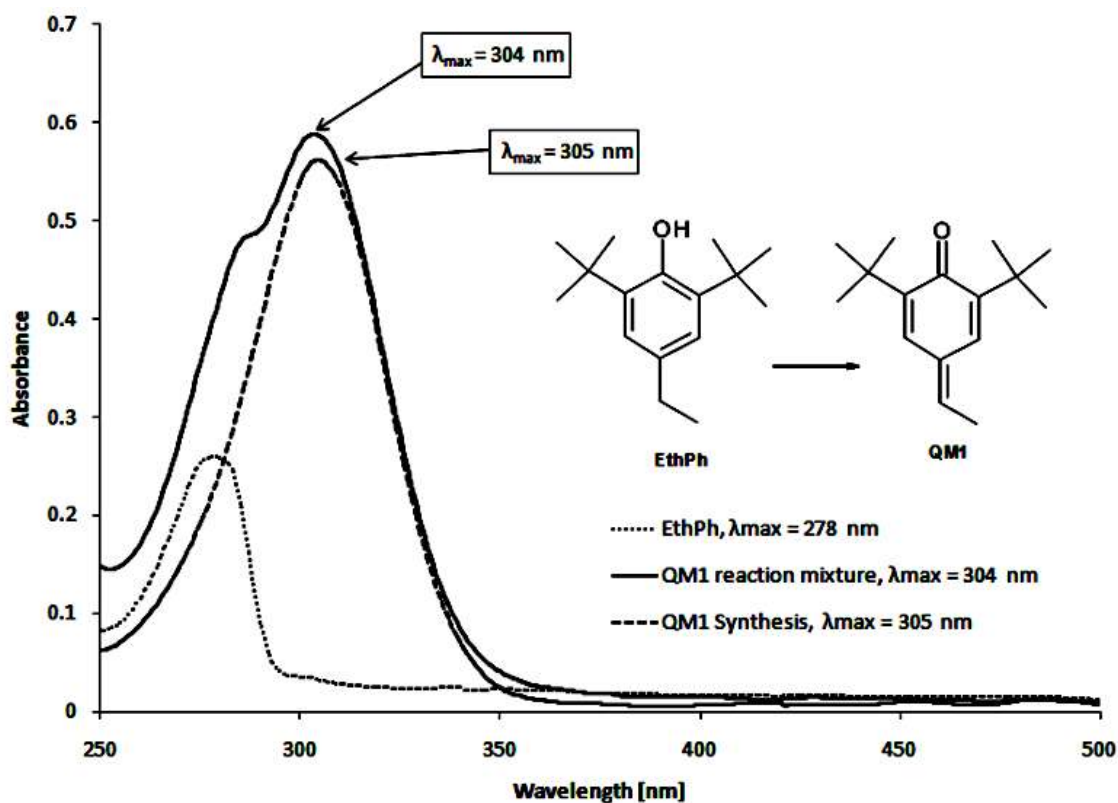


Figure 4.11: UV-Vis spectra of synthesised 2,6-di-*tert*-butyl-4-ethylidene-cyclohexa-2,5-dien-1-one (QM1), reaction mixture with quinone methide intermediate (QM1) and starting material (EthPh).

This result supports QM (from OHPP) identification as it shows that the characteristic absorption at approximately 305 nm is similar for other quinone methides.

Analysis of another standard component, hydroxy cinnamate, shows UV-Vis absorption at approximately $\lambda_{\max} = 314$ nm,¹¹³ which was compared with UV-Vis spectrum of reaction mixture containing OHPP intermediate product, Figure 4.12.

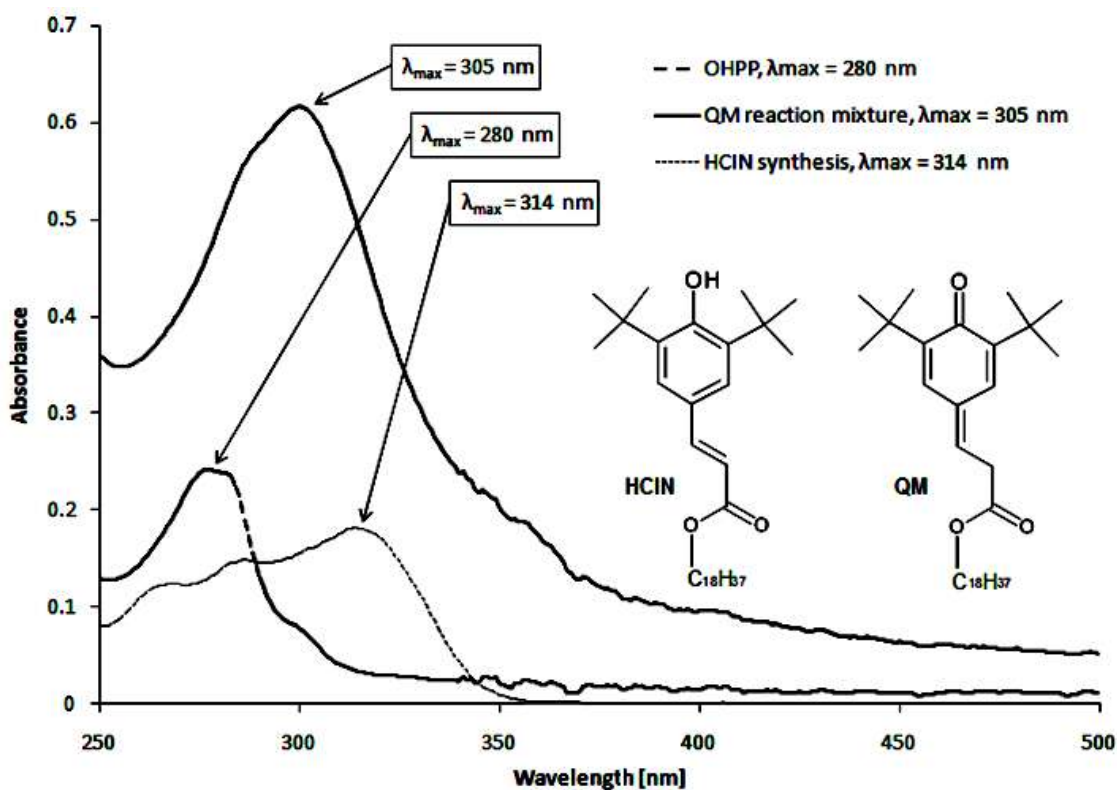


Figure 4.12: UV-Vis spectra of starting material with an antioxidant (OHPP) and reaction mixture with intermediate (QM) comparing to model compound of hydroxyl cinnamate (HCIN).

The UV-Vis analysis is consistent with QM formation, but does not completely exclude the formation of HCIN, which has a weaker absorption and could be part of the broad peak. Similar UV-Vis absorption have been observed using GPC UV-Vis analysis (in Appendix C), which separates molecules due to their size and which showed that the intermediate product (QM) is of a similar size to the antioxidant, and is not a dimer (a possible structure suggested by Pospisil et al. during oxidation studies).¹¹³

4.3.4 Product Identification - 1D and 2D proton NMR (COSY, DOSY)

The proton NMR identification of the reaction mixture was based on comparison to the model compounds (synthesised HCIN and QM1) and it was also supported using predicted ¹H NMR spectra, obtained using ACD/I-lab ¹H NMR Prediction Software, which spectra can be calculated to quoted accuracy of ± 0.3 ppm for ¹H NMR.

Samples were primarily run on the 1D proton NMR and the characteristic chemical shifts for both HCIN and QM were identified at 5 to 15 minutes of reaction; these results are shown in Figure 4.13 (full range NMR in Figure C11, Appendix C).

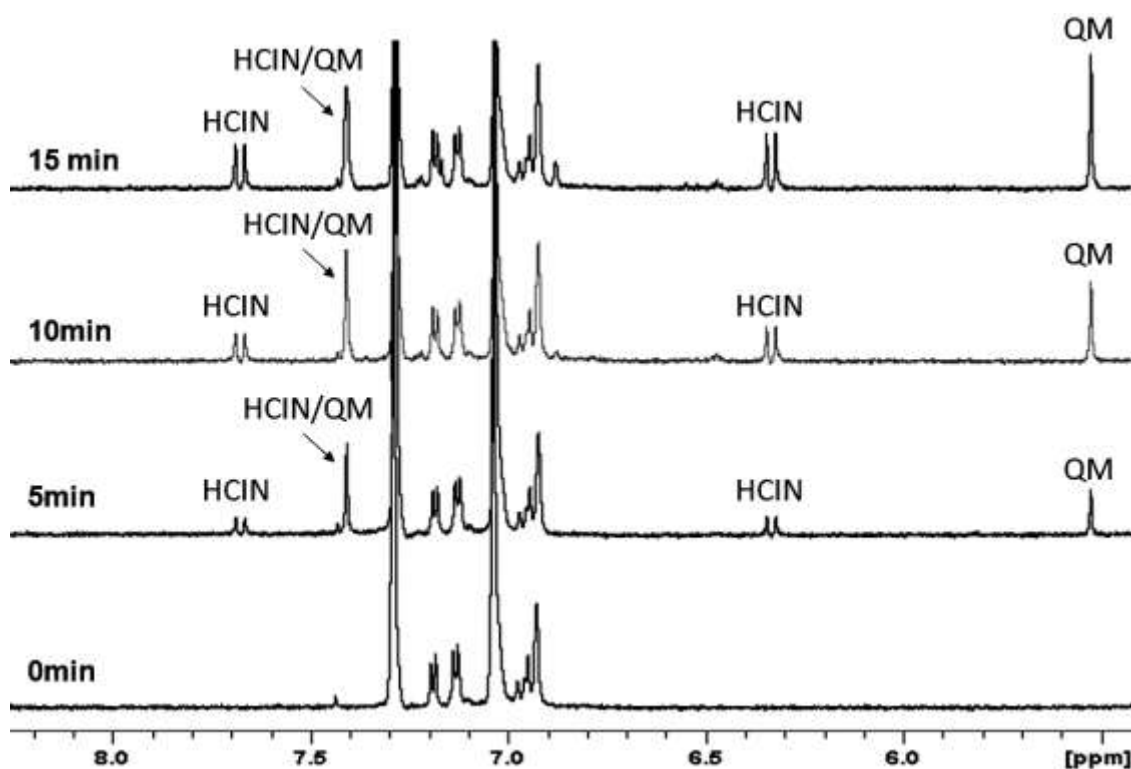


Figure 4.13: High resolution 700 MHz 1D ¹H NMR spectra of reaction mixture 0 to 15 min. (in CDCl₃) with identified products from antioxidant depletion: HCIN = Hydroxy Cinnamate and QM = Quinone Methide.

Two doublets $\delta = 7.7$ ppm (H, CH) and $\delta = 6.3$ ppm (H, CH) were identified as characteristic for trans coupling (-CH=CH- double bond) of HCIN, whereas the chemical shift at $\delta = 5.5$ ppm (H, CH at α carbon to the benzene ring) was identified as characteristic for QM.

The identification of HCIN in the reaction mixture was based on a comparison to the proton NMR of model compound (synthesised HCIN), which spectrum showed the same two doublets at approximately 7.7 ppm and 6.3 ppm characteristic for trans coupling, as in the reaction mixture, Figure 4.14.

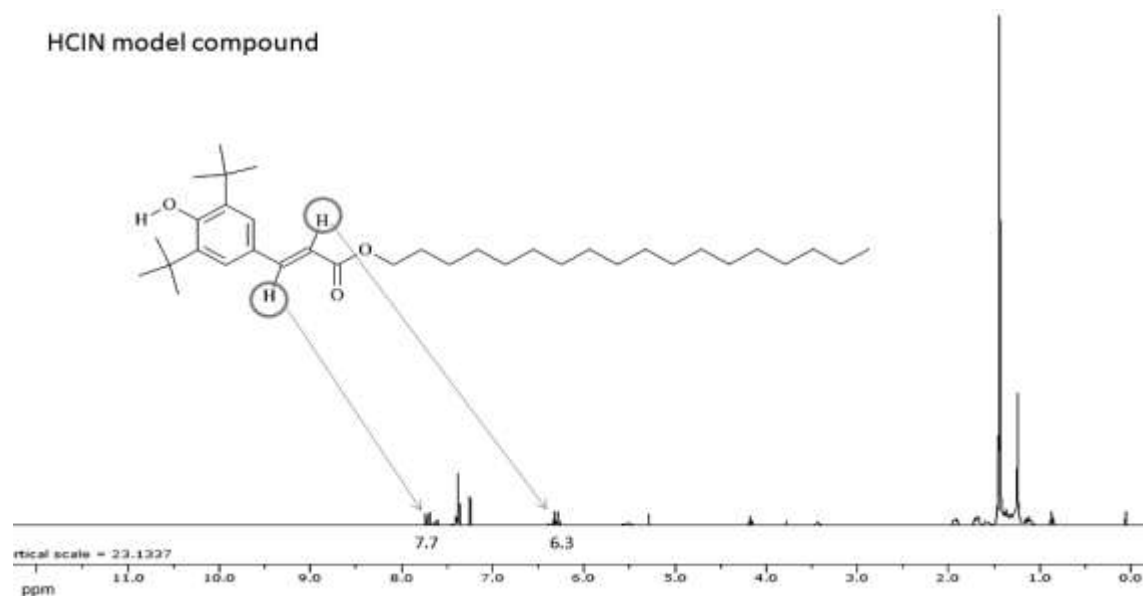


Figure 4.14: Proton NMR spectrum of hydroxy cinnamate (model compound), obtained using Bruker 400 MHz (solvent CDCl₃), synthesised at University of York by G. Moody.

These two doublets were also calculated for HCIN using prediction software (predicted spectrum of HCIN Figure 4.15) which supporting the identification of hydroxy cinnamate in the reaction mixture.

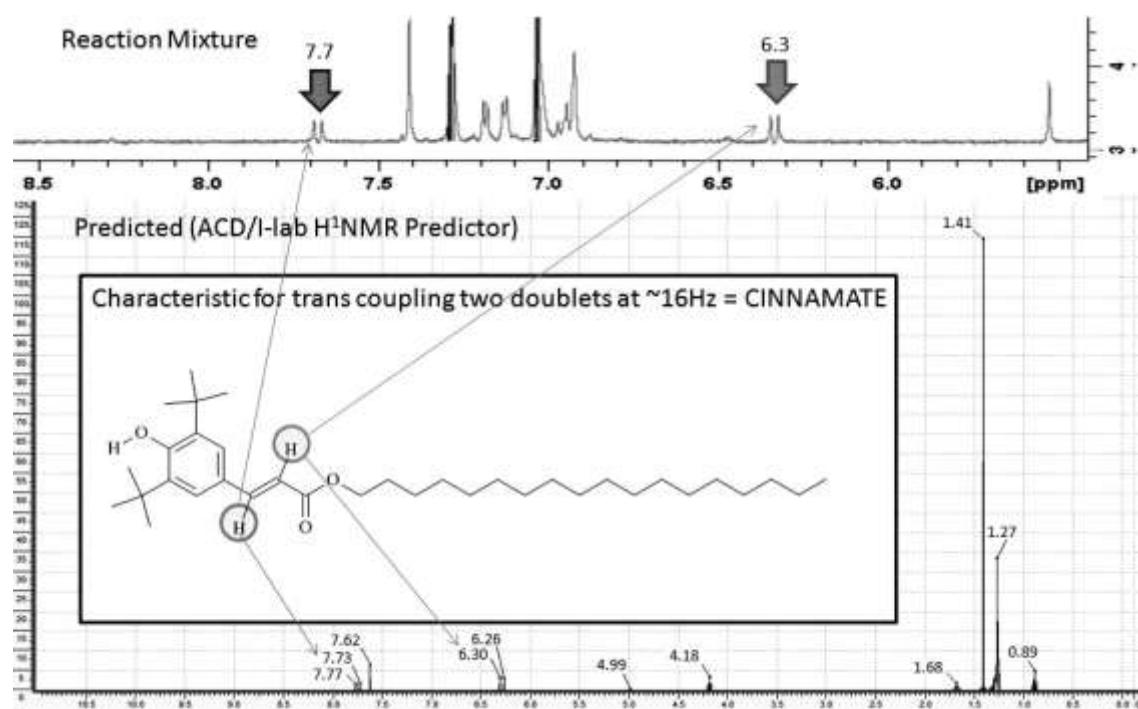


Figure 4.15: Comparison of predicted HCIN spectrum, obtained using ACD/I-lab ¹H NMR Prediction Software, to 5 min. reaction mixture.

The secondly predicted ¹H NMR spectrum of quinone methide has been obtained, in Figure 4.16.

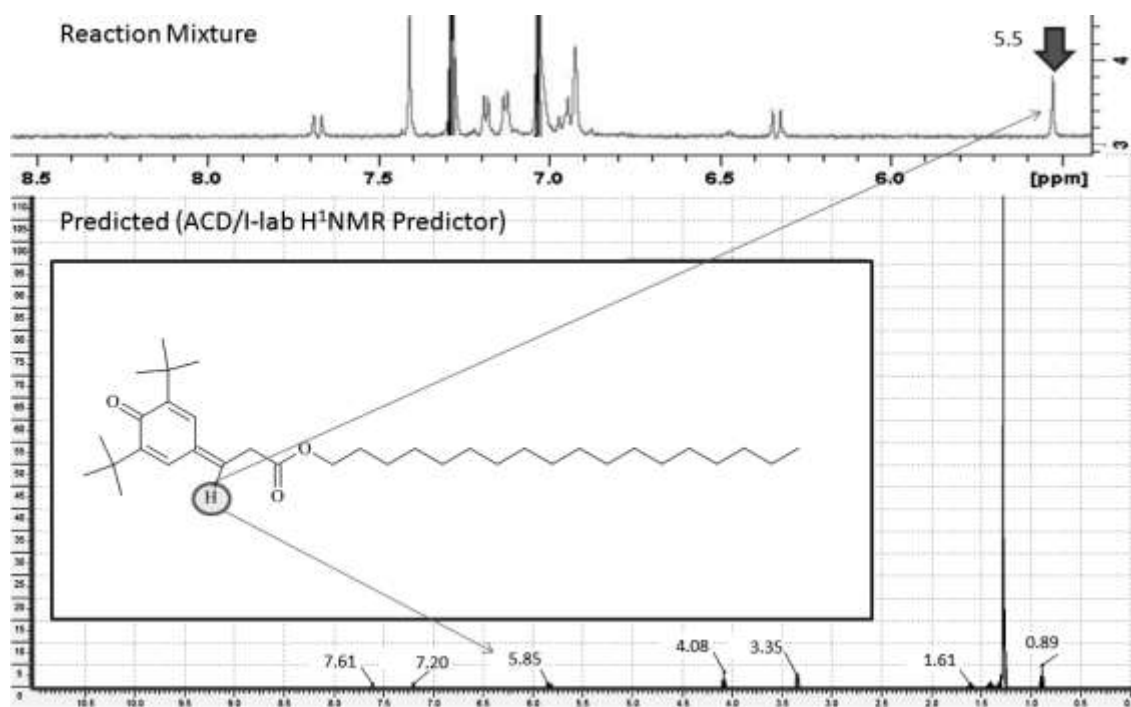


Figure 4.16: Comparison of predicted QM spectrum, obtained using ACD/I-lab ¹H NMR Prediction Software, to 5 min. reaction mixture.

The characteristic chemical shift at $\delta = 5.5$ ppm in the reaction mixture showed 5.8 ± 0.3 ppm on the predicted spectrum, which supports the identification of QM.

To compare, ¹H NMR of synthesised QM1 has been obtained with $\delta = 5.6$ ppm chemical shift (showed 5.9 ± 0.3 ppm on the predicted spectrum), and because of both QM and QM1 have similar structures, this analysis also supports the identification of QM.

All other chemical shifts characteristic for both, HCIN and QM, were reviewed, however they were not very useful in differentiating between the two. For example, the $\delta = 7.4$ ppm (predicted 7.6 ± 0.3 ppm) chemical shift, was common to both Hydroxy Cinnamate and Quinone Methide, details in Appendix C, Figures C12-C14.

Peaks between 7.5 to 6.5 ppm, sample 0 min., correspond to phenol region, hydrogens of benzene ring and quinone ring protons.

To determine the (OH) hydrogen of phenolic antioxidant the proton NMR is not a particularly helpful technique, as this hydrogen can appear in a very wide range of spectrum or sometimes cannot be seen at all, because it can H-bond or exchange with a solvent.

2D ¹H NMR DQF COSY and DOSY

Further qualitative analysis of the 10 minute sample by the 2D proton NMR (Figure 4.17), was undertaken using the double quantum filter correlation spectroscopy (DQF COSY sequence).

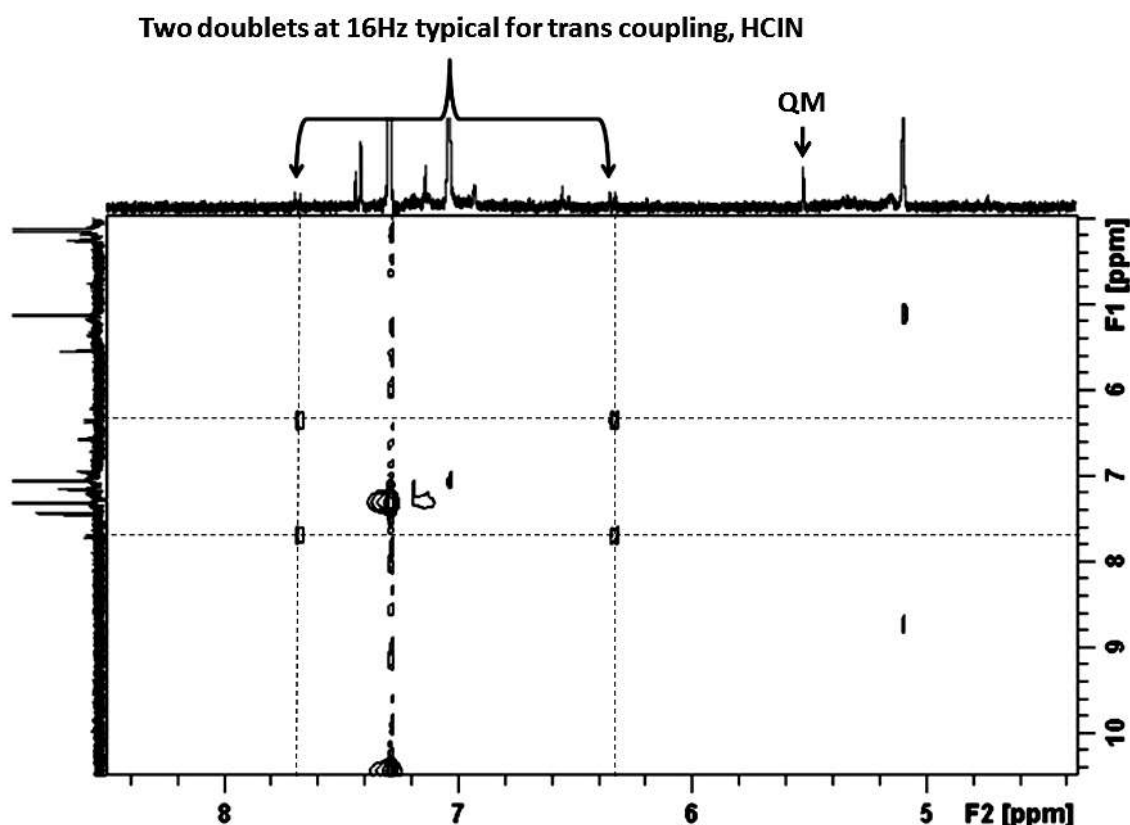


Figure 4.17: High resolution 700 MHz ¹H DQF COSY spectrum of 10 minutes sample (in CDCl₃), shows nearest neighbours diagonal and cross peaks of hydroxy cinnamate, proves that two doublets (~16Hz typical for trans coupling) are in the same molecule.

The COSY experiment was useful in the analysis of the nearest neighbours diagonal and cross peaks,¹⁵³ and demonstrates that the two doublets at approximately 16Hz (a value which is typical for trans coupling of alkenyl hydrogens) belonged to the same molecule of hydroxy cinnamate, but that the peak at 5.5 ppm did not belong to the same molecule as the doublets, consistent with it being a part of quinone methide.

The second 2D proton NMR analysis used the diffusion ordered spectroscopy (DOSY sequence), Figure 4.18.

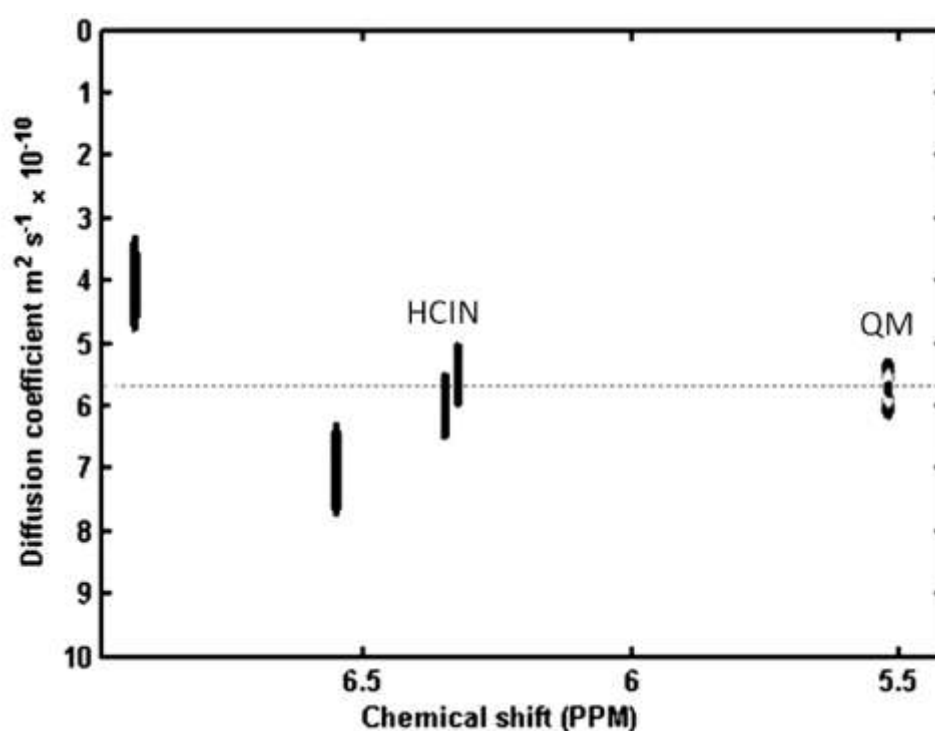


Figure 4.18: High resolution 700 MHz ¹H DOSY spectrum of 10 minutes sample (in CDCl₃), shows diffusion coefficient for Hydroxy Cinnamate and Quinone Methide proves that both molecules are the same size.

This analysis showed a diffusion coefficient for both molecules and proved that both molecules formed were the same size and similar to the starting antioxidant.

4.3.5 Product Identification by GC-NCD

The analysis of the samples using GC x GC with nitrogen chemiluminescence detector (NCD) shows that there were no nitrogenated compounds formed during the time when the antioxidant and its intermediate were present, Figure 4.19. The chromatogram of the 45 minutes sample shows no products from nitration, the peak at approximately 3 min (red marks on bottom left of 2D chromatogram) is associated with the nitrogen from the air injected together with the sample.

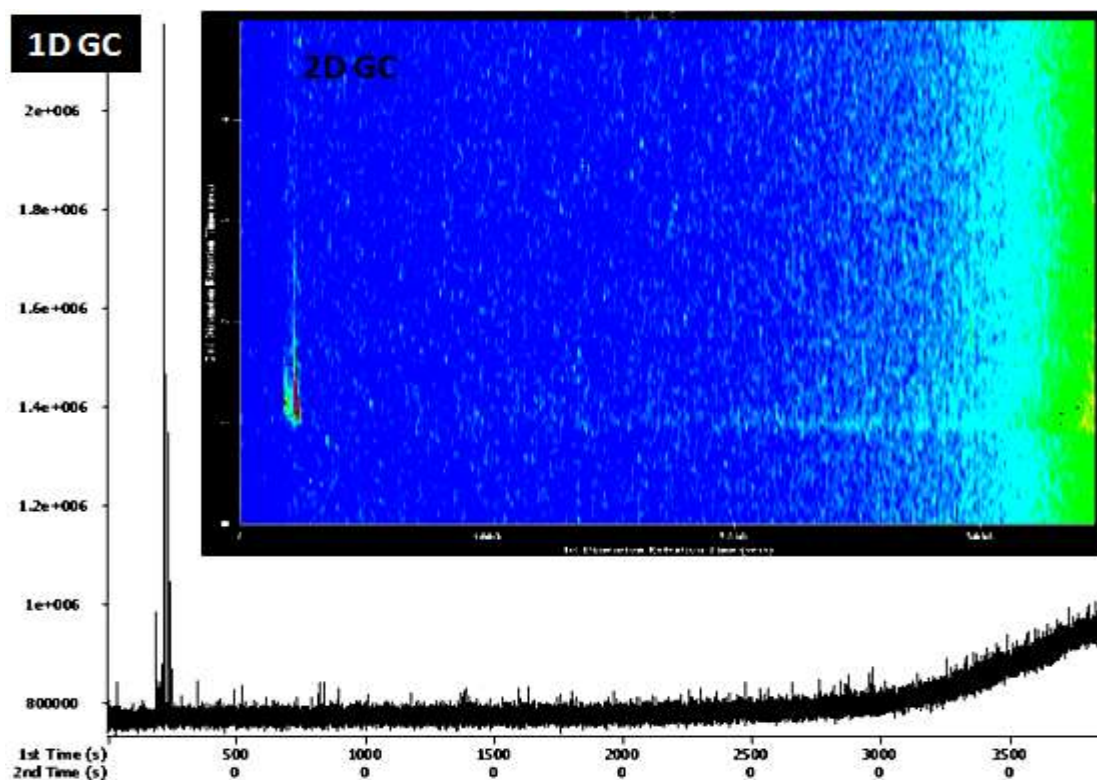


Figure 4.19: 1D and 2D GC NCD chromatograms of 45 min. sample with not detected nitrated products.

The 2D GC NCD technique was useful also in the analysis of squalane nitration products which were observed after both the antioxidant and its intermediates were consumed (example in Figure C11, Appendix C).

4.3.6 Product Identification by ATR/FTIR

Analysis of the samples 0-135 minutes using ATR shows no changes to the spectrum, this corresponds to the time when OHPP and its intermediate protect the base oil from nitration, Figure 4.20.

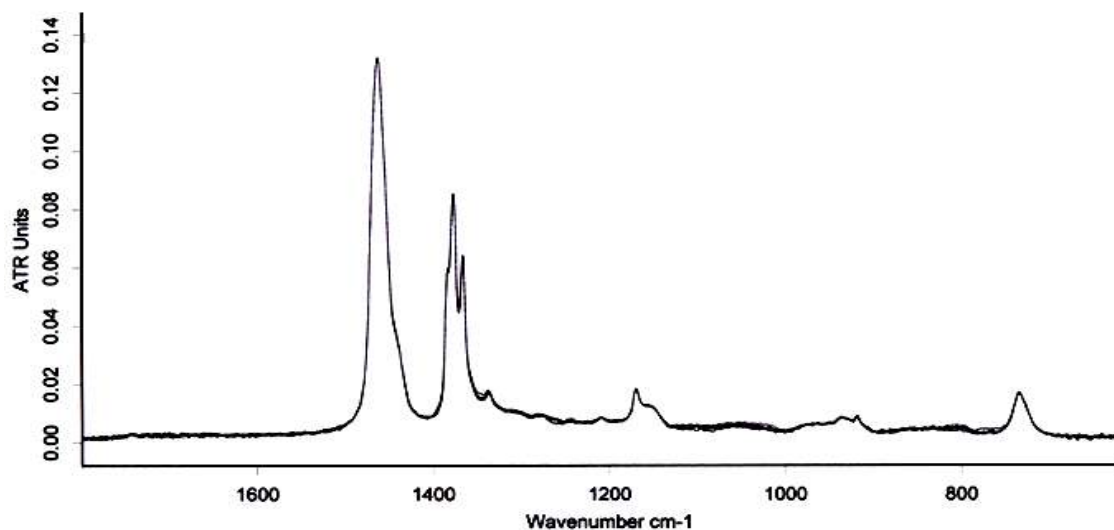


Figure 4.20: FTIR results show no changes up to 135 min. Overlaid spectra of samples: 0 - 135 minutes.

The samples taken after 135 minutes showed an increase in frequencies typical for nitration, such as: C–NO₂, two strong symmetrical and antisymmetrical stretching of N–O bonds in the range of 1570-1540 cm⁻¹,¹⁵⁴ Figure 4.21.

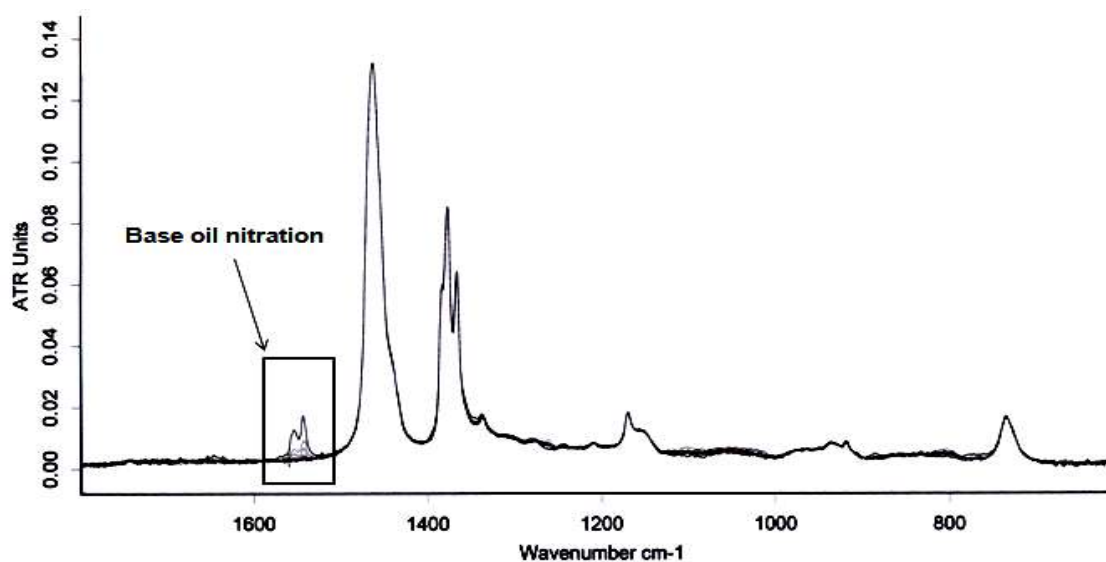


Figure 4.21: Overlaid FTIR spectra of samples: 135 - 240 minutes shows nitrated base oil.

To obtain more information on the antioxidant and its intermediate the 0 and 10 minute samples were analysed using FTIR with the Specac Omni-Cell System with CaF₂ windows (details in Chapter 2), which has a much larger effective path length than ATR, and therefore allows a much smaller concentration of components to be detected, Figure 4.22.

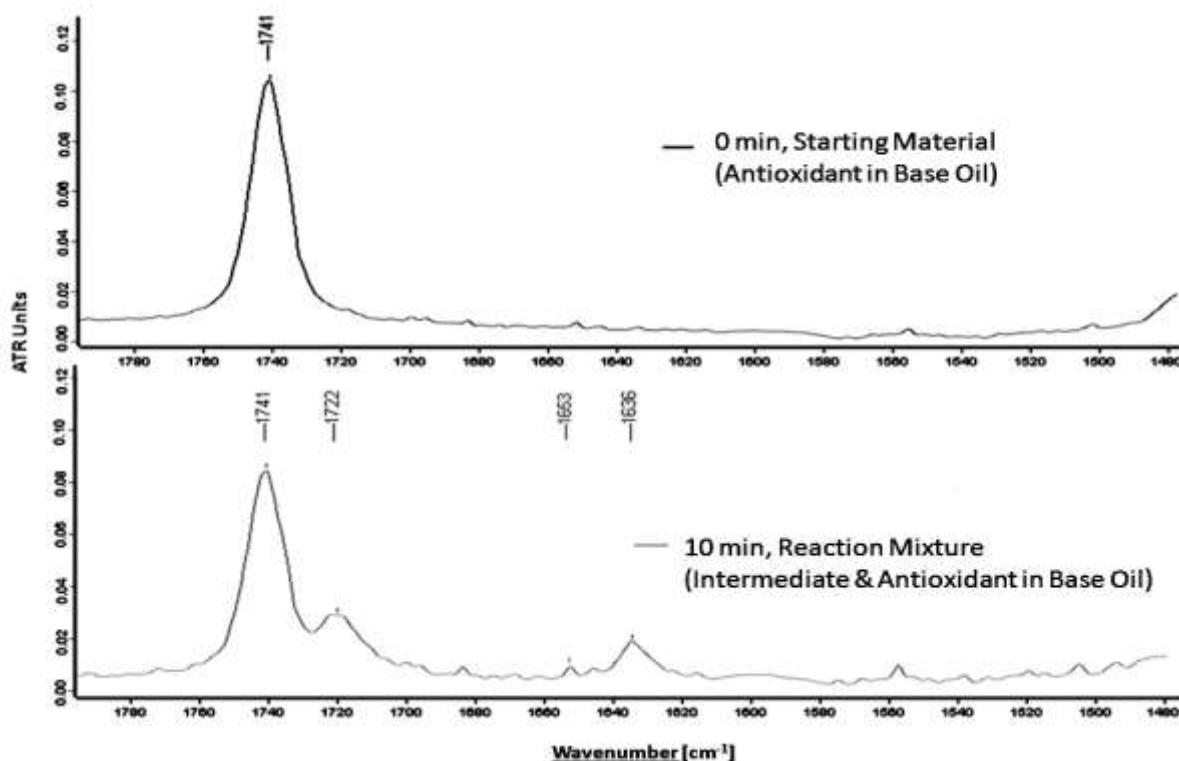


Figure 4.22: FTIR spectra of starting material and 10 minutes reaction mixture recorded in the thin layer cell (CaF₂).

The spectrum of starting material showed antioxidant carbonyl absorption from the ester group (C=O) at 1741 cm⁻¹, whereas the 10 minutes reaction mixture showed a shift to a lower frequency, 1722 cm⁻¹, which is possibly associated with olefinic conjugation with ester characteristic for the intermediate.¹⁵⁵ The 1653 cm⁻¹ absorption was associated with (C=O) carbonyl stretching frequency and 1636 cm⁻¹ with (C=C),¹⁵⁵ which was studied previously for quinones. Similar absorption was obtained for the model compound QM1.

4.3.7 Summary of Antioxidant Intermediate Identification

Various analytical techniques, such as: GC-FID, high resolution GC-MS FI and EI, UV-Vis (and also GPC with UV-Vis detector), ¹H NMR and ATR/FTIR, have been employed to establish the structure of an intermediate from the reaction of phenolic antioxidant (OHPP) with nitrogen dioxide at high temperature engine piston conditions. A short summary of the results is shown in Table 4.4.

Table 4.4: Summary of an intermediate product identification, from the reaction of antioxidant (OHPP) with NO₂ at 180 °C.

Analytical Technique/ Solvent	Identification of Quinone Methide	Identification of Hydroxy Cinnamate	Comments
GC-FID (hexane)	One peak on GC trace		
GC-MS FI (hexane)	m/z 528.458 ± 0.005; two possible structures (QM or HCIN)		
GC-MS EI (hexane)	m/z 217.158 ± 0.001	-	Supporting identification of QM
UV-Vis (DCM)	305 nm	-	Supporting identification of QM, however not excluding HCIN
GCP UV- Vis (THF)	305 nm	310 nm	Supporting identification of QM, 310 nm possibly indicates HCIN formation possibly due to a polar solvent effect
¹ H NMR (CDCl ₃)	δ = 5.5 ppm	δ = 7.7 ppm and δ = 6.3 ppm	Supporting identification of both HCIN and QM
GC x GC NCD (hexane)	Supporting the idea of non nitrated intermediate product from antioxidant (shows nitration of base oil when antioxidant and its intermediate have been consumed)		
ATR (no solvent)	Shows no nitration of base oil until antioxidant and its intermediate is present, however when both consumed increase in frequencies (1570- 1540 cm ⁻¹) typical for nitration observed.		
FITR (Omni- Cell) (no solvent)	1653 cm-1 (C=O) 1636 cm-1 (C=C) From quinone	1722 cm-1 (C=O)	Supporting identification of QM,

Results from all analysis support the identification of quinone methide in the reaction mixtures, which was the dominant product of the reaction of OHPP with nitrogen dioxide, in the early stage of the reaction. QM was stable in non-polar environment; however it slowly reacted to HCIN in polar solvents. Therefore the analysis by GPC and ¹H NMR, which used moderately polar solvents, such as: THF and CDCl₃, showed the formation of both products, QM and HCIN. The analysis of the samples exposed to daylight for a few days (at room temperature) also showed the formation of hydroxy cinnamate.

4.4 Reaction mechanism

The reaction of hindered phenolic antioxidants (OHPP) with 1000 ppm of NO₂ at 180 °C resulted in the formation of QM and then slow conversion to HCIN in polar solvent, in contrast to previous work at lower temperatures,^{82,83,147} which identified nitrated antioxidant products. Therefore a novel, high temperature mechanism is proposed as shown in Figure 3.

It is accepted that the reaction between phenolic antioxidant and gaseous NO₂ is initiated by the hydrogen abstraction from the hydroxyl group by nitrogen dioxide, reaction [4.1], as proposed by Brunton,⁸³ with the formation of phenoxyl radicals and nitrous acid, where the phenoxyl radical is stabilised by resonance. Previous authors who studied the low temperature mechanism suggested the addition of NO₂ to phenoxyl radical (reaction [4.2]).^{82,83,147}

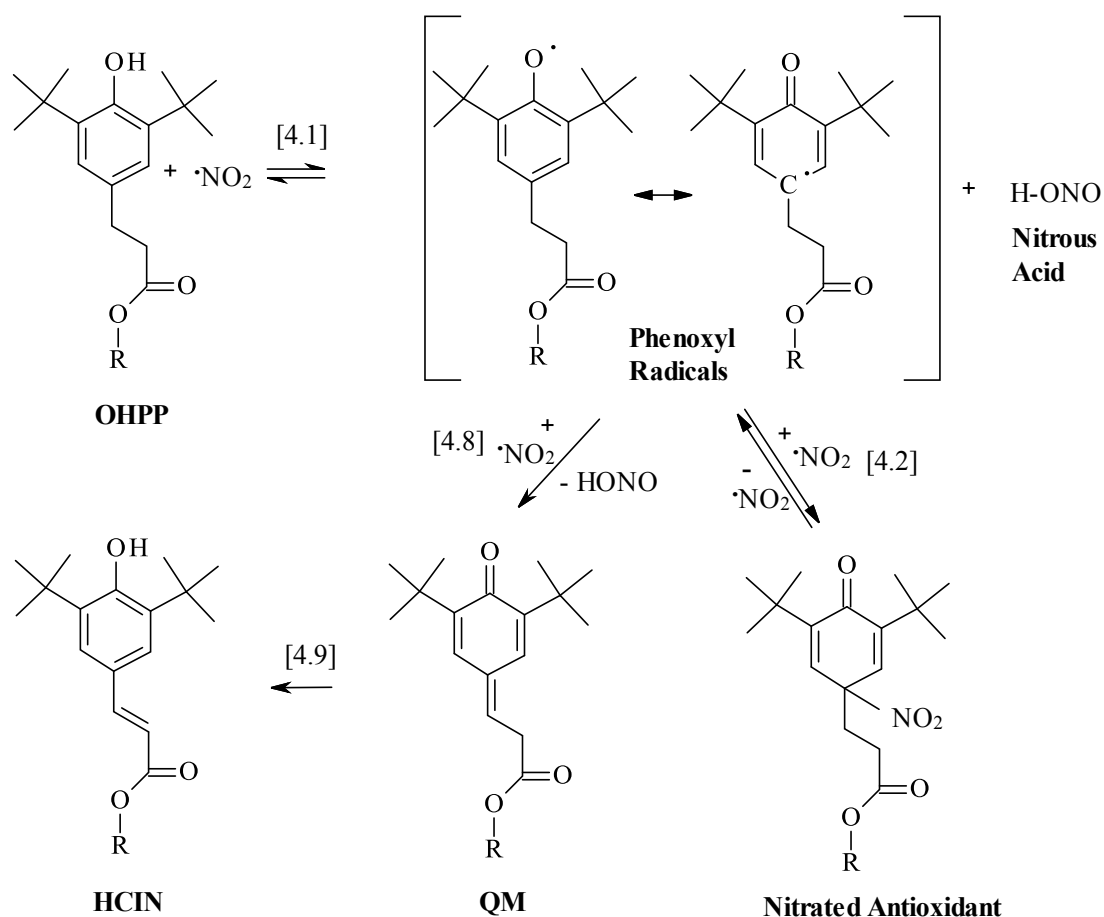


Figure 4.23: Novel reaction mechanism of phenolic antioxidant (OHPP) with NO₂.

The novel, high temperature pathway is illustrated in reaction [4.8], the direct abstraction of the hydrogen by NO₂. This mechanism has not been hitherto reported previously as QM has not been previously identified as a product of reaction with nitrogen dioxide. It is likely to be a comparatively slow reaction in comparison with addition of NO₂, which is likely to be barrierless; however, at elevated temperatures, the abstraction could be dominant due to the addition of NO₂ being reversible, (this is explained in detail in Chapter 5). Finally, the QM can re-arrange slowly to the second observed antioxidant intermediate product HCIN in polar environment, reaction [4.9].

4.5 Summary

In summary, the main products formed during the reaction of the hindered phenolic antioxidant (OHPP) with NO₂ at 180 ± 1 °C were quinone methide (QM), octadecyl 3-(3,5-di-*tert*-butyl-4-oxo-cyclohexa-2,5-dien-1-ylidene) propanoate and hydroxy cinnamate (HCIN), octadecyl-3-(3,5-di-*tert*-butyl-4-hydroxy-phenyl)prop-2-enoate, neither containing –NO₂ groups, in contrast to previous work at lower temperature where cyclohexadienone–NO₂ adducts were the main products observed.

Primarily, quinone methide has been identified, which then can react slowly to form another previously unidentified product of reaction with NO₂, a hydroxy cinnamate. Observation of these products is in apparent contradiction to previous studies on this reaction, which observed the formation of nitro phenols.

A novel reaction mechanism is proposed to account for this change in mechanism with temperature, which is explained in more detail in Chapter 5. The novel, high temperature reaction mechanism is the direct abstraction of the hydrogen from the phenoxyl radical by NO₂, which led to formation of QM. This is likely to be a comparatively slow reaction in comparison to the addition of NO₂, which is likely to be barrierless, but at elevated temperatures, the abstraction could be dominant due to the addition of NO₂ being reversible.

Chapter 5: Thermochemical calculations using Gaussian Software

5.1 Introduction

The aim of this chapter is to improve the understanding of the reaction mechanisms of phenolic antioxidants with NO₂ by the calculation of the bond dissociation energies (BDEs), their reaction enthalpies, entropies and Gibbs energies and for compounds discussed in Chapter 4, and an estimation of ceiling temperatures for their formation.

The experimental work reported in Chapter 4 was based mainly on octadecyl 3-(3,5-ditert-butyl-4-hydroxy-phenyl) propanoate (OHPP) a commercial phenolic antioxidant, and its interaction with NO₂ at high temperature piston conditions (180 °C). The product identification shows the formation of a non-nitrated intermediate from the antioxidant, in contradiction to previous work,^{83,94} which identified nitrated phenolics. These nitrated phenolics were reported mainly for low temperature conditions and only one author used a temperature as high as 160 °C.¹⁴⁶ To explain the phenomenon of non-nitrated products formation at 180 °C the thermochemistry of NO₂ addition to representative phenolic species was calculated, and all structures examined are shown in Figure 5.1.

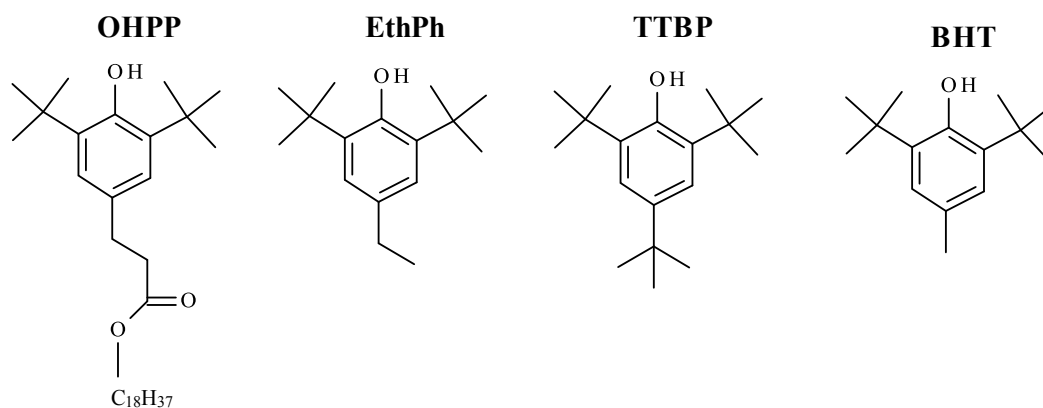


Figure 5.1: Structures of phenolic antioxidants; octadecyl 3-(3,5-di-tert-butyl-4-hydroxyphenyl)propanoate (OHPP), 2,6-di-tert-butyl-4-ethylphenol (EthPh), 2,4,6-tri-tert-butylphenol (TTBP), 4-methyl-2,6-di-tert-butylphenol (BHT).

The strength of a bond is measured by its bond dissociation energy (BDE), defined here as the energy required to separate the atoms to infinity¹⁵⁶ and this information is crucial for understanding reaction mechanisms. Unfortunately, the BDE for some key compounds is unavailable in the literature and so computational methods need to be employed to obtain this information. The bond strengths of relevance to this work were the: C—NO₂ of nitroaromatics, O—H of phenolics, and C—H of non-aromatics, such as quinone methide (QM) structures.

Choosing the appropriate computational technique and level of theory is crucial to achieve an acceptable level of accuracy of calculated thermochemical quantities, therefore the standard deviation for different methods and model compounds, for which experimental bond strength were known, were reviewed. Moreover the calculation time, which took up to a few days for the computer to run for large molecules (e.g. M = 530 g mol⁻¹), needs to be recognised. Primarily, the recommendation by Foresman *et. al.* 1996,¹⁵⁷ as the best hybrid functionals, the B3LYP and B3PW91 methods were considered. Secondly, the literature on the prediction of thermochemical information for nitroaromatic and phenolic compounds, which used Gaussian software with density functional theory (DFT), was reviewed.¹⁵⁸⁻¹⁶²

As nitroaromatic compounds play an important role as explosives, knowledge of the bond dissociation energies is the most fundamental property in this industry and so has been studied in detail, by Shao *et al.* 2006.¹⁵⁸⁻¹⁶⁰ To obtain the experimental BDE of some nitro aromatic compounds is very difficult, because they are very unstable and hard to synthesize. Previous studies of the energies of cleavage of C–NO₂ bonds for nitroaromatic molecules using DFT with different correlation functionals and basis set are shown in Appendix D, Tables D1-D3.¹⁵⁸⁻¹⁵⁹ This review compared the effectiveness of different hybrid density functional methods (the B3LYP, B3PW91, B3P86) with the basis sets, such as: 6-31G** [6-31G(d,p)], 6-31+G** [6-31+G(d,p)] and 6-311G** [6-311G(d,p)] and compared results with the experimental data of BDEs of various nitroaromatic compounds. Primarily, using 6-31G(d,p) basis set, different methods were compared: the B3LYP, B3W91 and B3P86 methods, which gave the average absolute differences of 1.51, 0.88 and 3.06 kcal mol⁻¹ (6.3, 3.7 and 12.8 kJ mol⁻¹), respectively. The best result was obtained using the B3W91 method. This method was also recommended by Foresman *et. al* for final, accurate energy calculations, for example for bond energies.¹⁵⁷ Secondly, using the higher level basis set, the 6-31+G(d,p) the best result was obtained with B3P86 method, giving a mean absolute deviation of 1.70 kcal mol⁻¹ (7.1 kJ mol⁻¹). Finally, using the 6-311G(d,p) basis set, which was the highest level of theory used by Shao, the best result gave the B3P86 method with a mean absolute deviation of 1.16 kcal mol⁻¹ (4.9 kJ mol⁻¹).

Summarising all previous results, the B3W91/6-31(d,p) and B3P86/6-311G(d,p) methods gave the best results for BDE of nitrocompounds with the lowest mean absolute deviations of 0.88 kcal mol⁻¹ and 1.16 kcal mol⁻¹ respectively and would give an acceptable level of accuracy for studies of the nitroaromatics discussed in Chapter 4. Unfortunately, the B3P86 method is not available using the software chosen for this

work, Gaussian 09, therefore a similar method, the BPV86, was tested before deciding on the method.

The second type of BDE reviewed was the O—H bond, which was important for hydrogen abstraction from phenolics. The literature predictions of O—H bond dissociation energy for model molecules, such as: H₂O (water), CH₃OH (methyl alcohol) and PhOH (phenol), which used the B3LYP and the (RO)B3LYP methods with the 6-311G(d,p) and 6-311++G(2df,2p) basis sets are shown in Appendix D, Table D4.¹⁶¹ Comparing basis sets the 6-311G(d,p) with the 6-311++G(2df,2p), better results were obtained using the higher basis set 6-311++G(2df,2p). However, comparing the two methods B3LYP and (RO)B3LYP, the mean absolute deviations were very similar. The main advantage was the computational time, which favoured the B3LYP method.

Other authors compared different basis sets with the B3LYP method using the dissociation of water as an example, Appendix D, Table D5.¹⁶² The result most comparable to experimental data was obtained using the lower basis set 6-31+G(d) or next favoured 6-311G(d,p) higher basis set. The same authors using the 6-31+G(d) basis set to compare different methods, Appendix D, Table D6. This revision shows that the best method for energy prediction for water dissociation was the BLYP/6-31+G(d), the result of which was 119.0 kcal mol⁻¹, essentially identical with experimental data. The second best was B3LYP/6-31+G(d) with only 0.5 kcal mol⁻¹ (2.1 kJ mol⁻¹) mean absolute deviation from the experimental value. Based on a literature review of both C—NO₂ and O—H BDE's predictions it was not possible to decide which method and basis set would be the best for both phenolics and nitroaromatics, therefore the best results were selected and pre-testing of different methods and basis sets was performed.

5.2 Method Development

Prediction of the thermochemical values in this work were obtained using Gaussian 09 software. The level of theory was decided based on the best results of BDE obtained for model molecules compared to experimental data and relatively short calculation time.

5.2.1 Testing the Model for the Level Theory

To choose the best computational method for study the thermochemical properties of both phenols and nitroaromatics, pre-testing of various DFT methods was performed. The selected methods were the B3LYP, B3PW91 and BPV86 combined with the most effective basis sets, based on the literature review.

In the thermodynamic calculations the bond enthalpies should be used instead of the bond dissociation energies,¹⁵⁶ therefore in this chapter the bond dissociation energies for a species at standard conditions (298 K and 1 bar) will correspond to the bond enthalpies, which could be defined as the reaction enthalpies of the bond homolysis reactions and are dependent on the standard enthalpies of formation of products and reactants.¹⁶³ The bond dissociation energies of representative molecules: nitrobenzene (C₆H₅—NO₂), phenol (PhO—H), 2,6-di-tert-butyl-4-methylphenol (BHTO—H) and nitrous acid (H—ONO), were calculated using computed energies (the standard enthalpies of formation, $\Delta_f H^\circ(X)$) and compared with experimental data, Table 5.1. The BDEs were calculated using expressions:

$$\text{BDE (C}_6\text{H}_5\text{—NO}_2\text{)} = \Delta_f H^\circ (\text{C}_6\text{H}_5) + \Delta_f H^\circ (\text{NO}_2) - \Delta_f H^\circ (\text{C}_6\text{H}_5\text{NO}_2)$$

$$\text{BDE (PhO—H)} = \Delta_f H^\circ (\text{PhO}) + \Delta_f H^\circ (\text{H}) - \Delta_f H^\circ (\text{C}_6\text{H}_5\text{OH})$$

$$\text{BDE (BHTO—H)} = \Delta_f H^\circ (\text{BHT-O}) + \Delta_f H^\circ (\text{H}) - \Delta_f H^\circ (\text{BHT})$$

$$\text{BDE (H—ONO)} = \Delta_f H^\circ (\text{ONO}) + \Delta_f H^\circ (\text{H}) - \Delta_f H^\circ (\text{HONO})$$

Table 5.1: The homolytic bond dissociation enthalpies of C₆H₅NO₂, PhOH, BHT and HONO calculated using different methods and basis sets.

Method and basis set	BDE [kJ mol ⁻¹]				M. abs. dev.*
	C ₆ H ₅ —NO ₂	PhO—H	BHT(O—H)	H—ONO	
DFT B3LYP/6-31G(d,p)	307.6 (11.6)	375.2 (2.6)	331.3 (10.3)	339.6 (12.1)	9.2
DFT B3LYP/6-31+G(d)	299.6 (3.6)	361.6 (11)	312.7 (28.9)	328.2 (0.7)	11.1
DFT B3LYP/6-311+G	313.9 (17.9)	363.0 (9.6)	317.2 (24.4)	337.9 (10.4)	15.6
DFT B3PW91/6-31G(d,p)	309.4 (13.3)	377.5 (4.9)	336.8 (4.8)	331.6 (4.0)	6.8
DFT B3PW91/6-311+G	319.8 (23.8)	363.9 (8.7)	316.4 (25.2)	328.5 (0.9)	14.7
DFT BPV86/6-31+G(d,p)	296.7 (0.6)	381.4(8.8)	340.9 (0.7)	334.0 (6.4)	4.1
DFT BPV86/6-311G(d,p)	293.7 (2.3)	379.9 (7.3)	338.1 (3.5)	327.2 (0.3)	3.4
Experimental/Calculated ^c	296.1 ± 4 ^a	362.8 ± 2 ^b	341.6 ± 8 ^a	330.9 ± 1 ^c	3.7

Values in the round brackets are the mean absolute deviation from computed BDE for experimental one.

^aRef.164, ^bRef.165, ^cRef.166, 167, 168

*M. abs. dev. – Mean Absolute Deviation (the experimental value the average of standard errors)

Based on the above comparison, the best method for predicting both O—H of phenolics, C—NO₂ of nitroaromatics and O—H of nitrous acid was the DFT BPV86/6-311G(d,p) with the mean absolute deviation calculated to be approximately 3.4 kJ mol⁻¹, which predicts values that are in fact comparable to the accuracy of the experimental results.¹⁶⁹

The BPV86 method (Becke style, which uses Perdew's 1986 functional with local correlation replaced, as suggested by Vosco)¹⁵⁷ was used for both geometry optimisation and frequency calculations. This level of theory was accurate enough for calculating the thermochemistry of phenolic antioxidants and their products from reactions with NO₂, and the computational time was acceptable, taking up to three days for the largest molecule examined, on the PC used (details in Chapter 2).

The example of calculation of the change in reaction enthalpy, Gibbs energy and entropy based on the thermochemical values computed using Gaussian for nitrobenzene are shown in Appendix D, Tables D7-D8.¹⁷⁰

5.3 Results

Primarily the thermochemical values for the reaction of nitrogen dioxide when added to different phenolic species were calculated.

5.3.1 Thermochemistry calculations of selected Phenoxy–NO₂ adducts

BHT–NO₂

Previous work suggested the addition of NO₂ to phenoxy radical from 4-methyl-2,6-di-tert-butylphenol (BHT) at room temperature, by Brunton et al. 1979,⁸³ reaction [5.1].

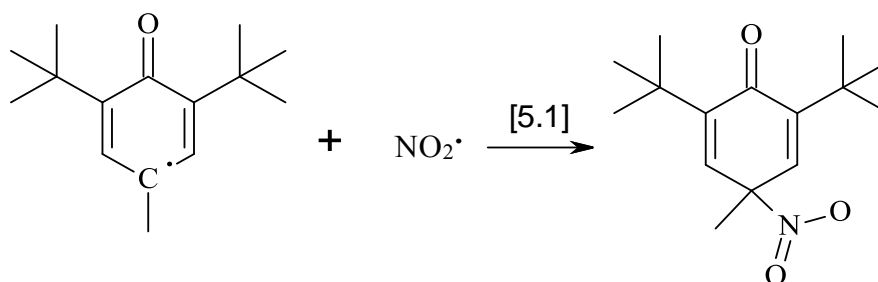


Figure 5.2: Reaction [5.1] of NO₂ addition to phenoxy radical from 4-methyl-2,6-di-tert-butylphenol (BHT).⁸³

The optimised geometry of BHT-NO₂ adduct is shown in Figure 5.3.

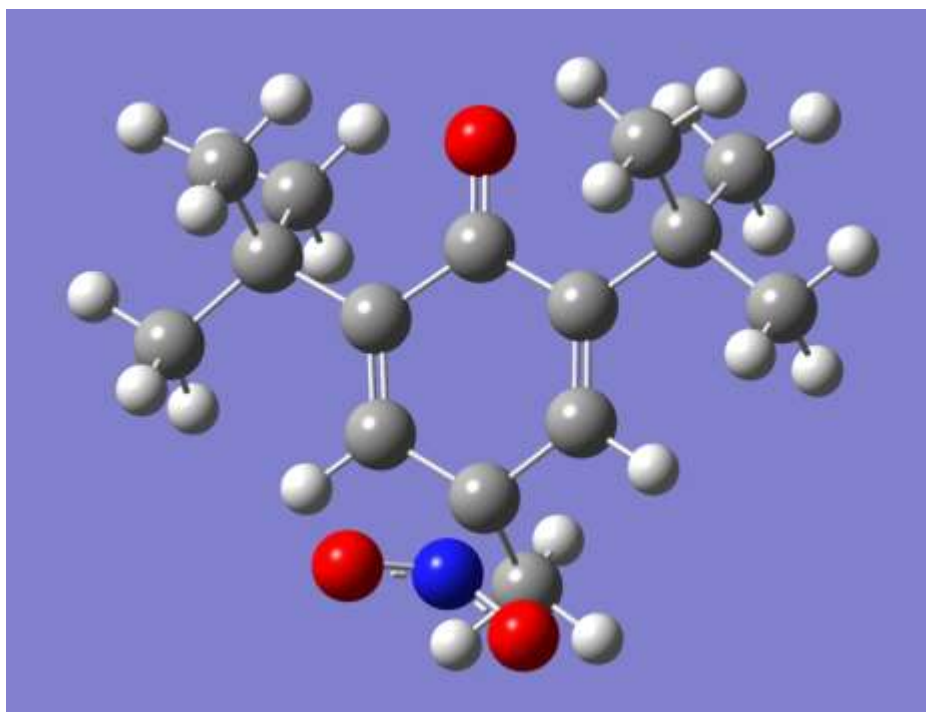


Figure 5.3: Optimised geometry of BHT–NO₂ using BPV86/6-311G(d,p) method (Output File).

The thermochemical values were obtained for reaction [5.1] using Gaussian, details Appendix D, Table D9. The enthalpy, Gibbs energy and entropy were calculated, as previously for nitrobenzene, (results in Table 5.2).

Table 5.2: Calculated changes in enthalpy, Gibbs energy and entropy for reaction 5.1, at standard temperature and pressure.

$\Delta_r H^\circ(298K)$ [kJ mol ⁻¹]	$\Delta_r G^\circ(298K)$ [kJ mol ⁻¹]	$\Delta_r S^\circ(298K)$ [J mol ⁻¹ K ⁻¹]
-67.8 ± 3.4	-10.8 ± 3.4	-191.0

The change in enthalpy for BHT–NO₂ formation was approximately -67.8 ± 3.4 kJ mol⁻¹, which showed that this reaction was exothermic (the error quoted here is the mean absolute deviation for this method from Table 5.1). The negative Gibbs energy -10.9 ± 3.4 kJ mol⁻¹ proved that the forward reaction is favourable and this reaction is spontaneous at standard temperature and pressure.

BHT–ONO

In addition to the usual C–N bond formation, Astolfi have suggested addition of NO₂ to phenoxyl radical through the oxygen atom at room temperature,⁹⁴ reaction [5.2].

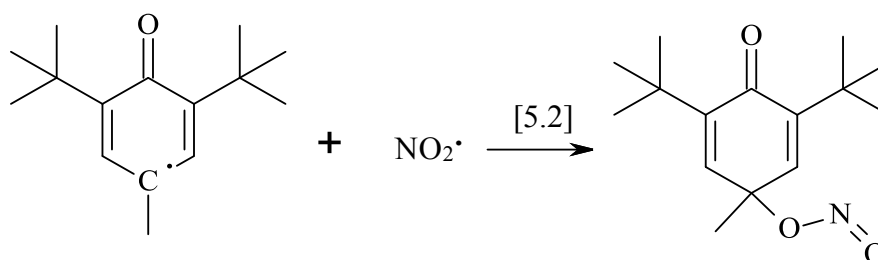


Figure 5.4: Reaction [5.2] of NO₂ addition through the oxygen atom to phenoxyl radical from 4-methyl-2,6-di-tert-butylphenol (BHT).⁹⁴

The optimised geometry of BHT–ONO adduct is shown in Figure 5.5.

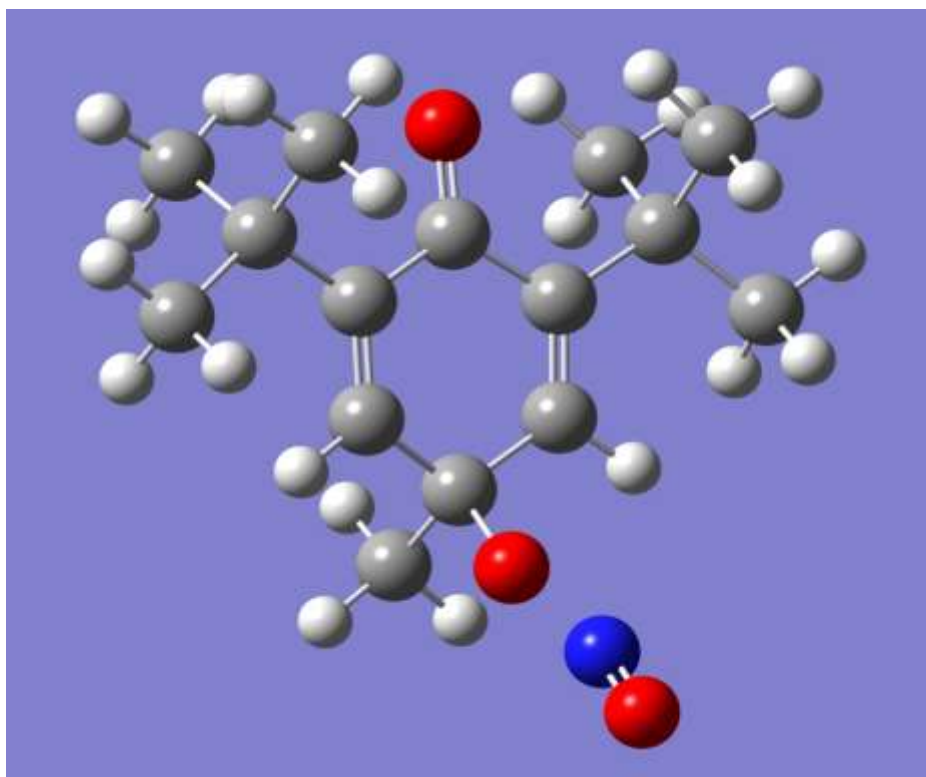


Figure 5.5: Optimised geometry of BHT–ONO using BPV86/6-311G(d,p) method (Output File).

The thermochemical values for reaction [5.2] are presented in Appendix D, Table D10.

The calculated enthalpy, Gibbs energy and entropy results are shown in Table 5.3.

Table 5.3: Calculated changes in enthalpy, Gibbs energy and entropy for reaction 5.2, at standard temperature and pressure.

$\Delta_r H^\circ(298K)$ [kJ mol ⁻¹]	$\Delta_r G^\circ(298K)$ [kJ mol ⁻¹]	$\Delta_r S^\circ(298K)$ [J mol ⁻¹ K ⁻¹]
-51.5 ± 3.4	3.4 ± 3.4	-184.2

The Gibbs energy was essentially zero 3.4 ± 3.4 kJ mol⁻¹ that suggested the reverse reaction proceeds spontaneously at standard temperature and pressure. The change in enthalpy and entropy for BHT–ONO formation were negative $\Delta_r H^\circ(298K) = -51.5 \pm 3.4$ kJ mol⁻¹ and $\Delta_r S^\circ(298K) = -184.2$ J mol⁻¹, hence irreversible BHT–ONO formation will be possible only below 298 K.

TTBP–NO₂

The TTBP (2,4,6-tri-*tert*-butylphenol) was studied previously by Davydov et al.1997,¹⁴⁸ therefore the thermochemistry of the addition of NO₂ to TTBP–phenoxy radical was examined and is shown below, reaction [5.3].

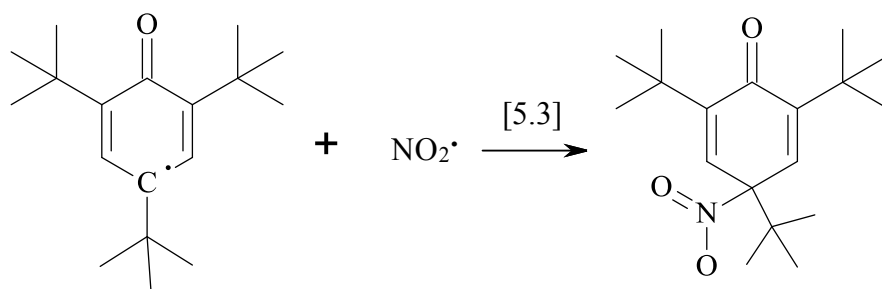


Figure 5.6: Reaction [5.3] of NO₂ addition to phenoxy radical from 2,4,6-tri-*tert*-butylphenol (TTBP).¹⁴⁸

The optimised geometry of TTBP–NO₂ adduct is shown in Figure 5.7.

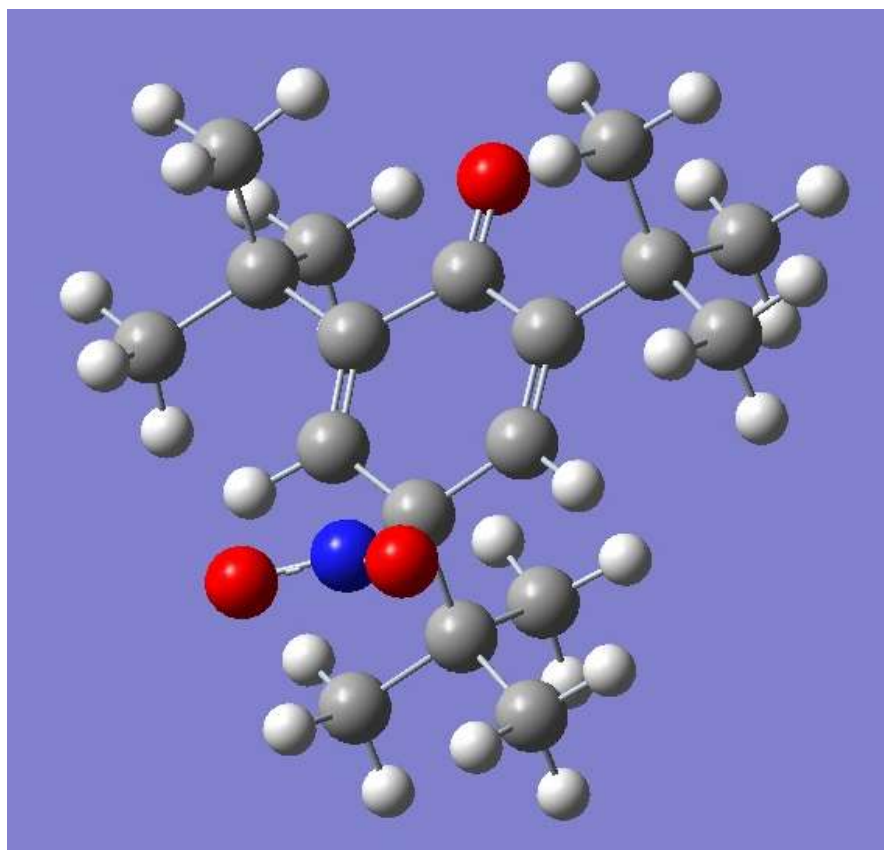


Figure 5.7: Optimised geometry of TTBP–NO₂ using BPV86/6-311G(d,p) method (Output File).

For reaction [5.3] the thermochemical values are shown in Appendix D, Table D11. The enthalpy, Gibbs energy and entropy were predicted for this reaction, Table 5.4.

Table 5.4: Calculated changes in enthalpy, Gibbs energy and entropy for TTBP–NO₂ at standard temperature and pressure.

$\Delta_r H^\circ(298K)$ [kJ mol ⁻¹]	$\Delta_r G^\circ(298K)$ [kJ mol ⁻¹]	$\Delta_r S^\circ(298K)$ [J mol ⁻¹ K ⁻¹]
-78.8 ± 3.4	-18.8 ± 3.4	-201.1

The enthalpy change for TTBP–NO₂ formation was -78.8 ± 3.4 kJ mol⁻¹, which suggested that this reaction is more exothermic; than BHT–NO₂ by 11 kJ mol⁻¹. The negative $\Delta_r S^\circ$ and $\Delta_r H^\circ$ shows that this reaction is spontaneous at standard temperature and pressure.

EthPh—NO₂

The addition of NO₂ to the phenoxy radical from 2,6-di-*tert*-butyl-4-ethyl-phenol (EthPh) at room temperature was studied next, reaction 5.4.

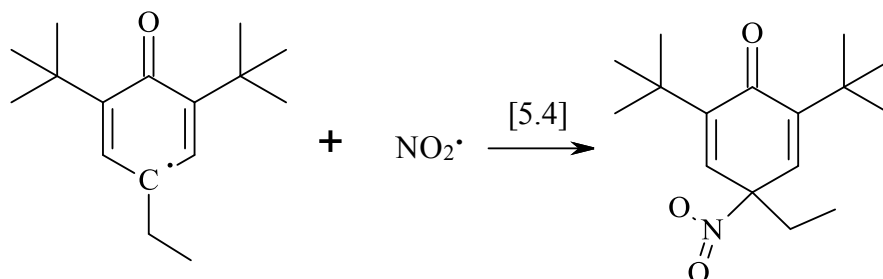


Figure 5.8: Reaction [5.4] of NO₂ addition to phenoxy radical from 2,6-di-*tert*-butyl-4-ethyl-phenol (EthPh).

The optimised geometry of EthPh-NO₂ adduct is shown in Figure 5.9.

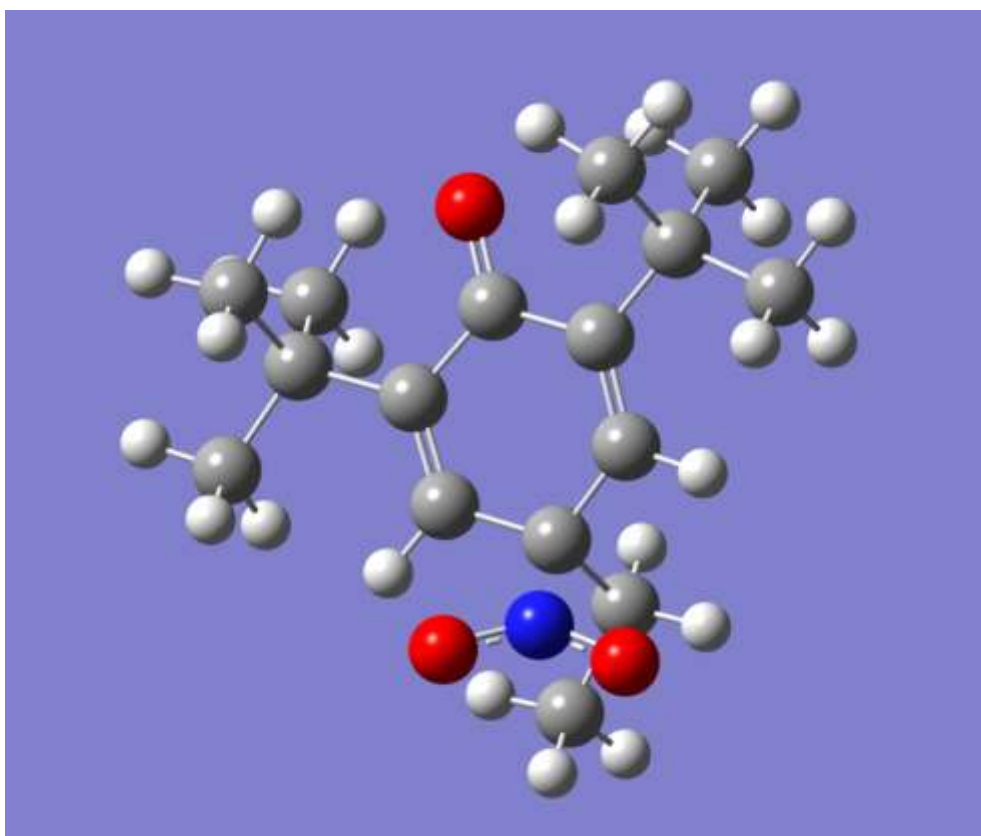


Figure 5.9: Optimised geometry of EthPh—NO₂ using BPV86/6-311G(d,p) method (Output File).

The thermochemical values were obtained for reaction [5.4] using Gaussian, as previously for nitrobenzene, calculation details in Appendix D, Table D12, then the enthalpy, Gibbs energy and entropy were calculated, Table 5.5.

Table 5.5: Calculated changes in enthalpy, Gibbs energy and entropy for reaction 5.4, at standard temperature and pressure.

$\Delta_r H^\ominus(298K)$ [kJ mol ⁻¹]	$\Delta_r G^\ominus(298K)$ [kJ mol ⁻¹]	$\Delta_r S^\ominus(298K)$ [J mol ⁻¹ K ⁻¹]
-66.7 ± 3.4	-12.8 ± 3.4	-180.7

The change in enthalpy for analogous EthPh–NO₂ formation was -66.7 ± 3.4 kJ mol⁻¹, which shows that this reaction is slightly less exothermic than for BHT–NO₂ by 1.1 kJ mol⁻¹. The Gibbs energy is negative (-12.8 ± 3.4 kJ mol⁻¹), the forward reaction will proceed spontaneously and it is more negative than for BHT–NO₂ by 2.0 kJ mol⁻¹. The negative $\Delta_r S^\ominus$ and $\Delta_r H^\ominus$ shows that this reaction is spontaneous at standard temperature and pressure.

Analogue of OHPP–NO₂

The addition of NO₂ to analogue OHPP–phenoxy radical is shown in reaction 5.5.

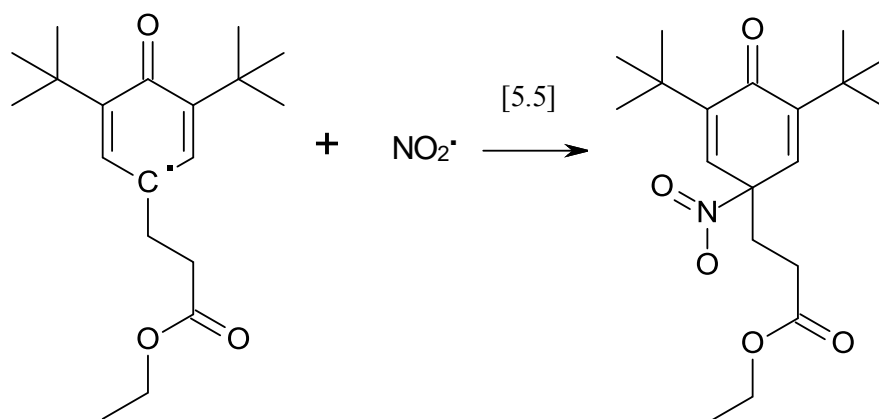


Figure 5.10: Reaction [5.5] of NO₂ addition to phenoxy radical from OHPP analogue.

The analogue of OHPP, (with a C₂ chain, 16 carbons shorter than OHPP) was used in Gaussian prediction to shorten the run time, but is not thought to influence significantly calculated values. The optimised geometry of analogue OHPP–NO₂ adduct is shown in Figure 5.11.

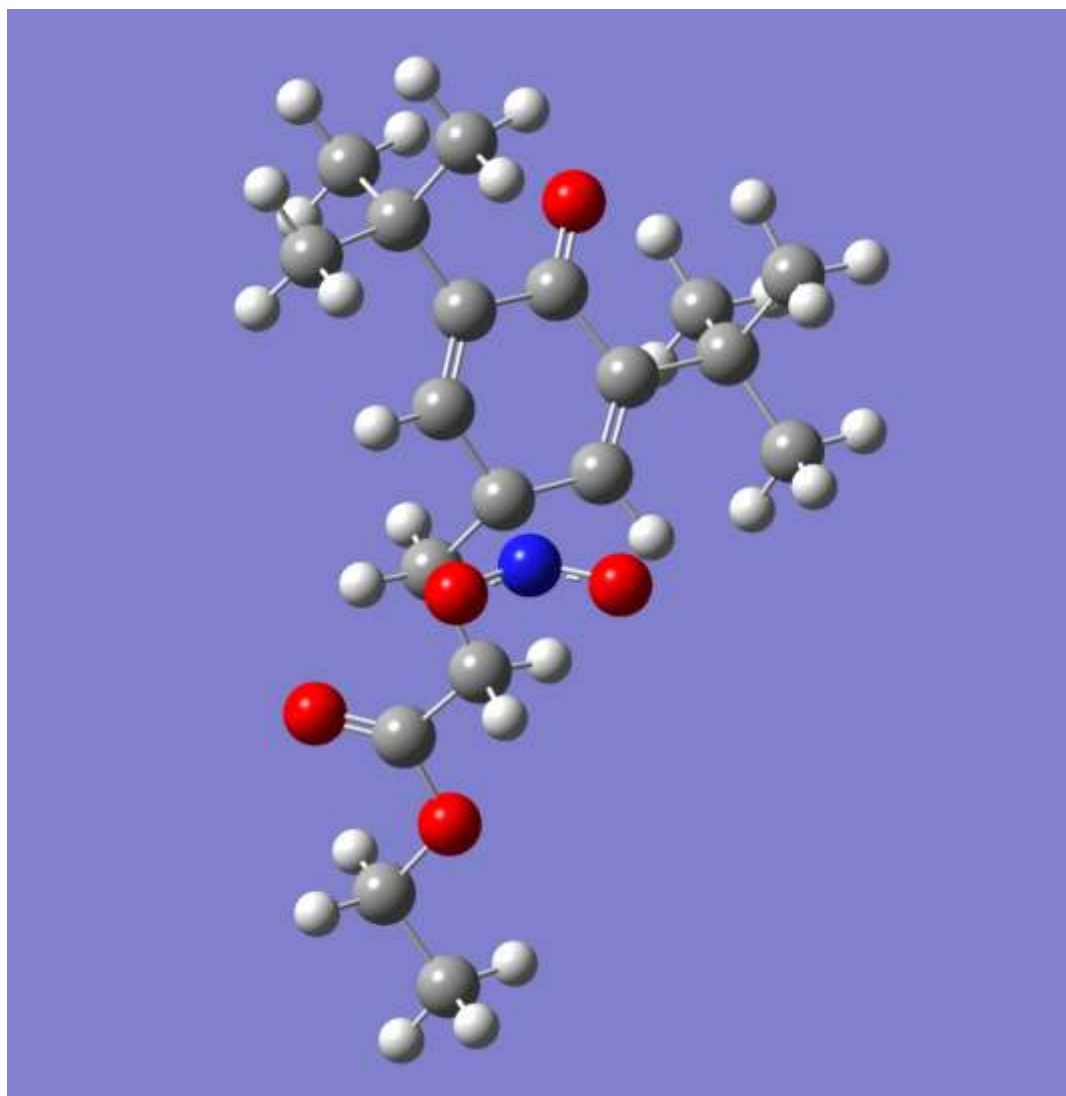


Figure 5.11: Optimised geometry of OHPP–NO₂ using BPV86/6-311G(d,p) method (Output File).

For reaction [5.5] the thermochemical values are shown in Appendix D, Table D13. The enthalpy, Gibbs energy and entropy were predicted for this reaction, Table 5.6.

Table 5.6: Calculated changes in enthalpy, Gibbs energy and entropy for analogue OHPP–NO₂ at standard temperature and pressure.

$\Delta_r H^\circ(298K)$ [kJ mol ⁻¹]	$\Delta_r G^\circ(298K)$ [kJ mol ⁻¹]	$\Delta_r S^\circ(298K)$ [J mol ⁻¹ K ⁻¹]
-69.4 ± 3.4	-20.0 ± 3.4	-165.8

The change in enthalpy for the analogue OHPP–NO₂ formation was -69.5 ± 3.4 kJ mol⁻¹, which suggested that this reaction is slightly more exothermic than for BHT–NO₂ by 1.7 kJ mol⁻¹. The Gibbs energy is negative -20.0 ± 3.4 kJ mol⁻¹, the forward reaction will proceed spontaneously and it is more negative than for BHT–NO₂ by 9.2 kJ mol⁻¹. The negative $\Delta_r S^\circ$ and $\Delta_r H^\circ$ shows that this reaction is spontaneous at standard temperature and pressure.

5.3.2 Thermochemistry calculations of selected Quinone Methides

Quinone Methide from EthPh (QM1)

The thermochemistry of the formation of 2,6-di-*tert*-butyl-4-ethylidene-cyclohexa-2,5-dien-1-one (QM1) from 2,6-di-*tert*-butyl-4-ethyl-phenol (EthPh) at room temperature, reaction [5.6], was studied.

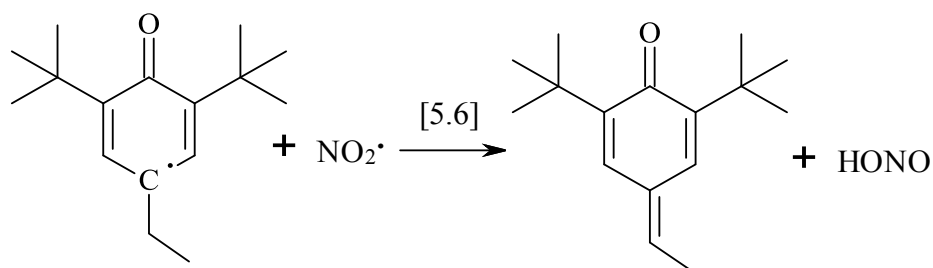


Figure 5.12: Reaction [5.6] of the formation of 2,6-di-*tert*-butyl-4-ethylidene-cyclohexa-2,5-dien-1-one (QM1) from 2,6-di-*tert*-butyl-4-ethyl-phenol (EthPh).

The optimised geometry of QM1 is shown in Figure 5.13.

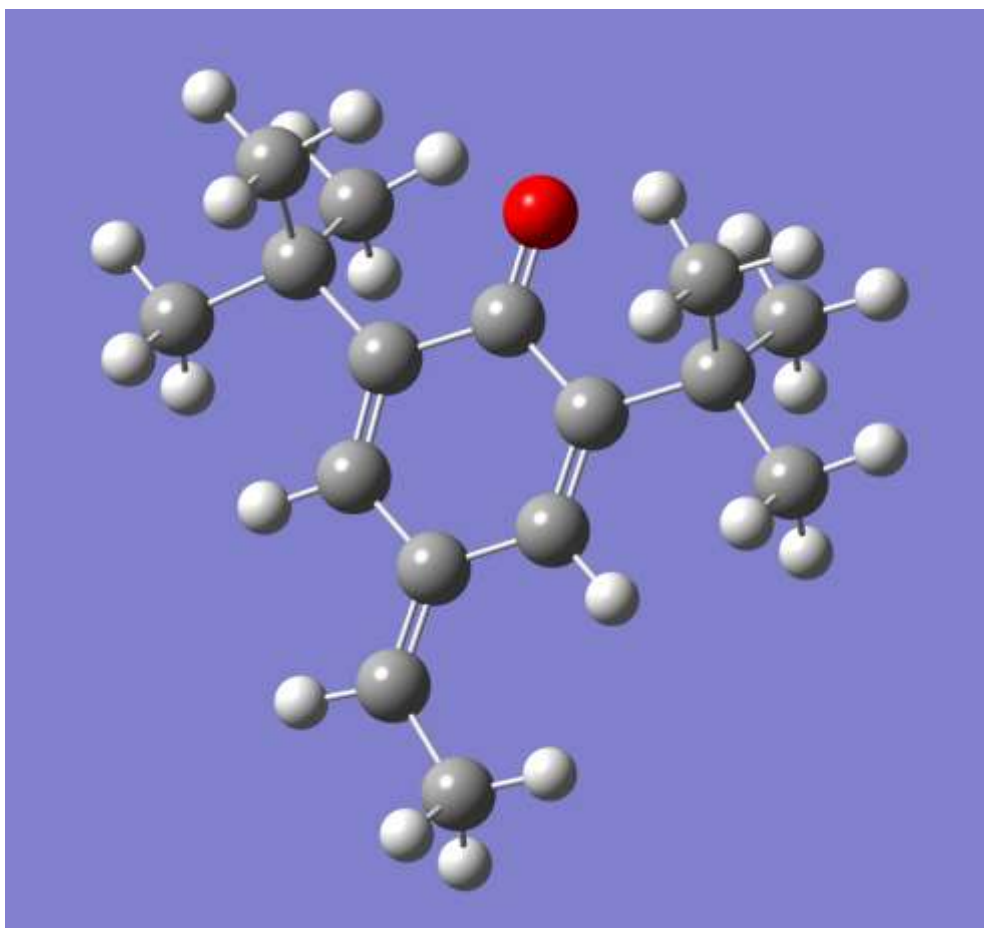


Figure 5.13: Optimised geometry of QM1 using BPV86/6-311G(d,p) method (Output File).

The thermochemical values were obtained for reaction [5.6] using Gaussian, as previously for nitrobenzene, Appendix D, Table D14. Afterwards the enthalpy, Gibbs energy and entropy were calculated, Table 5.7.

Table 5.7: Calculated changes in enthalpy, Gibbs energy and entropy for reaction 5.6 at standard temperature and pressure.

$\Delta_r H^\circ(298K)$ [kJ mol ⁻¹]	$\Delta_r G^\circ(298K)$ [kJ mol ⁻¹]	$\Delta_r S^\circ(298K)$ [J mol ⁻¹ K ⁻¹]
-65.0 ± 3.4	-63.4 ± 3.4	-5.35

The change in enthalpy for QM1 formation was -65.0 ± 3.4 kJ mol⁻¹, which shows that this reaction is slightly less exothermic than for EthPh–NO₂ by 1.8 kJ mol⁻¹. The Gibbs energy is negative -63.4 ± 3.4 kJ mol⁻¹, the forward reaction will proceed

spontaneously and it is much more negative (by 50.6 kJ mol⁻¹) than for EthPh–NO₂ formation.

Quinone Methide from OHPP (QM)

The second important reaction was the formation of octadecyl 3-(3,5-di-*tert*-butyl-4-oxo-cyclohexa-2,5-dien-1-ylidene) propanoate (QM), from OHPP–peroxyl radical reaction with NO₂, (reaction [5.7]). This reaction thermochemistry is crucial to explain the phenomenon of the formation of the non-nitrated quinone methide type product, identified in detail in Chapter 4.

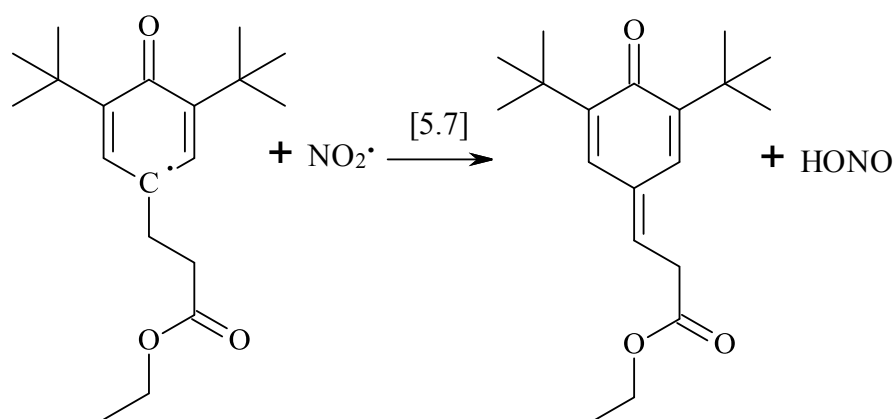


Figure 5.14: Reaction [5.7] of formation of octadecyl 3-(3,5-di-*tert*-butyl-4-oxo-cyclohexa-2,5-dien-1-ylidene) propanoate (QM), from OHPP–peroxyl radical.

The optimised geometry of analogue QM is shown in Figure 5.15.

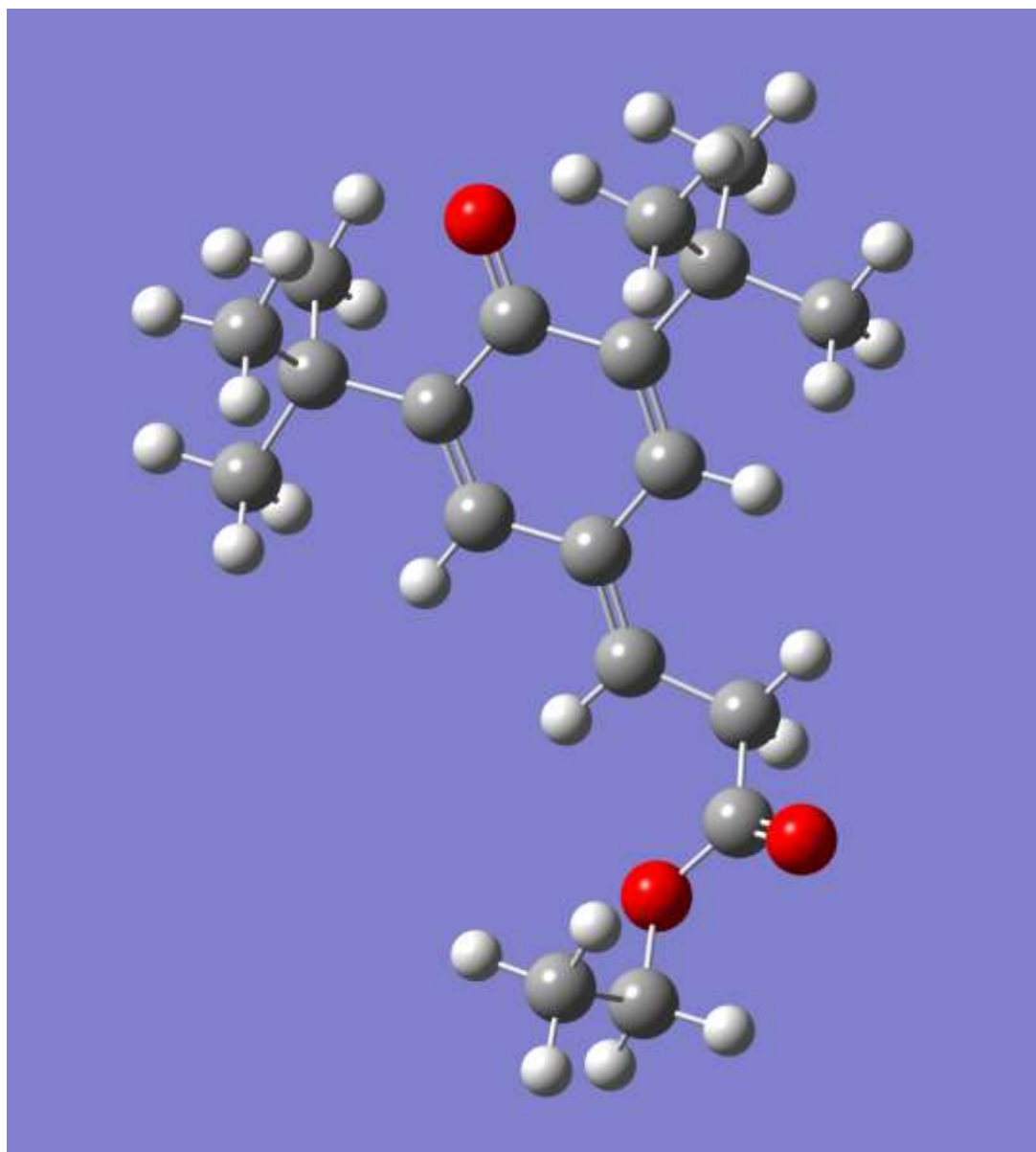


Figure 5.15: Optimised geometry of analogue QM using BPV86/6-311G(d,p) method (Output File).

For this reaction the thermochemical values are shown in Appendix D, Table D15.

The enthalpy, Gibbs energy and entropy were predicted for this reaction, Table 5.8.

Table 5.8: Calculated changes in enthalpy, Gibbs energy and entropy for QM formation at standard temperature and pressure.

$\Delta_r H^\circ(298K)$ [kJ mol ⁻¹]	$\Delta_r G^\circ(298K)$ [kJ mol ⁻¹]	$\Delta_r S^\circ(298K)$ [J mol ⁻¹ K ⁻¹]
-61.4 ± 3.4	-59.9 ± 3.4	-5.04

The change in enthalpy for analogue QM formation was $-61.4 \pm 3.4 \text{ kJ mol}^{-1}$, which suggested that this reaction is less exothermic by 8.2 kJ mol^{-1} than for analogue OHPP–NO₂ adduct. The Gibbs energy is negative $-59.9 \pm 3.4 \text{ kJ mol}^{-1}$, the forward reaction will proceed spontaneously and it is more negative than for OHPP–NO₂ formation; by 39.9 kJ mol^{-1} .

5.4 Discussion

Calculated reaction enthalpies, entropies and Gibbs energies of the formation of nitrated phenolics and quinone methides, are useful in examining the reaction mechanism presented in Chapter 4. A potential energy diagram was proposed for all phenolic species studied here and the ceiling temperatures for the formation of nitrated and non-nitrated products were predicted.

5.4.1 Potential Energy Diagram for Reactions of Phenolics with NO₂

The enthalpies and entropies of formation of key species involved in the reaction of NO₂ with phenolic compounds were calculated and four phenolic species were examined 4-methyl-2,6-di-*tert*-butylphenol (BHT), ethyl-substituted butylated phenol (EthPh), tri-*tert*-butylphenol (TTBP) and an ethyl analogue of octadecyl 3-(3,5-di-*tert*-butyl-4-hydroxy-phenyl)propanoate (OHPP analogue).

The OHPP analogue values have been used to construct a potential energy diagram for the system, which is representative for all studied phenolics, shown in Figure 5.16.

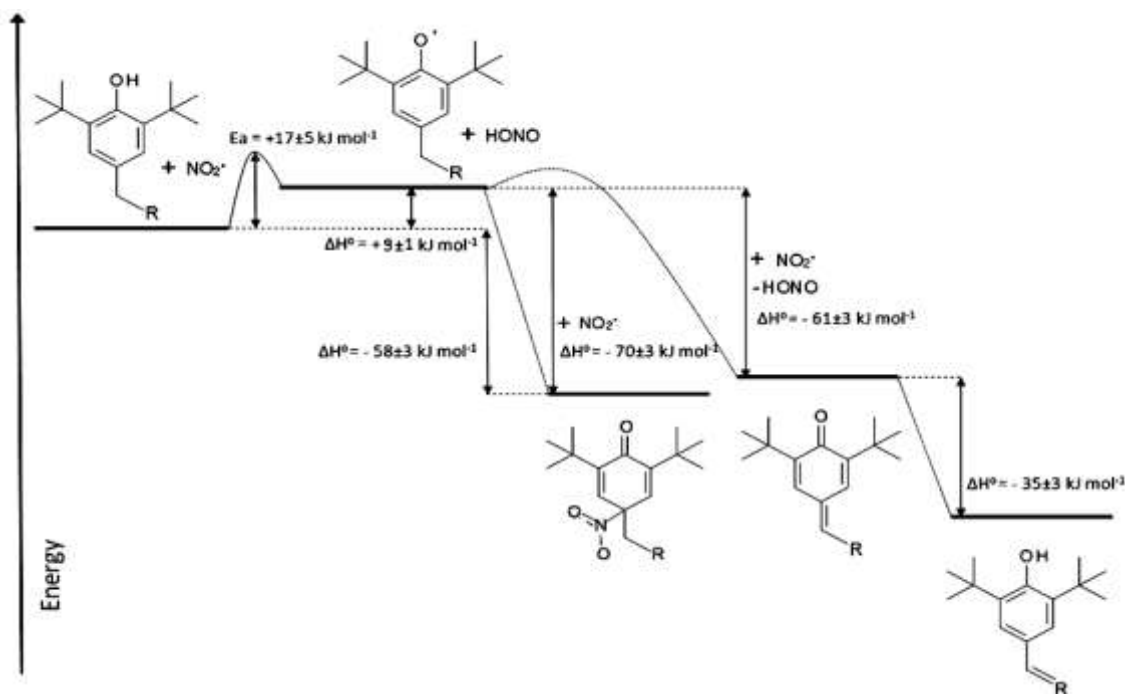


Figure 5.16: Potential energy diagram of reactions phenolic species with NO_2 .

There are four reactions in the diagram, for which heats of formation need to be considered. Firstly initiation, i. e. hydrogen abstraction from the antioxidant by nitrogen dioxide, the second is the addition of NO_2 to the phenoxyl radical at low temperature; the third is where the second weakest hydrogen is abstracted by NO_2 with the formation of quinone methide and nitrous acid. The fourth reaction is the conversion of quinone methide to hydroxycinnamate.

In the initiation step the literature (O—H) OHPP bond dissociation energy of $339.6 \pm 0.4 \text{ kJ mol}^{-1}$ was used,¹⁶⁴ which is taken as representative of all phenols. The (O—H) BDE for different phenolic species was studied in this work and the difference in predicted and experimental (O—H) BDE for all was approximately 1.9 kJ mol^{-1} (Appendix D, Table D16). Therefore it is considered to be negligible, and OHPP values are used here as an example.

The literature (O—H) BDE of OHPP the $339.6 \pm 0.4 \text{ kJ mol}^{-1}$ and nitrous acid of $330.9 \pm 1 \text{ kJ mol}^{-1}$ have been used,^{164, 166-168} to calculate the enthalpy of initiation reaction, which is positive $9 \pm 1 \text{ kJ mol}^{-1}$, and suggests that the reaction is slightly endothermic; a similar value of 11 kJ mol^{-1} was calculated previously for sterically hindered phenols by Denisov *et al.* 1995.¹⁷¹

To complete the first reaction, the activation energy of $17 \pm 5 \text{ kJ mol}^{-1}$, for the reaction of phenolic hydrogen abstraction by NO₂, measured by Davydov *et al.* in 1997 was used.¹⁴⁸

Davydov's experimental data for the rate constant against the temperature in Arrhenius diagram (Figure 5.17) resulted in a straight line with an activation energy of $E_a = +17 \pm 5 \text{ kJ mol}^{-1}$, which is higher than quoted in their paper ($E_a = 10 \text{ kJ mol}^{-1}$). This discrepancy in activation energies was due to Davydov's error in calculations. The $+17 \pm 5 \text{ kJ mol}^{-1}$, calculated activation energy value is assumed for all phenolic species.

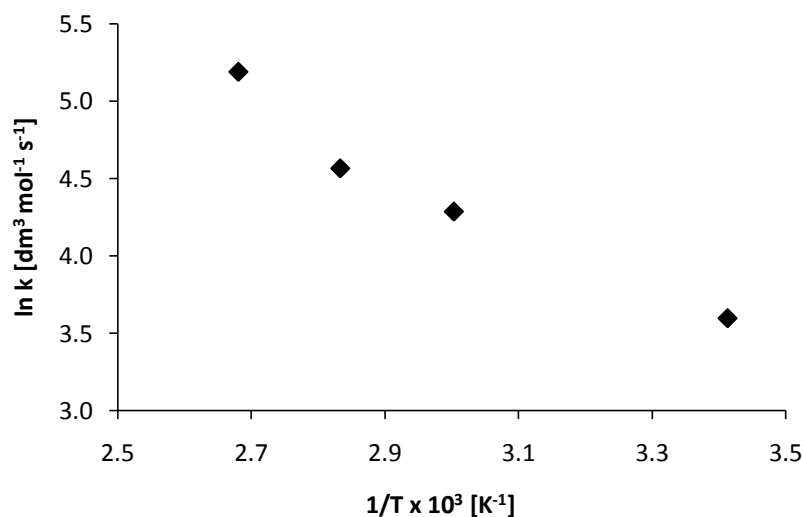


Figure 5.17: Arrhenius equation of the dependence of the rate constant $\ln k$ on the temperature $1/T$ for TTBP (previous studies).¹⁴⁸

The second reaction, the formation of nitrated phenolics is a radical-radical termination, which is therefore assumed here to be barrierless, as is the case with the addition

of NO₂ to peroxy radicals.¹⁵⁹ The enthalpy of formation the OHPP–NO₂ adduct was calculated to be $-70 \pm 3 \text{ kJ mol}^{-1}$, using predicted thermochemical values from Gaussian.

The third reaction was the formation of quinone methide by hydrogen abstraction from the phenoxyl radical by NO₂, which was slightly less exothermic, $\Delta_r H^\circ = -61 \pm 3 \text{ kJ mol}^{-1}$, than for NO₂ addition. The activation energy for this reaction is unlikely to be barrierless; however, comparing the relevant calculated C–H bond strength of the phenoxyl radical with the comparable O–H bond strength in the parent phenol, Table 5.9, shows that it is considerably weaker at $79.3 \pm 3 \text{ kJ mol}^{-1}$, hence it is likely that the activation energy for the third reaction is much lower than for the first reaction. Therefore the activation energy measured for the overall reaction by Davydov is assumed to be that for the initial abstraction (first reaction), with the barrier for (lower) third reaction.

Previous studies of the difference between the O–H and C–H BDE in phenols, suggested that the phenolic O–H bond is more likely to be attacked than C–H.^{171,159} Therefore the energy difference for O–H and C–H BDE's in OHPP were predicted in Table 5.9. In general, the weakest bonded hydrogen from (O–H) will be abstracted first, then next most favourable will be hydrogen at α carbon (C–H) and the last, the hydrogen at the β carbon (C–H).

Table 5.9: Comparison of experimental and calculated bond strengths for phenol O-H, phenoxy & benzyl-NO₂ adducts and C-H bond strengths for phenoxy radicals.

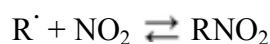
Phenolic	BDE [kJ mol ⁻¹]
	Calculated using DFT BPV86/6-311G (d,p) (this work)
OHPP(O-H)	341.3 ± 3.4
OHPP (C-H) α carbon	378.5 ± 3.4
OHPP (C-H) β carbon	405.6 ± 3.4
(OHPP) phenoxy-NO ₂	79.3 ± 3.4

One feature of the potential energy diagram is that the first reaction is endothermic, hence the initial hydrogen atom abstraction from phenols by NO₂ could be reversible, were it not for a fast reaction for the phenoxy radicals of reaction with an additional NO₂ molecule. The second feature is that the addition of NO₂ to phenoxy radicals (second reaction) is both slightly more exothermic than the competing hydrogen atom abstraction reaction (third reaction) and is also barrierless. Therefore, at sufficiently low temperatures, the addition of NO₂ (second reaction) will dominate over the hydrogen abstraction by NO₂ (third reaction). However, the second reaction is not greatly exothermic, so it is possible that at sufficiently high temperature the addition could become reversible.

Finally, there was another product identified from further reaction of QM with NO₂, the octadecyl (E)-3-(3,5-ditert-butyl-4-hydroxy-phenyl) prop-2-enoate (Hydroxy Cinnamate, HCIN), which is formed by the rearrangement of the quinone methide with the transfer of a hydrogen from the β carbon of the alkyl chain, which restores the aromaticity. The formation of HCIN was more exothermic than the formation of QM (by 35 ± 3 kJ mol⁻¹), which is consisted with HCIN being formed from QM in polar solvent.

5.4.2 The Ceiling Temperature

The thermodynamic calculations given in the section above can be used to predict the equilibrium constant of the reactions examined. In this section prediction of the ceiling temperature are based on the example of equilibrium reaction [5.1] (the reaction of formation of nitrated phenolics, where R is BHT):



For reaction [5.1], the calculated Gibbs energy was negative that suggests this reaction is spontaneous at standard conditions (i.e. at 1 bar of NO_2 and 298K). The calculated enthalpy and entropy changes were both negative, which indicates that the equilibrium constant will be favourable at low temperatures, but that at high temperatures is not favourable, and will have a noticeable reverse reaction.

In elementary applications, equilibrium constant can be expressed using for example: molar concentrations $[X]$ (as $[X]/[X]^\ominus$, where $[X]^\ominus = 1 \text{ mol dm}^{-3}$) and the equilibrium constant K_c is using subscript “c” for the “concentration”,

$$K_c = \frac{[RNO_2]}{[R][NO_2]} \quad \text{Equation 5.1}$$

or the numerical values of partial pressures p_X (as p_X/p_X^\ominus , where $p_X^\ominus = 1 \text{ bar}$), where the equilibrium constant K_p using subscript “p” for the “pressure”. At low overall pressures (when gas cannot be treated as a perfect), the activities are represented using ratios of partial pressures and the approximate equilibrium constant is expressed as:

$$K_p = \frac{(p_{RNO_2}/p^\ominus)}{(p_R/p^\ominus)(p_{NO_2}/p^\ominus)} = \frac{p_{RNO_2} p^\ominus}{p_R p_{NO_2}} \quad \text{Equation 5.2}$$

These equilibrium constants interpreted as K_c or K_p are only approximations.

In thermodynamic calculations the equilibrium constant K is expressed in terms of activities and is called a thermodynamic equilibrium constant.¹⁵⁶ For example, the thermodynamic equilibrium constant for the heterogeneous equilibrium, reaction [5.1]

$R(l) + NO_{2(g)} \rightleftharpoons RNO_{2(l)}$ can be expressed as:

$$K = a_{R(l)}^{-1} a_{NO_{2(g)}}^{-1} a_{RNO_{2(l)}} = \frac{a_{RNO_{2(l)}}}{\underbrace{a_{R(l)} a_{NO_{2(g)}}}_1} = \frac{1}{a_{NO_{2(g)}}} \quad \text{Equation 5.3}$$

The thermodynamic equilibrium constant is dimensionless, because activities “ a ” are dimensionless numbers.¹⁵⁶ Provided the nitrogen dioxide can be treated as a perfect gas, the equilibrium constant can be written:

$$K \approx \frac{p^\ominus}{p_{NO_2}} \quad \text{Equation 5.4}$$

Consequently, the ceiling temperature (T_c) can be calculated, as previously described for oxidation studies by Benson,¹⁷² and can be defined as the temperature at which the rates of the forward and backward reactions will be equal ($k_{5.1} = k_{-5.1}$), so the equilibrium constant, for the reaction [5.1] will be unity ($K = k_{5.1} / k_{-5.1} = 1$), and above which the reverse reaction is favourable, e.g. Figure 5.18.

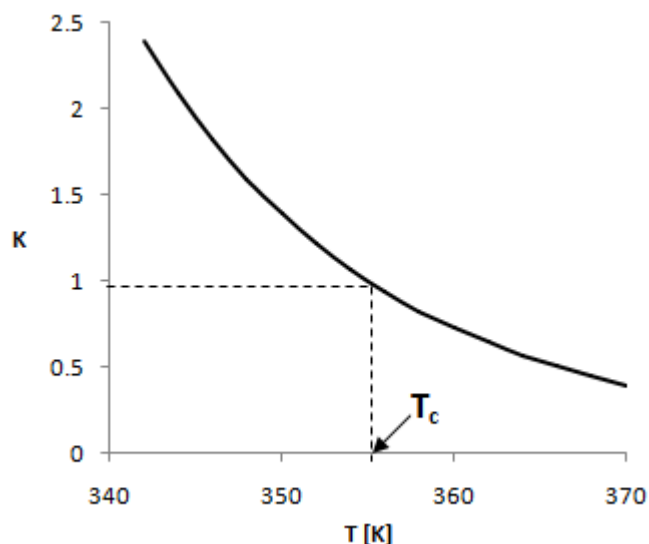


Figure 5.18: Equilibrium constant vs. temperature. Example of determination of ceiling temperature for reaction $R + NO_2 \rightleftharpoons RNO_2$ [5.1], when $K=1$.

The temperature dependence of the equilibrium constant (dimensionless) is taken from the Gibb's energy law, where at equilibrium ($\Delta G = 0$):

$$\Delta G = \Delta G^\circ + RT \ln K \quad \text{Equation 5.5}$$

At standard conditions:

$$\Delta G^\circ = \Delta H^\circ - T\Delta S^\circ \quad \text{Equation 5.6}$$

Combining equations 5.5 and 5.6:

$$K = e^{\left(\frac{-\Delta G}{RT}\right)} = e^{\left(\frac{-\Delta H^\circ}{RT}\right)} e^{\left(\frac{\Delta S^\circ}{R}\right)} \quad \text{Equation 5.7}$$

With $K = 1$, when $T = T_c$ therefore at standard pressure:

$$T_c = \frac{\Delta H^\circ}{\Delta S^\circ} \quad \text{Equation 5.8}$$

The ceiling temperature is pressure dependent and the correlation between the temperature and pressure will play a crucial role in explaining the products of reactions.

5.4.2.1 Pressure Dependence of Ceiling Temperatures

Previous nitration studies were performed at standard pressure (1bar NO₂),^{83,94,146} whereas this work uses 1000 times lower concentration of NO₂ (0.001 bar = 1000 ppm), therefore the effect of pressure on ceiling temperature needs to be calculated.

Combining equation 5.2 and 5.7 gives:

$$\frac{p^\ominus}{p_{NO_2}} = e^{\left(\frac{-\Delta H^\ominus}{RT}\right)} e^{\left(\frac{\Delta S^\ominus}{R}\right)} \quad \text{Equation 5.9}$$

Taking natural logs of both sides and cancelling gives:

$$\ln\left(\frac{p^\ominus}{p_{NO_2}}\right) = \frac{\Delta S^\ominus}{R} - \frac{\Delta H^\ominus}{RT_c} \quad \text{Equation 5.10}$$

Finally, rearranging equation 5.10 gives equation 5.11 (where p^\ominus/p_{NO_2} corresponds to [NO₂], because the relation between the K_p and K_c equilibrium is proportional, $K_p = K_c/RT$):

$$T_c = \frac{\Delta H^\ominus}{\Delta S^\ominus + R \ln\left(\frac{p_{NO_2}}{p^\ominus}\right)} \quad \text{Equation 5.11}$$

Equation 5.11 gives the correction due to having a different pressure to the standard pressure. By using the subsequent ΔH^\ominus and ΔS^\ominus values the ceiling for reactions [5.1]-[5.7] can be calculated, Figures 5.19-5.25. The importance of ceiling temperature is that for given NO₂ pressure, it explains the change in observed products at different temperatures and how the experiment temperature compares with the ceiling temperature. The ceiling temperature was studied here to examine the apparent irreversible addition of NO₂ to phenolics at low temperatures (1 bar NO₂), which change to reversible at high temperature (0.001 bar NO₂), as discussed in Chapter 4.

5.4.2.2 Ceiling Temperature for NO₂ Addition

T_c calculations for BHT• + NO₂ ⇌ BHT–NO₂

The ceiling temperature for the liquid phase reaction of BHT radical with gaseous NO₂ will be approximately 34 ± 34 °C at 1000 ppm (0.001 mbar) of NO₂, as shown in Table 5.10, (graphical in Figure 5.12), but 126 ± 44 °C at 1 bar of NO₂.

Table 5.10: Estimated Ceiling Temperature for reaction BHT• + NO₂ ⇌ BHT–NO₂ at Different Partial Pressures of NO₂

NO ₂ */NO ₂		Ceiling Temperature DFT calculations	
	[ppm]	T _c [K]*	T _c [°C]*
0.00001	10	266	-7 ± 29
0.0001	100	285	12 ± 32
0.001	1000	307	34 ± 34
0.01	10000	332	59 ± 37
0.1	100000	363	90 ± 40
1	1000000	399	126 ± 44
10	10000000	443	171 ± 49

*mean temperature range

Nitrated BHT was identified previously by Brunton *et al.* 1979,⁸³ for a reaction performed at room temperature and 1 bar NO₂. Figure 5.19 shows the ceiling temperature for BHT–NO₂, which suggest that addition of NO₂ to BHT radical will indeed be irreversible at room temperature.

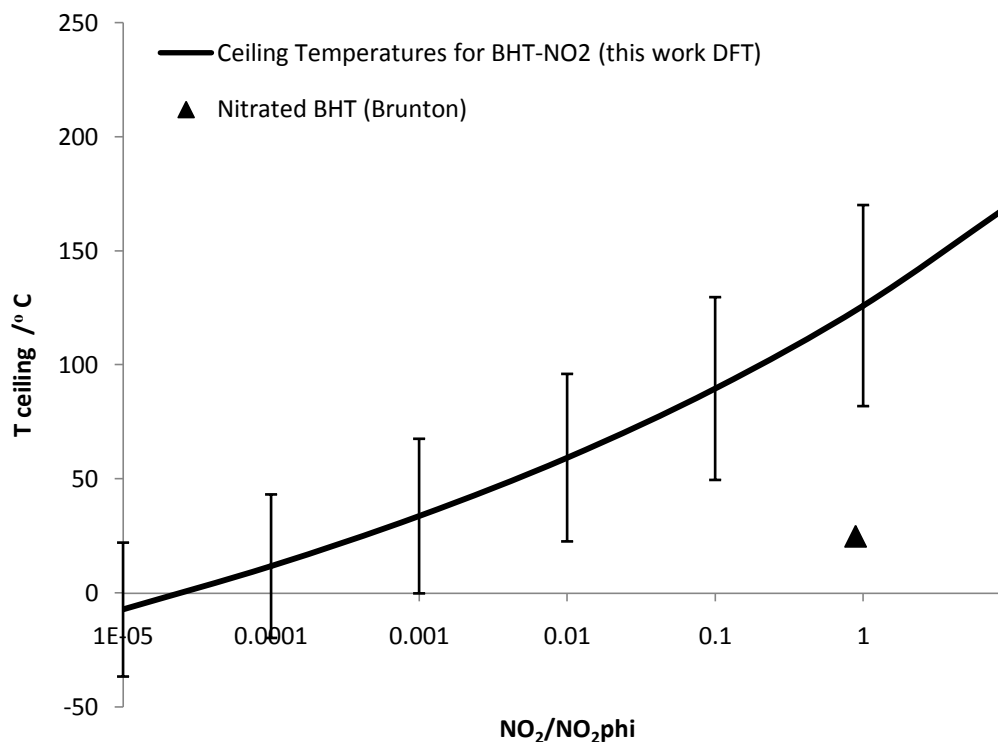


Figure 5.19: Calculated ceiling temperatures for BHT–NO₂ formation (the line) (this work), compared to the experimental conditions 25 °C and 1 bar NO₂ used by Brunton (the triangle) (previous studies), which product was nitrated BHT.

However in work reported here, experiments were performed at 180 °C and with approximately 1000 ppm of NO₂, which is significantly above the ceiling temperature (34 ± 34 °C) for BHT–NO₂ formation. At these conditions, the addition to BHT radical would be probably be reversible and this was proven with the identification of non-nitrated, quinone methide products from EthPh and OHPP.

Addition through Nitrogen or Oxygen of NO₂

Comparing BHT–NO₂ with BHT–ONO (Figure 5.20) where the difference is in the addition of NO₂ radical through the nitrogen or oxygen atom (NO₂ mesomeric structures),⁹⁴ the estimated ceiling temperature for BHT–ONO was approximately 59 °C lower than for BHT–NO₂.

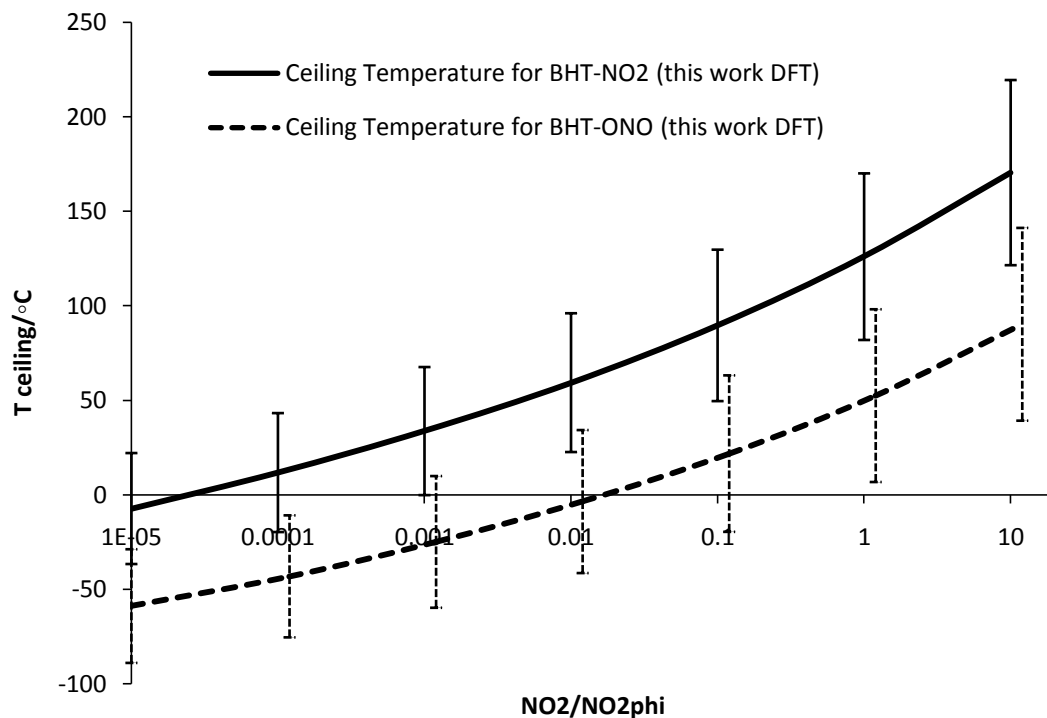


Figure 5.20: Ceiling Temperatures for BHT-ONO formation.

The mesomeric structures effect was studied previously by Astolfi *et. al* 2005,⁹⁴ who performed reactions at room temperature (1 bar NO_2) and proposed a two-way mechanism for both products of addition through the oxygen and nitrogen of NO_2 .

The ceiling temperatures for BHT- NO_2 and BHT-ONO is consistent with previous thermodynamics calculations, which suggested that BHT-ONO was weaker bonded than BHT- NO_2 ,⁹⁴ the calculation of ceiling temperature for BHT-ONO is shown in Table 5.11.

Table 5.11: Estimated Ceiling Temperature for reaction $\text{BHT}^\bullet + \text{NO}_2 \rightleftharpoons \text{BHT-ONO}$ at Different Partial Pressures of NO₂.

NO ₂ [*] /NO ₂		Ceiling Temperature DFT calculations	
	[ppm]	T _c [K]*	T _c [°C]*
0.00001	10	214	-59 ± 30
0.0001	100	230	-43 ± 32
0.001	1000	248	-25 ± 35
0.01	10000	269	-4 ± 38
0.1	100000	295	22 ± 41
1	1000000	326	52 ± 46
10	10000000	363	90 ± 51

*mean temperature range

Previous authors identified nitrated phenolics at room temperature (1 bar NO₂); this work supports existing results and will explain the ceiling temperature for the formation of both possible products.

T_c calculations for $\text{TTBP}^{\bullet} + \text{NO}_2 \rightleftharpoons \text{TTBP}-\text{NO}_2$

The estimated ceiling temperature from Table 5.12 for TTBP nitration was approximately 160 ± 42 °C at 1 bar of NO_2 , Figure 5.21.

Table 5.12: Estimated Ceiling Temperature for reaction $\text{TTBP}^{\bullet} + \text{NO}_2 \rightleftharpoons \text{TTBP}-\text{NO}_2$ at Different Partial Pressures of NO_2

$\text{NO}_2^*/\text{NO}_2$		Ceiling Temperature DFT calculations	
	[ppm]	T_c [K]*	T_c [°C]*
0.00001	10	294	-21 ± 28
0.0001	100	314	41 ± 30
0.001	1000	337	64 ± 33
0.01	10000	364	91 ± 35
0.1	100000	396	123 ± 38
1	1000000	434	160 ± 42
10	10000000	479	206 ± 46

*mean temperature range

Kinetics and the mechanism of nitration of TTBP was studied previously by Davydov *et al.* 1997,¹⁴⁸ therefore the ceiling temperature was predicted in this work, in order to compare with previous studies.

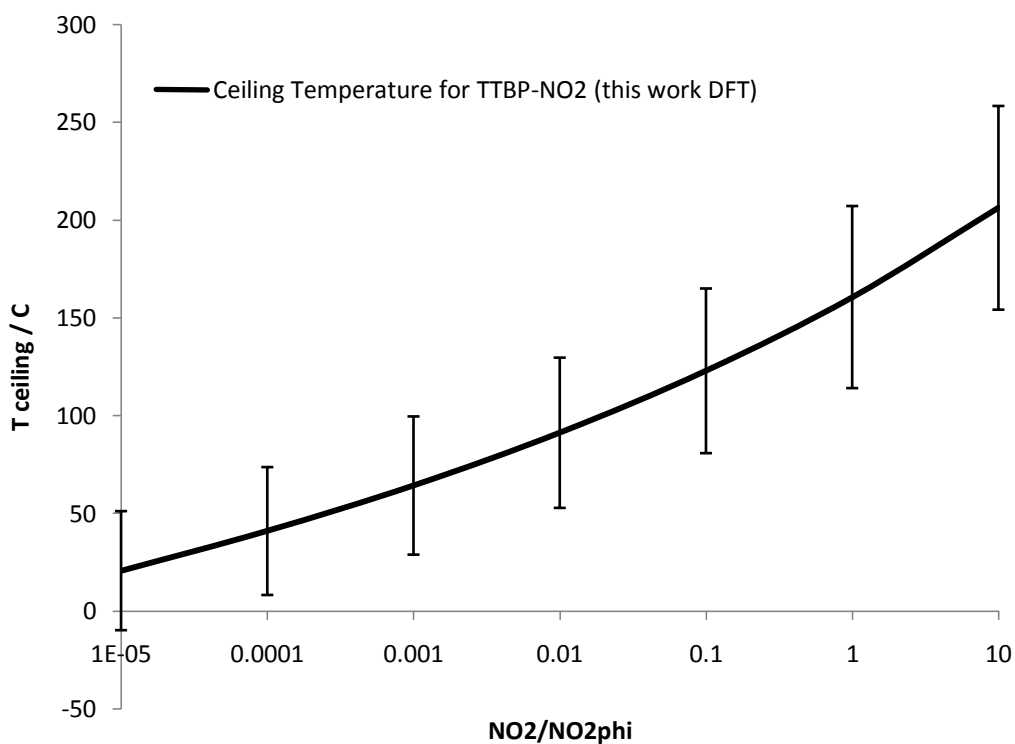


Figure 5.21: Ceiling Temperatures for TTBP–NO₂ formation.

Result of the ceiling temperature calculations for TTBP supported Davydov's mechanism, suggesting nitrated TTBP formation at room temperature.

T_c calculations for EthPh• + NO₂ ⇌ EthPh–NO₂

Another important reaction was the nitration of 2,6-ditert-butyl-4-ethyl-phenol (EthPh), the ceiling temperature prediction was plotted in Figure 5.22 (data Table 5.13).

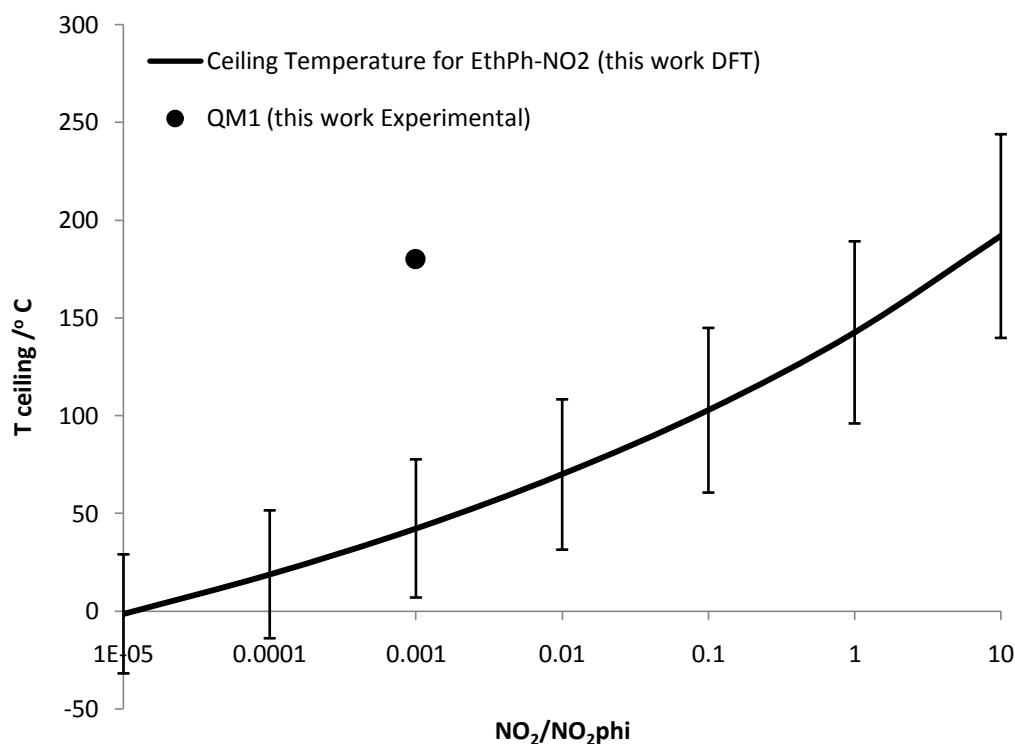


Figure 5.22: Calculated ceiling temperatures for EthPh–NO₂ formation (line) (this work), compared to the experiment carried out at 180 °C and 0.001 bar (the dot), which produced quinone methide (QM1) product from EthPh (this work).

The experimental result was plotted together with T_c , which was obtained using 1000 ppm NO₂ and 180 °C; under these conditions only a non-nitrated antioxidant product was observed (quinone methide from EthPh, QM1) which is consistent with the reaction conditions being above the ceiling temperature (at 1000 ppm NO₂) of 42 ± 35 °C, as shown in Figure 5.22.

Table 5.13: Estimated Ceiling Temperature for reaction $\text{EthPh}^{\cdot} + \text{NO}_2 \rightleftharpoons \text{EthPh-NO}_2$ at Different Partial Pressures of NO₂

NO ₂ [*] /NO ₂		Ceiling Temperature DFT calculations	
	[ppm]	T _c [K]*	T _c [°C]*
0.00001	10	272	-1 ± 30
0.0001	100	292	19 ± 33

0.001	1000	315	42 ± 35
0.01	10000	343	70 ± 38
0.1	100000	376	103 ± 42
1	1000000	416	143 ± 47
10	10000000	465	192 ± 52

*mean temperature range

Finally, the EthPh result was compared with OHPP, a commercial phenolic antioxidant, calculation below.

T_c calculations for OHPP• + NO₂ ⇌ OHPP–NO₂

Estimated ceiling temperatures for the reaction of the analogue OHPP radical with 1000 ppm of NO₂ (Table 5.14) with the formation of the nitrated product was approximately 76 ± 38 °C, which was below the experimental temperature of 180 °C at 1000 ppm NO₂, shown in Figure 5.23. This was consistent with product identification, where a non-nitrated antioxidant product (quinone methide from OHPP, QM) was identified, (details in Chapter 4).

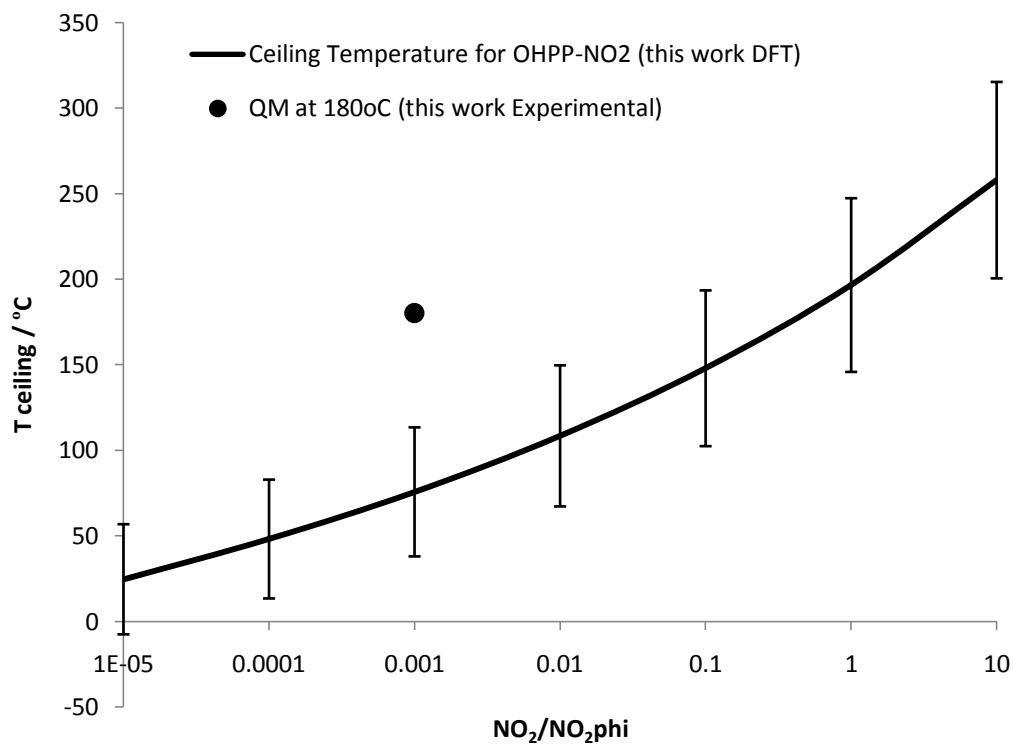


Figure 5.23: Calculated ceiling temperatures for OHPP–NO₂ formation (the line) (this work), compared to the experiment conditions 180 °C and 0.001 bar (this work), which produced quinone methide (QM) product from OHPP.

That explains why at 180 °C and 0.001 bar NO₂, which is above the ceiling temperature of nitration, the only product identified was the non-nitrated, Quinone Methide (QM).

Table 5.14: Estimated Ceiling Temperature for reaction $\text{OHPP}^\bullet + \text{NO}_2^\bullet \rightleftharpoons \text{OHPP-NO}_2$ at Different Partial Pressures of NO₂

NO ₂ [*] /NO ₂		Ceiling Temperature DFT calculations	
	[ppm]	T _c [K]*	T _c [°C]*
0.00001	10	298	25 ± 32
0.0001	100	321	48 ± 35
0.001	1000	349	76 ± 38
0.01	10000	382	109 ± 41
0.1	100000	421	148 ± 46
1	1000000	470	197 ± 51
10	10000000	531	258 ± 57

*mean temperature range

To obtain more information on quinone methides formation, further ceiling temperature calculations were undertaken.

5.4.2.3 Ceiling temperature for Quinone Methides formation

The ceiling temperatures for formation of non-nitrated products from EthPh and OHPP were predicted Tables 5.15 and 5.16, and were compared with experimental results in Figure 5.24.

Table 5.15: Estimated Ceiling Temperature for reaction EthPh[•] + NO₂ ⇌ QM1 + HONO at Different Partial Pressures of NO₂

NO ₂ [*] /NO ₂		Ceiling Temperature DFT calculations	
	[ppm]	T _c [K]*	T _c [°C]*
0.00001	10	726	453 ± 83
0.0001	100	896	623 ± 103
0.001	1000	1169	896 ± 134
0.01	10000	1681	1408 ± 193
0.1	100000	2995	2722 ± 344

*mean temperature range

The calculation of the ceiling temperature for QM was based on the reaction of hydrogen abstraction by NO₂ from phenoxy radical with the formation of a non-nitrated quinone methide product.

Table 5.16: Estimated Ceiling Temperature for reaction OHPP[•] + NO₂[•] ⇌ QM + HONO at Different Partial Pressures of NO₂

NO ₂ [*] /NO ₂		Ceiling Temperature DFT calculations	
	[ppm]	T _c [K]*	T _c [°C]*
0.00001	10	693	420 ± 84
0.0001	100	856	583 ± 103
0.001	1000	1118	845 ± 135
0.01	10000	1612	1339 ± 194
0.1	100000	2888	2615 ± 348

*mean temperature range

A comparison of the experimental results, where QM1 and QM were identified, to estimated ceiling temperatures are shown in Figure 5.24.

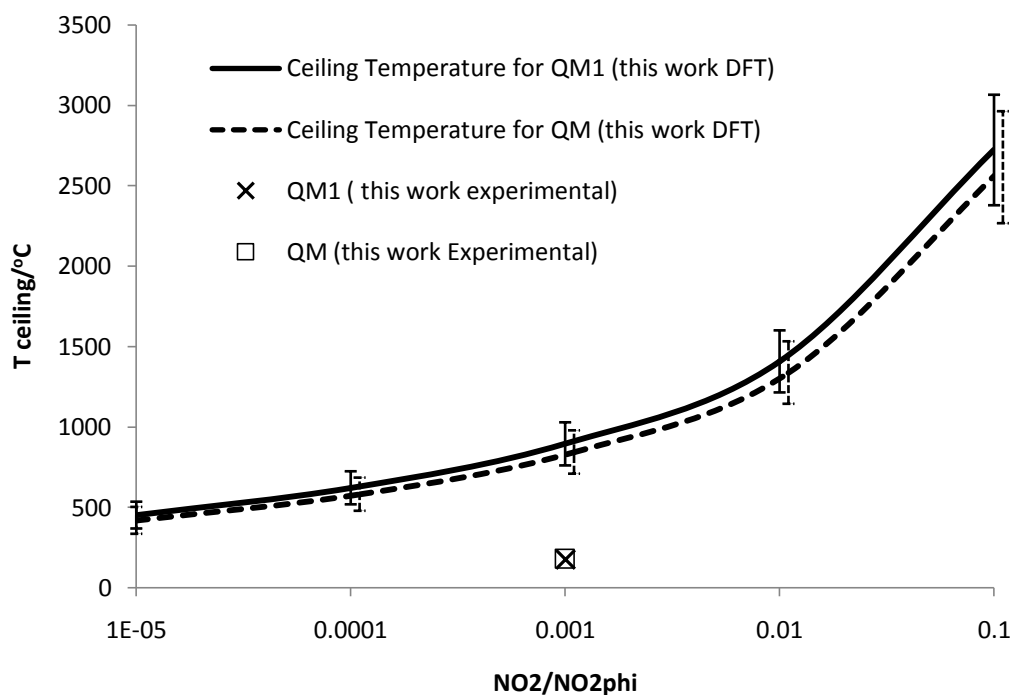


Figure 5.24: Calculated ceiling temperatures for QM and QM1 formation (lines) compared to the experimental conditions (two experiments), which produced QM and QM1.

The ceiling temperature for quinone methide formation from OHPP (at 1000 ppm NO₂) will be approximately 845 ± 135 °C; this is the temperature below which the formation of non-nitrated product (QM) will be spontaneous. This supports the product identification presented in Chapter 4.

5.4.2.4 Summary of T_c Calculations

Results of ceiling temperatures for different phenolic- NO_2 adducts were similar and shown increase of T_c with a size of molecule, Figure 5.25.

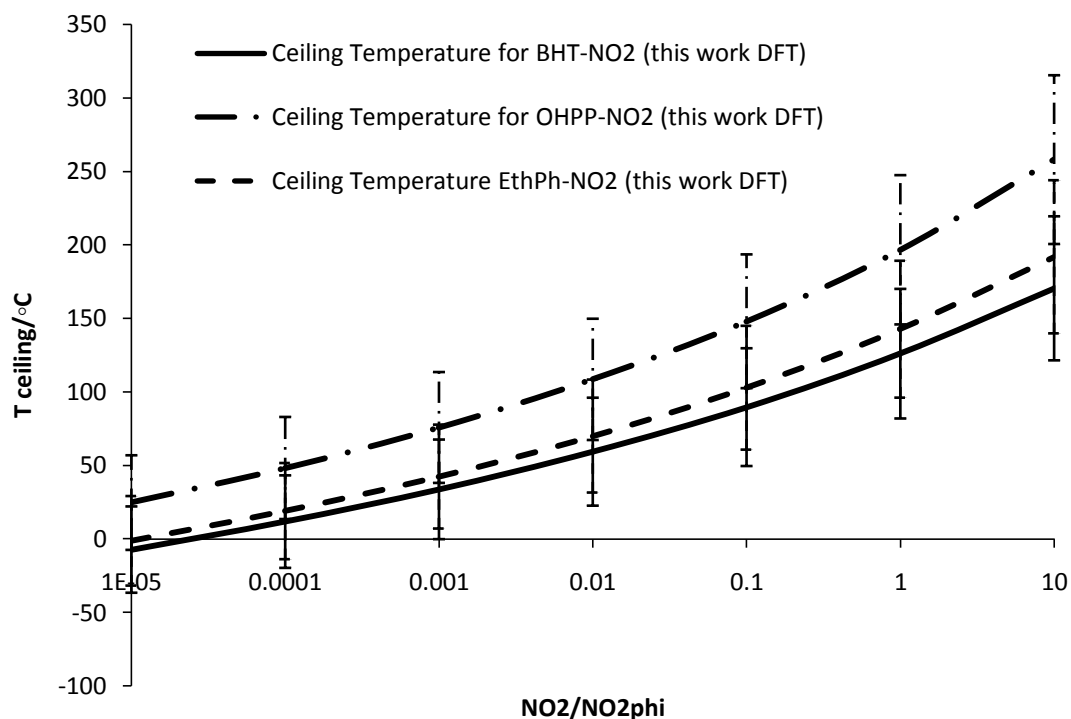


Figure 5.25: Estimated ceiling temperatures for nitrated BHT, EthPh and OHPP.

Therefore the overall ceiling temperature, for all nitrated phenolic species, was estimated as approximately 51 ± 57 °C (at 0.001 bar NO_2) and compared to previous and current experimental results, Figure 5.26.

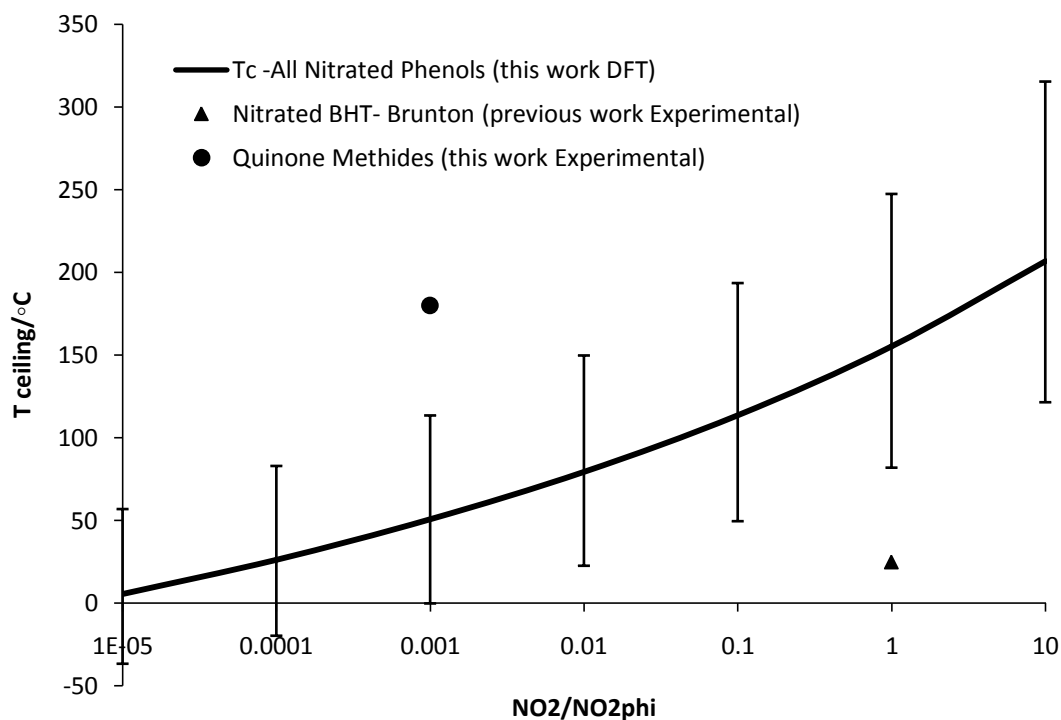


Figure 5.26: Comparison of previous experimental conditions (25 °C and 1 bar), which produced nitrated BHT (the triangle) and current experiments (with EthPh, OHPP; at 180 °C and 0.001bar NO₂), which produced quinone methides (the dot), to the calculated ceiling temperature for nitrated phenolics (the line).

This summary (Figure 5.26) shows that the ceiling temperature for phenolic–NO₂ adducts formation increases with increasing reaction temperature and pressure of NO₂. It supports experimental identification as it suggests that below T_c (such as room conditions, Brunton’s studies) nitrated products will form spontaneously and reaction is irreversible, but above T_c (e.g. 180 °C, engine ring pack conditions with low NO₂ concentration, this study) nitration will be reversible and non-nitrated products will preferably form.

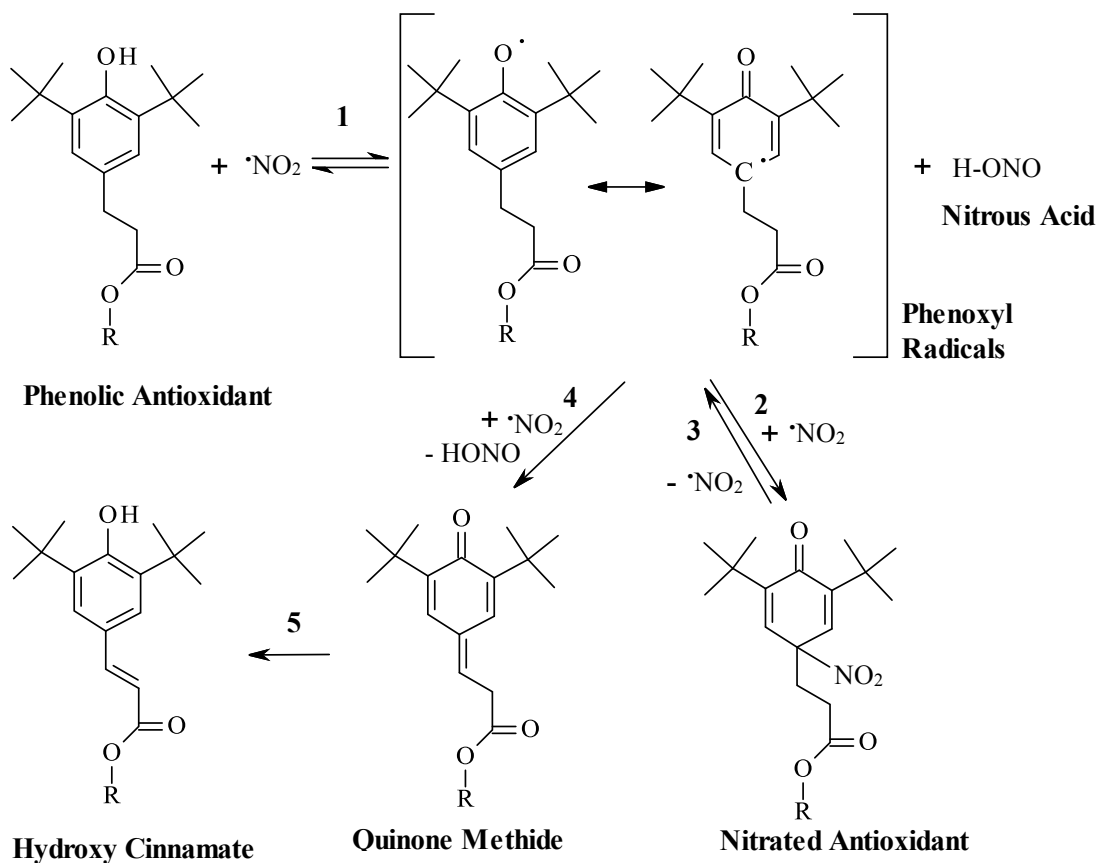


Figure 5.27: Proposed reaction mechanism based on product identification for the reaction of 0.5% OHPP in squalane with 1000 ppm of NO_2 at 180 °C.

The ceiling temperature estimation helps to explain the temperature and pressure limitations for OHPP– NO_2 formation (reaction 2), which is reversible above 76 ± 38 °C (at 0.001 bar NO_2) (reaction 3) and supports the novel reaction mechanism of formation of quinone methide (reaction 4) at 180 °C.

5.5 Summary

Gaussian software 09 has been used successfully to explain the thermochemistry of the reaction mechanisms of phenolic antioxidants with NO₂ under the piston ring pack conditions (180 °C and 1000 ppm NO₂) and supported the reaction mechanism based on products identification, proposed in Chapter 4.

Four phenolic species were studied here octadecyl 3-(3,5-di-tert-butyl-4-hydroxyphenyl)propanoate (OHPP), 2,6-di-tert-butyl-4-ethylphenol (EthPh), 2,4,6-tri-tert-butylphenol (TTBP) and 4-methyl-2,6-di-tert-butylphenol (BHT), and two main reactions were investigated; the addition of NO₂ to phenoxy radical with formation of nitrated phenolic and the abstraction of hydrogen by NO₂ from phenoxy radical at α carbon with the formation of the non-nitrated product, quinone methide.

The effect of the pre-testing of various density functional theory (DFT) methods resulted in choosing the best DFT BPV86/6-311G(d,p) computational method for studying phenols, phenol–NO₂ adducts and quinone methides. The decision was based on comparison of predicted and experimental bond dissociation energies (BDE) of model compounds with the mean absolute deviation calculated approximately 3.4 kJ mol⁻¹ and relatively short calculation time.

Computed thermochemical values were used in calculations of enthalpies, entropies and Gibbs energies and the overall energy diagram was proposed for NO₂ reactions with phenolic species.

The estimated ceiling temperature for nitration of phenolics agrees with experimental results and shows the temperature and pressure limitations for addition of NO₂ to phenoxy radical. Previous studies reported nitrated phenolics at room temperature

(1 bar NO₂), which is below the ceiling temperature predicted here for nitration, calculated to be approximately 155 ± 82 °C, so it agrees that at this conditions the reaction proceeds spontaneously and irreversibly. Experimental studies (Chapter 4), which were undertaken at 180 °C and 0.001 bar NO₂ are above the ceiling temperature of formation of phenolic–NO₂ adducts, was calculated as approximately 51 ± 57 °C at 0.001 bar NO₂, therefore under engine ring pack conditions, nitration will be reversible and the non-nitrated (quinone methide) product will form, supporting the novel reaction mechanism proposed in Chapter 4.

Chapter 6: Reaction of Aminic Antioxidant with NO₂ at Elevated Temperature

6.1 Introduction

The reaction of aminic antioxidants with NO₂ at high temperature, (i.e. engine piston conditions) have not been previously studied in detail; however, aminic antioxidants have been explored as oxidation inhibitors in engine lubricants and their interactions with different radicals have been proposed, with details given in Chapter 1.^{102,107,173}

Furthermore nitrogen dioxide has been used as a cheap reagent in chemical synthesis, where reaction of diphenylamine with NO₂ have been studied at slightly elevated temperatures in solvent-free environments and the dimeric product was reported, reaction [1.93] in Chapter 1.¹¹⁴ Other characteristic products formed by the reaction of amines with NO₂ were N-nitrosamines and N-nitramines.¹⁷⁴

This chapter shows the result of interactions of the commercial aminic antioxidant, 4,4'-Diocetyl Diphenylamine (DODPA), Figure 6.1, (BASF, Irganox® L01) with 1000 ppm NO₂ at 180 °C, the same conditions as previously studied for phenolic antioxidant in Chapter 4.

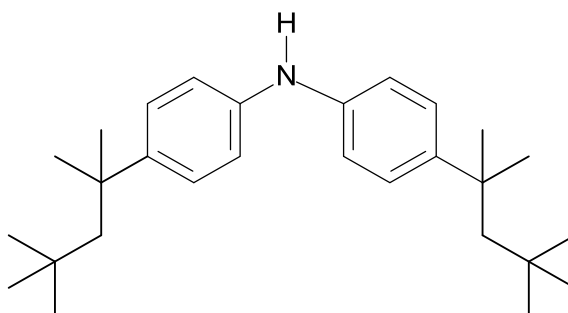


Figure 6.1: Structure of the commercial aminic antioxidant; 4,4'-Diocetyl Diphenylamine (DODPA), BASF Irganox® L01.

Therefore, the work reported here is novel and complements the work described in Chapters 4 and 5 on the reaction of phenolic antioxidants with NO₂.

6.2 Results and discussion

6.2.1 Reaction Procedure

The reaction of the aminic antioxidant (DODPA), at concentration of 1.0×10^{-2} mol dm⁻³ (0.5% w/w) in squalane, with 1000 ppm of nitrogen dioxide was undertaken in a similar manner as described for phenolic antioxidant in Chapter 4. The reaction was run until the antioxidant and its intermediates were consumed in their entirety. Reaction mixtures were extracted frequently at: 0, 5, 10, 15, 20, 30, 45, 60, 75, 90, 120 minutes and analysed by GC-FID, accurate GC/TOF MS (EI).

6.2.2 Product Identification using GC-FID

Examination of the reaction mixture (60 min. sample) by GC-FID showed seven products (labelled here A, B, 1, 2, 3, 4 and 5), Figure 6.2, which formed from interactions of aminic antioxidant with NO₂.

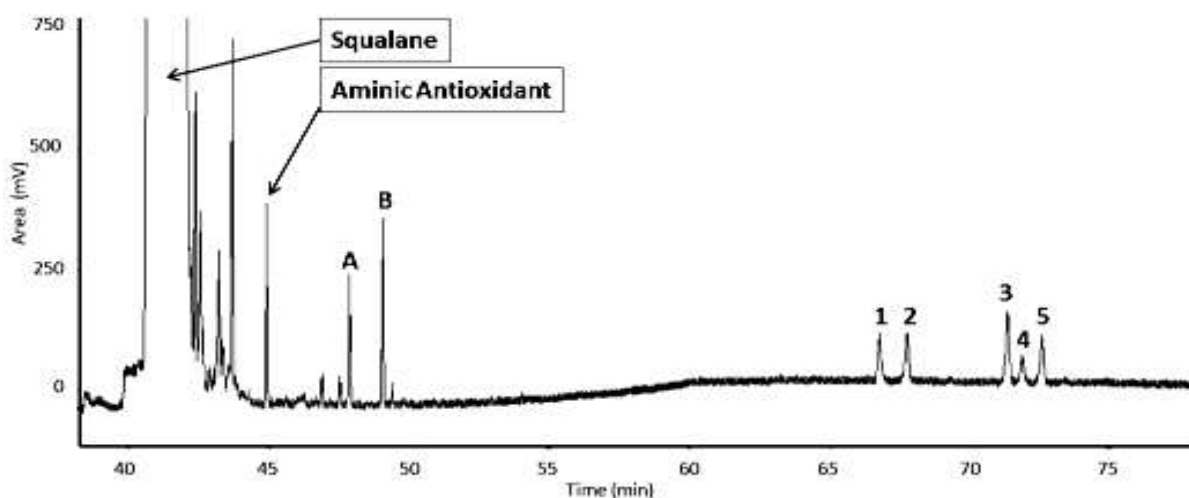


Figure 6.2: GC-FID chromatogram of 60 minutes sample mixture of aminic antioxidant and its products (A, B, 1, 2, 3, 4, 5).

DODPA is alkylated at *para*- position, which stabilises the structure, and which was suggested would have an effect on the products formed from it by dimerisation and oligomerisation.^{173,174}

6.2.3 Product Identification using High Resolution GC-MS EI

Antioxidant intermediates were analysed by accurate GC/TOF MS combined with EI ionisation, with method details in Chapter 2. A chromatogram was obtained using a solvent suppression technique, which improved the signal of the peaks of interests and reduced the impact of the large solvent and squalane peaks, Figure 6.3.

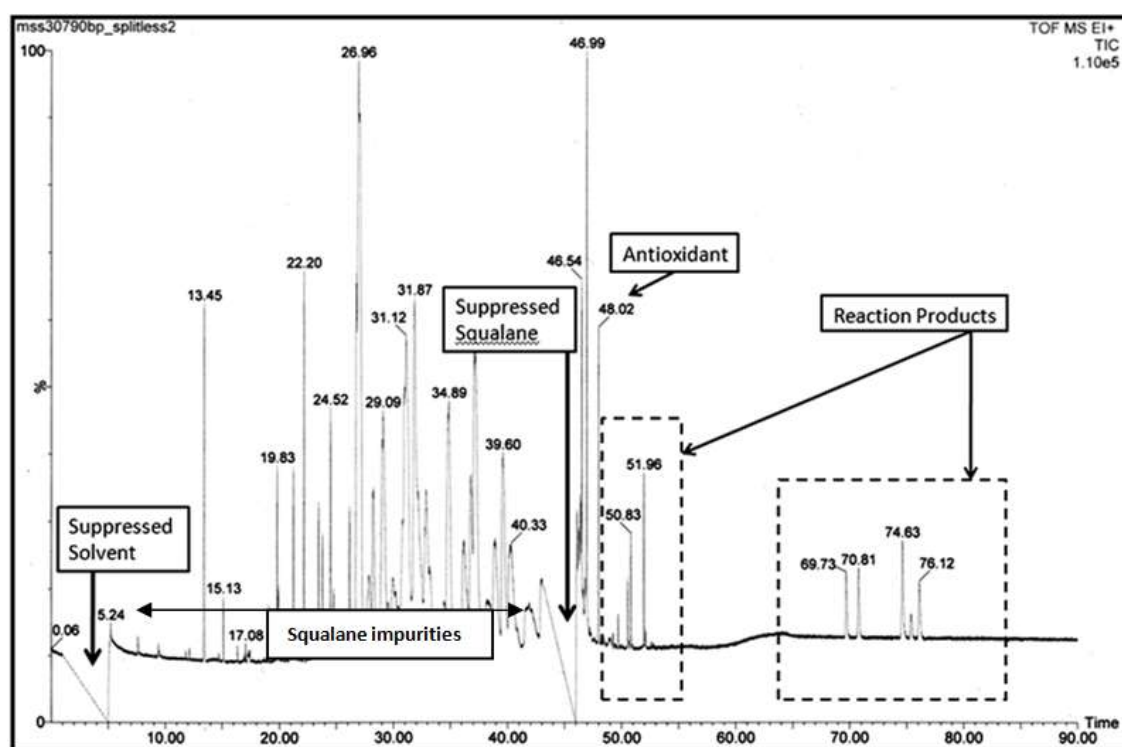


Figure 6.3: GC MS-EI (Total Ion Count) chromatogram of 60 minutes sample with suppressed solvent and squalane peaks. Peaks between 20-40 minutes are squalane impurities.

The aminic antioxidant mass spectrum was obtained, Figure 6.4, to allow a comparison with the products formed from it. The main fragments of the antioxidant were: 393, 322, 250 and 236, consistent with the known structure of the antioxidant; the details of

likely fragments are provided in Appendix E, Figure E1. The peak m/z 393.342 ± 0.003 was characteristic for the molecular ion of DODPA (calculated m/z 393.340 for the formula C₂₈H₄₃N) and followed the “nitrogen rule”, which suggests the formation of an odd mass number if there is an odd number of nitrogen atoms.¹⁷⁵ The largest, fragment peak m/z 322.234 ± 0.003 (calculated m/z 322.253 for the formula C₂₃H₃₂N) was formed by the loss of the pentyl group with the formation of a positive charge on the tertiary carbon and the m/z 250.162 ± 0.003 (calculated m/z 250.159 for the formula C₁₈H₂₀N) by the loss of the second pentyl group. This fragmentation is characteristic of compounds containing electro-attracting hetero atoms, such as nitrogen in amines, which decrease the ionisation energy of alkanes and lead to the loss of large alkyl groups¹⁷⁵ this was followed by the loss of another methyl group to produce the fragment m/z 236.146 ± 0.003 (calculated m/z 236.143 for C₁₇H₁₈N).

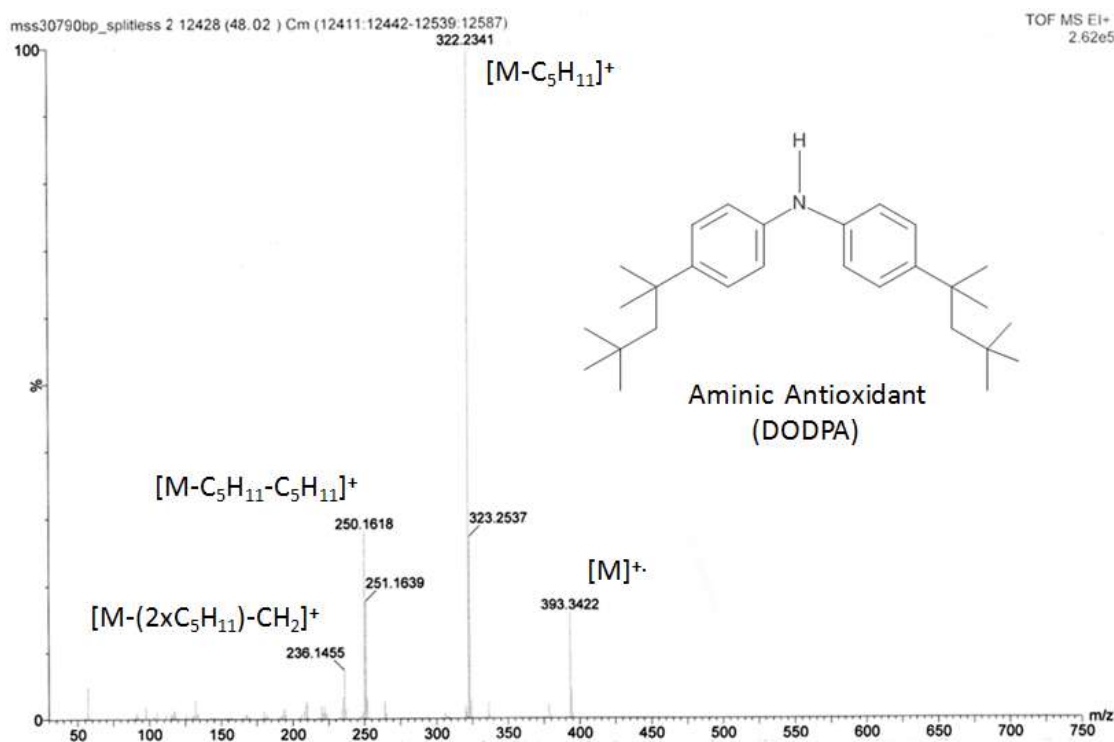


Figure 6.4: GC/TOF MS (EI) spectrum of aminic antioxidant (DODPA).

The DODPA spectrum was compared to library data found in NIST database (Figure 6.5) and was also confirmed with mass spectra obtained by GC-MS in previous work.¹⁷⁶

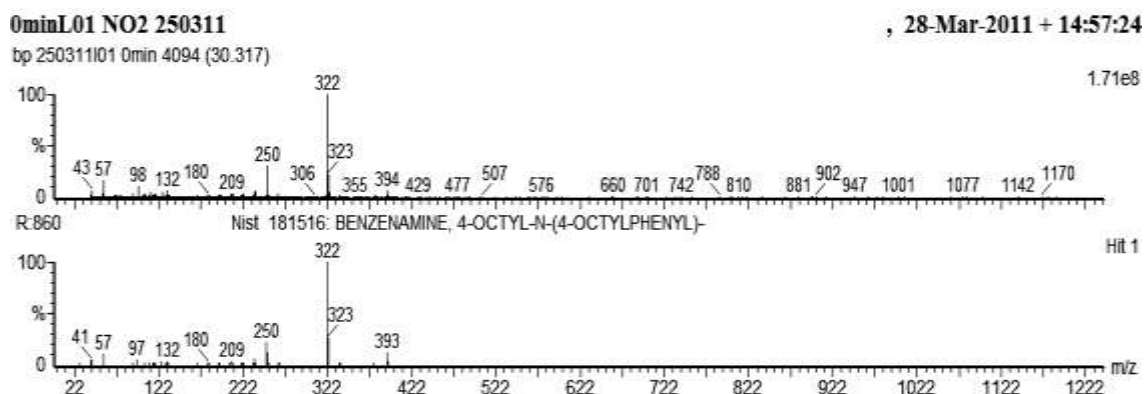


Figure 6.5: Confirmation of EI mass spectrum of the aminic antioxidant (DODPA) (top spectrum) with NIST Library database (bottom spectrum). Analysis by GC Perkin Elmer Clarus 500, details in Chapter 2.

The likely initiation reaction of an aminic antioxidant with NO₂ would be expected to be by hydrogen abstraction with the formation of the aminyl radical and nitrous acid, Figure 6.6.

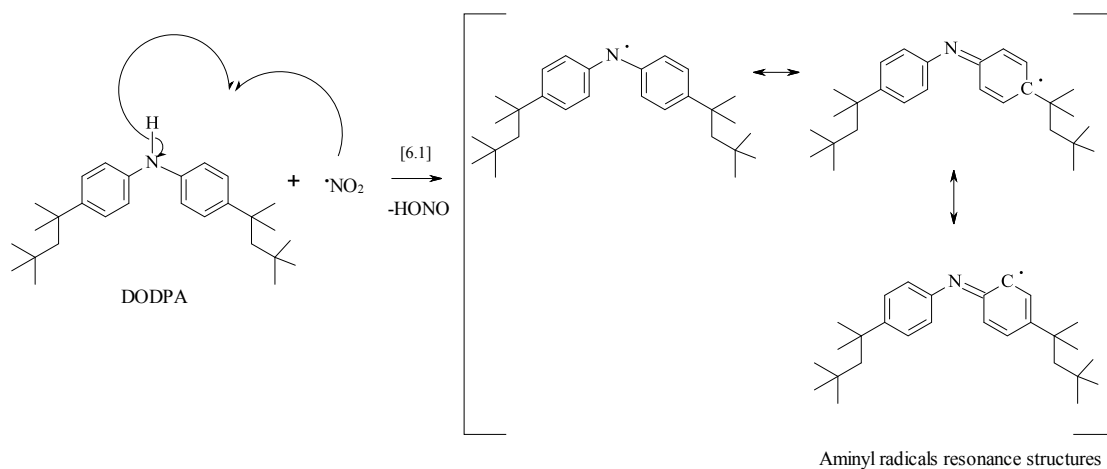


Figure 6.6: Resonance structures of aminyl radical from DODPA.

The aminyl radical is stabilised by a series of resonance structures, as shown in Figure 6.6.

Identification of Intermediates from DODPA using GC/TOF MS (EI)

To identify detected intermediates, assignments have been made using mass spectrum data as Library spectra were unavailable.

Product A - GC/TOF MS (EI)

The first eluting antioxidant intermediate was product A, (EI spectrum in Figure 6.7), a monomeric species containing an odd number of nitrogen's, with a molecular mass ion m/z 407.325 ± 0.005 (calculated exact mass m/z 407.319 for the formula C₂₈H₄₁NO, i.e. a loss of two hydrogen atoms and a gain of one oxygen atom).

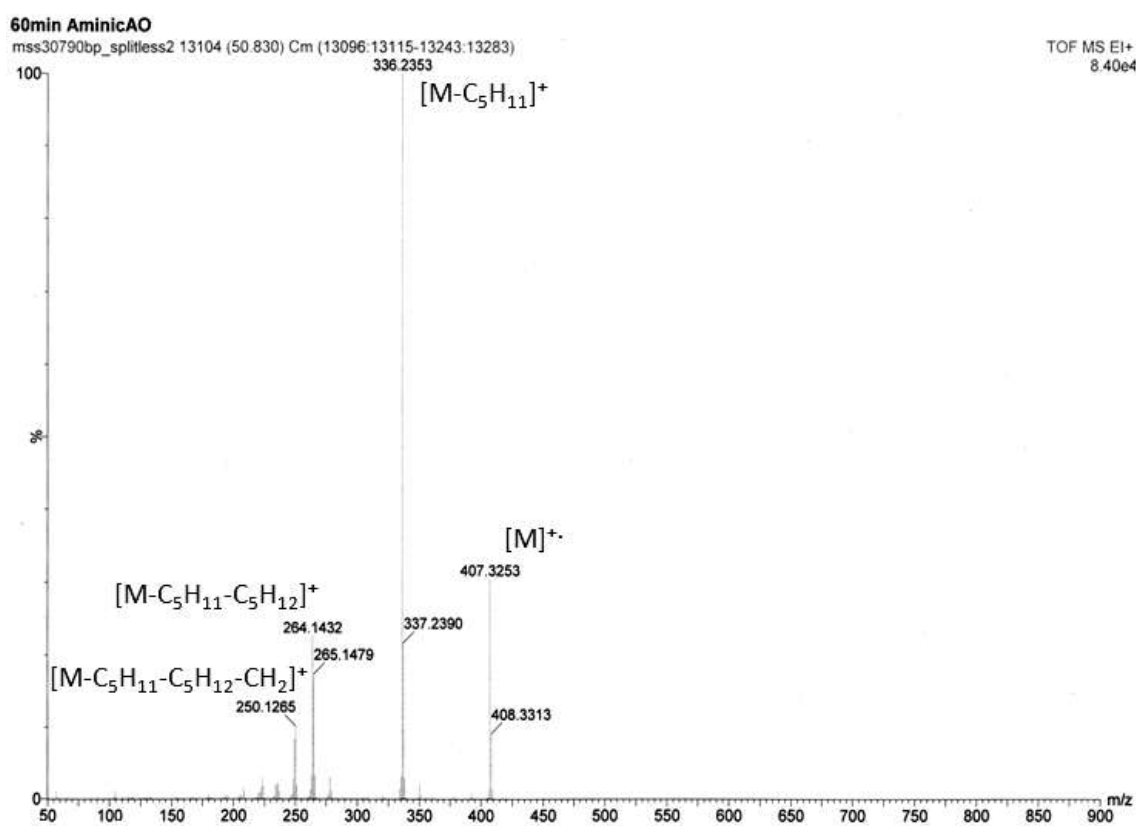


Figure 6.7: GC/TOF MS (EI) spectrum of product A from the reaction of aminic antioxidant (DODPA) with NO₂ at 180 °C.

Other characteristic fragments were: 336, 264 and 250, i. e. the fragmentation patterns follow a similar fragmentation rule as the antioxidant, by the formation of an amine radical cation and alkyl radical.¹⁷⁷ Based on the fragmentation pattern, a possible structure of product A is suggested as shown in Figure 6.8.

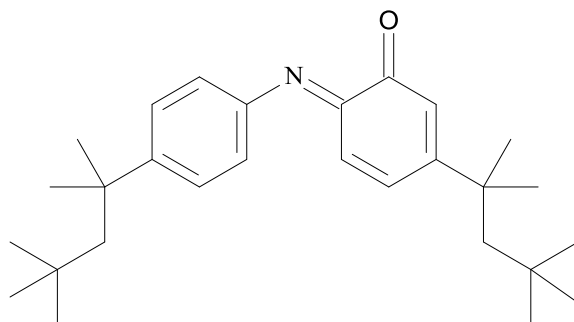


Figure 6.8: Possible structure of product A based on GC/TOF MS (EI) fragmentation.

The example of signal assignments with structures of the fragments for product A, is shown in Appendix E, Figure E2.

Product B - GC/TOF MS (EI)

The second monomeric product identified by GC was Product B (Figure 6.9), with a molecular mass ion m/z 438.333 ± 0.005 - an even number and therefore an even number of nitrogen atoms were expected in this molecule, consistent with the formula of C₂₈H₄₂N₂O₂, which has a calculated accurate mass of 438.325. The main fragments were: 367, 333, 262 and 234.

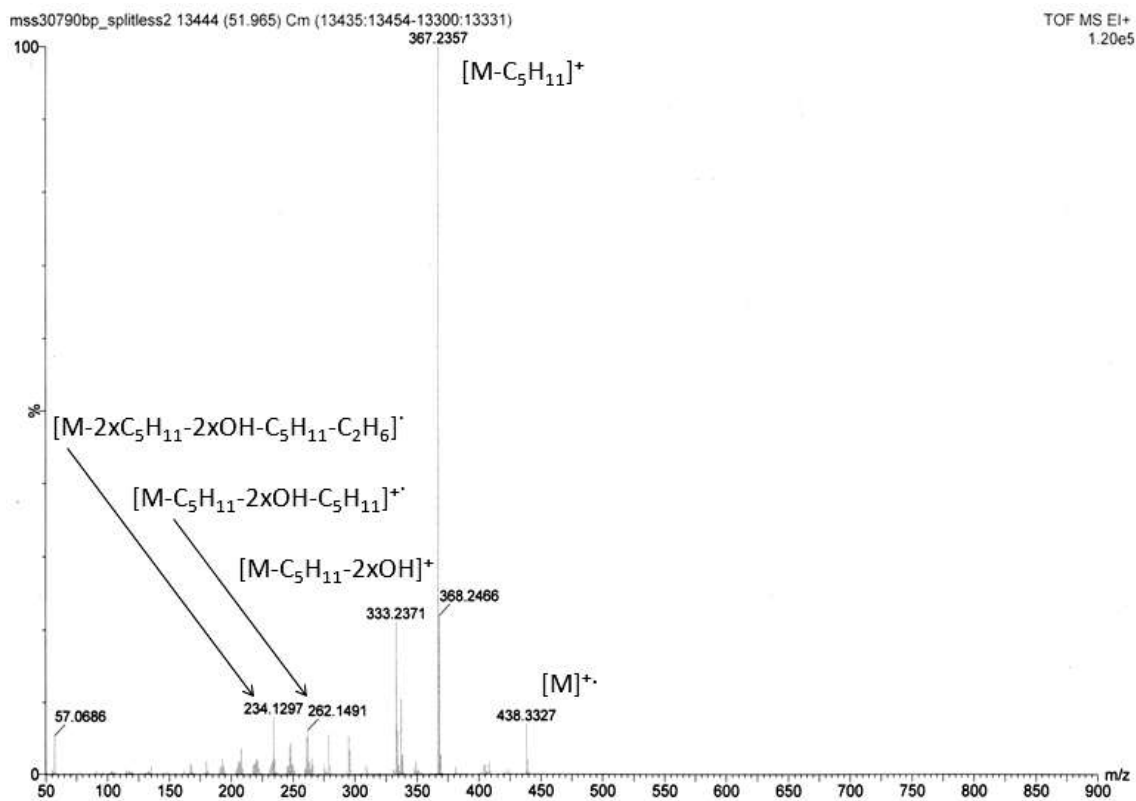


Figure 6.9: GC/TOF MS (EI) spectrum of product B from the reaction of aminic antioxidant (DODPA) with NO₂ at 180 °C.

This product is possibly formed by the addition of NO₂ to the aminyl radical (46 + 392 = m/z 438) at the *ortho*-position of the benzene ring, confirmed by an identified mass fragment of m/z 333.237 ± 0.005 (calculated m/z 333.233 for the formula C₂₃H₂₉N₂) corresponding to dibenzopyrazine, the possible EI fragmentation in Figure 6.10 (more details in Appendix E, Figure E3). A similar EI fragmentation and rearrangement process for *N*-alkyl-*o*-nitroanilines was proposed by Danikiewicz et al.¹⁷⁸

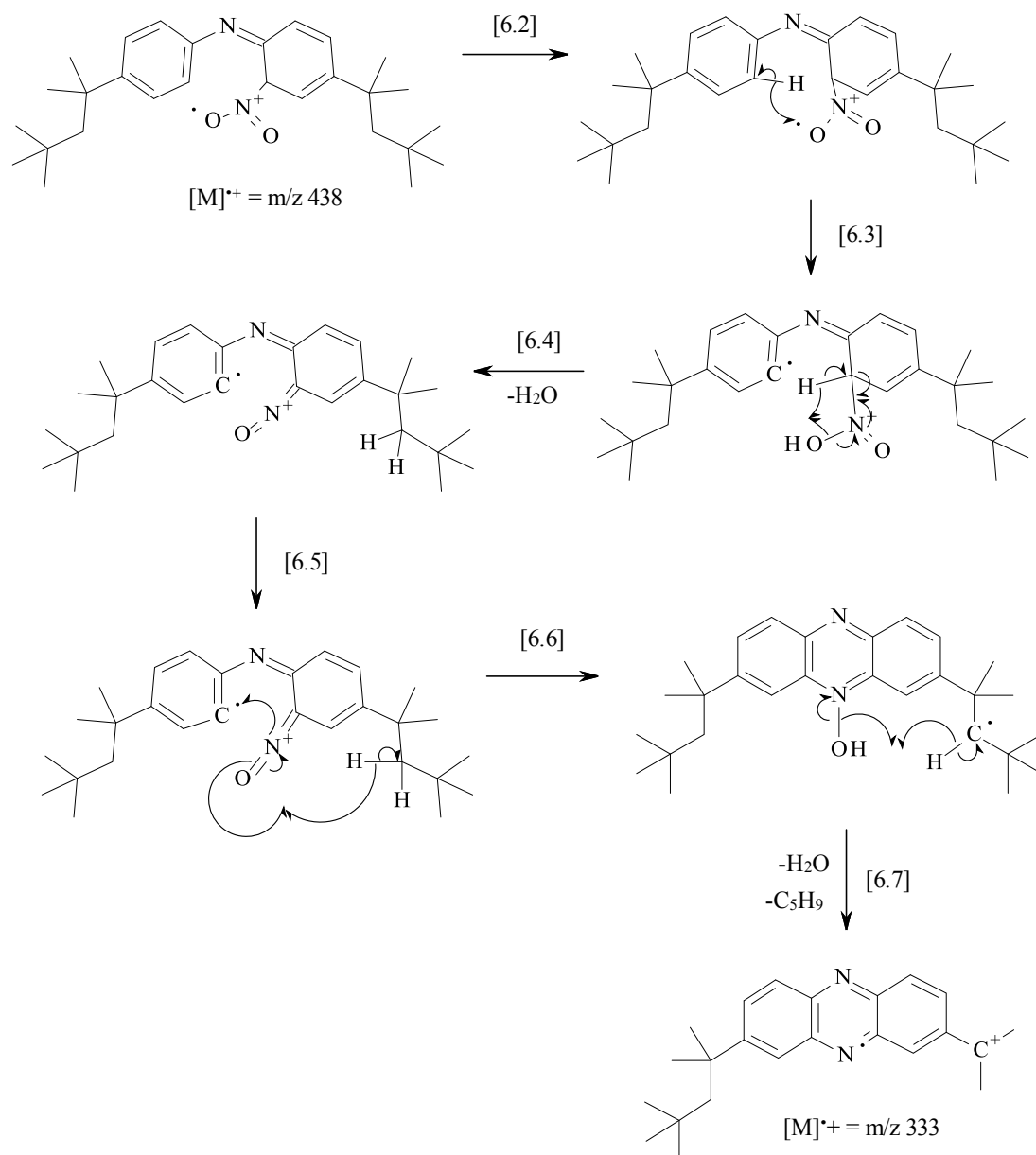


Figure 6.10: EI fragmentation mechanism of the H₂O elimination from the molecular ion of Product B with formation of characteristic m/z 333 fragment.

Other possible structures of product B have been revised (structures in Appendix E, Figure E4), however based on the fragment m/z 333, they were unlikely to form.

Product 1 and 2 - GC/TOF MS (EI)

The identical mass spectra of products 1 and 2 (Figures 6.11 and 6.12) have been identified as dimers of DODPA with the mass ion m/z 784.694 ± 0.005 (calculated 784.663 for the formula $C_{56}H_{84}N_2 = 2C_{28}H_{43}N - 2H$). The characteristic mass fragments were: 713, 641, 321 and 250, and followed the same fragmentation pattern as the antioxidant. The example of signal assignment with structures of the fragments is shown in Appendix E, Figure E5 and E6.

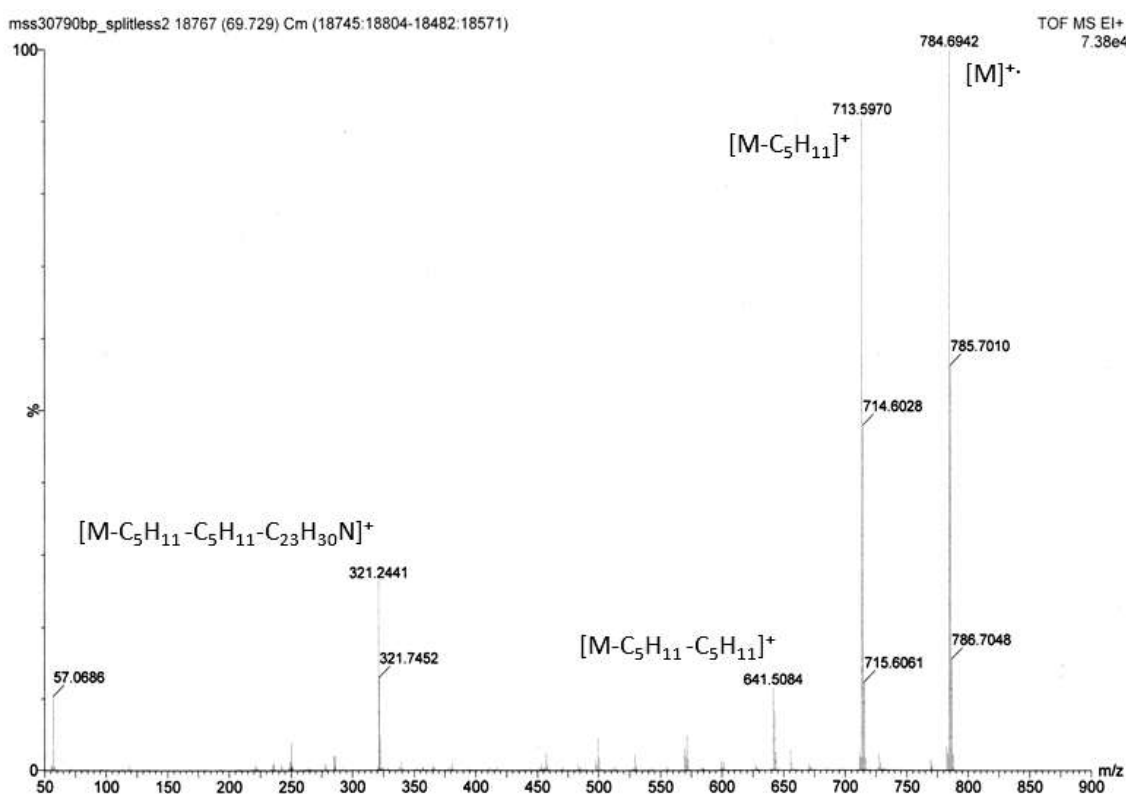


Figure 6.11: GC/TOF MS (EI) spectrum of product 1 from the reaction of aminic antioxidant (DODPA) with NO₂ at 180 °C.

These products have been formed by the coupling of two aminyl radicals, as previously suggested in literature for the reaction of diphenylamine with NO₂,¹¹⁴ possible structures shown in Figure 6.13.

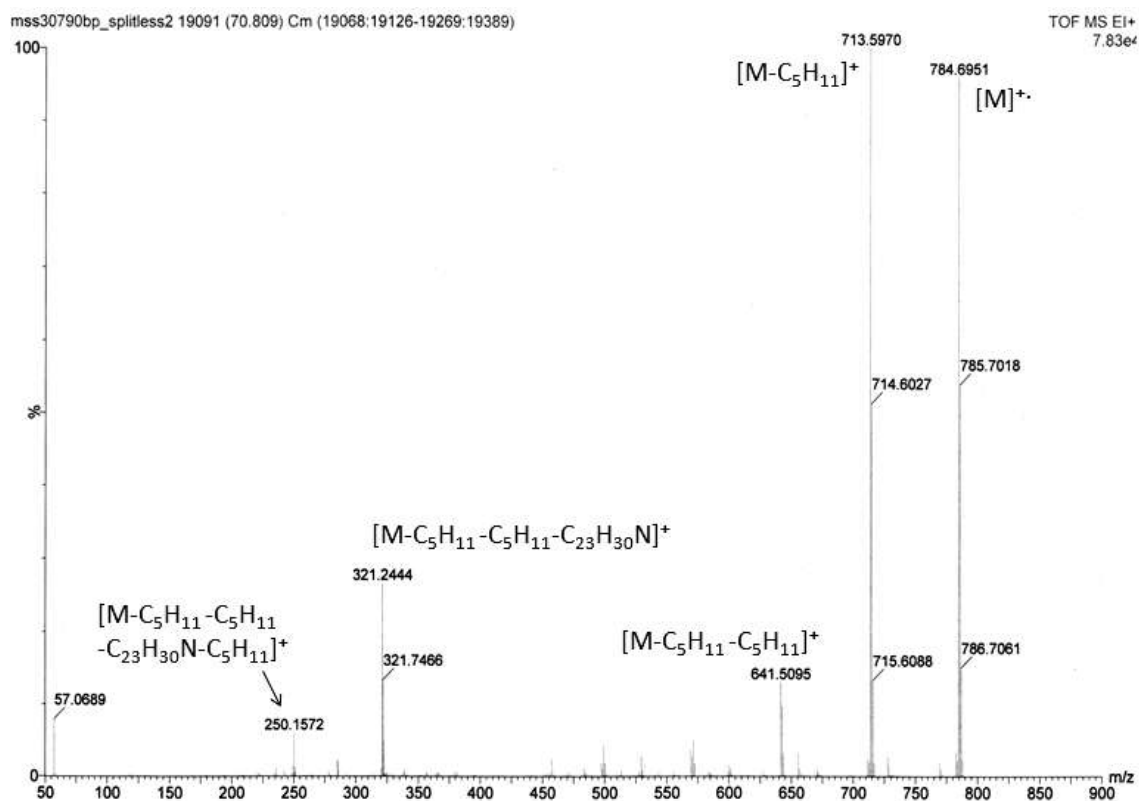


Figure 6.12: GC/TOF MS (EI) spectrum of product 2 from the reaction of aminic antioxidant (DODPA) with NO₂ at 180 °C.

Based on the resonance structures of aminyl radical, different combination of dimers were reviewed, including: nitrogen – nitrogen bonded (1a); nitrogen – carbon bonded (1b; *para*, 1c; *ortho*) and carbon – carbon bonded (1d; *para - para*, 1e; *ortho - ortho*, 1f; *para - ortho*).

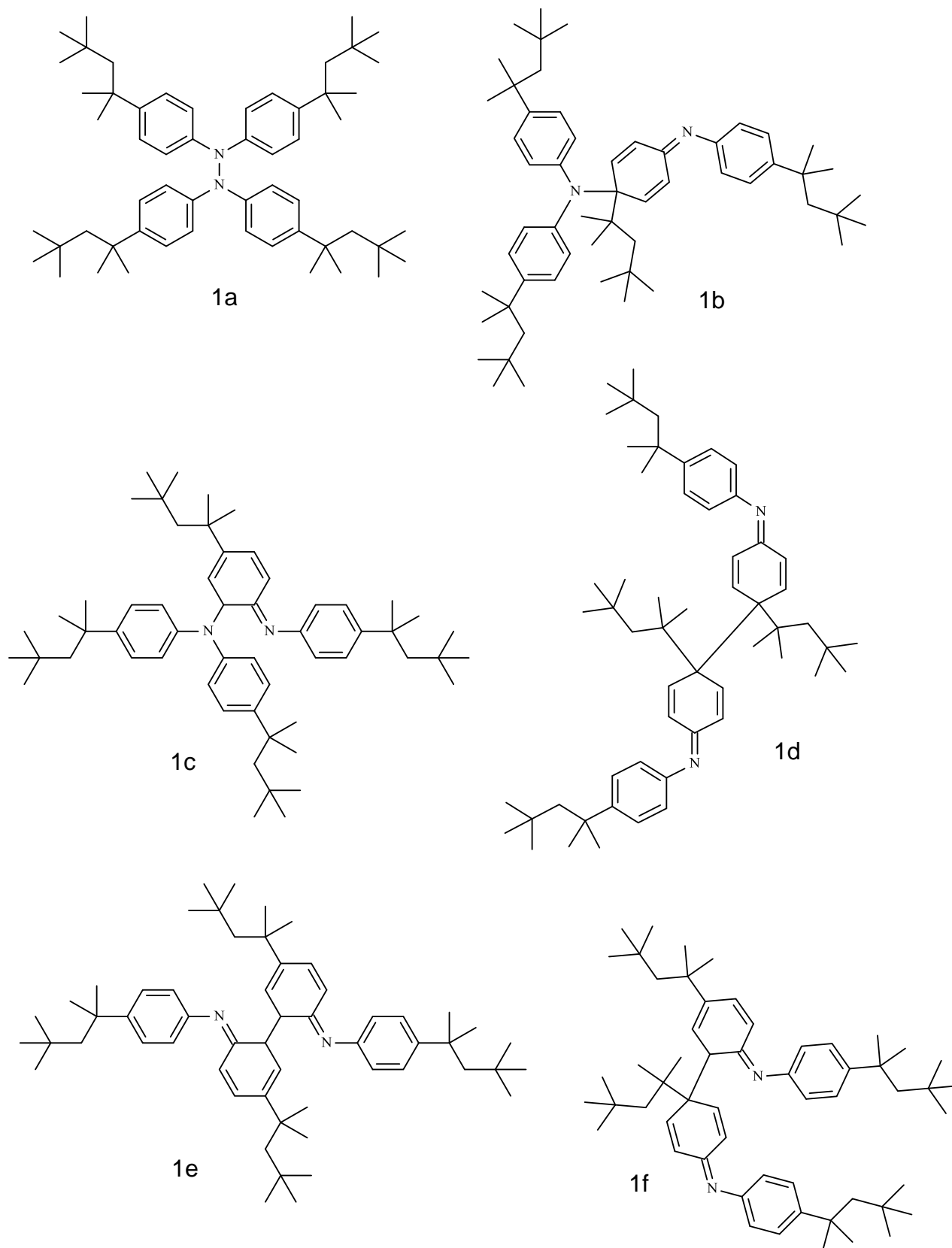


Figure 6.13: Possible dimer structures of products 1 or 2, numbered 1a - .1f.

It was not possible to differentiate the structures of product 1 and 2 using GC-MS EI, however proposed structure 1a would be expected to be energetically favourable, with four benzene rings, compared to only two benzene rings in other possible dimers.

Product 3 - GC/TOF MS (EI)

The next product identified by GC was product 3, mass spectrum in Figure 6.14, with molecular mass ion m/z 798.678 ± 0.006 (calculated 798.673, $C_{56}H_{82}N_2O = 2C_{28}H_{43}N_2 + O - 4H$) suggesting an even number of nitrogen atoms in the molecule.

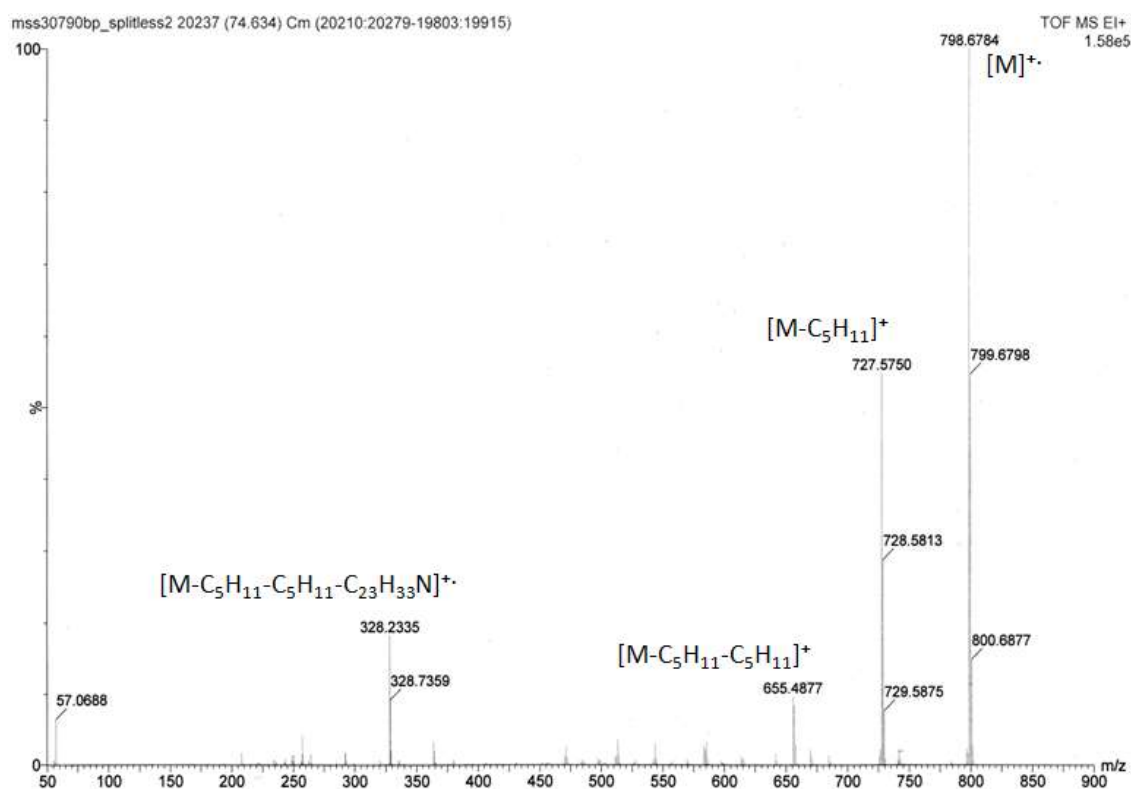


Figure 6.14: GC/TOF MS (EI) spectrum of product 3 from the reaction of aminic antioxidant (DODPA) with NO₂ at 180 °C.

Characteristic fragments were formed by the loss of large alkyl fragments as for other products; however the size of the molecule suggested the dimer with oxygen atom and three possible structures were proposed in Figure 6.15.

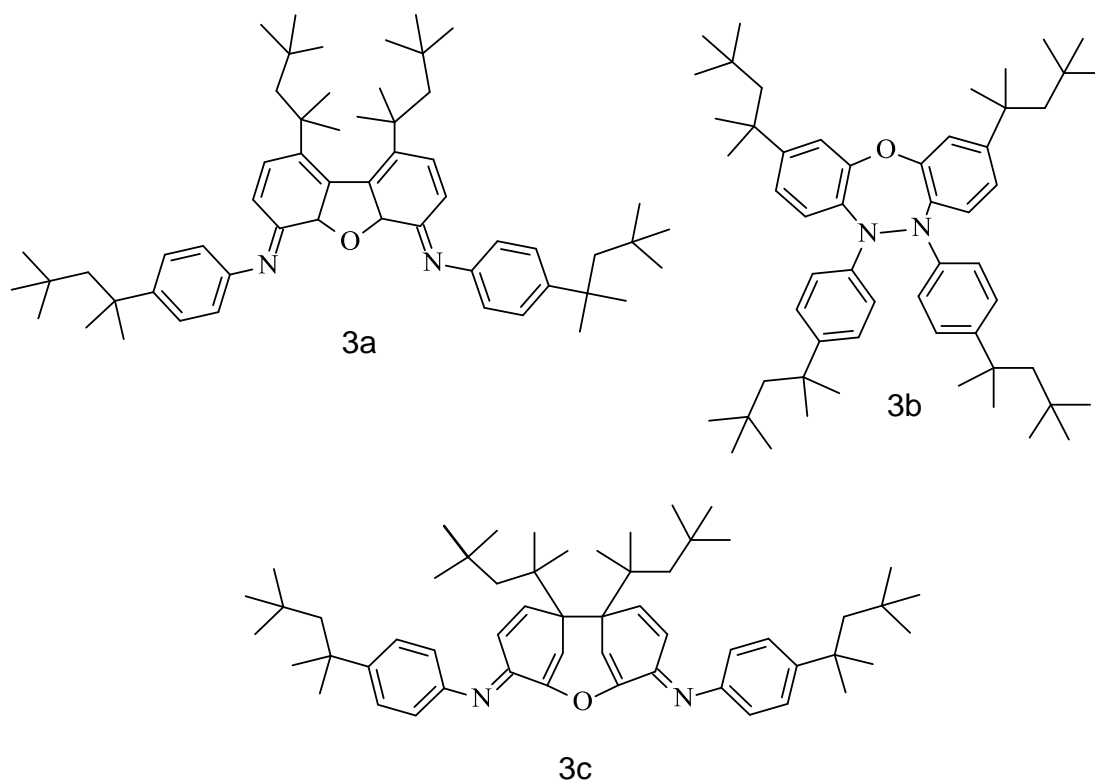


Figure 6.15: Possible dimer structures of products 3.

Dimer 3b is the most energetically favourable of all possible structures, as it contains four benzene rings. There is also a possible mechanism of its formation from monomeric, product A (containing oxygen at the *ortho* position of the ring) suggesting structure 3b, as discussed in section 6.3. The example of fragment assignment based on product 3b is illustrated in Appendix E, Figure E7.

Product 4 and 5 - GC/TOF MS (EI)

The mass spectra of products 4 and 5 were identical, Figures 6.16 and 6.17. Their molecular mass ion fragment m/z 782.681 ± 0.005 (calculated 782.648 for formula $C_{56}H_{82}N_2 = 2C_{28}H_{43}N-4H$) were two Daltons lower than for identified dimers (product 1 and 2), suggesting a loss of a further two hydrogen atoms from products 1 or 2.

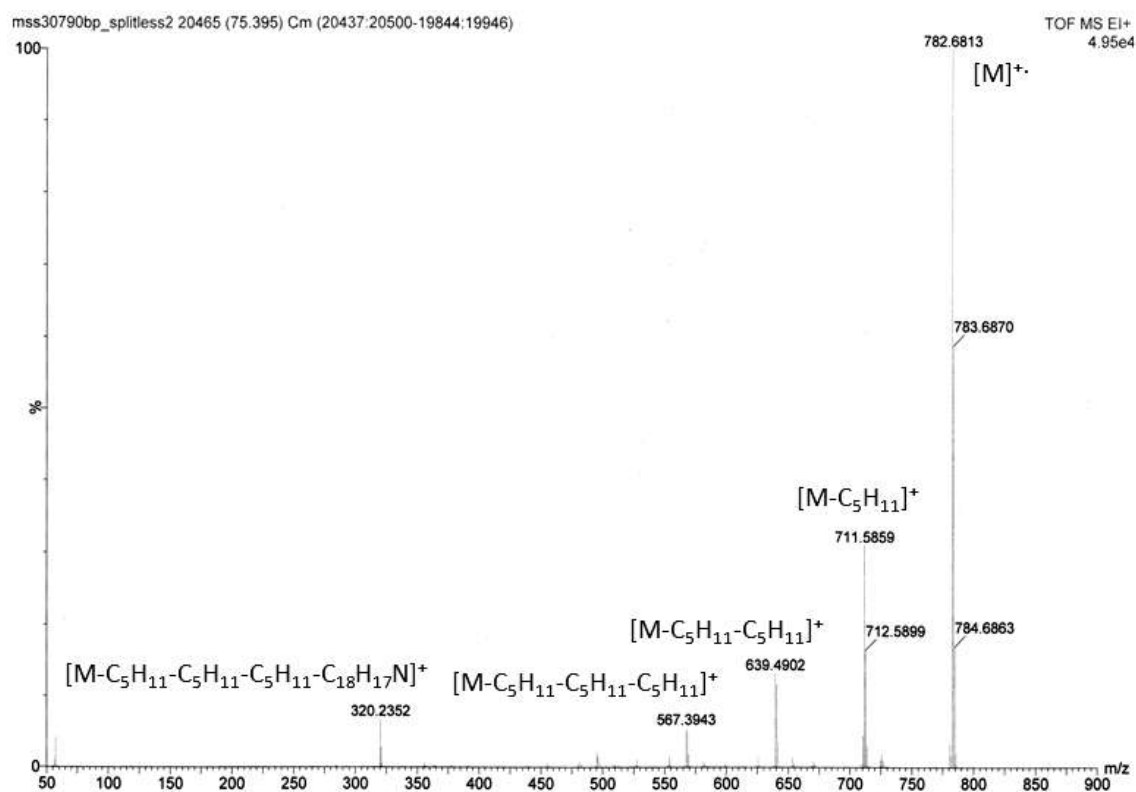


Figure 6.16: GC/TOF MS (EI) spectrum of product 4 from the reaction of aminic antioxidant (DODPA) with NO₂ at 180 °C.

The structures of possible conformational isomers were proposed, which differ by the rotation of C=C double bond (4a and 4b), (isomer 4b could also conceivably rearrange to the more stable structure 4c restoring aromaticity, Figure 6.18).

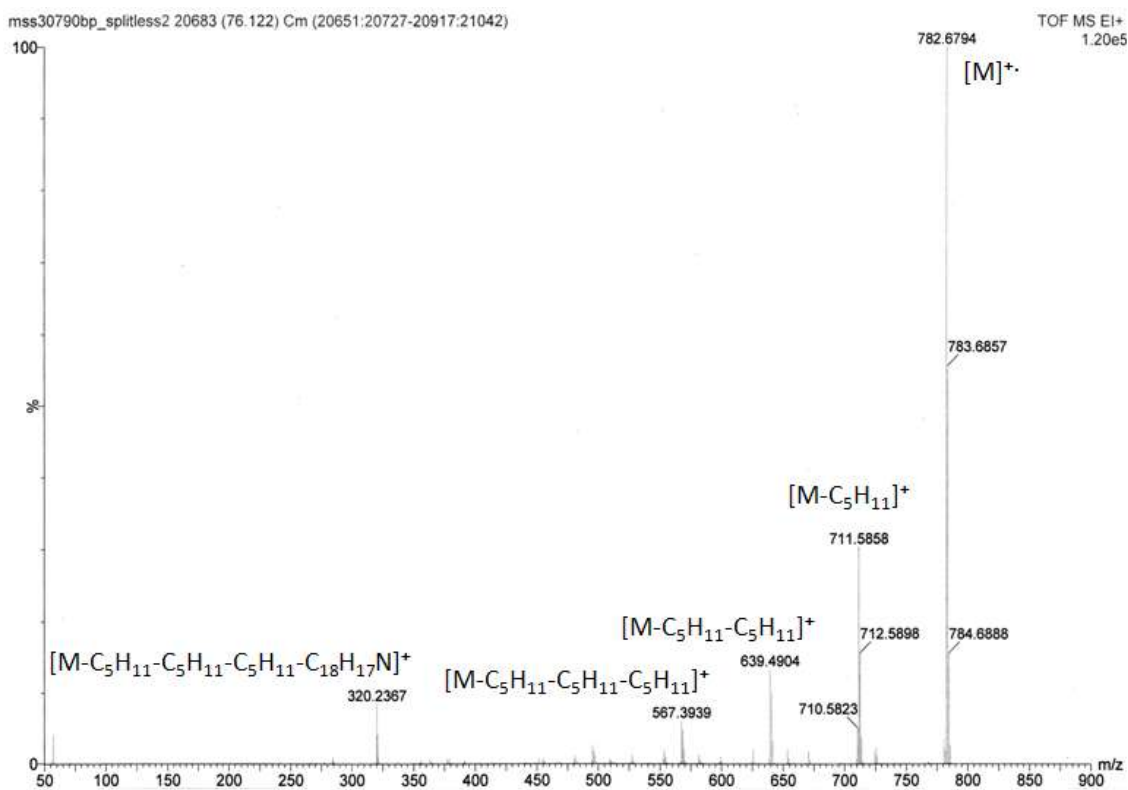


Figure 6.17: GC/TOF MS (EI) spectrum of product 5 from the reaction of aminic antioxidant (DODPA) with NO₂ at 180 °C.

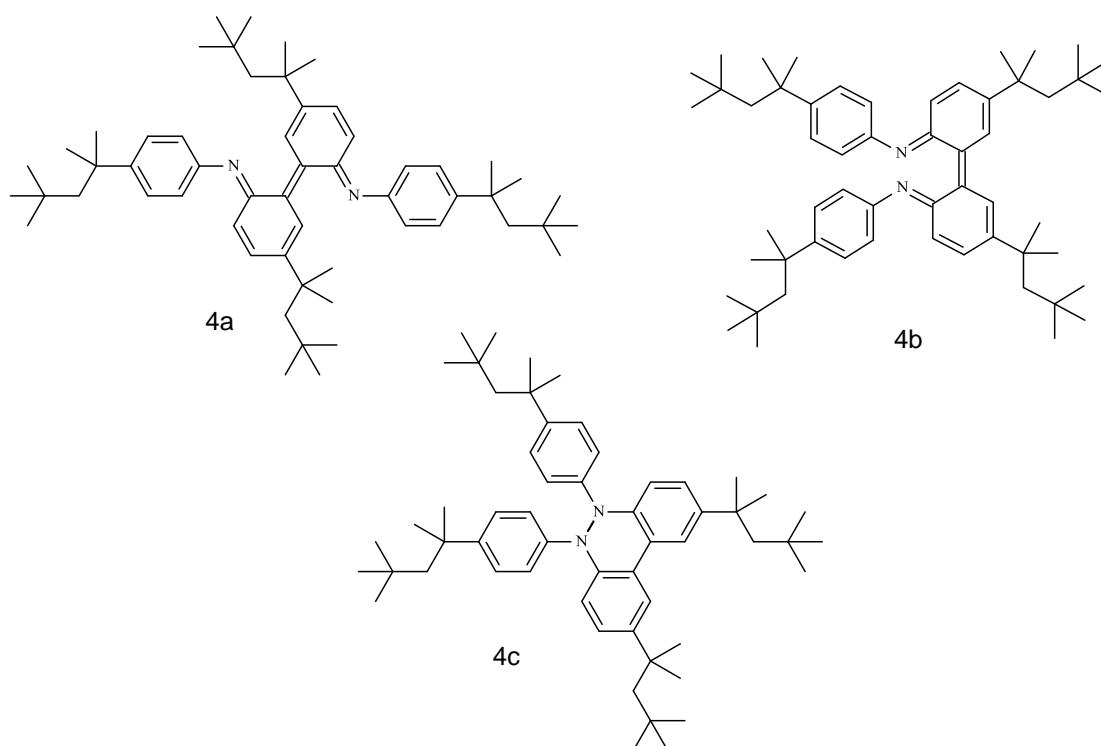


Figure 6.18: Possible dehydrodimers structures of products 4 or 5, numbered 4a-4c.

Using EI analysis, it was not possible to conclusively identify which of the proposed structures (4a-4c) are products 4 and 5, although as the mass spectra for these two species were essentially identical, this strongly suggests that they are the E and Z isomers, structures 4a and 4b. The example of fragment assignment, including the structures, is illustrated in Appendix E, Figures E8.

6.2.4 Quantitative Analysis using GC-FID

Decay of the antioxidant and the formation of its intermediates were quantified by GC and by using an effective carbon number method, as described in Chapter 2. Concentration of all products and antioxidant were plotted vs. reaction time in Figure 6.19. The quantified analysis shows that at 30 minutes approximately 60 % of the antioxidant was reacted to the intermediates, which suggests that they were the main products of antioxidant interaction with NO₂.

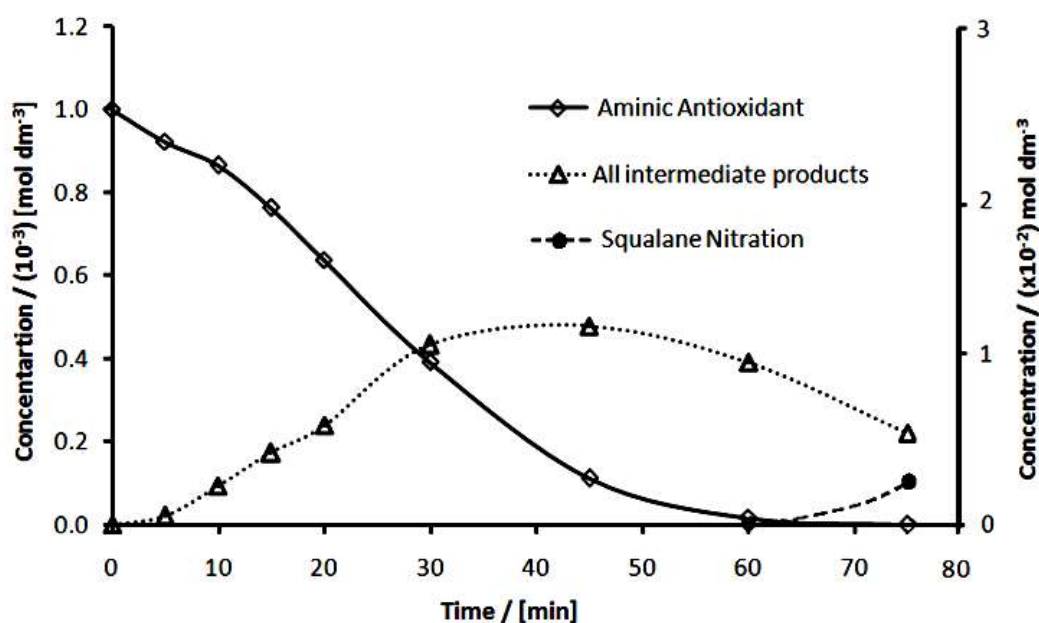


Figure 6.19: Aminic antioxidant consumption vs. total of intermediate products formation for the reaction of DODPA with NO₂ at 180 °C. Squalane nitrate products are on the right hand axis.

The DODPA was protecting the base oil until all the antioxidant was consumed up to 60 minutes. The next sample at 75 minutes showed squalane nitration, even though there were still some antioxidant intermediates present. The formation of aminic antioxidant intermediates is shown in Figure 6.20.

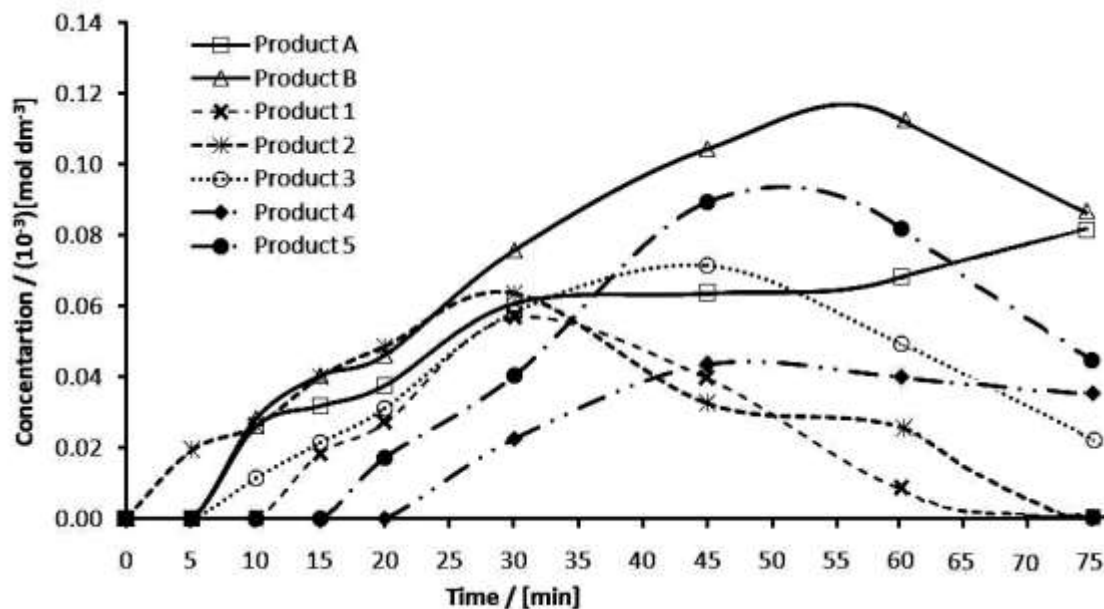


Figure 6.20: Calculated concentrations of intermediates products for the reaction of DODPA with NO₂ at 180° C.

The first product to be formed, at 5 minutes, was product 2 (an antioxidant dimer), then at 10 minutes three more products were detected; monomers A and B, and the dimer product 3. At 15 minutes, product 1 was identified, then at 20 minutes product 5, and product 4 the last at 30 minutes. By 60 minutes almost no antioxidant remained and the dimer products were decaying.

The order of product formation could give some more tentative information on the mechanism of the products, and potentially also their respective structures.

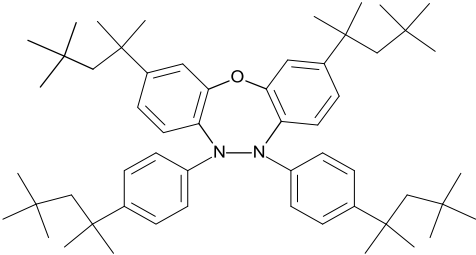
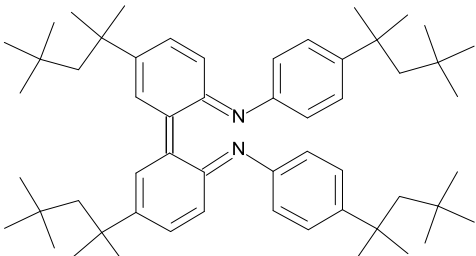
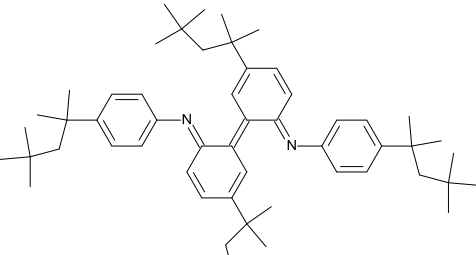
6.2.5 Summary of Identification

The first two products, A & B, eluting at approximately 48-49 minutes were identified as monomers of the antioxidant, whereas products 1 to 5, eluting at approximately 67-78 minutes were found to be dimers of the antioxidant. A summary of their identification, including possible chemical structures, names, formulae and calculated exact masses are shown in Tables 6.1 and 6.2.

Table 6.1: Chemical structures and molecular weights of DODPA and its intermediates (A, B, 1, 2) from the reaction with NO₂.

Peak No	IUPAC Name / Formula	Exact Mass [g mol ⁻¹]	Structure
DODPA	4-(1,1,3,3-tetramethylbutyl)-N-[4-(1,1,3,3-tetramethylbutyl)phenyl]aniline C ₂₈ H ₄₃ N [AO]	393.342	
A	(6E)-3-(1,1,3,3-tetramethylbutyl)-6-[4-(1,1,3,3-tetramethylbutyl)phenyl]imino-cyclohexa-2,4-dien-1-one C ₂₈ H ₄₁ NO [AO - 2H + O]	407.319	
B	6-nitro-4-(1,1,3,3-tetramethylbutyl)-N-[4-(1,1,3,3-tetramethylbutyl)phenyl]cyclohexa-2,4-dien-1-imine C ₂₈ H ₄₂ N ₂ O ₂ [AO - H + NO ₂]	438.325	
1	4-(1,1,3,3-tetramethylbutyl)-N-[4-(1,1,3,3-tetramethylbutyl)phenyl]-6-[(6E)-3-(1,1,3,3-tetramethylbutyl)-6-[4-(1,1,3,3-tetramethylbutyl)phenyl]imino-cyclohexa-2,4-dien-1-yl]cyclohexa-2,4-dien-1-imine C ₅₆ H ₈₄ N ₂ [2AO - 2H]	784.663	
2	1,1,2,2-tetrakis[4-(1,1,3,3-tetramethylbutyl)phenyl]hydrazine C ₅₆ H ₈₄ N ₂ [2AO-2H]	784.663	

Table 6.2: Chemical structures and molecular weights of intermediates (3, 4, 5) formed from the reaction of DODPA with NO₂.

Peak No	IUPAC Name / Formula	Exact Mass [g mol ⁻¹]	Structure
3	2,9-bis(1,1,3,3-tetramethylbutyl)-5,6-bis[4-(1,1,3,3-tetramethylbutyl)phenyl]benzo[c][5,1,2]benzoxadiazepine C ₅₆ H ₈₂ N ₂ O [2AO-4H+O]	798.643	
4	(6Z)-4-(1,1,3,3-tetramethylbutyl)-N-[4-(1,1,3,3-tetramethylbutyl)phenyl]-6-[(6E)-3-(1,1,3,3-tetramethylbutyl)-6-[4-(1,1,3,3-tetramethylbutyl)phenyl]iminocyclohexa-2,4-dien-1-ylidene]cyclohexa-2,4-dien-1-imine C ₅₆ H ₈₂ N ₂ [2AO-4H]	782.648	
5	(6E)-4-(1,1,3,3-tetramethylbutyl)-N-[4-(1,1,3,3-tetramethylbutyl)phenyl]-6-[(6E)-3-(1,1,3,3-tetramethylbutyl)-6-[4-(1,1,3,3-tetramethylbutyl)phenyl]iminocyclohexa-2,4-dien-1-ylidene]cyclohexa-2,4-dien-1-imine C ₅₆ H ₈₂ N ₂ [2AO-4H]	782.648	

6.3 Reaction Mechanism of DODPA with NO₂

The interaction of the commercial aminic antioxidant (DODPA) with 1000 ppm NO₂ at 180 °C resulted in the formation of seven intermediates from the antioxidant. Based on product identification reaction mechanisms are proposed in Figures 6.21 to 6.27.

The initiation reaction would be by the hydrogen abstraction from DODPA by nitrogen dioxide with the formation of aminyl radical and nitrous acid, reaction 6.1. Aminic antioxidants are scavenging antioxidants with a relatively weak N–H bond, which influences their reactivity. Previously reported N–H bond dissociation energy of DODPA was $358 \pm 4 \text{ kJ mol}^{-1}$,¹⁸² which is somewhat higher than the O–H bond dissociation energy of nitrous acid, $330.9 \pm 1 \text{ kJ mol}^{-1}$,¹⁶⁶⁻¹⁶⁸ with an energy difference (ΔH) is $37 \pm 3 \text{ kJ mol}^{-1}$. This value is higher than the enthalpy of the reaction for the reaction of phenolic antioxidants with NO₂, $12 \pm 3 \text{ kJ mol}^{-1}$ (described in chapter 5), and so this reaction is more endothermic, therefore the aminic hydrogen abstraction by NO₂ may be less favourable than for phenolics.

DODPA is an aromatic amine with alkylated *para* positions, it was suggested (in the reaction with peroxy radicals) that this would have an effect on product formation, mainly formed by dimerisation and oligomerisation,¹⁷³ however, not many details of this analysis was given. Other autoxidation studies similarly, suggested a high probability of recombination of formed radicals, however this is also currently lacking in detailed analysis.^{184,185}

The first reaction mechanism for product 2 (the dimer), which was the first product identified by GC in the 5 minute sample, was by the recombination of two aminyl radicals (reaction [6.9]) shown in Figure 6.21.

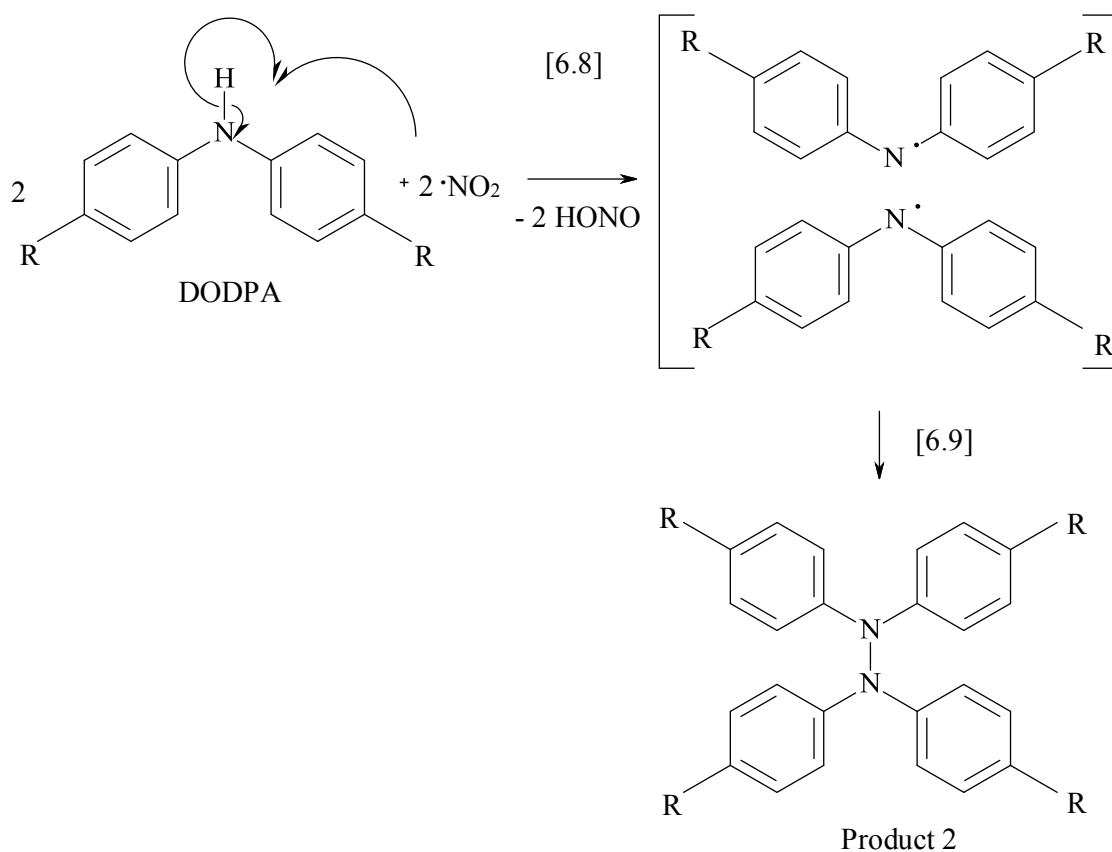


Figure 6.21: Reaction mechanism of the formation of product 2 (R=C₈H₁₁).

The next products, identified in the 10 minute sample, were the two monomers A and B, and the dimer with oxygen, product 3.

There are three possible mechanisms for the formation of Product A (numbered here as mechanism I, II and III), Figure 6.22. The initial reaction for mechanisms I and II is the same; namely the addition of NO₂ via the oxygen atom to the aminyl radical (reaction [6.10]). The next reaction of mechanism I is by loss of nitric oxide (reaction [6.11]), followed by abstraction of the next weakest hydrogen by NO₂ with the formation of Product A and nitrous acid, reaction [6.12]. The mechanism II was by the cyclic transition state and led to loss of HNO.

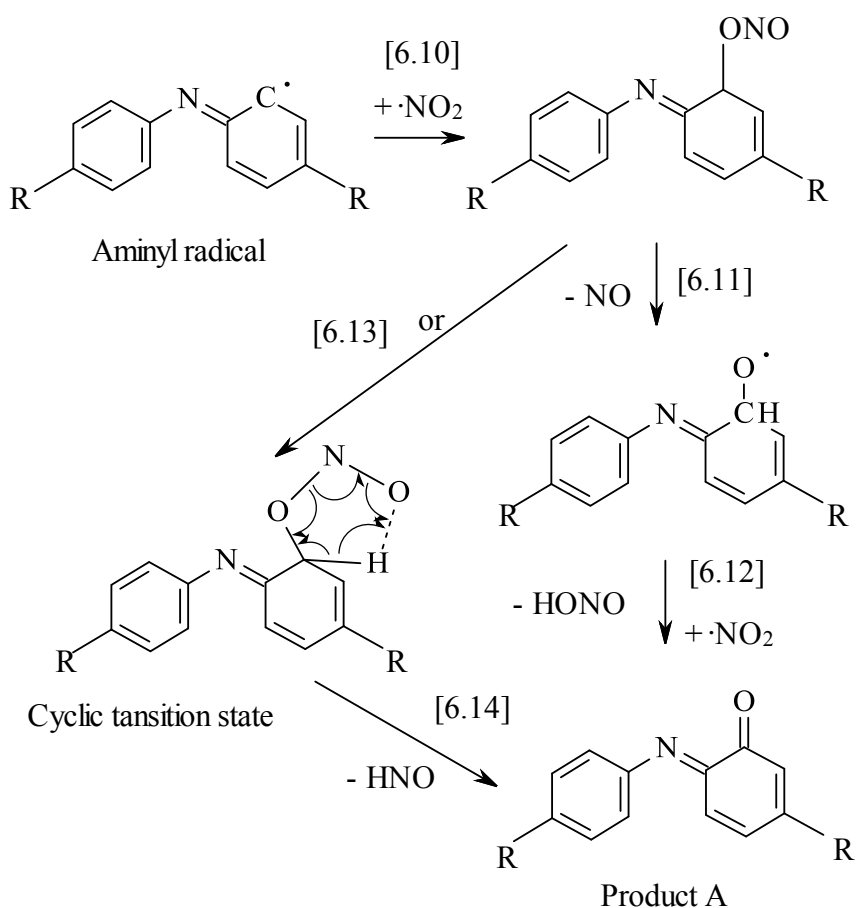


Figure 6.22: Mechanism I and II – possible reaction mechanisms of formation of product A. ($\text{R}=\text{C}_8\text{H}_{11}$).

In mechanism III (Figure 6.23), Product A possibly forms during several stages, firstly the addition of nitrogen dioxide to the aminyl radical via nitrogen (reaction [6.15]), followed by the hydrogen migration via σ -cleavage (reaction [6.16]), followed by the hydroxyl transfer (reaction [6.17]), which led to the loss of nitric oxide through the heterolytic cleavage, reaction [6.18]. Then the abstraction of the next weakest hydrogen atom by the second NO₂ radical occurred, followed by the bond rearrangement to product A, reaction [6.19].

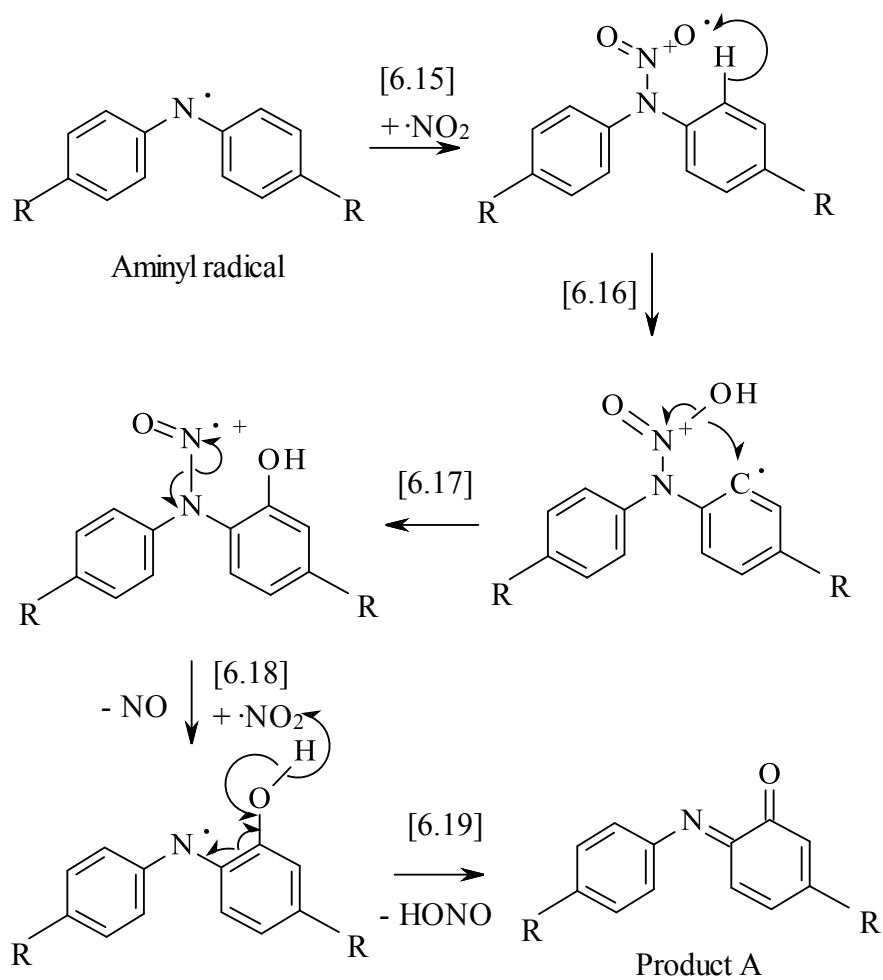


Figure 6.23: Mechanism III – first possible reaction mechanism of formation of product A (R=C₈H₁₁).

Product B forms by the addition of NO₂, through the nitrogen atom, to the aminyl radical, reaction [6.20].

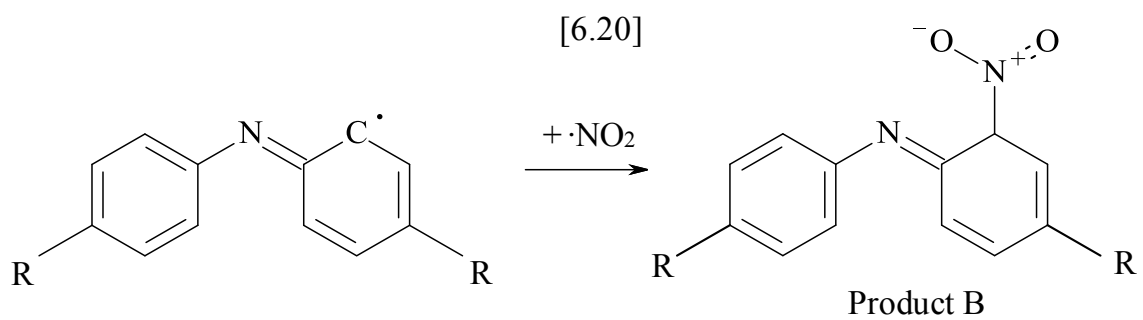


Figure 6.24: Reaction mechanism of formation of product B ($\text{R}=\text{C}_8\text{H}_{11}$).

Product 3 is the dimer, which forms by the combination of *o*-aminyl radical and product A, reactions [6.21]-[6.22].

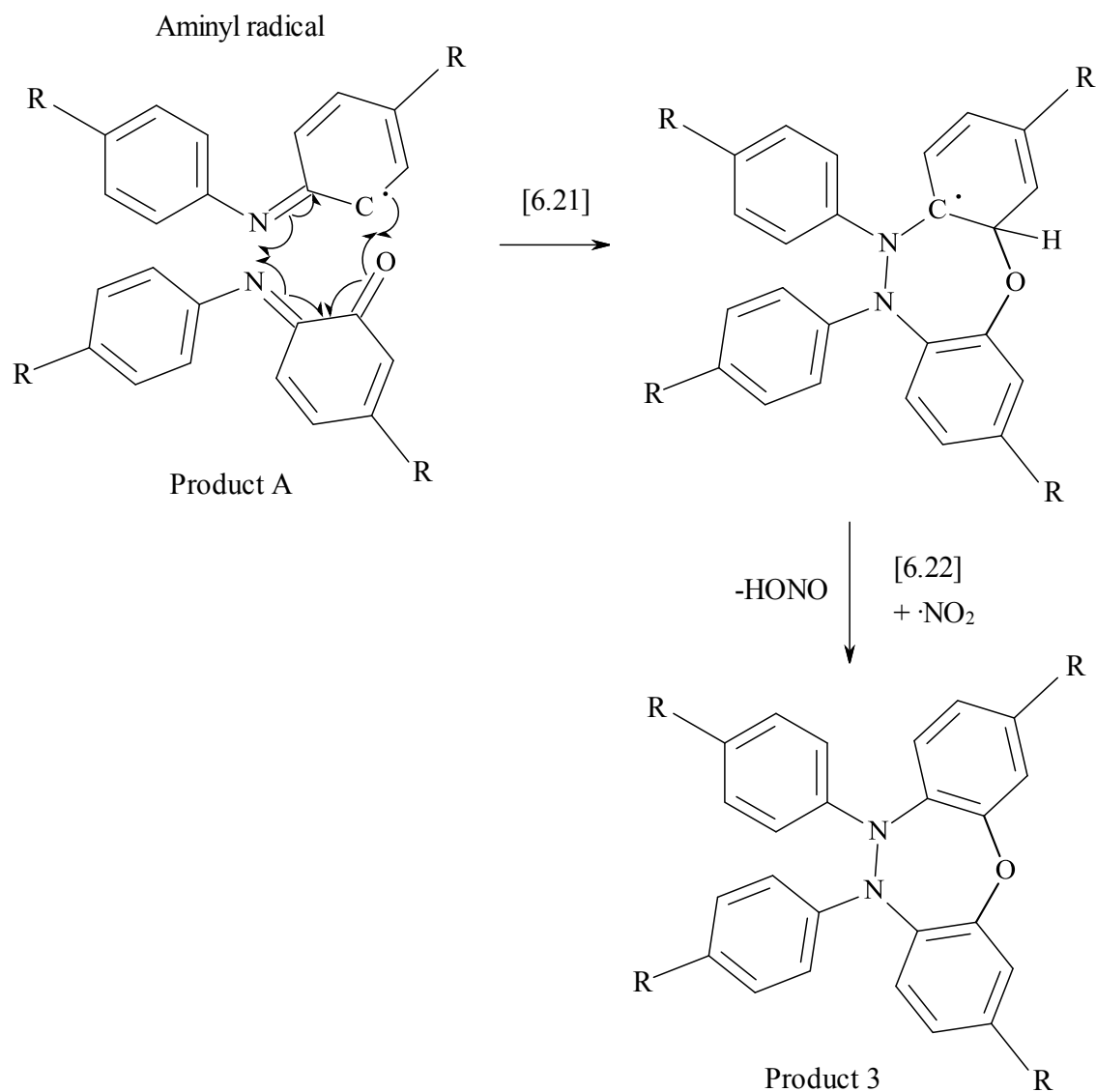


Figure 6.25: Reaction mechanism of formation of product 3 ($\text{R}=\text{C}_8\text{H}_{11}$).

The last products identified are: the dimer (product 1), which forms by the combination of two *o*-aminyl radicals and then two more dimers (products 4 and 5), Figure 6.26.

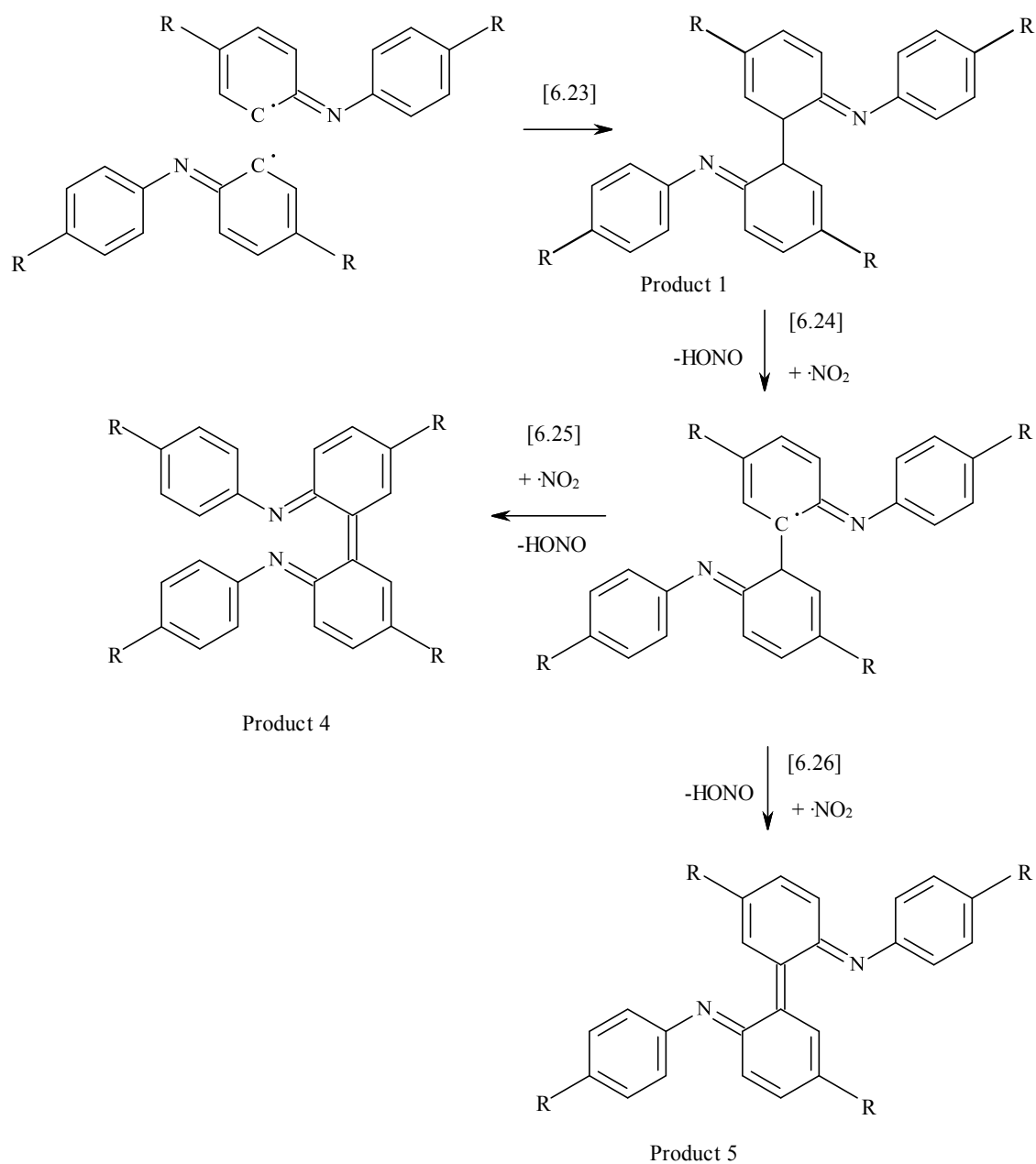
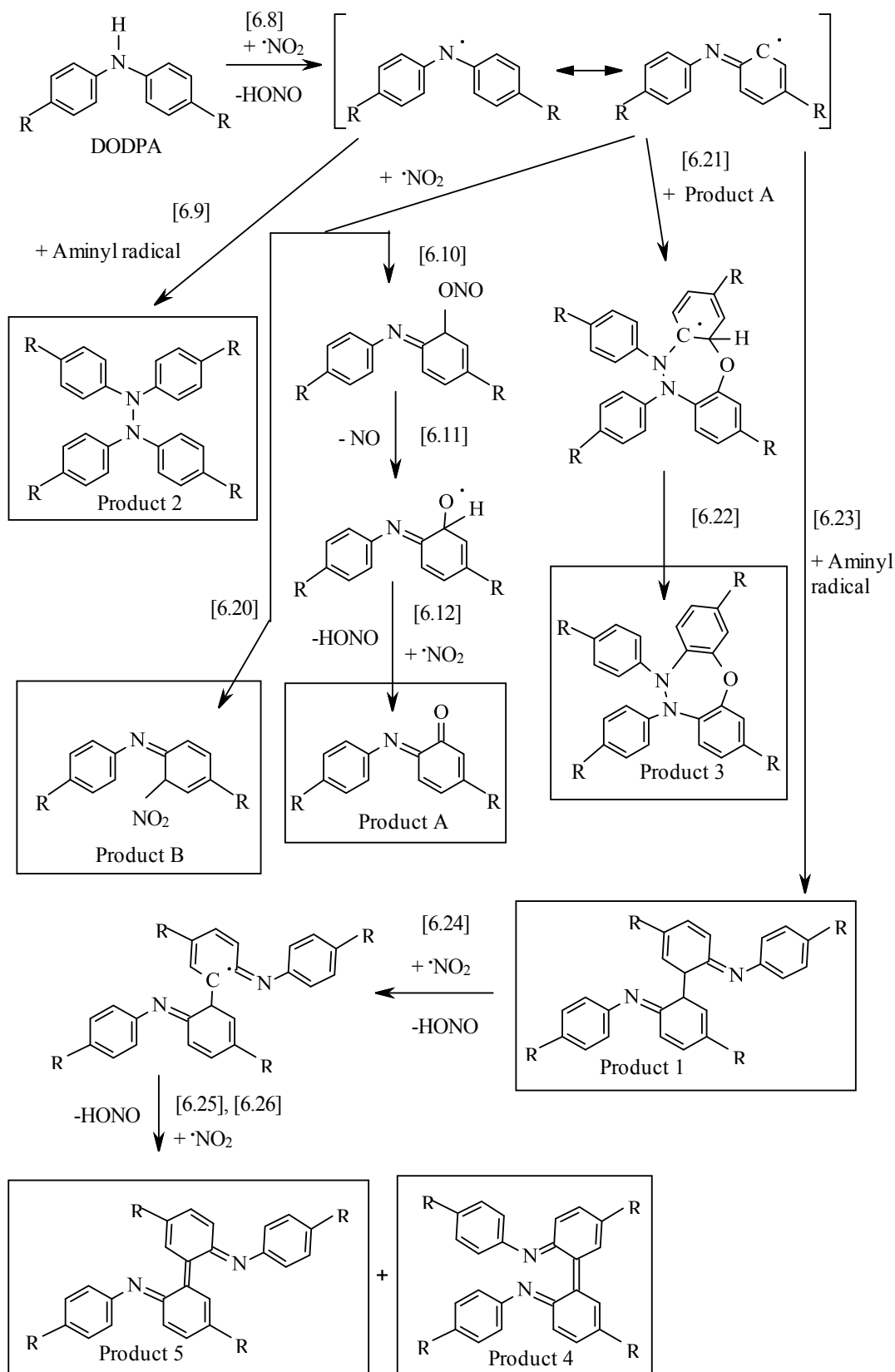


Figure 6.26: Reaction mechanism of formation of product 1, 4 and 5 ($\text{R}=\text{C}_8\text{H}_{11}$).

Both dimers (product 4 and 5) are formed by the elimination of two hydrogen's from product 1 by NO_2 with the formation of a $\text{C}=\text{C}$ double bond.

The summarising mechanism for all products formed from the aminic antioxidant reaction with NO_2 is shown in Figure 6.27.



6.27: Summarising mechanism of intermediates formed from DODPA in the reaction with NO₂ (R=C₈H₁₁).

6.4 Summary

The reaction of 0.5% w/w DODPA in squalane with 1000 ppm of NO₂ at 180 °C (piston conditions) has not been studied previously and so was examined here, and resulted in the identification of seven products formed from the antioxidant.

The concentration of the antioxidant intermediates was significant accounting for well over half of the antioxidant was reacting.

The inhibiting effect of the aminic antioxidant under the harsh NO₂ conditions was observed up to 60 minutes until all of the antioxidant was consumed, at which point squalane nitration products started to form, despite the presence of many antioxidant intermediates. This observation was in contrast to phenolic antioxidant intermediates, which gave protection to the base oil until all the intermediates were consumed.

Based on product identification and the order of product formation by GC, a reaction mechanism was proposed which can account for all seven intermediates. Products 1 and 2 are dimers, which form by the combination of aminyl radicals, products 4 and 5 are dimers formed from dimer 1. Product B is a nitrated amine and forms by the addition of NO₂ to the aminyl radical in the *ortho*-position of the ring. Product A forms by the addition of NO₂ to the aminyl radical, followed by the loss of nitric oxide, which led to the C=O double bond formation. Product 3 forms from the aminyl radical and product A.

Chapter 7: Interactions of Phenolic and Aminic Antioxidant with NO₂ at 180 °C

7.1 Introduction

The inhibiting effect of a single antioxidant in preventing engine lubricant degradation may sometimes not be satisfactory; consequently a common solution to this problem is the use of two or more antioxidants in conjunction with each other.¹⁸⁶ Work reported in previous chapters has been based on single additive systems, whereas in this chapter the interaction of phenolic with aminic antioxidants when used together with NO₂ will be examined. Two commercial antioxidants: phenolic, octadecyl 3-(3,5-ditert-butyl-4-hydroxy-phenyl) propanoate (OHPP), (BASF, Irganox® L107) and aminic, 4,4'-Diocetyl Diphenylamine (DODPA),(BASF, Irganox® L01) have been used here, Figure 7.1.

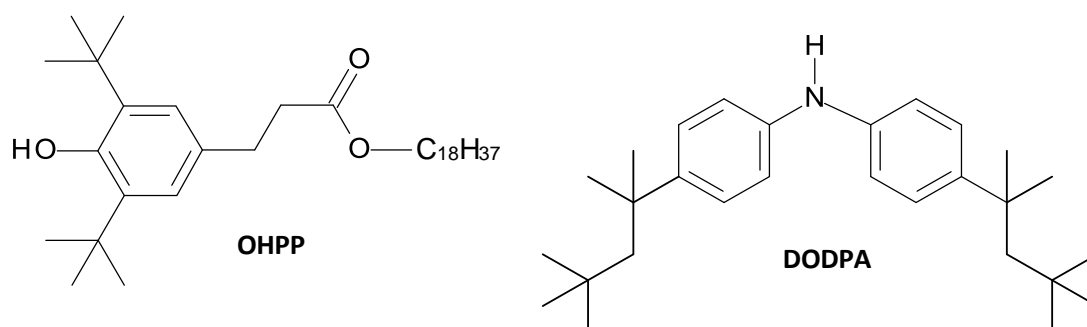


Figure 7.1: Structures of commercial phenolic (OHPP) and aminic (DODPA) antioxidants.

A model lubricant mixture containing OHPP and DODPA in squalane was reacted with 1000 ppm of NO₂ at 180 °C; products were analysed by GC-FID and by using high resolution TOF/GC MS (EI). The interaction between both antioxidants in preventing nitration was examined and reaction mechanisms are proposed.

7.2 Interaction of Phenolic and Aminic Antioxidants during Autoxidation

There is no previously published work on the interaction of both phenolic and aminic antioxidants with NO₂, therefore, background literature on the interaction of these two classes of antioxidants during autoxidation has been examined to provide context. Phenolic and aminic antioxidants are both radical scavengers, so act in similar ways and therefore the interaction between them is sometimes termed homosynergism.^{186,187} Previous studies have examined the interaction of phenolic with aminic antioxidants during the prevention of hydrocarbon autoxidation. The proposed mechanism for the interaction suggested that the aminic antioxidant is more reactive with peroxy radicals than the phenolic, therefore, when used together in mixtures the aminic will preferentially react primarily with peroxy radicals to give the aminyl radical. These aminyl radicals will then react with the phenolic antioxidant to regenerate the amine with the formation of more stable phenoxyl radical, Figure 7.2,^{102,187,188} because the N–H bond in aminic antioxidants is stronger than the O–H bond in phenolic antioxidants.

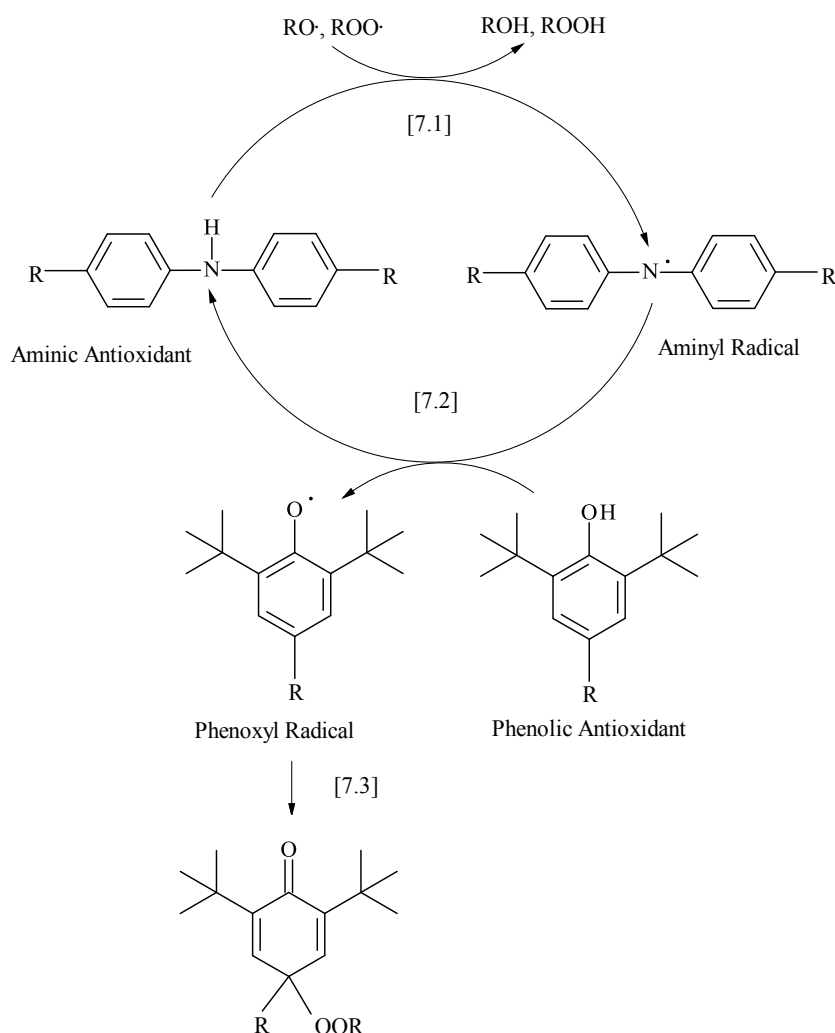


Figure 7.2: Synergistic mechanism between phenolic and aminic antioxidant in the reaction with peroxy radicals.^{187,188}

As a consequence, during autoxidation the phenolic antioxidant is initially consumed followed by the consumption of the amine. Overall, the combination of antioxidants has been reported to increase the inhibition effectiveness in comparison to a single antioxidant system.¹⁸⁷

Previous studies focused on hydrocarbon oxidation, whereas in this chapter the results of interaction of phenolic and aminic antioxidant with NO₂.

7.3 Results and discussion

The starting reaction mixture consisted of 0.25% w/w ($4.4 \times 10^{-3} \text{ mol dm}^{-3}$), phenolic antioxidant (OHPP) and 0.25% w/w ($5.4 \times 10^{-3} \text{ mol dm}^{-3}$), aminic antioxidant (DODPA) in squalane the total antioxidants concentration was 0.50% w/w. The reaction with 1000 ppm of NO₂ at 180°C was performed as previously in Chapters 4 and 6 for single additive model lubricants. Samples were taken frequently during the reaction and quantified by GC-FID and identified by accurate mass TOF/GC MS (EI).

7.3.1 Quantitative Analysis using GC-FID

The quantitative analysis of antioxidants decay and intermediates formation is summarised in Figure 7.3 (Squalane nitration on right hand axis).

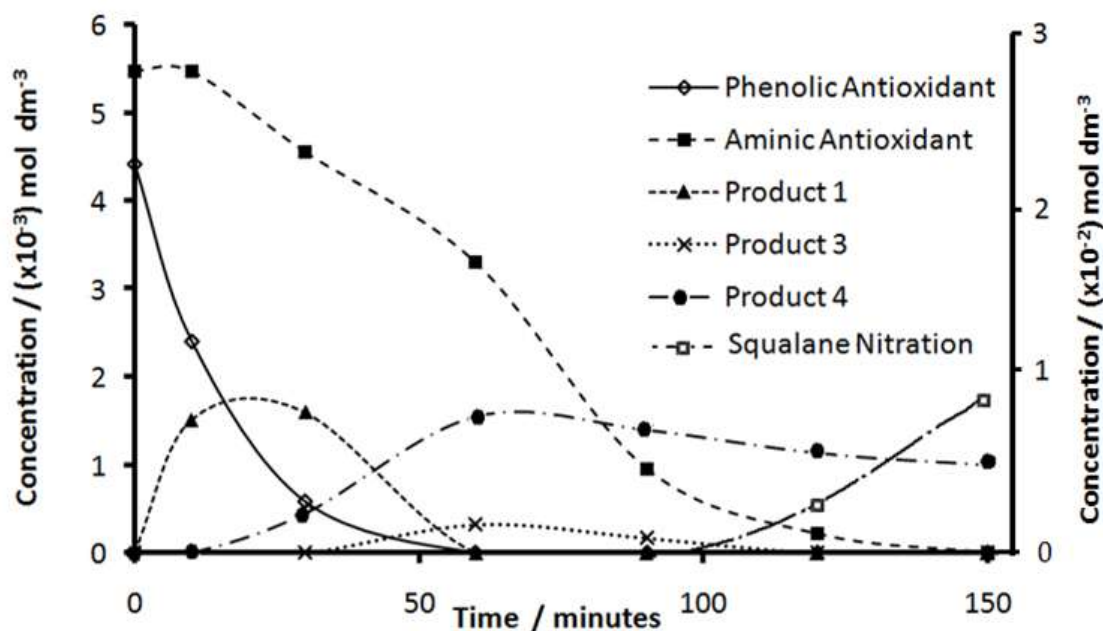


Figure 7.3: Decay of phenolic (0.25 % w/w) and aminic (0.25 % w/w) antioxidants, and their intermediates formation (products 1, 3 and 4) in the reaction with NO₂ at 180 °C.

Initially, the decay of the phenolic antioxidant is observed and one intermediate product forms, as shown in Figure 7.4 (10 min. sample); no decay of the aminic component is seen at this stage.

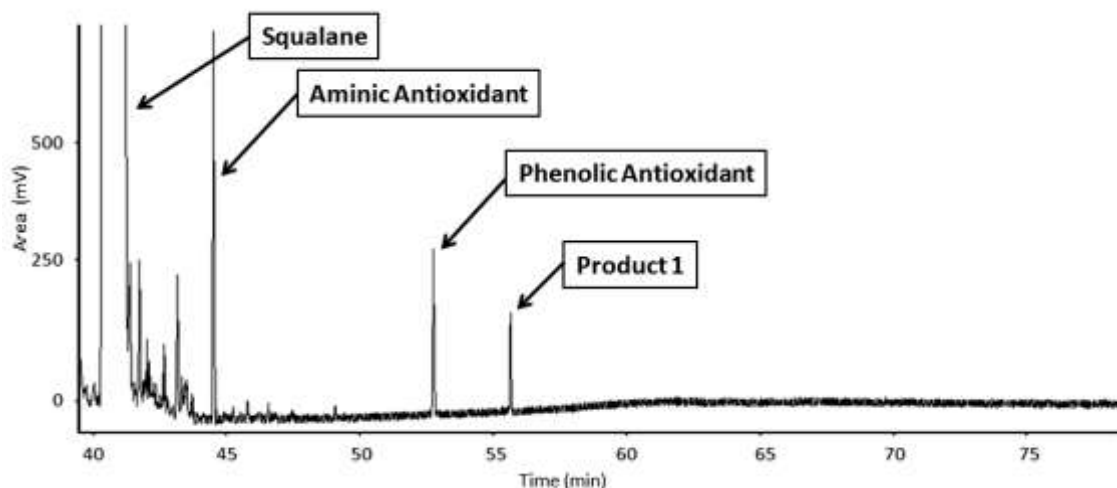


Figure 7.4: GC chromatogram of 10 minutes reaction mixture containing phenolic and aminic antioxidants and a phenolic antioxidant intermediate product (Product 1), other peaks are squalane impurities. Analysis using GC-FID, Shimadzu GC, column ZB-5HT, inj. 350 °C, oven 50-350°C at 5 °C/min, hold for 20 min , FID 350 °C.

As the reaction progresses, by 30 minutes most of the phenolic antioxidant is consumed, however there is still a significant concentration of product 1. At this time aminic antioxidant starts being consumed and a new intermediate forms, product 4. Sample at 60 min. shows that product 1 decays and that there are two new intermediates (product 2 and 3), chromatogram in Figure 7.5.

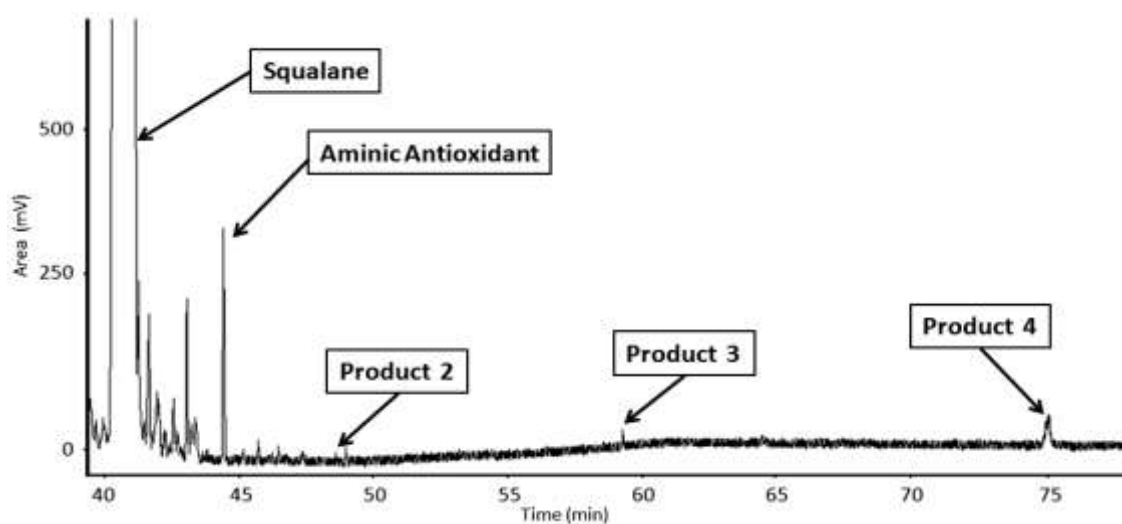


Figure 7.5: GC chromatogram of 60 minutes reaction mixture containing aminic antioxidant and three intermediates (products 2, 3 and 4).

The next sample at 90 minutes shows significant decrease in the concentration of the aminic antioxidant approximately 80 % is consumed and a slow decay of products 3 and 4 is evident. At the same time, there is a significant increase of product 2 and five new intermediates form in the region characteristic for aminic dimers, previously identified in Chapter 6.

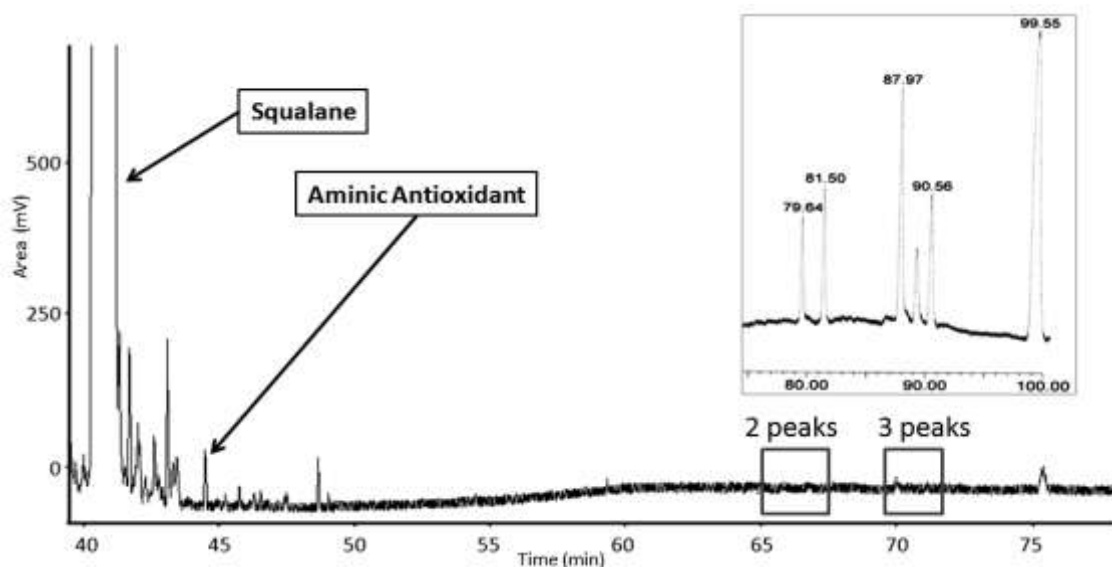


Figure 7.6: GC chromatogram of 90 minutes reaction mixture containing the aminic antioxidant, products 2, 3, 4 and five new intermediates (shown in insert from analysis different on different GC with lower baseline noise, Agilent 7890A GC). Analysis using GC-FID, Shimadzu GC, column ZB-5HT, inj. 350 °C, oven 50-350°C at 5 °C/min, hold for 20 min , FID 350 °C.

Finally at 150 min. when all of the aminic antioxidant is consumed, its intermediate products decay and squalane nitration is observed. This analysis of products formation will be used in establishing the reaction mechanism.

7.3.2 Identification of Intermediates using High Resolution GC-MS EI

The intermediate products formed from the interaction of the model lubricant containing two antioxidants (OHPP and DODPA) in reaction with NO₂ were analysed using an accurate GC-MS (EI) and were compared to results obtained using a single additive systems, as discussed in Chapters 4 and 6.

The EI spectrum of product 1 (Figure 7.7) showed a molecular mass ion of m/z 528.460 ± 0.004 (calculated exact mass m/z 528.454 for formula C₃₅H₆₀O₃) and other characteristic fragments such as: 513, 261 and 219. This suggests the formation of an intermediate formed from the phenolic antioxidant (OHPP), as previously studied in Chapter 4. However, a detailed analysis showed the formation of a m/z 219.174 ± 0.004 fragment (calculated exact mass m/z 219.173), which is more likely for hydroxyl cinnamate (HCIN), the second intermediate product identified for OHPP studied alone.

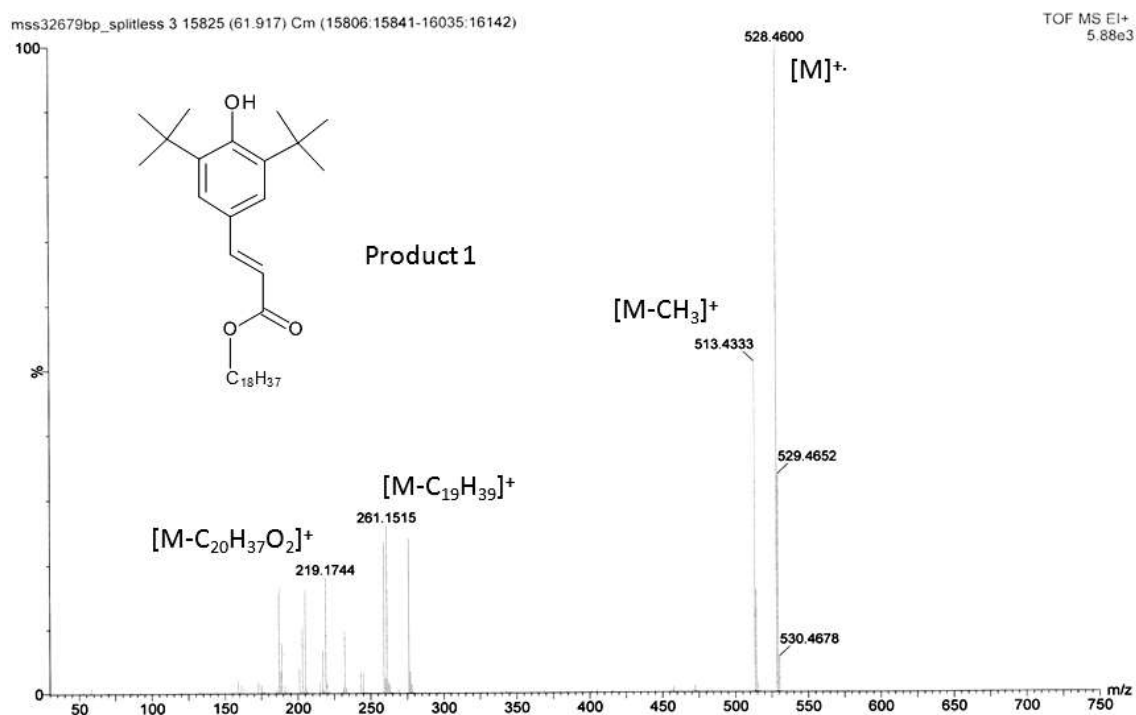


Figure 7.7: GC/TOF MS (EI) spectrum of Product 1 from the reaction of aminic (DODPA) and phenolic (OHPP) antioxidant with NO₂ at 180°C.

The next species identified was product 4 (retention time. = 75 min. by GC) its molecular mass ion was m/z 713.617 \pm 0.005 (calculated exact mass m/z 713.611 for formula C₄₉H₇₉NO₂), spectrum in Figure 7.8. Reviewing GC retention times, a dimerized molecule was expected, however dimers previously identified for DODPA had an even numbered m/z . The odd number of molecular mass fragment of product 4 suggested an odd number of nitrogens in this molecule.¹⁷⁵ Other fragments identified were: m/z = 642, 570, 444, 390, 318 and 274, and the detailed peak assignment is shown in Figure 7.9 and 7.10. From the analysis of fragmentation pattern a possible structure was proposed of octadecyl 5-(1,1,3,3-tetra-methylbutyl)-1-[4-(1,1,3,3-tetra-methylbutyl) phenyl] indole-3-carboxylate.

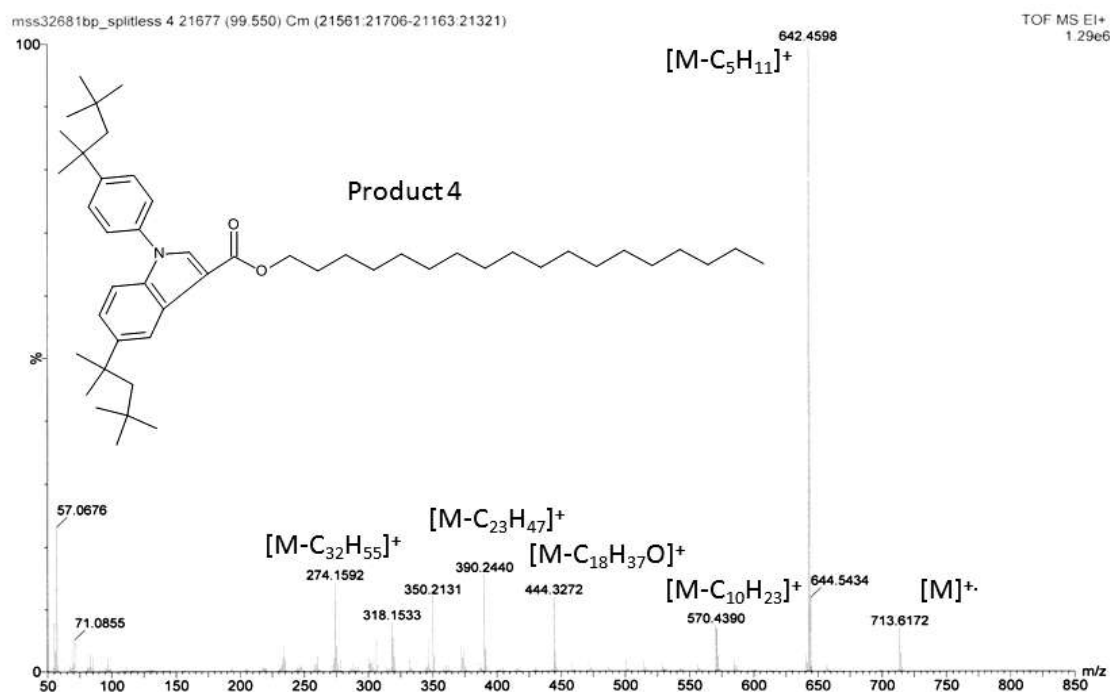


Figure 7.8: GC/TOF MS (EI) spectrum of Product 4 from the reaction of aminic (DODPA) and phenolic (OHPP) antioxidant with NO₂ at 180 °C.

The reaction analysis further suggested that this product possibly forms from the interaction of the phenolic intermediate and the aminyl radical, as they are both present at 30 min. of reaction.

Product 4

Peak at 75.0 min.: octadecyl 5-(1,1,3,3-tetramethylbutyl)-1-[4-(1,1,3,3-tetramethyl butyl) phenyl] indole-3-carboxylate

Assignment

713.617
(calc.713.611)
(C₄₉H₇₉NO₂)

642.500
(calc.642.524)
(C₄₄H₆₈NO₂)
M – C₅H₁₁

570.439
(calc.570.431)
(C₃₉H₅₆NO₂)
M – C₁₀H₁₃

444.327
(calc.444.326)
(C₃₁H₄₂NO)
M – C₁₈H₃₇O

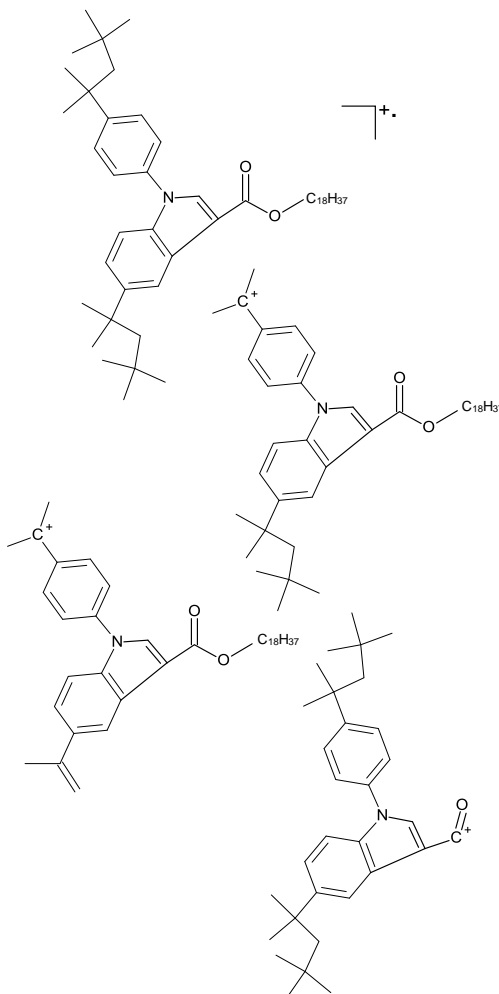
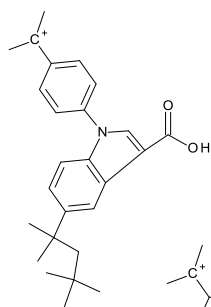


Figure 7.9: Possible fragment structures of Product 4 from the reaction of aminic (DODPA) and phenolic (OHPP) antioxidant with NO₂ at 180 °C - Part 1.

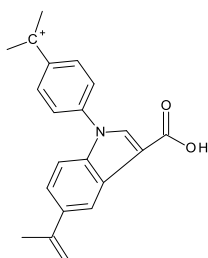
390.244

(calc. 390.243)

(C₂₆H₃₂NO₂)M – C₂₃H₄₇

318.153

(calc. 318.149)

(C₂₁H₂₀NO₂)M – C₂₈H₅₉

274.159

(calc. 274.181)

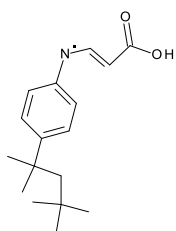
(C₁₇H₂₄NO₂)M – C₃₂H₅₅

Figure 7.10: Possible fragment structures of Product 4 from the reaction of aminic (DODPA) and phenolic (OHPP) antioxidant with NO₂ at 180 °C - Part 2.

Two products were identified at the 60 minutes sample (product 2 and 3); at this time the phenolic intermediate (product 1) was completely consumed. Figure 7.11 shows the spectrum of product 2, of which fragmentation was identical to the previously identified nitrated aminic antioxidant (product B in Chapter 6).

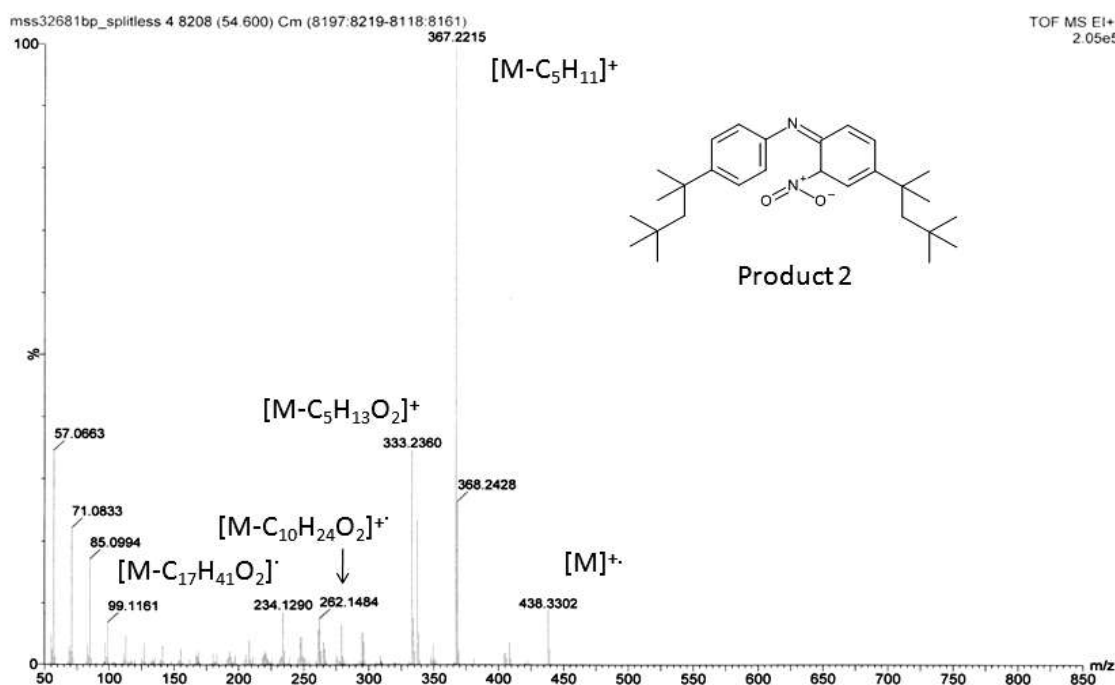


Figure 7.11: GC/TOF MS (EI) spectrum of Product 2 from the reaction of aminic (DODPA) and phenolic (OHPP) antioxidant with NO₂ at 180 °C.

Analysis of Product 3 (Figure 7.12) shows a molecular mass ion m/z 609.500 ± 0.008 (calculated m/z 609.491 for formula C₄₃H₆₃ON), which again suggests an odd number of nitrogen atoms. The characteristic fragments are: m/z = 594, 552, 525, 522 and 454, the analysis of peaks assignment is shown in Figure 7.13. Interestingly, there have also been identified a few fragments characteristic only for phenolic (m/z 219) or aminic (m/z 393, 322, 250) antioxidants (details in Chapters 4 and 6). Following the analysis a possible structure of product 3 was proposed as 2,6-ditert-butyl-4-[[4-(1,1,3,3-tetra-methylbutyl)-N-[4-(1,1,3,3 tetra-methylbutyl) phenyl] anilino] methylene] cyclohexa-2,5-dien-1-one, which is an intermediate formed by combining fragments of both antioxidants.

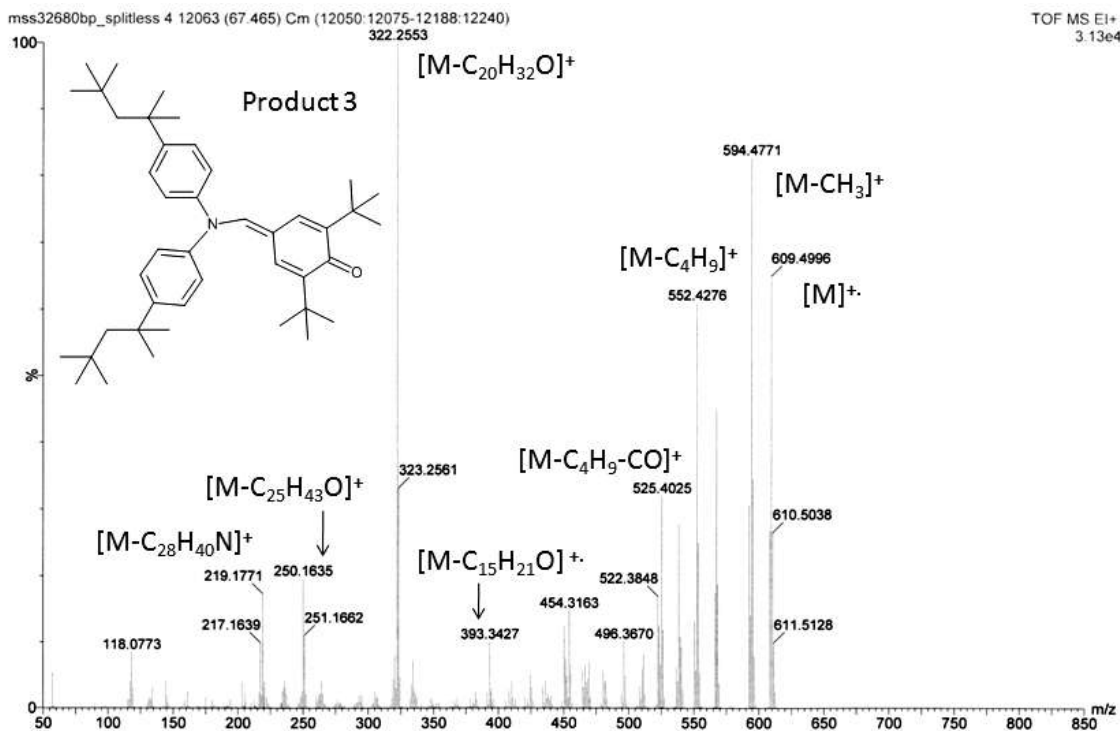


Figure 7.12: GC/TOF MS (EI) spectrum of Product 3.

It possibly forms by combining the aminyl radical with methylene cyclohexadienone radical (semiquinone radical), a product of phenolic antioxidant decay.

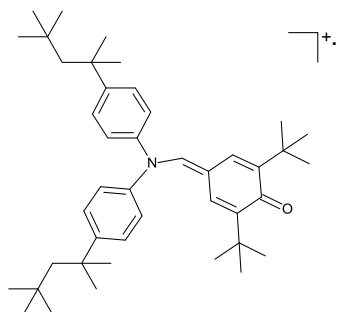
Product 3

Peak at 59.0 min.: 2,6-ditert-butyl-4-[[4-(1,1,3,3-tetramethylbutyl)-N-[4-(1,1,3,3-tetramethylbutyl)phenyl]anilino]methylene]cyclohexa-2,5-dien-1-one

Assignment

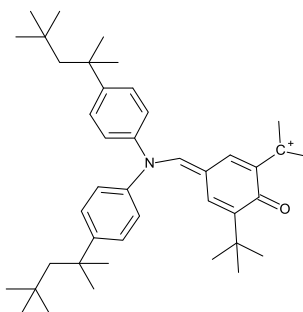
609.499

(calc. 609.491)

(C₄₃H₆₃NO)

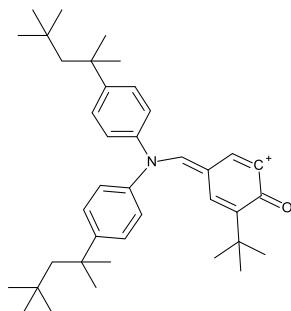
594.477

(calc. 594.467)

(C₄₂H₆₀NO)M-CH₃

552.428

(calc. 522.421)

(C₃₉H₅₄NO)M-C₄H₁₂

525.403

(calc. 525.433)

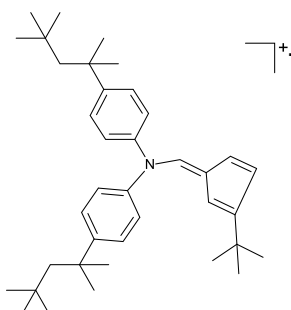
(C₃₈H₅₅N)M-C₅H₈O

Figure 7.13: Possible fragment structures for Product 3 from the reaction of aminic (DODPA) and phenolic (OHPP) antioxidant with NO₂ at 180 °C.

Finally at 90 min., five products are observed, which have been identified by EI as the previously detected dimers, products of interaction of aminic antioxidant with NO₂, details in Chapter 6.

7.4 Reaction mechanism

Initially, only the phenolic antioxidant is consumed due to the presence of NO₂, reactions [7.4]-[7.6]; this mechanism has been presented in Chapter 4.

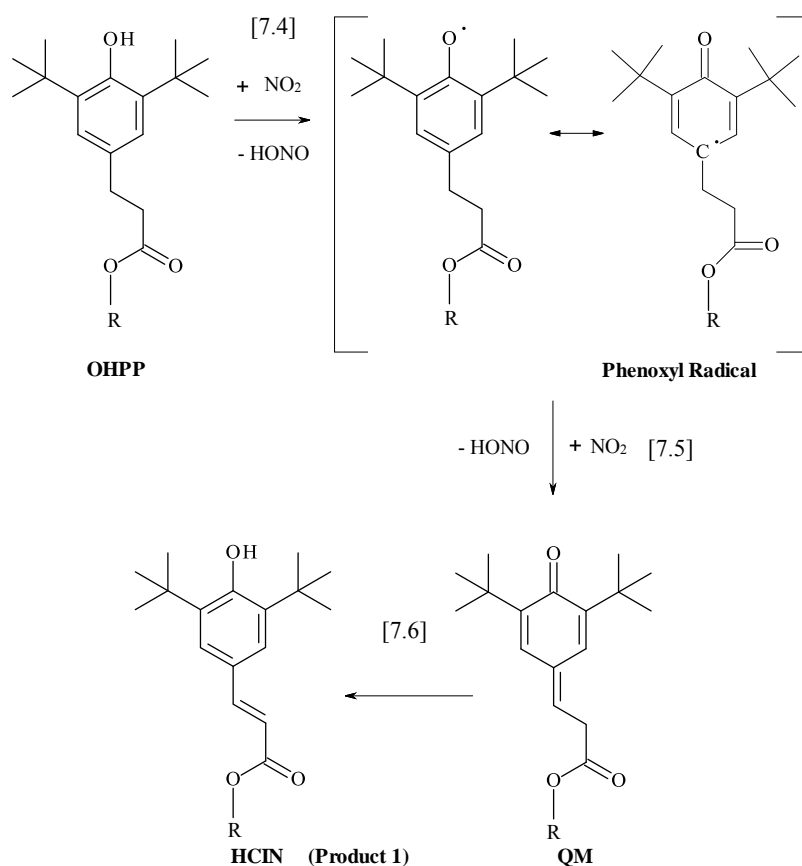


Figure 7.14: Mechanism of the formation of HCIN, from the experiment studying the reaction of the model lubricant containing both aminic and phenolic antioxidants with NO₂ at 180 °C, (R=C₁₈H₃₇).

In reaction [7.2], the phenoxyl radical reacts with NO₂ to form the quinone methide (not identified in this chapter), which rearranges to form the hydroxyl cinnamate (HCIN, Product 1) identified at 10 minutes of reaction (by reaction [7.3]). At this time

approximately 70 % OHPP has reacted to HCIN. Product quantification suggests that this reaction progresses in a similar way comparing to the use of phenolic on its own (see Figures 7.3 and 4.6 in Chapter 4).

The interactions of phenolic and aminic antioxidant with NO₂ are proposed in Figures: 7.15 - 7.17.

The first can be explained by comparing the bond dissociation energies of OHPP and DODPA antioxidants, which shows that the BDE of phenolic O–H ($339.7 \pm 0.4 \text{ kJ mol}^{-1}$)¹⁶⁴ is weaker than aminic N–H ($358.3 \pm 4 \text{ kJ mol}^{-1}$)¹⁸⁹ and therefore phenol could be expected to react preferentially with NO₂. This is consistent with previous studies on the inhibition of autoxidation by aminic and phenolic antioxidants used in conjunction, where the phenolic is consumed first, followed by consumption of the aminic antioxidant. The preferential consumption could be due to a faster rate of reaction with NO₂ due to its weaker O–H bond strength in comparison to the N–H bond strength of the aminic antioxidant. Alternatively, the aminic antioxidant could react first, if kinetically favourable, but then can be regenerated in the analogous way presented in Figure 7.2 for peroxy radicals, reaction with NO₂ in Figure 7.15.

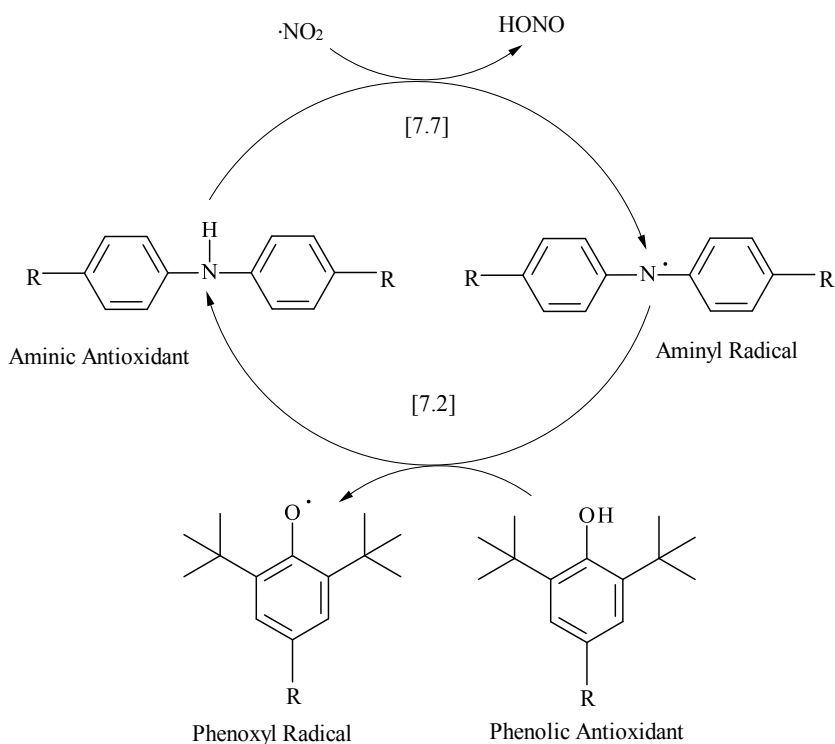


Figure 7.15: Possible synergistic mechanism between phenolic and aminic antioxidant in the reaction with NO₂, similar to mechanism previously studied for peroxy radicals.^{186,187}

Based on product identification two reaction mechanisms for formation of product 4 and 3, formed from the interaction of both antioxidants in the presence of NO₂, have been proposed in Figures 7.16 and 7.17. At the same time, when almost all the phenolic antioxidant is consumed, the aminic antioxidant, DODPA, starts to be consumed and Product 4 is identified, (see the reaction mechanism in Figure 7.16). Primarily, the ester radical is formed by the addition of nitrogen dioxide via the oxygen atom to the *para*-phenoxyl radical, reaction [7.8], followed by the loss of nitrous oxide (reaction [7.9]); which is then followed by cleavage with the formation of quinone and the ester radical (reaction [7.10]). At the same time the aminic hydrogen is abstracted by NO₂ from DODPA with the formation of the aminyl radical and nitrous acid (reaction in Chapter 6). The ester radical from OHPP is combined with the aminyl radical, in the radical-radical termination step, followed by the abstraction of the two weakest

hydrogens by NO₂ and the internal addition, followed by the abstraction of the next weakest hydrogen by NO₂ with the formation of product 4, reactions [7.11]-[7.16].

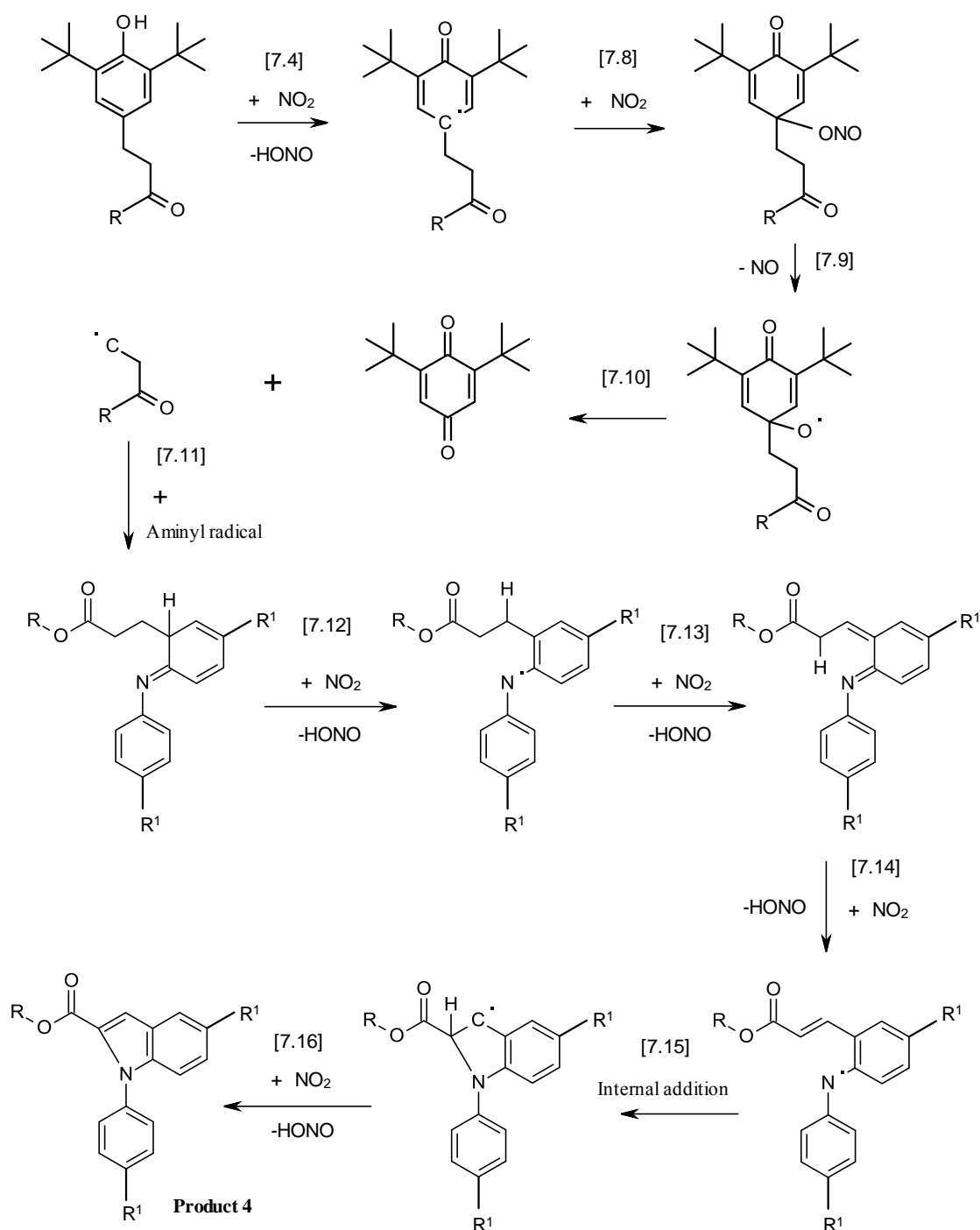


Figure 7.16: Possible mechanism of the formation of Product 4 in the reaction of the model lubricant (containing both aminic and phenolic antioxidants) with NO₂ at 180 °C: (R=C₁₈H₃₇; R¹=C₈H₁₇).

At 60 min. Product 1 is completely consumed and only its decay products potentially remain, therefore the termination reaction occurs. The third mechanism shows the formation of product 3, which is also an interaction product of both antioxidants (Figure 7.17) and which forms by reaction of the aminyl radical with QM.

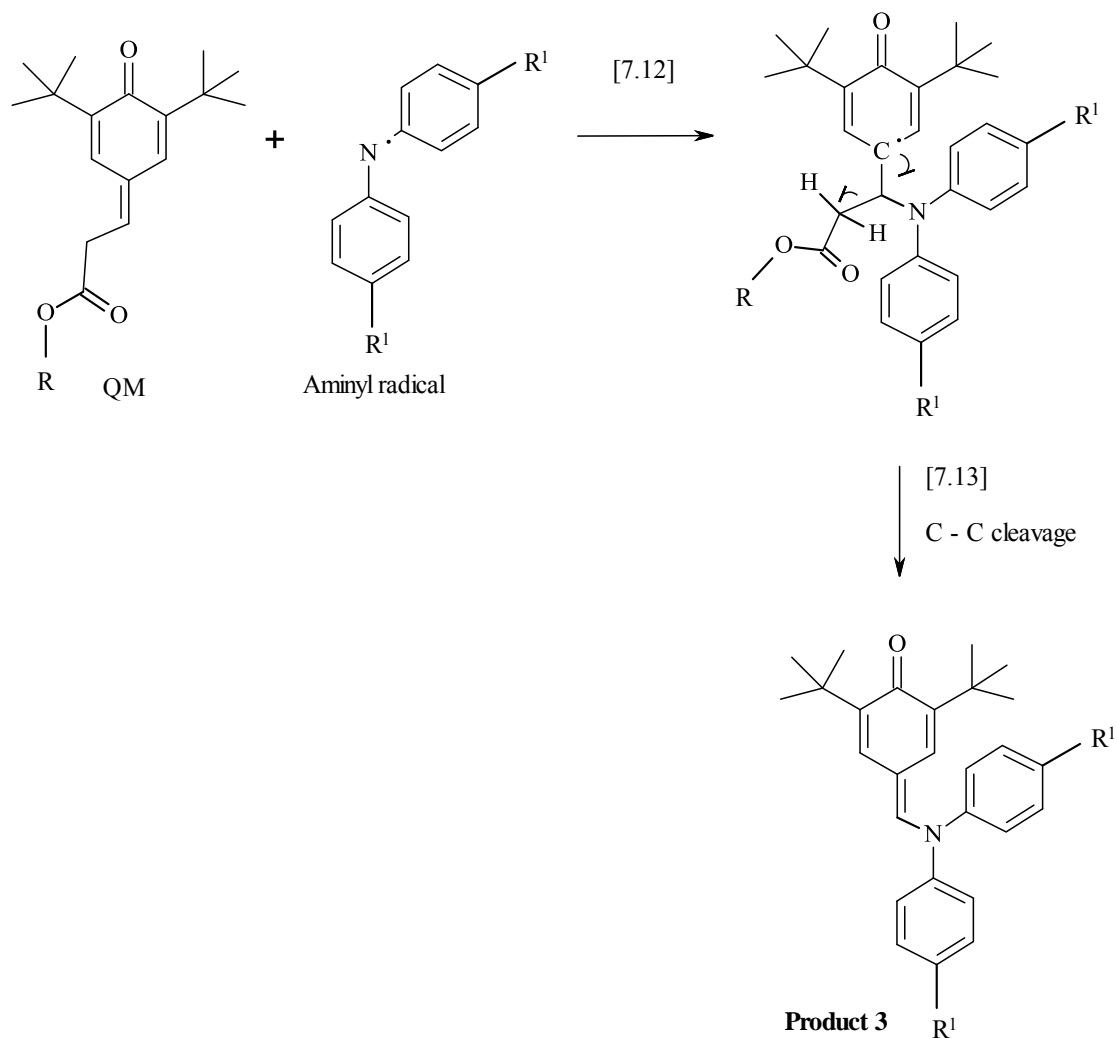


Figure 7.17: Possible mechanism of formation of Product 3 from the reaction of the model lubricant (containing both aminic and phenolic antioxidants) with NO₂ at 180 °C. (R¹=C₈H₁₇ and R=C₁₈H₃₇).

The synergistic interaction of quinones with aromatic amines was reported previously by Denisov *et. al.*¹⁰² who proposed a mechanism ultimately resulting in radical polymerization,¹⁸³ but which starts with the reaction of quinone with the aminic antioxidant to semiquinone and then a further rapid termination of radicals.¹⁷¹ At 90

min. decay of product 3 and 4 is observed, which is related to the consumption of intermediates from the decay of HCIN. At this point there is only 20 % of aminic antioxidant left, which rapidly reacts with NO₂, which increases the formation of Product 2 (nitrated amine) together with aminic dimers, as described by the reaction mechanism as shown in Chapter 6. At 120 min. most of the aminic antioxidant is used and nitration of squalane commences.

It has been suggested that the interaction of quinone with the aminic antioxidant prolongs the induction time by 2-3 times during autoxidation.¹⁰² Therefore the synergistic effect of both antioxidants was reviewed in this study. There have been three categories of interactions between antioxidants proposed by Denisov *et. al.*; the additive effect, which is equal to the sum of both antioxidant effectiveness's, the antagonistic effect, where the antioxidants used in conjunction is less effective than when used individually, or synergistic, where the total inhibition effect is increased.¹⁰² This study shows an increased inhibition effectiveness using a mixture of both aminic (0.25 % w/w) and phenolic (0.25 % w/w) antioxidants up to 120 minutes; compared to the aminic antioxidant (0.5 % w/w) used alone, which was up to 75 minutes, there is evidence of a synergistic interaction. However, comparing to the phenolic antioxidant (0.5% w/w) used alone, under which conditions squalane nitration products form at 165 min., suggests that addition of amine decreases its inhibition effectiveness, thus overall the interaction of aminic and phenolic antioxidants is antagonistic when it comes to reactions with NO₂.

7.5 Summary

The interaction between phenolic (OHPP, 0.25 %) and aminic (DODPA, 0.25 %) antioxidants has been studied, to understand how they inhibit the nitration of base oil under high temperature piston conditions.

Nine intermediate products have been identified by accurate GC-MS (EI): Product 1 (HCIN), forms from the phenolic antioxidant identified previously in Chapter 4, Products 3 and 4 are products of interaction of phenolic and aminic antioxidants (new products), and six products from the aminic antioxidant identified previously in Chapter 6.

Based on a quantified analysis of product formation, identification by GC-MS (EI) and review of bond dissociation enthalpies possible reaction mechanisms have been proposed.

The inhibition effectiveness using two antioxidants have been compared to single additive systems, which suggested that the best protection against NO₂ is provided by phenolic antioxidant (OHPP) used alone; the mixture of both antioxidants is less effective, and the least effective is the aminic antioxidant (DODPA) used alone.

Chapter 8: Conclusions and Suggestions for Future Work

8.1 Summary and conclusions

Recently, the main drivers for change in automotive engine technology have been to improve fuel economy, reduce exhaust emissions and increase power density. Unfortunately, one consequence of this is that this has led to an increase of the harmful product of combustion, NO_x, in the combustion chamber. The interaction of engine oils with a high concentration of NO_x can cause degradation of the lubricant, with unwanted increases in viscosity leading to reduced fuel economy and increase emissions of the green house gas CO₂, as well as increased formation of insoluble precipitates, sludge, which also have serious implications on the performance and working lifetime of the engine.

NO_x reacts with hydrocarbons causing engine oil nitration, therefore the importance of this study was to improve the understanding of the reactions of phenolic and aminic antioxidants with NO_x and to investigate the chemical mechanisms by which these inhibitors react with NO_x, because, without antioxidants, nitration would quickly decompose engine oil in use. The piston assembly is the first place where lubricants come into contact with harsh combustion products such as NO_x, therefore the temperature studied here was as high as 180 °C, which was representative of for lubricants in the vicinity of the piston rings.

Experiments were carried out using a bench-top test developed at University of York. Initially the bench test was designed and optimised, and the series of test experiments,

including oxidation, nitration and nitro-oxidation were undertaken, as described in Appendix A, Chapter 2.

The preliminary studies also included an investigation of the autoxidation of squalane ($C_{30}H_{62}$) in the liquid phase, as described in Chapter 3. Squalane has been used in this work as a representative chemical model of lubricant base fluid, because its chemical and physical properties are similar to those in commercial base fluids. The autoxidation of squalane resulted in the identification of alkanes (this work) and ketones (previously identified by Alfadhl, 2008),¹¹⁵ which are smaller and more volatile than squalane itself. These products are associated with the decomposition via beta-scission of the tertiary alkoxy radicals (2-squaloxyl, 6-squaloxyl and 10-squaloxyl) in a similar way to pristine ($C_{19}H_{40}$), a smaller branched alkane, which was studied previously by Wilkinson 2006. Investigation of the liquid phase oxidation products of squalane is a very effective way of monitoring degradation of the parent molecule.

The main experiments reported in this work include the reactions of 1000 ppm of NO_2 in N_2 with model lubricants consisting of phenolic, aminic, or both (phenolic and aminic) antioxidants in squalane, which have been studied at 180 ± 1 °C, representative of the lubricant in the piston assembly. Products arising from the antioxidants interactions with NO_2 have been identified using robust analysis including GC with accurate mass FI-MS and EI-MS, 1H NMR, UV-Vis, FTIR and GC x GC with NCD detection, and reaction mechanisms were proposed. Additionally Gaussian software has been used successfully in explaining the thermochemistry of the reaction mechanisms of phenolic antioxidants with NO_2 at piston ring pack temperatures.

The reaction of the phenolic antioxidant, octadecyl 3-(3,5-di-*tert*-butyl-4-hydroxyphenyl) propanoate (OHPP) with NO_2 at 180 °C resulted in the formation of quinone

methide, octadecyl 3-(3,5-di-*tert*-butyl-4-oxo-cyclohexa-2,5-dien-1-ylidene) propanoate, QM, (as described in Chapter 4), in an apparent contradiction to previous studies, which observed nitro-phenols formation.⁸³ Therefore, a novel reaction mechanism has been proposed to account for this change in mechanism with the temperature. At ambient temperatures and high concentrations of NO₂, the main reaction of NO₂ with phenoxy radicals is addition, with the formation of nitrated phenolic (as reported previously).⁸³ At elevated temperatures and low concentrations of NO₂, however this addition of NO₂ to the phenoxy is reversible, allowing a slower reaction to dominate the abstraction of hydrogen by NO₂ from phenoxy radical at α carbon with the formation of a non-nitrated product, quinone methide (described in this work in Chapter 5). Thermochemical calculations allowed the ceiling temperature for formation of nitrated phenolics to be estimated as approximately 51 ± 57 °C for 0.001 bar NO₂ therefore under engine piston conditions nitration will be reversible and the formation of non-nitrated (quinone methide) products will dominate. This is consistent with experimental results being dependent on the temperature and pressure and supported limitations for the addition of NO₂ to phenoxy radical at piston ringpack temperatures.

The reaction of the aminic antioxidant, 4,4'-dioctyl diphenylamine (DODPA) in squalane, with 1000 ppm NO₂ at 180 °C was also investigated for this work, and resulted in the identification of seven products from the antioxidant, as reported in Chapter 6. Previous work on the synthesis reaction of diphenylamine with NO₂ suggested the formation of the dimers or nitrated amines, however no chemical analysis has yet been reported. The work reported here is novel as it is investigating in details the aminic antioxidant interaction with nitrogen dioxide at elevated temperatures representative of piston assembly, something which has not been previously

investigated. Two monomers and five dimers were identified from the reaction of DODPA with NO_2 , using accurate GC/TOF-MS EI and ^1H NMR, and possible reaction mechanisms were proposed. The first monomer was nitrated amine (product A) formed by the addition of NO_2 to aminyl radical and the second cyclohexadienone imine (product B) formed by the addition of NO_2 through the oxygen to aminyl radical followed by the loss of nitric oxide, which led to $\text{C}=\text{O}$ double bond formation. Two dimers were formed by the combination of two aminyl radicals (products 1 and 2), product 3 formed from the reaction of aminyl radical with product A, which gave the dimer with an oxygen atom and the last products were two dehydrodimers (products 4 and 5), formed from the dimers.

Understanding of the elementary reactions of how the harsh combustion products, such as NO_x , react with lubricants is key in the development of long lived lubricants. It is a common solution in industry, to use two or more antioxidants, where synergistic interactions improve the inhibiting effectiveness, comparing to a single additive system. The final studies therefore included the interaction of phenolic and aminic antioxidants, used together, in the reaction with nitrogen dioxide at $180\text{ }^\circ\text{C}$, which have not been studied before and is reported here in Chapter 7. During the reaction nine intermediate products from the antioxidants have been identified; however, of these only two were new products from the interaction of phenolic (OHPP) and aminic (DODPA) antioxidants (product 3 and 4). Possible reaction mechanisms of their formation were proposed, which have not been presented before. Product 3 was a combination of the aminyl radical and semi-quinone radical, whereas product 4 was a combination of aminyl radical with the long chain ester from the phenolic antioxidant.

The analysis of the samples taken periodically during the reaction showed that at the first stage of the reaction the phenolic antioxidant was consumed and only one intermediated product from the phenolic antioxidant was identified, which was the hydroxyl cinnamate. When all the phenolic was consumed further reactions showed the formation of products from the interaction of the phenolic with the aminic antioxidant (product 3 and 4); at the end of reaction a small concentration of the dimers from the aminic antioxidant have been observed (identified here in Chapter 6).

The inhibition effectiveness using two antioxidants have been compared to single additive systems. All experiments used in total 0.5 % w/w of inhibitor; the results showed that the best protection against NO₂ will provide phenolic antioxidant (OHPP) used alone, as there was no squalane nitration observed up to 130 min. of the reaction (Figure 4.6, Chapter 4). Comparing the phenolic result to the experiment using a mixture of both the phenolic and the aminic antioxidants, no squalane nitration was identified up to 90 min. of the reaction (Figure 7.3, Chapter 7). The least experiment with the aminic antioxidant (DODPA) used alone, with no nitration observed up to 60 min. of the reaction, (Figure 6.19, Chapter 6). Therefore, in the reaction with NO₂, aminic antioxidants will have an antagonistic effect on phenolics.

8.2 Future Work

8.2.1 The effect of Oxygen on Nitration Lubricants

The real engine combustion environment contains air as a source of oxygen, however the main experimental work presented here used 1000 ppm of NO₂ in nitrogen (or 100% of oxygen, in Chapter 3). The possible interaction of oxygen with NO₂ and its

effect on lubricant degradation can be raised. Thus, to further this work, reactions should be undertaken at 180 °C, replacing approximately 10 % of an inert gas (N₂) with oxygen, which is a representative concentration remaining in blow-by gases after combustion.

8.2.2. Effect of other Lubricant Additives on Engine Oil Degradation in Bench Top Reactor

Future work should involve extending the reaction matrix to include the interaction of other lubricant additives with NO₂ and the effect on lubricant degradation; potential additives include ZDDPs, detergents and dispersants.

8.2.3. The effect of NO on Engine Lubricant Degradation at 180 °C

Nitric oxide and nitrogen dioxide are the main components of NO_x in automotive engines. The effect of NO₂ has been studied and reported in Chapters 4 to 7. However the concentration of nitric oxide in blow-by gases is significant and cannot be ignored. Therefore 1000 ppm of NO have been used in preliminary studies (in a similar way to NO₂), however it showed no reaction with the base fluid and antioxidant consequently the main studies concentrated on NO₂. This need to be explored in further detail, in future work and preferentially should preferably be based on the thermochemical calculation using Gasussian software, in a similar way to the results presented for NO₂ reaction with phenolics in Chapter 5.

8.2.4. Monitoring of NO₂ Consumption

A specially designed NO₂ automotive sensor was mounted to the apparatus used for this work to monitor NO₂ consumption; however the Henry's law solubility of NO₂ in non-polar solvents (similar to squalane) at 180 °C have not been reported previously, and interpretation of these results proved problematic, therefore the NO₂ uptake has not

been reported in this work; however, it would be informative to explore this in more detail.

8.2.5. Identifying the Nitration Products from Squalane

The screening of the nitrated squalane sample showed the formation of a large number of the products which could be difficult to separate and identify by GC-MS alone, however using GC x GC analysis with NCD and FID detectors shows a great improvement in separation of the products and demonstrates it to be a good analysis tool for resolving the complex mixtures of used lubricants. Nevertheless, the key research of this thesis was the interaction of NO_x with antioxidants; squalane nitration should be investigated in future work.

A. Appendix to chapter 2.

Oxygen uptake calculations using raw data recorded from oxygen sensor

The example of calculated oxygen uptake in $[\text{mol dm}^{-3}]$ using the ideal gas law equation and raw data of oxygen consumption in $[\text{mV}]$ is shown in Table A1. This was previously described by Alfadh1 2008.¹¹⁵

Table A1: Example of the oxygen uptake calculations from squalane oxidation in bench-top reactor at 180° C. (this work results)

Time (min)	O2 (mV)	O ₂ uptake (%)		O ₂ flow rate (dm ³ min ⁻¹)	O ₂ uptake (dm ³ min ⁻¹)	Pressure (mbar)	O ₂ uptake (mol min ⁻¹)	Δ Time (min)	Integral (mol min ⁻¹)	Sum (mol)	[O ₂] in 7 cm ³ (mol dm ⁻³)
		Recorded	Actual								
0.00	996.749	100	0.00	0.10	0.00E+00	1034.487	0.00E+00	0	0.00E+00	0.00E+00	0.000
0.03	993.724	99.69651	0.30	0.10	3.03E-04	1034.567	8.34E-06	0.03	2.78E-07	2.78E-07	0.000
0.07	993.718	99.69591	0.30	0.10	3.04E-04	1034.275	8.35E-06	0.03	2.78E-07	5.56E-07	0.000
0.10	993.727	99.69681	0.30	0.10	3.03E-04	1034.113	8.32E-06	0.03	2.77E-07	8.34E-07	0.000

Details of calculations:

$$[\text{O}_2] (\text{mol dm}^{-3}) = \text{sum (mol)} / \text{substrate volume (dm}^{-3}\text{)}$$

$$\text{Sum (mol)} = \text{latter sum cell} + \text{adjacent integral cell}$$

$$\text{Integral (mol min}^{-1}\text{)} = \text{O}_2 \text{ uptake (mol min}^{-1}\text{)} \times \text{time difference (min)}$$

$$\Delta \text{Time (min)} = \text{latter time cell} - \text{former time cell}$$

$$\text{O}_2 \text{ uptake (mol min}^{-1}\text{)} = (\text{pressure in mbar} \times 100) \times (\text{O}_2 \text{ uptake in dm}^{-3} \text{ min}^{-1} / 1000) / (\text{gas constant} \times \text{temperature in [K]})$$

$$\text{O}_2 \text{ uptake (dm}^3 \text{ min}^{-1}\text{)} = \text{O}_2 \text{ actual uptake (\%)} \times \text{O}_2 \text{ flow rate (dm}^3 \text{ min}^{-1}\text{)} / 100$$

Pre-testing of experimental set-up with analysis of the samples from nitro-oxidation

Initially the bench test was designed and optimised, and the series of test experiments, such as: oxidation, nitration and nitro-oxidation were undertaken. Studies included comparison of calculated (this work) oxygen uptake for different experiments, such as: with and without antioxidant and with and without nitrogen dioxide. Figure A1.

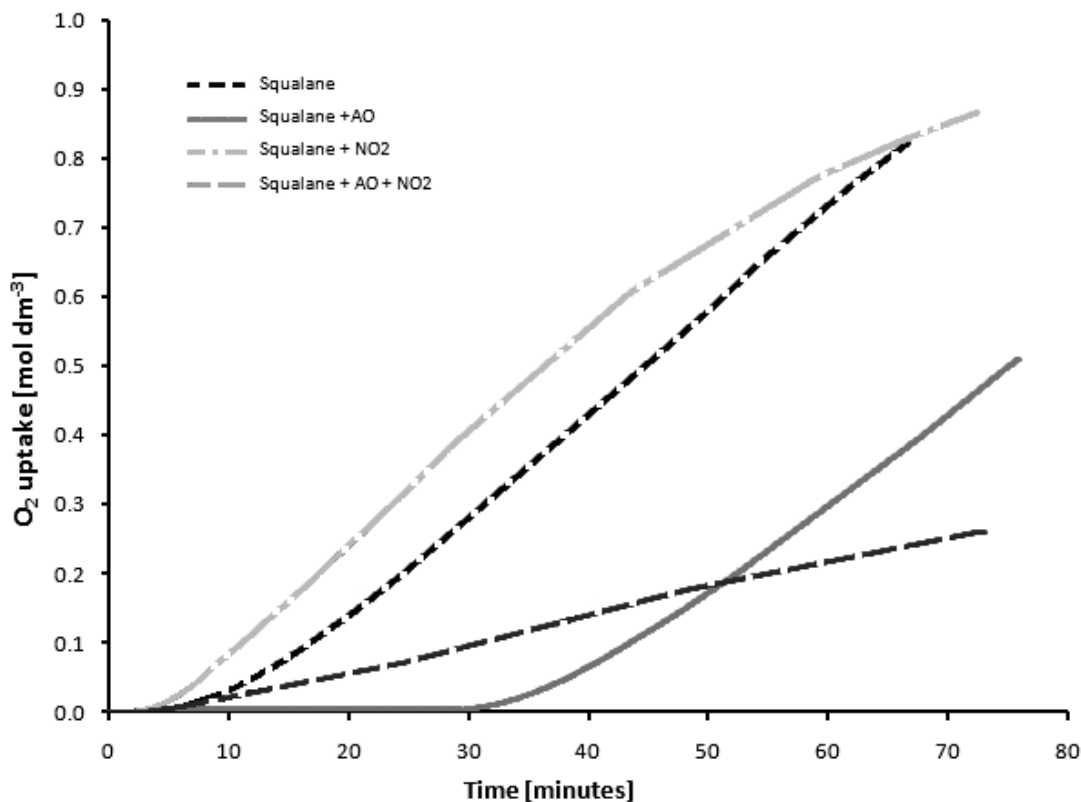


Figure A1: Calculated oxygen uptake for four different oxidation experiments using: 1. – squalane (model base oil); 2. – squalane with OHPP (phenolic antioxidant); 3. – squalane with NO₂; 4. - squalane with OHPP and with NO₂. Reaction conditions: 180 ± 1 °C, 1000 mbar, oxygen flow rate 0.1 dm³ min⁻¹, [NO₂]~1700 ± 200 ppm, [OHPP] 0.5% w/w.

The oxygen uptake results were depended on the presence or absence of NO₂ or antioxidant in the reactions and were monitored using automotive oxygen sensor. All four reactions were undertaken in bench-top reactor at 180 °C. The oxidation induction time (OIT) method was used to characterise squalane oxidative stability to highly

reactive NO₂ and to determine the effectiveness of phenolic antioxidant. Therefore the moment of the significant oxygen increase was monitored for each of the reaction. Oxygen uptake results show that in the presence of nitrogen dioxide oxygen consumption was twice as fast as reaction without NO₂ and the OIT was also reduced from (8 ± 1 min.) to (3 ± 1 min.) approximately. The addition of antioxidant during reaction with NO₂ slows down oxygen uptake but the antioxidant effect is smaller (6 ± 1 min.) than for reaction without NO₂ (28 ± 1 min.).

To support oxygen uptake data samples obtained from the reactions, were analysed using FTIR spectroscopy, Figures A2 to A5 and the viscosity changes were monitored, Figure A6. The level of oxidation and nitration products formed during the reactions was monitored using infrared spectroscopy. Each of the Figures A2 to A5 contained overlaid spectra from all stages of the reaction. The carbonyl groups, characteristic for squalane oxidation, were identified in the 1770 to 1710 cm⁻¹ region, as shown in Figure A2.

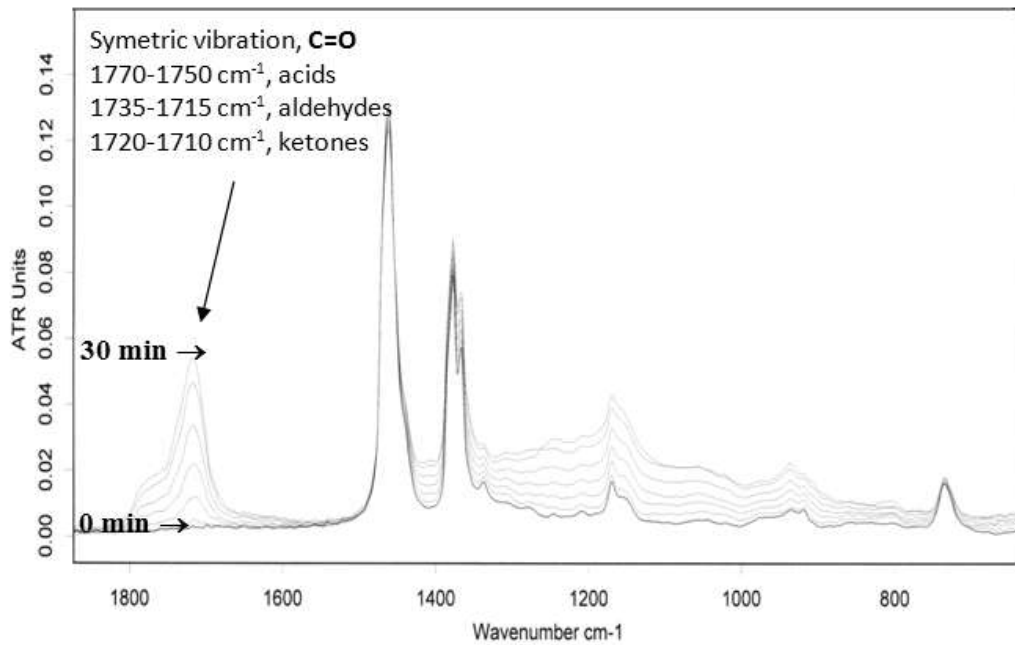


Figure A2: Identification of carbonyl functional groups from oxidation squalane in bench-top reactor at 180 °C, overlaid IR spectra of samples from: 0, 5, 10, 15, 20, 15, 25 and 30 minutes.

For reaction with antioxidant, inhibition was observed up to 25 minutes and at 30 minutes rapid increase in carbonyl finger print region was observed, Figure A3.

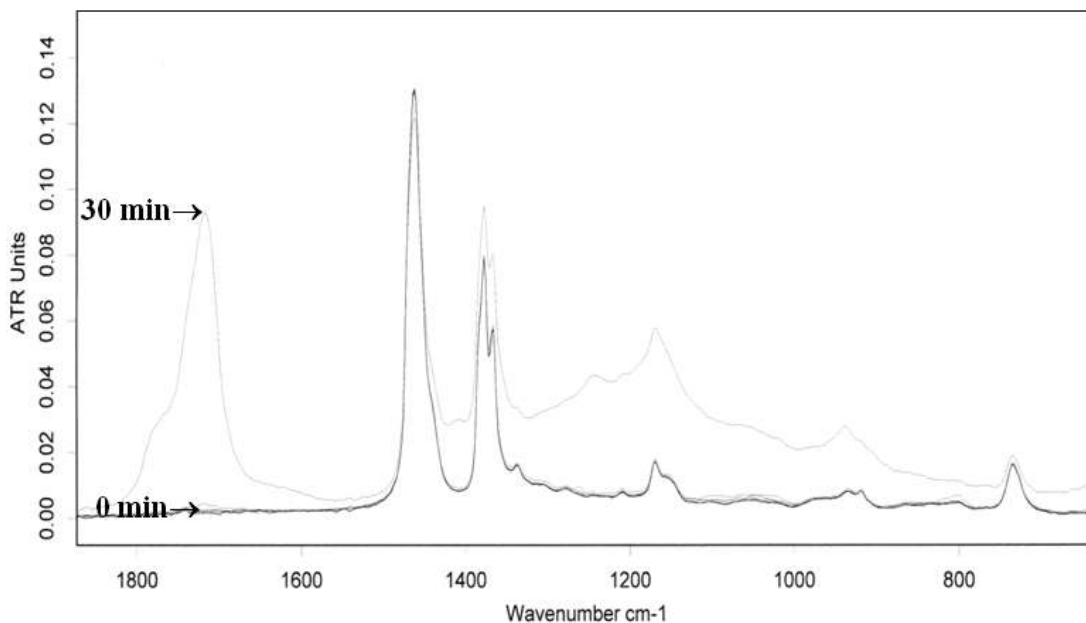


Figure A3: Inhibited (phenolic antioxidant) oxidation of squalane in bench-top reactor at 180 °C, overlaid IR spectra of samples from: 0, 5, 10, 15, 20, 25 and 30 minutes.

For reaction of squalane with NO_2 , three functional groups such as: carbonyl, nitrate ester and nitro groups were identified, Figure A4. The reaction with nitrogen dioxide gave four extra peaks characteristic for C-NO_2 , O-NO_2 and N-O bonds and the concentration of carbonyl functional groups was higher than in oxidation reaction.

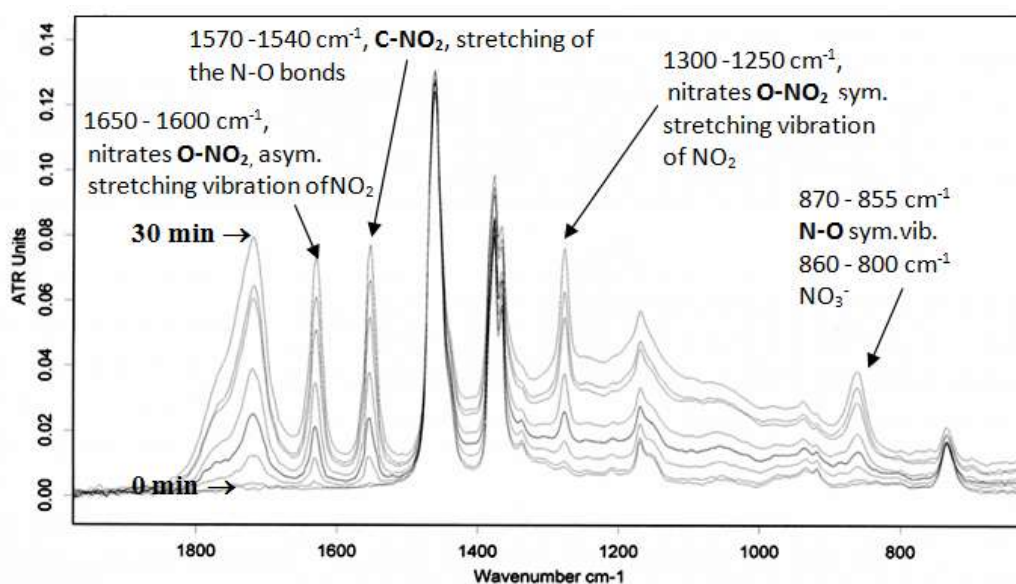


Figure A4: Identification of nitrate and nitro functional groups from the nitro-oxidation of squalane in bench-top reactor at 180°C , samples 0, 5, 10, 15, 20, 23, 25 and 30 minutes.

Antioxidant effect on nitration is shown in Figure A5.

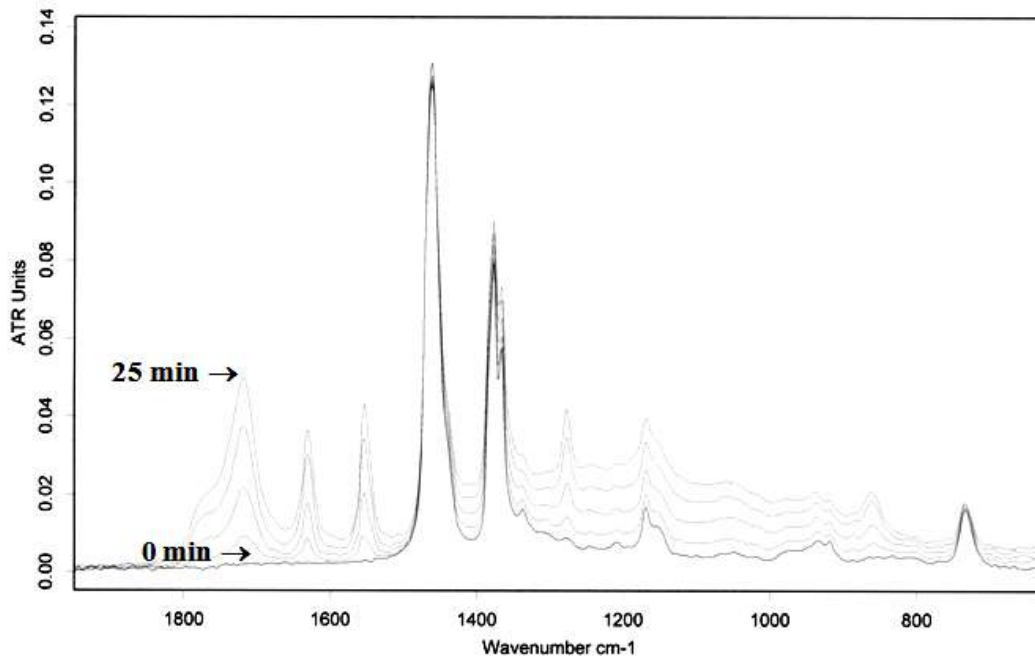


Figure A5: Antioxidant effect on nitro-oxidation of squalane in bench-top reactor at 180 °C, overlaid IR spectra of samples from: 0, 5, 10, 15, 20, 15 and 25 minutes.

The infrared results from inhibited nitro-oxidation show that the concentration of carbonyl, nitrate ester and nitro groups was smaller comparing to none inhibited nitro-oxidation. For inhibited oxidation the formation of carbonyls was stopped until the antioxidant was present.

The viscosity changes of model lubricants, in the reactions with and without NO₂ and with and without AO, have been compared. The viscosity measurements were performed using standard industry method, KV at 40 °C. The rapid increase in viscosity was observed due to reaction of squalane with NO₂ and the smallest increase was obtained due to inhibiting action of antioxidant, as shown in Figure A6.

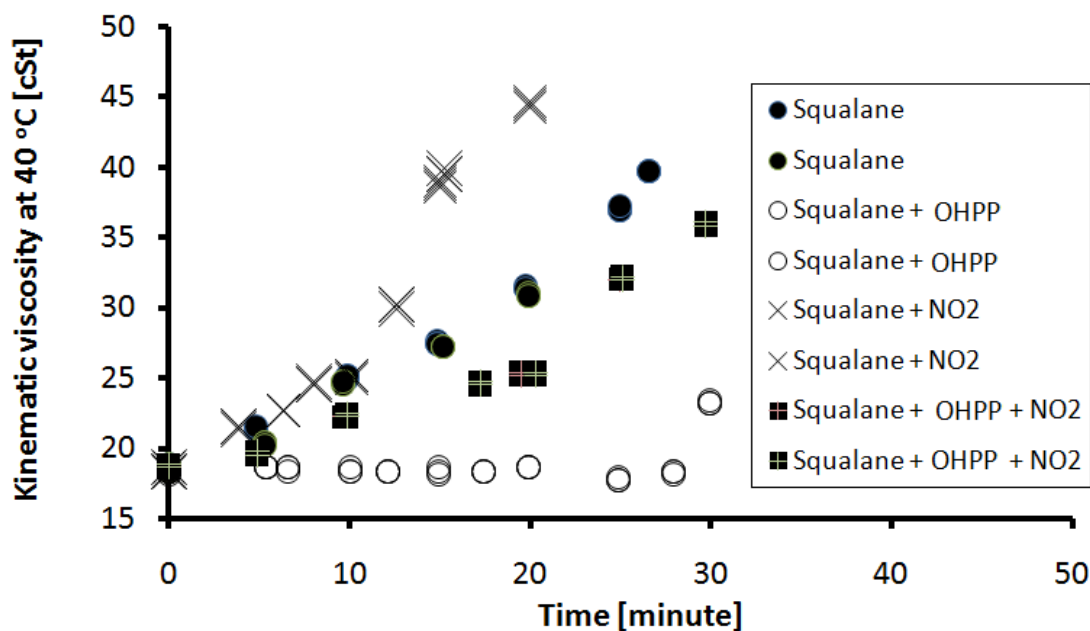


Figure A6: Kinematic viscosity change reported for oxidation of squalane in bench-top reactor at 180 °C, comparison of the reactions with presence or absence nitrogen dioxide (1700 ± 200 ppm) and with presence or absence of antioxidant OHPP (0.5 %, wt/wt).

The results from nitration show the maximum increase in viscosity up to 45.0 ± 0.1 cSt from 19.0 ± 0.1 for last sample. For inhibited nitration increase in viscosity was slower approximately 38.0 ± 0.1 cSt after 25 minutes. For reaction with antioxidant and without NO_2 oxidation was completely prevented up to 25 minutes, when all AO was used up and rapid increase in viscosity was observed.

The effect of pressure on degradation of lubricants

The reaction in bench-top reactor was carried out under ambient pressure condition (1050 ± 10 mbar); whereas for real engines, the pressure is typically higher and depends on the piston position. To study the effect of the pressure on lubricant degradation the Standard Test Method for Oxidation Stability of Steam Turbine Oils by Rotating Pressure Vessel, ASTM D2272, has been employed in preliminary experiments to oxidise model lubricant containing 0.5% of phenolic antioxidant, OHPP, in base oil. The standard test method used 90 psi (6205 mbar) pressure and 150 °C temperature, and also H₂O and copper as a catalyst. That was different to the conditions studied in bench top reactor at the University of York, where the typical experimental temperature was 180 °C and 1050 mbar pressure, with no catalyst. Therefore to compare this results the test experiment was undertaken in bench-top reactor at 150 °C and the result showed approximately 4 hours oxidation induction time which was similar to results obtained using the industrial high pressure oxidation test. This comparison proof that results obtained using the bench-top reactor at University of York are comparable to those used in industry.

Response factor calculations using effective carbon number (ECN) method

The effective carbon number (ECN) concept was used in calculations of GC-FID response factors for products, which standards were unavailable:

$$ECN = (GC \text{ response} / \text{Carbon constant}) \times (1/\text{Compound carbon atoms})$$

Experimentally obtained response factors for standard compounds were plotted together with an effective carbon numbers as shown in Figure A7.

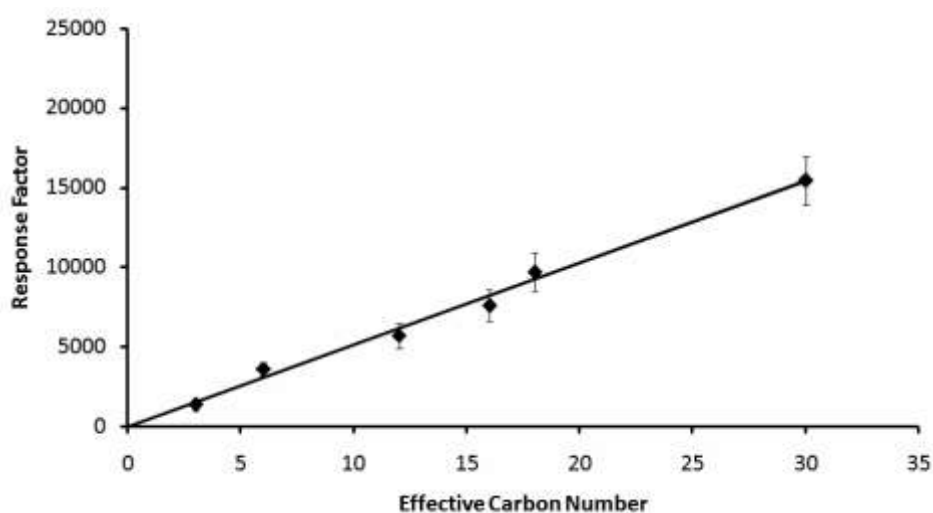


Figure A7: GC response factors plotted against effective carbon number of various compounds (this work).

Response factors of authentic compounds correlate to the number of combustible carbon atoms and carbon constants can be calculated, Table A2.

Table A2: Carbon constant calculated for standard compounds.

Compound	Response factor	Carbon number	Carbon constant
Squalane	15440	30	514
Octadecane	9702	18	539
Hexadecane	7612	16	475
Dodecane	5717	12	476
Hexane	3621	6	603
Acetone	1364	2	457
Average	-	-	≅510

Solvent suppression technique

To improve the accurate GC-EI analysis suppression technique was employed to minimise effect of large squalane peak and maximise small intermediates.

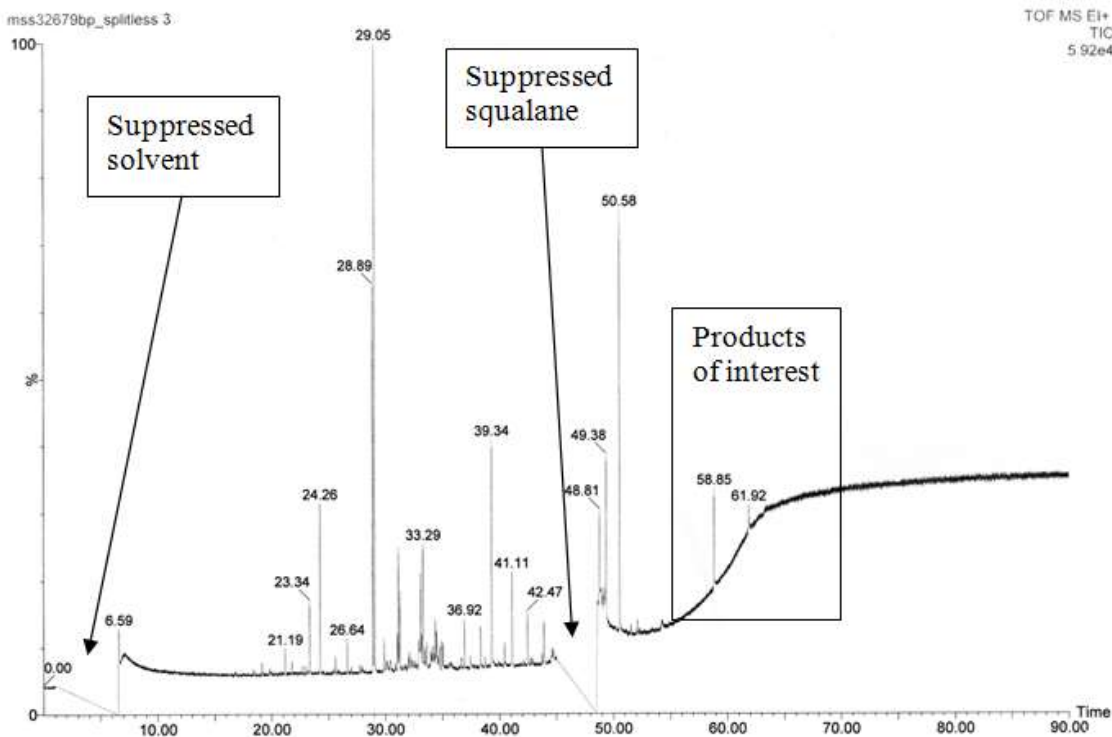


Figure A8: Example of chromatogram obtained by suppression solvent and squalane. (this work)

Peaks between approximately 10 to 50 minutes are squalane impurities. This GC trace was compared to fresh lubricant sample and there was no indication of any new products formed in the region between 10 to 50 minutes.

Table A3 gives some more details of GC-MS EI and FI analysis.

Table A3: Example of 6-methyl-2-heptanone EI and FI fragmentation. (this work)

Product	EI mass spectrum (m/z)	FI-MS m/z
6-methylhept-2-one	43 (90) 58 (100) 71 (18) 85 (12) 95 (21) 110 (24) 128 (6)	110 (15) [M-18], 128 (100) [M], 129 (12) [M+1]

Examples of 2D GC chromatograms

The additional information was obtained using comprehensive two-dimensional gas chromatography GC x GC equipped with flame ionization detector (FID) detector or nitrogen chemiluminescence detector (NCD). This analysis was useful in screening the used lubricant samples, which contain a mixture of different products which might have similar retention times in one dimension and could be hard to separate. The example of 2D chromatogram obtained using FID detector is shown in figure A9.

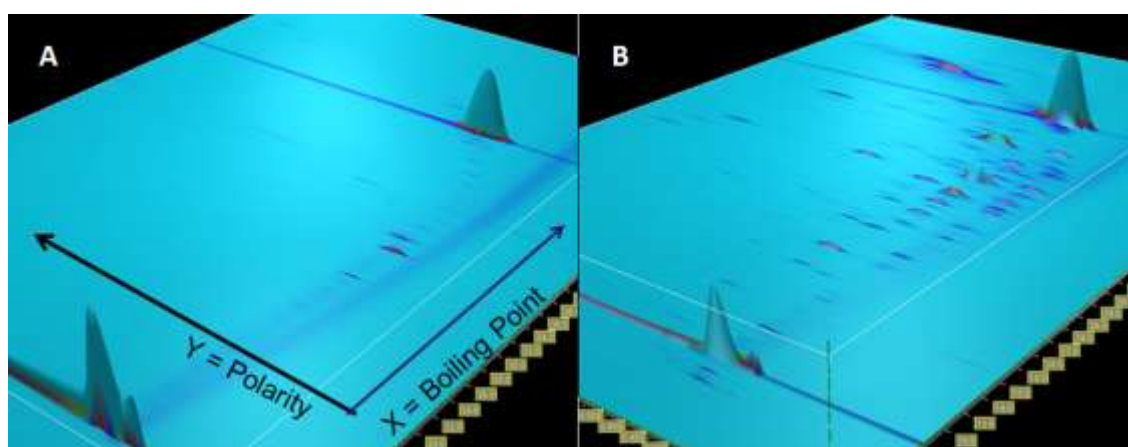


Figure A9: Example of 2D GC chromatogram obtained using FID detector: C – before reaction, D – after reaction. Reaction details: model lubricant (squalane), reactive gas NO_2 , at 180 °C (this work).

In the first dimension, non-polar column (X-axis), separation is essentially related to differing boiling points, where in the second dimension, polar column (Y-axis), separation is achieved based on differing polarity. Using FID detector different group of products can be separated such as: alkanes, ketones, aldehydes etc. The example of 2D chromatogram with nitrated products from the reaction of squalane with NO_2 identified using NCD detector is shown in figure A10.

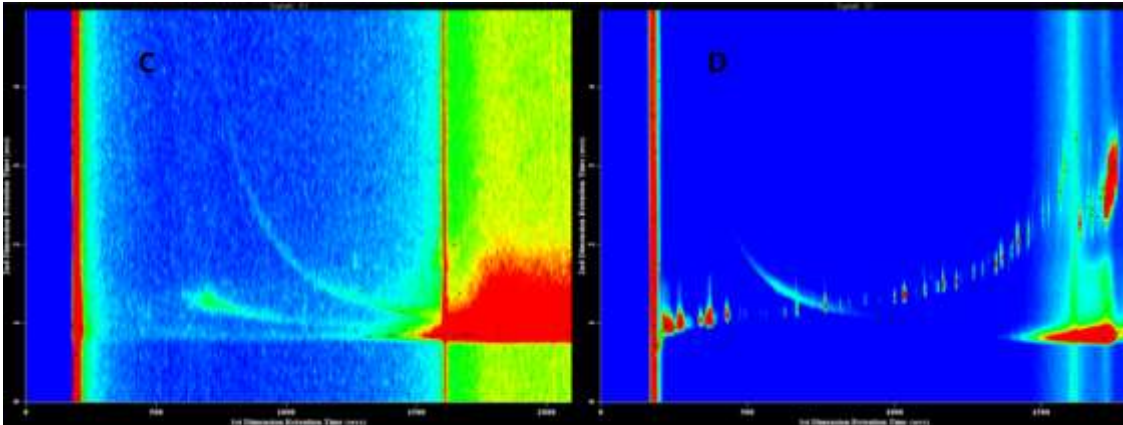


Figure A10: Example of 2D GC chromatograms obtained using NCD detector: A - before reaction, B - after reaction. Reaction details: model lubricant (squalane), reactive gas NO₂, at 180 °C. (this work)

Chromatogram (C) of the starting material, before reaction, shows only noise, where chromatogram (D) of the sample after reaction shows nitrated products. The NCD detector produced a liner response to nitrogen compounds of the same polarity, which allowed separation from other nitrated products.

Table A4: Examples of characteristic frequencies of carbonyl functional groups .¹²⁵

Group	Band (cm ⁻¹)	
Ketones		
C=O stretch	1725-1705	Saturated branching at α position
Aldehydes		
C=O stretch	1740-1720	Saturated
Acid anhydrides		
C=O stretch	1850-1800	Saturated
C=O stretch	1790-1740	Saturated
C-O stretch	1300-1050	All classes
Carboxylic Acids		
C=O stretch	1725-1700	Saturated
O-H stretch	3000-2500	All types
Esters and Lactones		
C=O stretch	1750-1735	Saturated
C-O stretch	1300-1050	All classes

Table A5: Examples of characteristic frequencies of nitro, nitroso, N-O functional groups.¹²⁵

Group	Band (cm⁻¹)
C-NO ₂	1570-1540 (s) 1390-1340(s)
Nitrates O-NO ₂ ,	1650-1600(s) 1270-1250(s)
Nitramines	1630-1550(s)
N-NO ₂ ,	1300-1250(2)
C-N=O	1600-1500(s)
O-N=O	1680-1610(s)
N-N=O	1500-1430(s)
N ⁺ -O ⁻	
Aromatic	1300-1200(s)
Aliphatic	970-950(s)
NO ₃ ⁻	1410-134 860-800

B. Appendix to chapter 3.

Model Hydrocarbons vs. Commercial Base Fluids

Previous work compared the tertiary carbon composition in different commercial base fluids, such as: Group I, II, III and PAO to model hydrocarbons, such as squalane and n-hexadecane.⁹

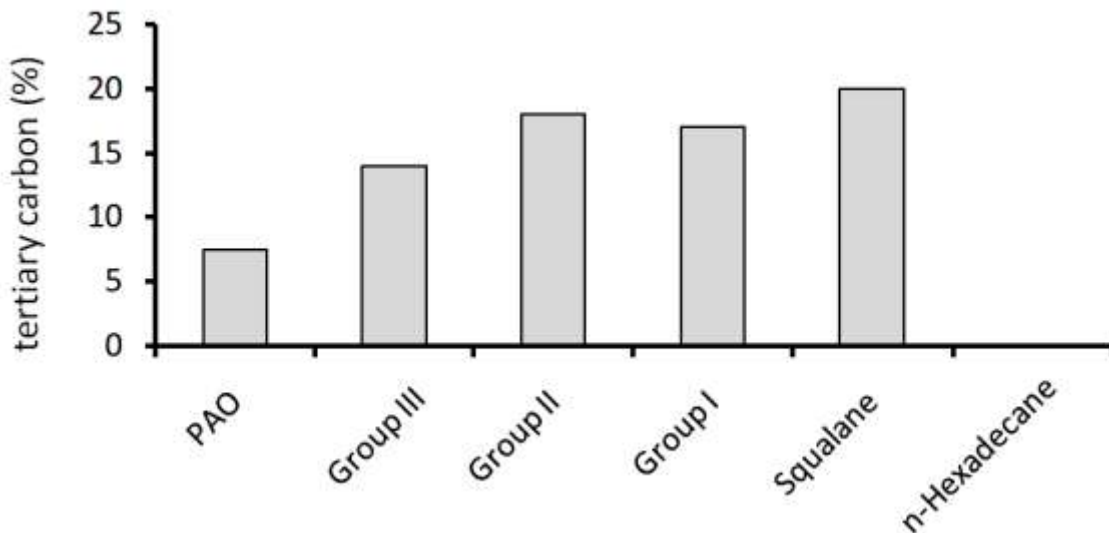


Figure B1: Comparison of tertiary carbon composition of the different commercial base fluids to squalane and n-hexadecane.⁹

Results shown that branched alkanes were more representative as a model lubricant as their tertiary carbon composition is similar to commercial base fluids, what is likely to influence its oxidation properties.

The GC-FID analysis (this work) of fresh, commercial, Group III base fluid (Yubase 4) was undertaken to compare with model hydrocarbon squalane. The analysis shown the range of different size of hydrocarbons for Yubase 4 (the top trace), where the bottom trace shown a single peak of squalane (99.0 % of purity). Squalane has also a similar boiling point as the commercial base fluid and therefore is a good model compound for study lubricant degradation.

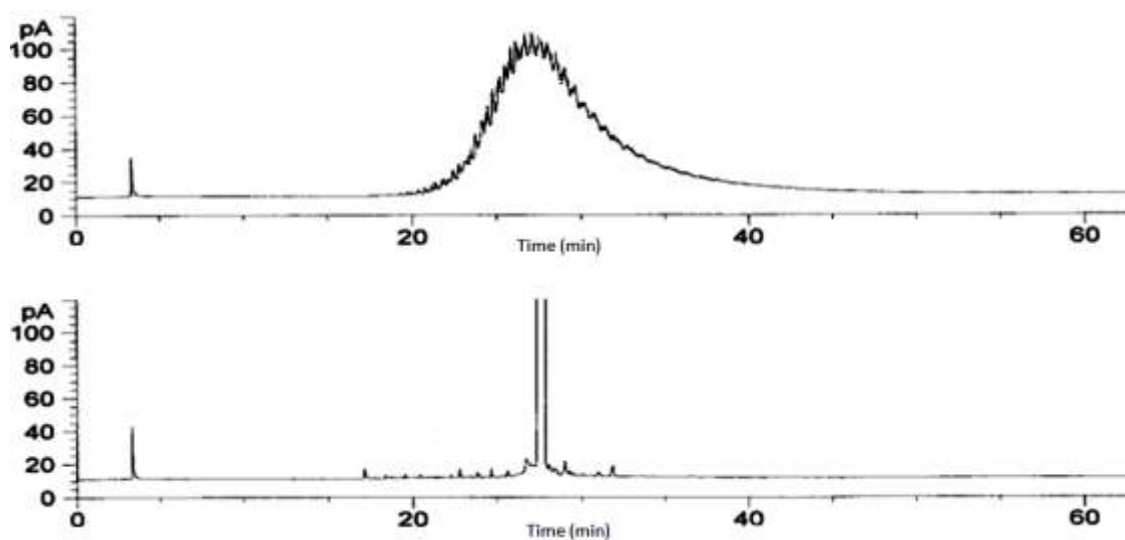


Figure B2: GC-FID traces of commercial base fluid, Yubase 4 (top trace) and model base fluid, Squalane 99% purity (bottom trace). (This work results)

Autoxidation of Pristane

Table B1: Products formed during the autoxidation of pristane, the pristoxyl or pristyl radicals from which they are formed by the reactions given.⁸

Peak no.	Product	pristoxyl or pristyl radical	Reactions
1	propanone	2-pristoxyl	6
2	2-methylpentane	6-pristoxyl	6,7
3	ethanoic acid	not known	not known
5	2-methylheptane	7-pristoxyl	6,7
6	2,6-dimethylheptane	8-pristoxyl	6,7
7	2,6-dimethyl-1-heptene	6-pristyl	13
8	3-methylbutanoic acid	5-pristoxyl	6,1,2,3,8,9,10
9	2,6-dimethyloctane	6-pristoxyl	6,7
10	6-methylheptan-2-one	6-pristoxyl	6
11	5,5-dimethyldihydrofuran-2-one	6-pristoxyl	6,12,11,2,3,4,8,13,4,14,15,12
12	2,6-dimethylnonane	6-pristoxyl	6,7
13	2,6-dimethylundecane	4-pristoxyl	6,7
14	4,8-dimethylnonan-1-ol	6-pristoxyl	6,1,2,3,4
15	2,6,10-trimethylundecane	4-pristoxyl	6,7
16	2,6,10-trimethylundec-1-ene	2-pristyl	13
17	4,8-dimethylnonanoic acid	6-pristoxyl	6,1,2,3,8,9,10
18	6,10-dimethylundecan-2-one	6-pristoxyl	6
19	5-methyl-5-(4-methylpentyl)dihydrofuran-2-one	6-pristoxyl	6,12,11,2,3,4,8,13,4,14,15,12
20	2,6,10-trimethyltridecane	2-pristoxyl	6,7
22	pristanone (e.g. 2,6,10,14-tetramethylpentadecan-3-one)	secondary	5
23	pristan-6-ol (2,6,10,14-tetramethylpentadecan-6-ol)	6-pristoxyl	5
24	pristan-2-ol (2,6,10,14-tetramethylpentadecan-2-ol)	2-pristoxyl	4
25	<i>sec</i> -pristanol (e.g. 2,6,10,14-tetramethylpentadecan-3-ol)	secondary	5

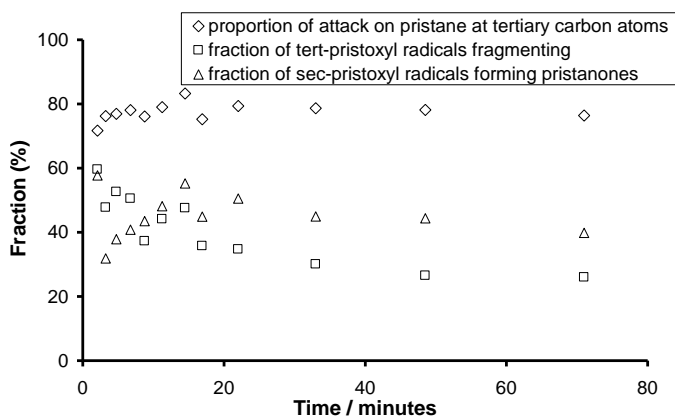


Figure B3: Proportion of radical attack at tert-carbons of pristane, and quantified reaction pathways for sec- and tert-pristoxyl radicals.^{8&17}

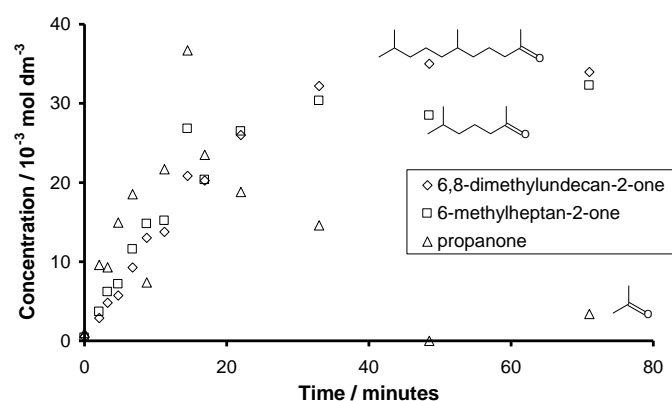


Figure B4: Fragment ketone products formed during the autoxidation of pristane at 170°C.^{8&17}

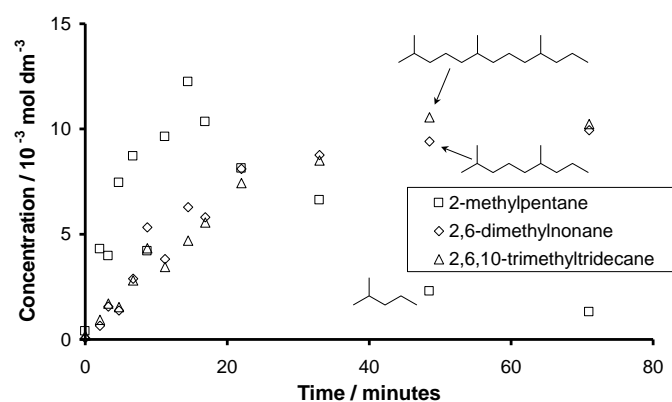


Figure B5. Fragment alkane products formed during the autoxidation of pristane at 170°C.^{8&17}

C. Appendix to chapter 4.

High Resolution GC-MS EI and FI

The high resolution GC-MS EI and FI spectra of phenolic antioxidant (OHPP) and its intermediate, which form by the reaction of antioxidant with nitrogen dioxide, shown in Figures C1 - C4.

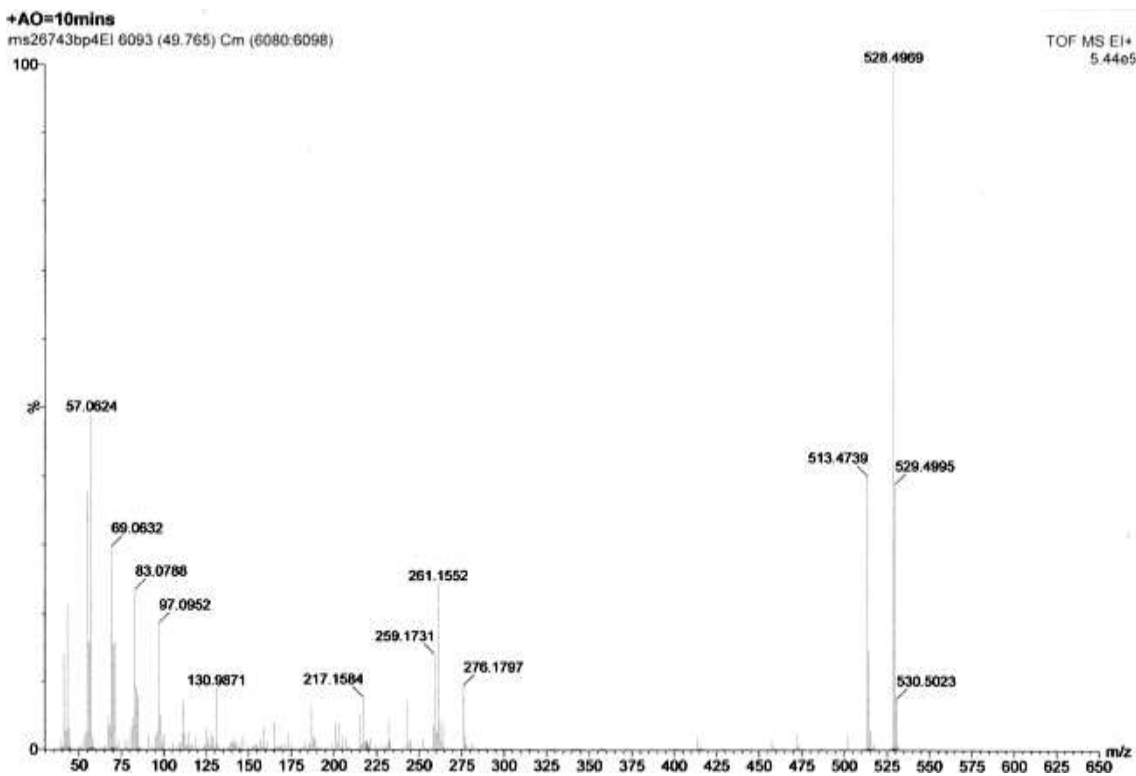


Figure C1: High Resolution GC-MS EI of OHPP Intermediate.

The GC-MS EI showed the characteristic fragmentation patterns for an intermediate from the antioxidant (Figure C1), which could be compared to an antioxidant in starting material (Figure C2).

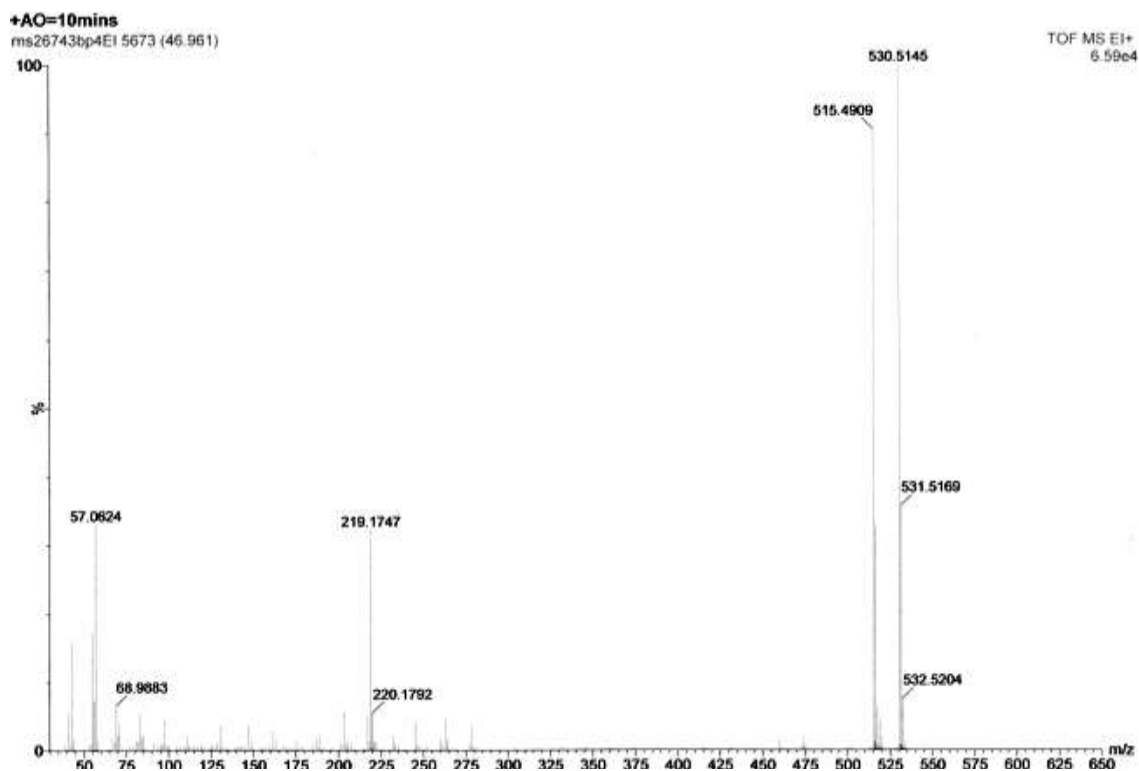


Figure C2: High Resolution GC-MS EI of OHPP.

The molecular mass of both (antioxidant and an intermediate) have been studied using GC-MS FI.

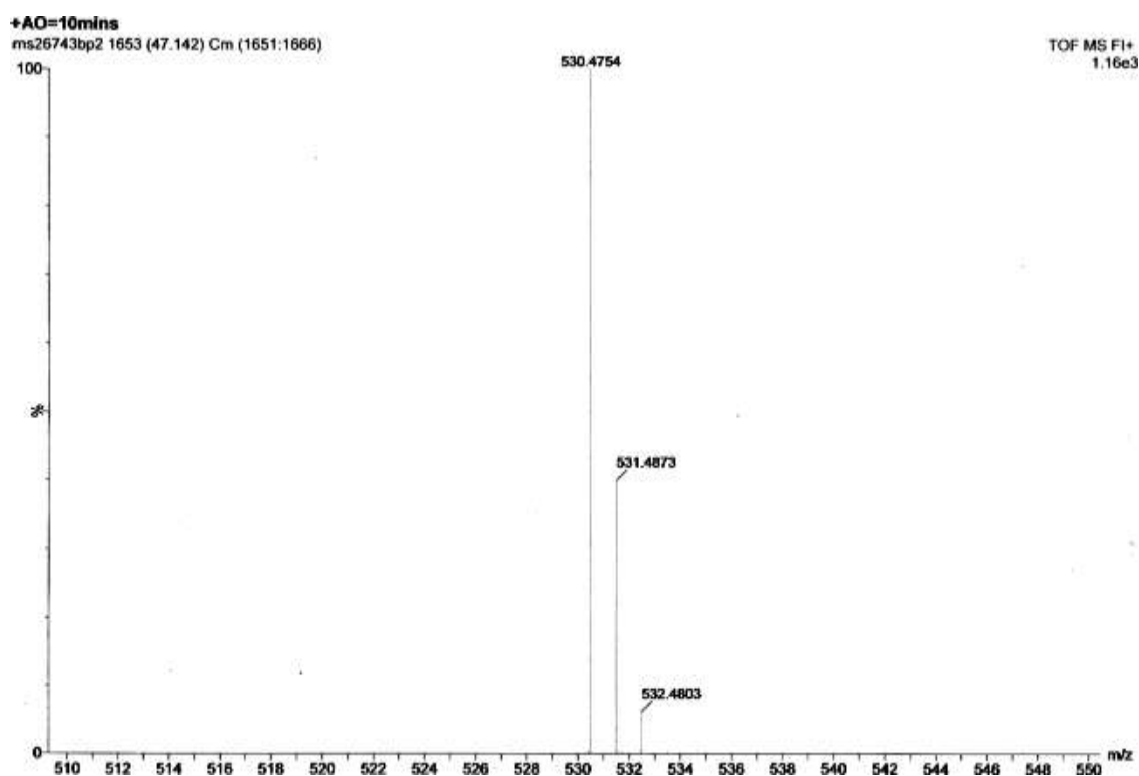


Figure C3: High Resolution GC-MS FI of OHPP.

The molecular mass ion m/z 530.475 ± 0.005 measured for antioxidant (Figure C3) and m/z 528.458 ± 0.003 for an intermediate (Figure C4), showed the difference of two Daltons between the antioxidant (OHPP) and its intermediate.

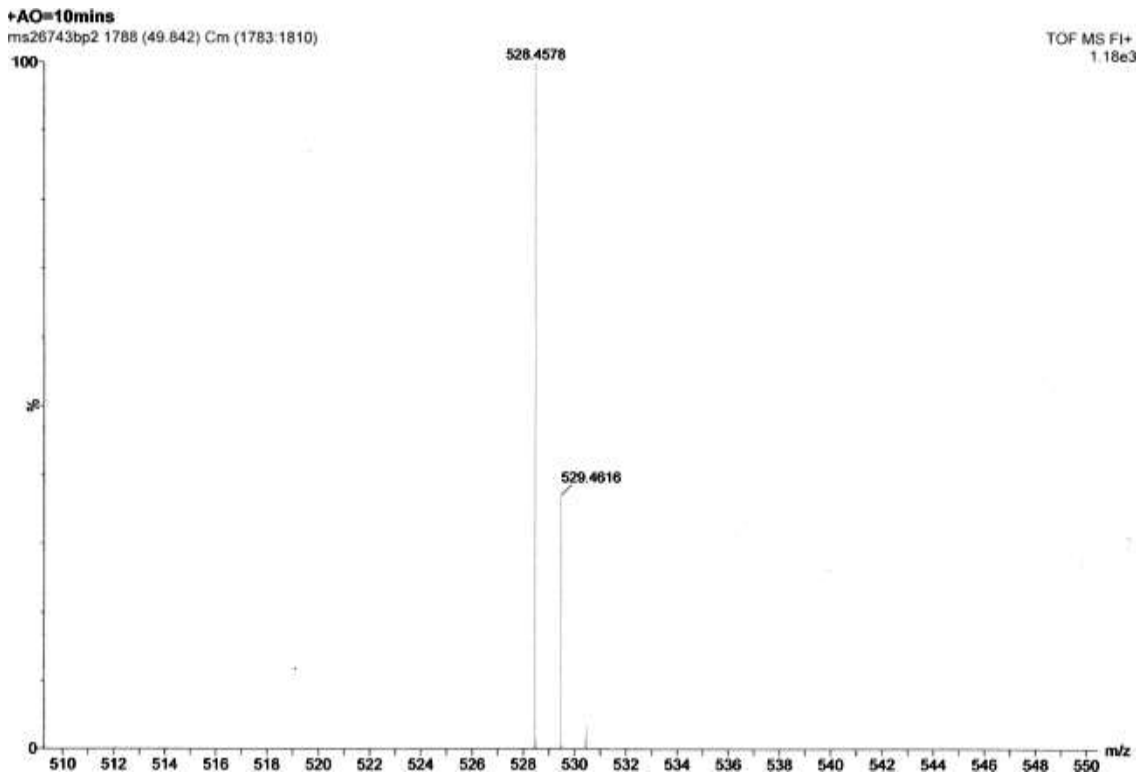


Figure C4: High Resolution GC-MS FI of OHPP Intermediate.

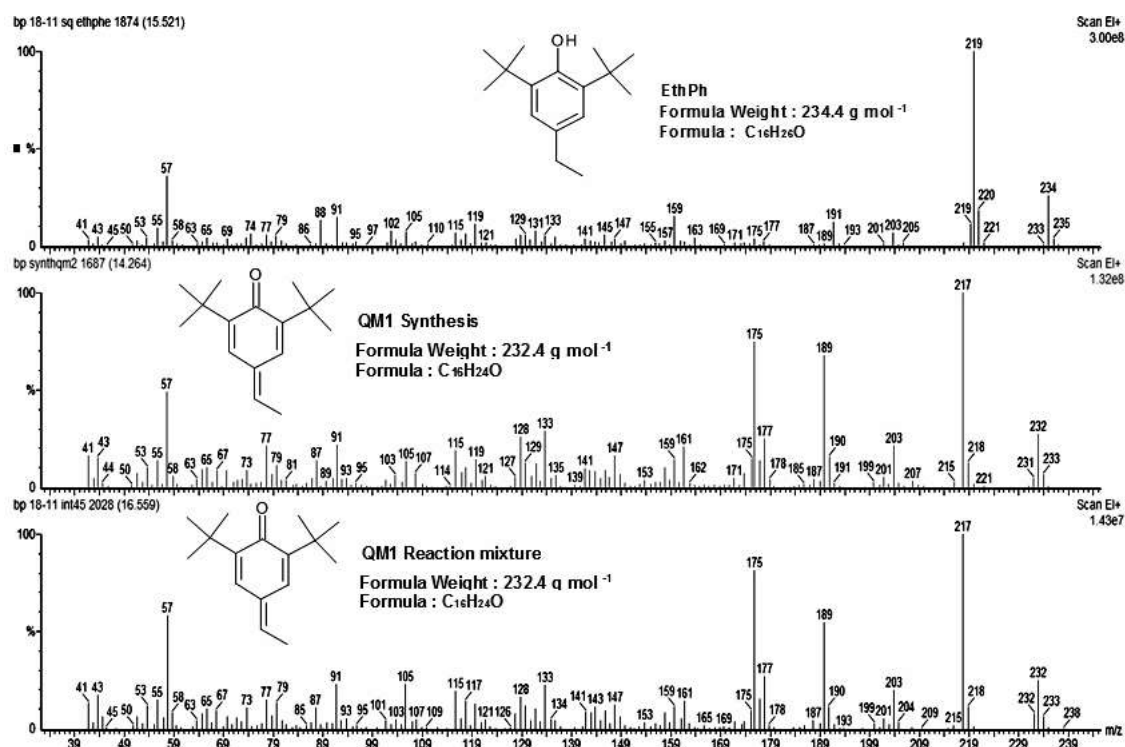


Figure C5: GC MS EI Perkin Elmer analysis of 2,6-di-tert-butyl-4-ethyl phenol (EthPh), syntheses 2,6-ditert-butyl-4-ethylidene-cyclohexa-2,5-dien-1-one (QM1) and QM1 product of reaction with NO_2 at 180°C .

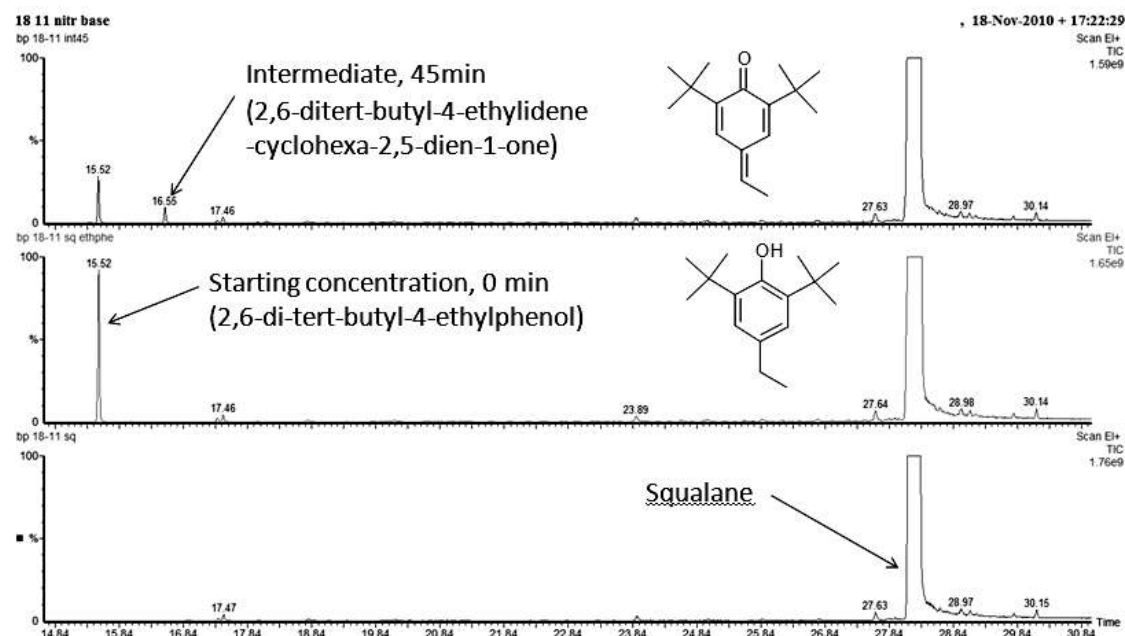


Figure C6: GC Chromatograms of squalane, squalane with EthPh and reaction mixture containing product of reaction EthPh with NO_2 , the 6-ditert-butyl-4-ethylidene-cyclohexa-2,5-dien-1-one (QM1).

Product Identification by GPC

Gel Permeation Chromatography (GPC), also known as Size Exclusion Chromatography was used with an eight channel UV-Vis detector to separate molecules depending on their size and absorption. The UV-Vis detector was set up to monitor 260, 280, 305, 310, 315, 320, 340 and 360 nm absorptions characteristic for antioxidant and products,^{11,12} analysed previously by UV-Vis.

The analysis of starting material showed a peak at approximately 8.4 min. with a maximum absorption at 280 nm, characteristic for phenolic antioxidant (OHPP),¹¹

Figure C7.

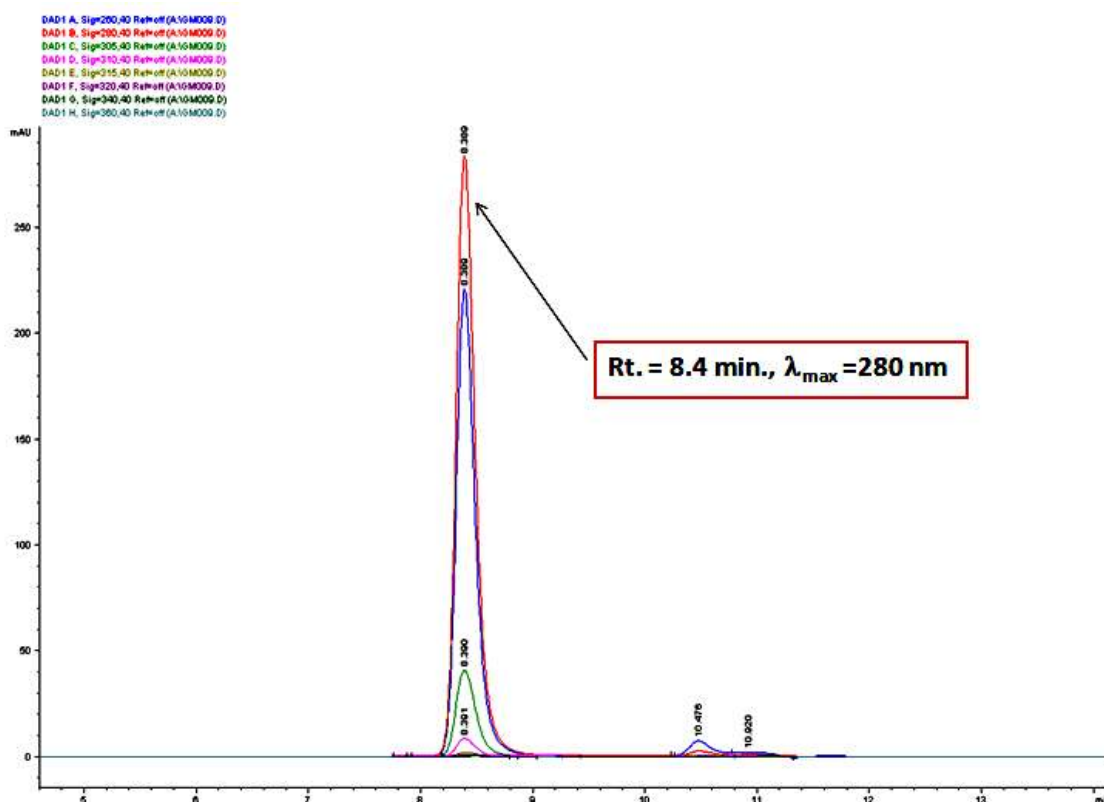


Figure C7: GPC chromatogram sample 0 min. (in THF), 0.5 % w/w OHPP in squalane.

The 10 minutes sample of reaction mixture showed peaks of an antioxidant at 8.4 min. and an intermediate at approximately 8.5 min. with maximum absorption of 305 nm,

consistent with formation of quinone methide, analysed previously by UV-Vis, Figure C8, and that this quinone methide is of similar size to the starting antioxidant, and is not, for example, a dimer.

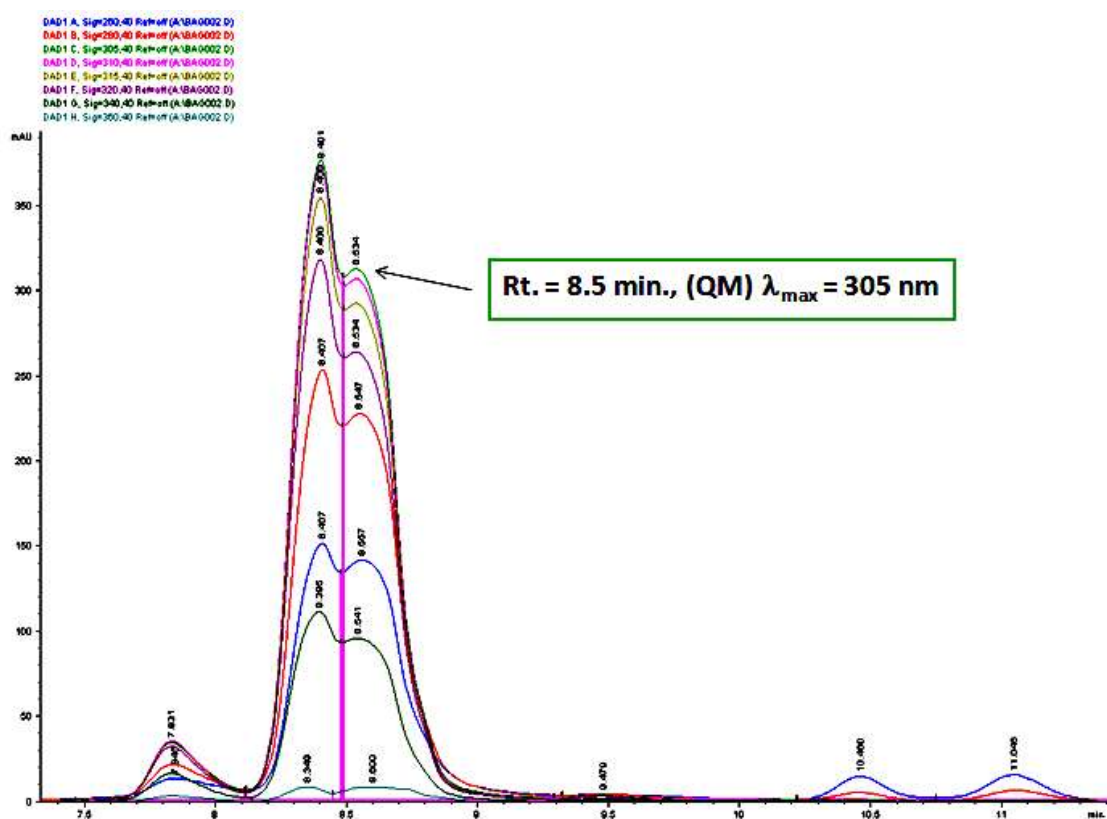


Figure C8: GPC chromatogram 10min (in THF), reaction mixture with max. absorption of 305 nm characteristic for QM.

The 45 minutes sample, according to GC quantified analysis contained $\frac{1}{4}$ of antioxidant and similar concentration of intermediate, there are still peaks at 8.4 and 8.5 min. but the maximum absorption is shifted to 310 nm, which might be related to formation of hydroxy cinnamate (Figure C9).

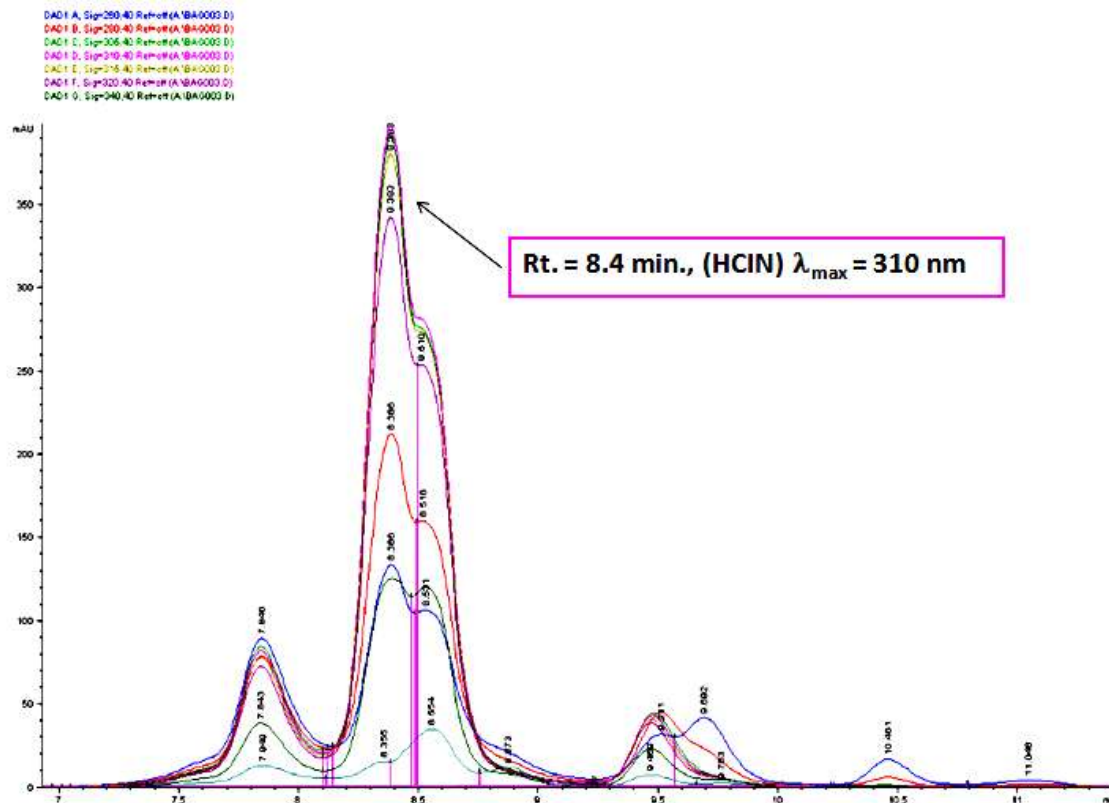


Figure C9: GPC chromatogram 45min, reaction mixture with max absorption of 310 nm characteristic for HCIN.

UV-Vis analysis of synthesised HCIN shown absorption of 314 nm and not 310 nm, therefore the synthesised hydroxy cinnamate was analysed by GPC to compare it with reaction mixtures, Figure C10.

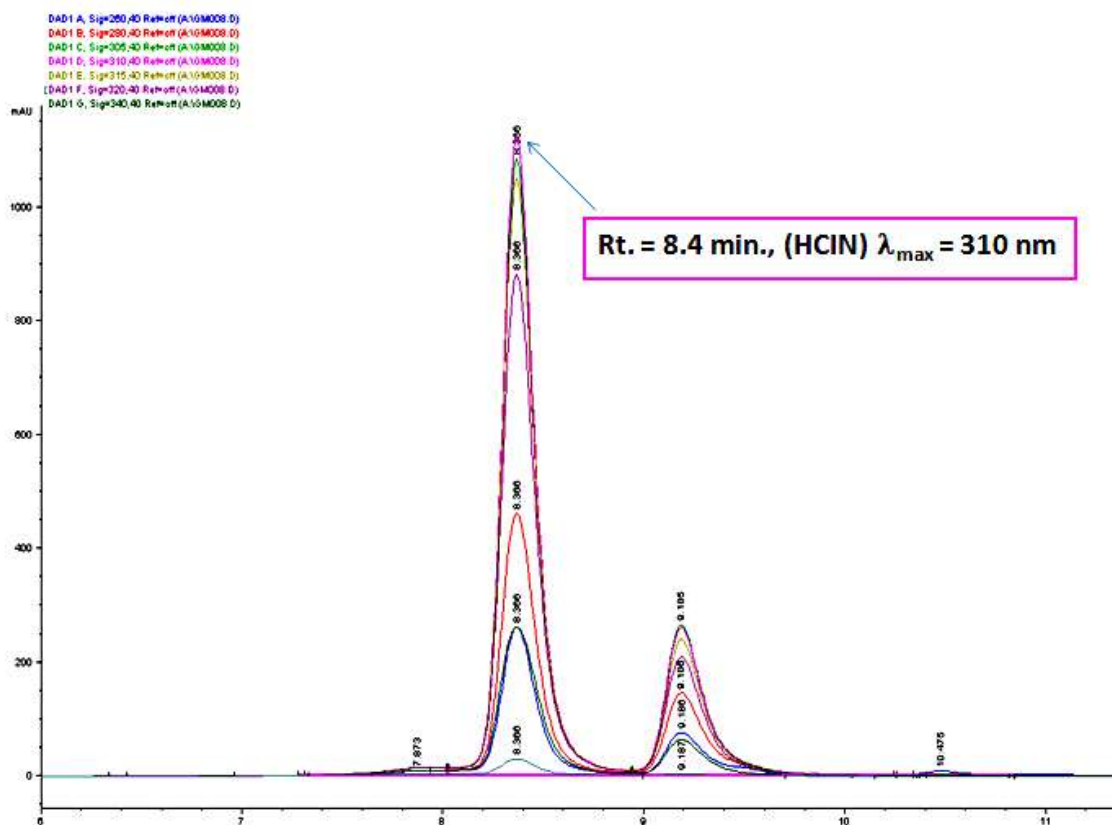


Figure C10: GPC chromatogram of synthesised HCIN with max absorption of 310 nm.

The GPC chromatogram of synthesised hydroxy cinnamate shows the retention time for HCIN of approximately 8.4 min., which was the same as for antioxidant, but its absorption was 310 nm, as observed in analysed 45 min. reaction mixture (figure C9), that suggests that the HCIN will be one of the reaction products, which will dominate in later stage of reaction. The difference in elution time between QM (8.5 min.) and HCIN (8.4 min.), even both have the same molecular masses, could be explain by the difference in polarity.¹⁷⁻¹⁸

GPC was not very good in separating the products of reaction mixture, because their molecular masses were very similar. Also the HCIN cannot be excluded as a product of 10 min. sample as its absorption is weaker than in quinone methide.

During analysis by GPC, negligible concentrations of other intermediates were detected, those products have not been confirmed by GC analysis. It might be that their concentration was too small to be identified or these are interaction products with the moderately polar solvent (THF).¹⁷

Product Identification by NMR

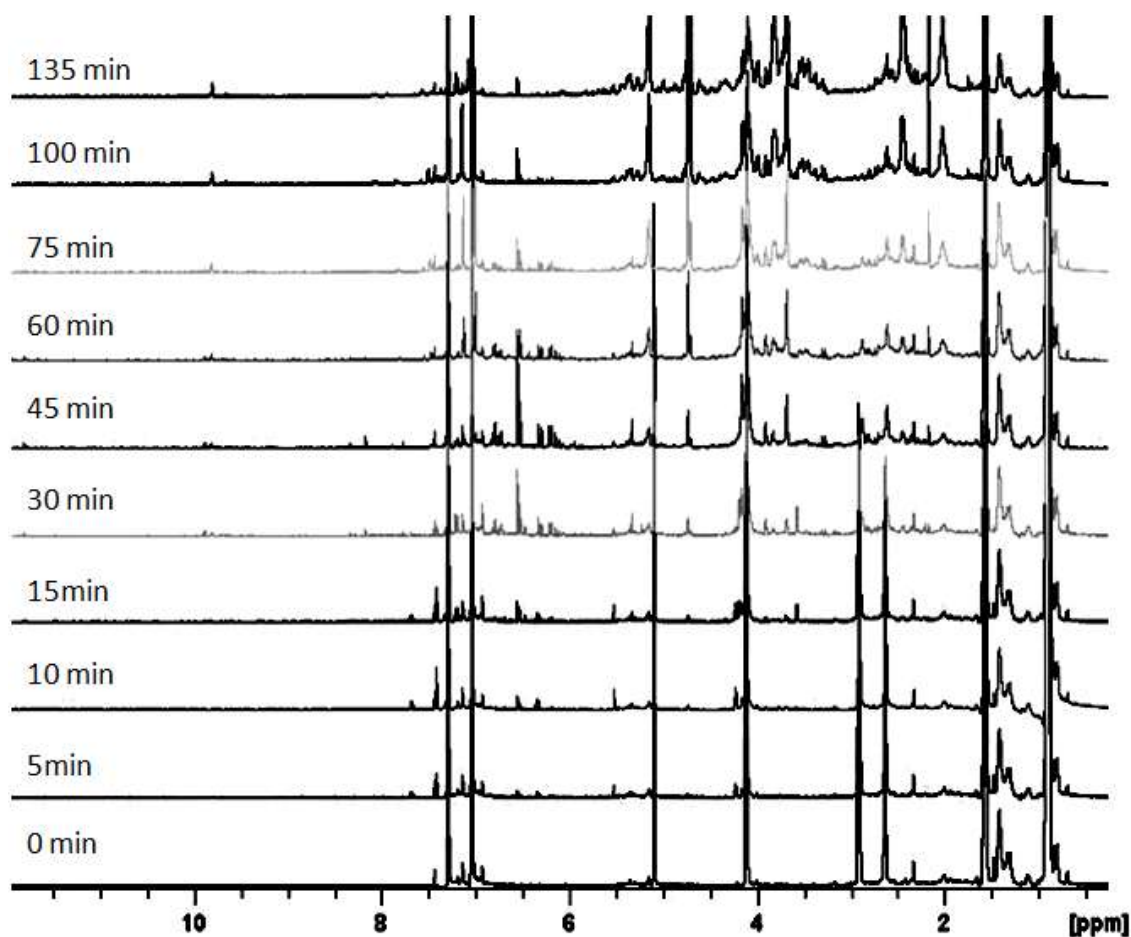


Figure C11. High resolution 700 MHz 1D proton NMR spectra of reaction mixture 0 to 135 min. (in CDCl_3), full range. Reaction of OHPP in squalane with NO_2 at 180°C .

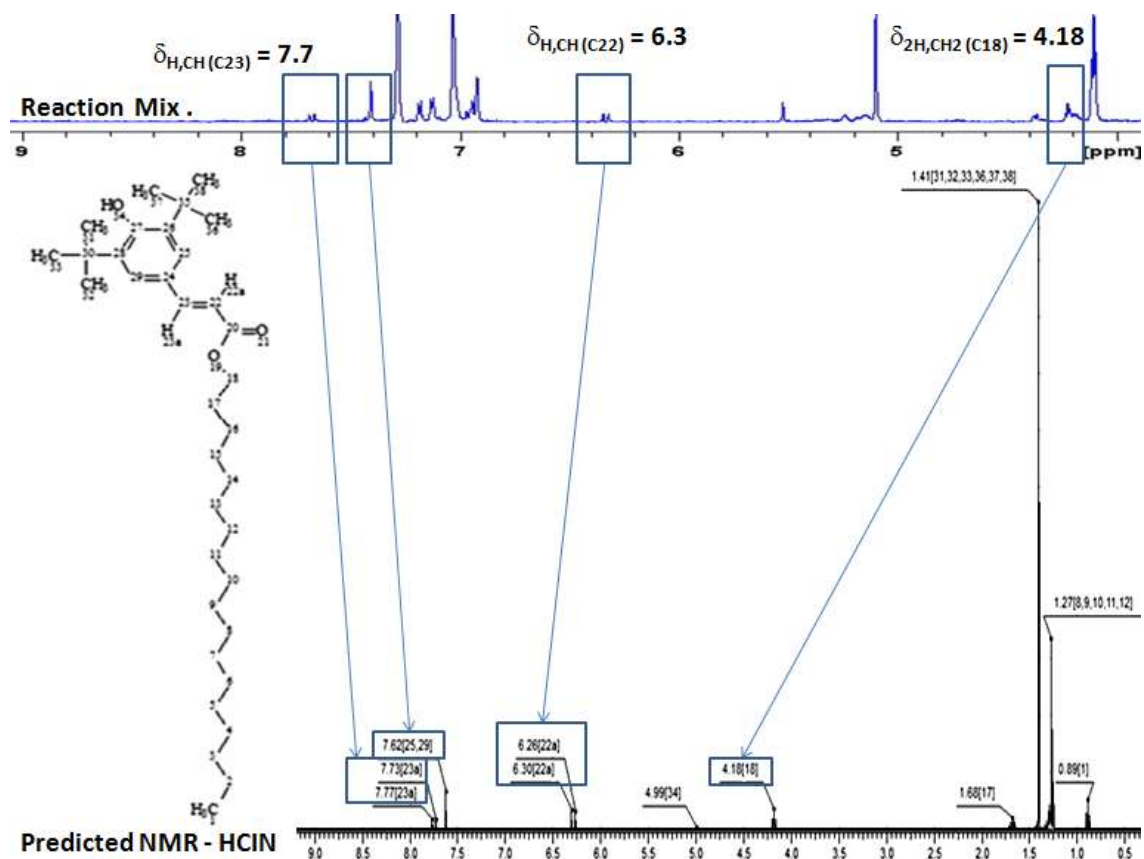


Figure C12: Comparison of 5 min. reaction mixture with predicted proton NMR of HCIN.

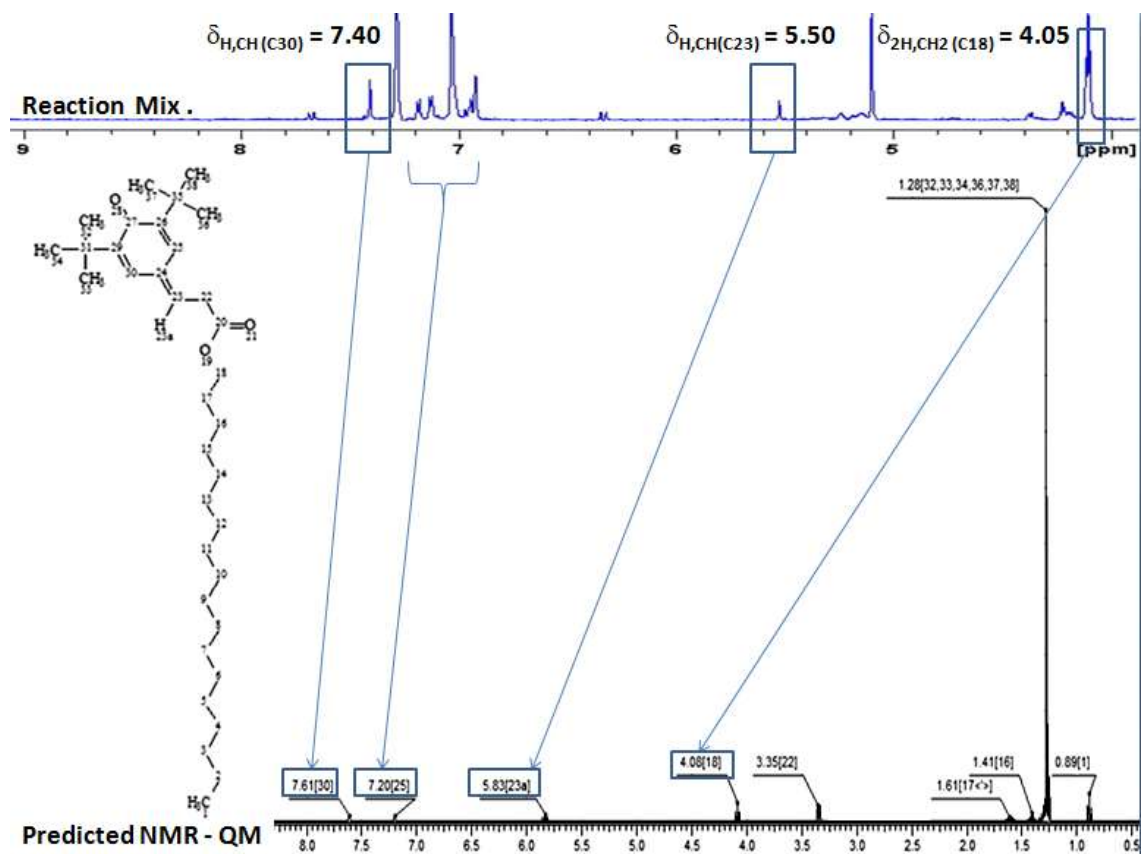


Figure C13: Comparison of 5 min. reaction mixture with predicted proton NMR of QM.

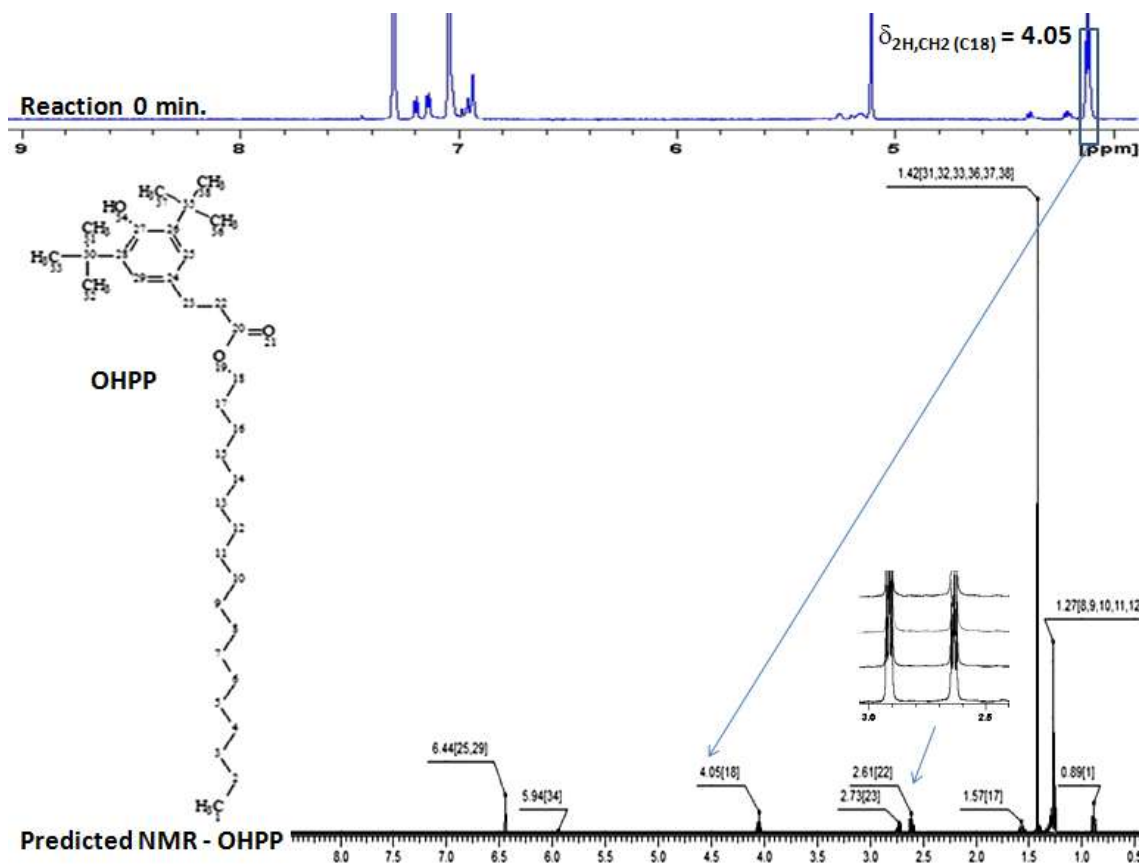


Figure C14: Comparison of 0 min. reaction mixture with predicted H^1 NMR of OHPP.

Analysis of nitrated sample of squalane by GC x GC with nitrogen detector suggest formation of similar polarity products, possibly formed by addition of NO_2 group to the tertiary alkyl radicals.

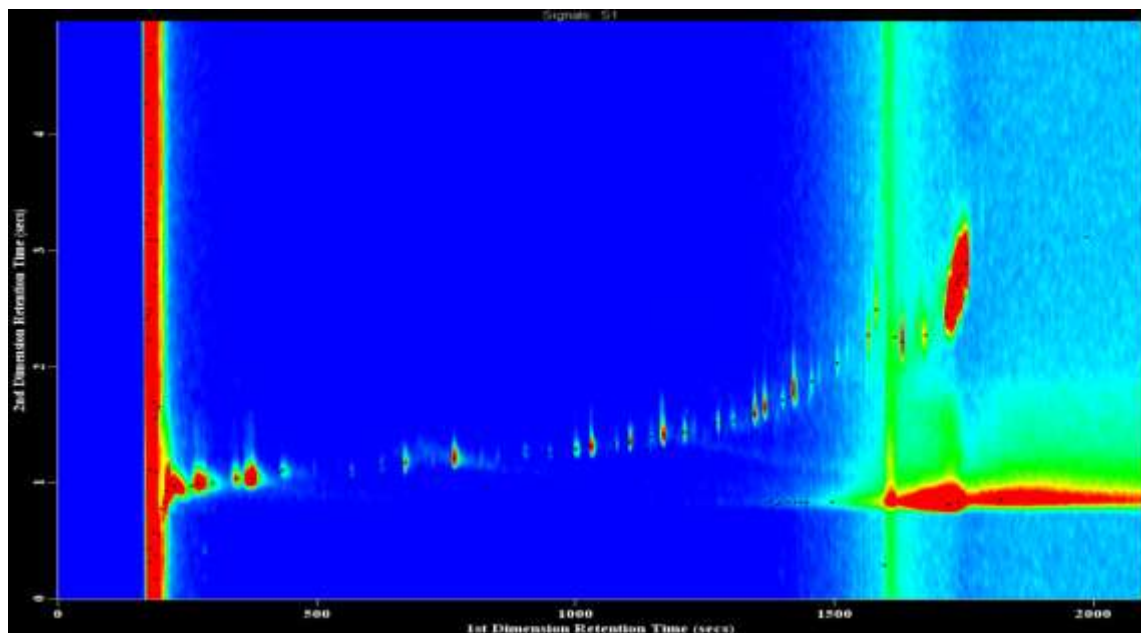


Figure C15. 2D GCxGC NCD chromatogram of nitrated squalane.

D. Appendix to chapter 5.

Table D1: Computed bond dissociation energies at 298K with various DFT methods at 6-31G (d,p) basis set. The value in the parenthesis is the deviation from computed BDE for experimental one.[Ref.¹⁵⁷]

Molecule	B3LYP [kcal mol ⁻¹]	B3W91 [kcal mol ⁻¹]	B3P86 [kcal mol ⁻¹]	Exp. [kcal mol ⁻¹][kJ mol ⁻¹]	
C ₆ H ₅ -NO ₂	69.02 (1.68)	69.47 (1.23)	72.90 (-2.2)	70.7±1	295.8
3-NH ₂ -C ₆ H ₄ -NO ₂	69.53 (0.97)	70.00 (0.5)	73.44 (-2.94)	70.5	295.0
4-NH ₂ -C ₆ H ₄ -NO ₂	73.38 (-1.18)	73.98 (-1.78)	77.47 (-5.27)	72.2	302.1
3-NO ₂ -C ₆ H ₄ -NO ₂	66.30 (0.2)	66.80 (-0.3)	70.19 (-3.69)	66.5	278.2
4-NO ₂ -C ₆ H ₄ -NO ₂	66.09 (0.91)	66.58 (0.42)	69.97 (-2.97)	67.0	280.3
2-CH ₃ -C ₆ H ₄ -NO ₂	66.32 (3.88)	69.60 (0.6)	73.05 (-2.63)	70.2±2.5	293.7
4-CH ₃ -C ₆ H ₄ -NO ₂	70.10 (1.3)	70.59 (0.81)	74.03 (-2.63)	71.4±2.3	298.7
3,5-(NO ₂) ₂ -C ₆ H ₄ -NO ₂	64.05 (1.95)	64.58 (1.42)	67.93 (-1.93)	66.00	276.3
Mean absolute Deviation	1.51	0.88	3.06	-	-

Table D2: Computed bond dissociation energies at 298K with various DFT methods at 6-31+G (d,p) basis set. The value in the parenthesis is the deviation from computed BDE for experimental one. [Ref.¹⁵⁸]

Molecule	B3LYP [kcal mol ⁻¹]	B3W91 [kcal mol ⁻¹]	B3P86 [kcal mol ⁻¹]	Exp. [kcal mol ⁻¹]
C ₆ H ₅ -NO ₂	67.19 (3.51)	68.12 (2.58)	71.60 (-0.9)	70.7±1
3-NH ₂ -C ₆ H ₄ -NO ₂	67.60 (2.90)	68.58 (1.92)	72.06 (-1.56)	70.5
4-NH ₂ -C ₆ H ₄ -NO ₂	71.77 (0.43)	72.76 (0.56)	76.30 (-4.10)	72.2
3-NO ₂ -C ₆ H ₄ -NO ₂	64.37 (2.13)	65.38 (1.12)	68.82 (-1.48)	66.5
4-NO ₂ -C ₆ H ₄ -NO ₂	64.09 (2.91)	65.05 (1.95)	68.48 (-1.48)	67.0
2-CH ₃ -C ₆ H ₄ -NO ₂	64.25 (5.95)	65.16 (5.04)	68.92 (1.28)	70.2±2.5
4-CH ₃ -C ₆ H ₄ -NO ₂	68.42 (2.98)	69.39 (2.01)	72.88 (-1.48)	71.4±2.3
3,5-(NO ₂) ₂ -C ₆ H ₄ -NO ₂	62.00 (4.00)	63.15 (2.85)	66.54 (-0.54)	66.0
Mean absolute Deviation	3.10	2.25	1.70	-

Table D3: Computed bond dissociation energies at 298K with various DFT methods at 6-311G (d,p) basis set. The value in the parenthesis is the deviation from computed BDE for experimental one. [Ref.¹⁵⁸]

Molecule	B3LYP [kcal mol ⁻¹]	B3W91 [kcal mol ⁻¹]	B3P86 [kcal mol ⁻¹]	Exp. [kcal mol ⁻¹]
C ₆ H ₅ -NO ₂	66.30 (4.40)	67.29 (3.41)	70.66 (0.04)	70.7±1
3-NH ₂ -C ₆ H ₄ -NO ₂	66.84 (3.66)	67.85 (2.65)	71.22 (-0.72)	70.5
4-NH ₂ -C ₆ H ₄ -NO ₂	70.67 (1.53)	71.76 (0.44)	75.18 (-2.98)	72.2
3-NO ₂ -C ₆ H ₄ -NO ₂	64.10 (2.4)	61.73 (4.77)	68.25 (-1.75)	66.5
4-NO ₂ -C ₆ H ₄ -NO ₂	63.74 (3.26)	64.74 (2.26)	68.07 (-1.07)	67.0
2-CH ₃ -C ₆ H ₄ -NO ₂	63.51 (6.69)	64.44 (5.76)	68.08 (2.12)	70.2±2.5
4-CH ₃ -C ₆ H ₄ -NO ₂	67.45 (3.95)	68.47 (2.93)	71.84 (-0.44)	71.4±2.3
3,5-(NO ₂) ₂ -C ₆ H ₄ -NO ₂	61.83 (4.17)	62.84 (3.16)	66.15 (-0.15)	66.0
Mean absolute Deviation	3.76	3.17	1.16	-

Table D4: Computed bond dissociation energies for H₂O, CH₃OH and Ph-OH at 298K using B3LYP and (RO)B3LYP methods with 6-311G(d,p) and 6-311++G(2df,2p) basis sets. [Ref.¹⁶⁰]

Molecule	B3LYP [kcal mol ⁻¹]		(RO)B3LYP [kcal mol ⁻¹]		Exp. [kcal mol ⁻¹]
	6-311G (d,p)	6-311++G (2df,2p)	6-311G (d,p)	6-311++G (2df,2p)	
H ₂ O	114.2	117.0	115.1	118.2	117.6 ± 0.1
CH ₃ OH	99.7	101.2	100.8	102.6	104 ± 0.9
Ph-OH	84.1	-	86.4	87.5	87.3 ± 1.5

Table D5: Total energies (a.u.) and energy of dissociation (kcal mol⁻¹) for HOH→OH +H calculated by using B3LYP Hybrid DFT method and different basis sets. [Ref.¹⁶¹]

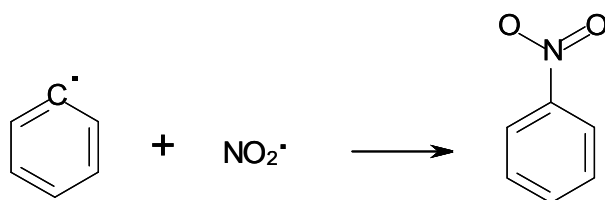
Basis set	E _{HOH} [a.u.]	E _{OH} [a.u.]	E _H [a.u.]	ΔE [kcal mol ⁻¹]
6-31G(d)	-76.4089486	-75.7234612	-0.5002728	116.2
6-31+G(d)	-76.4225695	-75.7334956	-0.5002728	118.5
6-311G(d,p)	-76.4474453	-75.7545244	-0.5021559	119.7
6-311+G(2d,2p)	-76.4619823	-75.7642379	-0.5021559	122.7
6-311++G(3dpf,3pd)	-76.4645106	-75.7662300	-0.522569	123.0
Exp.				119±1

Table D6: Total energies (a.u.) and energy of dissociation (kcal mol⁻¹) for HOH→OH +H calculated by using 6-31+G(d) basis set and different methods. [Ref.¹⁶¹]

Methods	E _{HOH} [a.u.]	E _{OH} [a.u.]	E _H [a.u.]	ΔE [kcal mol ⁻¹]
SVWN	-76.0552961	-75.3391352	-0.4939369	139.4
B3LYP	-76.4225695	-75.7334956	-0.5002728	118.5
B3P86	-76.5990405	-75.8873638	-0.5168186	122.3
BLYP	-76.4051031	-75.7199799	-0.4954462	119.0
MP2	-76.4229082	-75.7290161	-4981050	122.9
Exp.				119±1

The example of calculating the enthalpy, Gibbs energy and entropy from the thermochemical values computed using Gaussian [This work]

Formation of nitrobenzene (Figure D1.) was used as a model reaction for calculations of enthalpy, Gibbs energy and entropy from Gaussian thermochemical output values,¹⁶⁶ computed using the DFT BPV86/6-311G (d,p) method (standard conditions of 1 bar and 298.15K).¹⁶² Reaction D1 below:



The optimised geometry of nitrobenzene is shown in Figure D1.

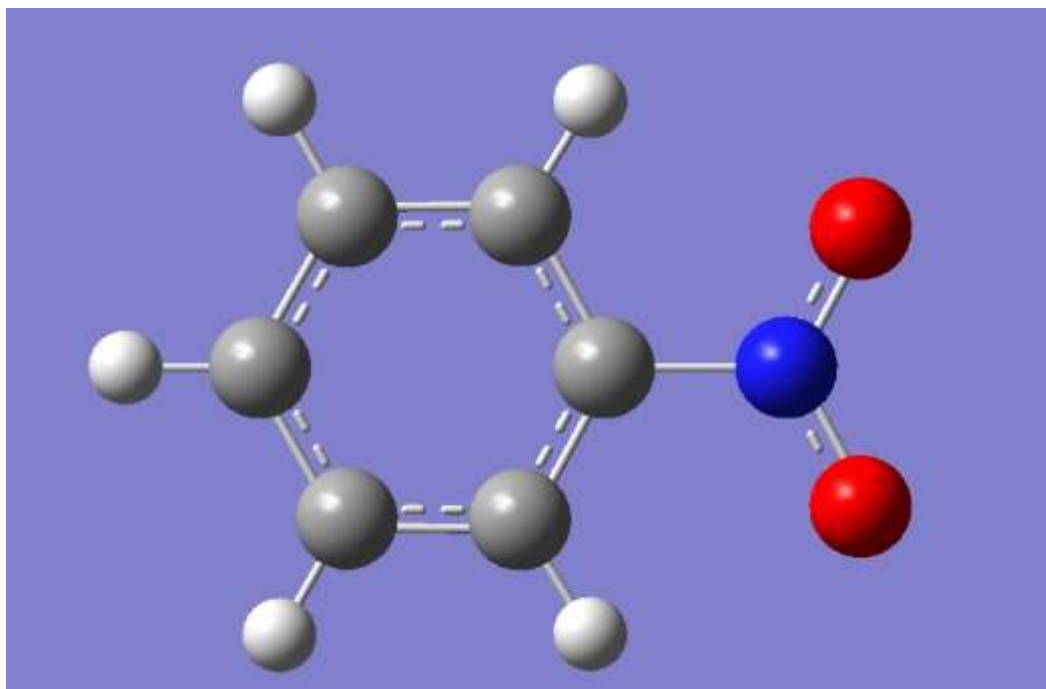


Figure D1: Optimised geometry of nitrobenzene C₆H₅NO₂ using BPV86/6-311G (d,p) method (Output File).

Various thermochemical information were calculated for each of the reactants and product using the BPV86/6-311G (d,p) method, such as:

ϵ_0 - Total electronic energy

ϵ_{ZPF} - Zero-point correction

E_{tot} - Thermal correction to energy

H_{corr} - Thermal correction to enthalpy

G_{corr} - Thermal correction to Gibbs free energy

$\epsilon_0 + \epsilon_{ZPE}$ - Sum of electronic and zero-point energies

$\epsilon_0 + E_{tot}$ - Sum of electronic and thermal energies

$\epsilon_0 + H_{corr}$ - Sum of electronic and thermal enthalpies

$\epsilon_0 + G_{corr}$ - Sum of electronic and thermal free energies

S_{tot} - Total entropy – which is represented by sum of ($S_t + S_r + S_v + S_e$), where S_t – entropy due to translation, S_r – entropy due to rotational motion, S_v – entropy due to vibrational motion, S_e – entropy due to electronic motion

The Gaussian thermochemistry output results for product and reactants are shown in Appendix D, Table D7.

Table D7: Thermochemical values from Gaussian, calculated for reactants and product for nitrobenzene formation using BPV86/6-311G (d,p) method, units Hartees. [This work]

	$C_6H_5-NO_2$	$C_6H_5^\cdot$	NO_2
ϵ_0	-436.906696	-231.624526	-205.170364
ϵ_{ZPF}	0.099706	0.084586	0.008452
E_{tot}	0.10673	0.089105	0.011395
H_{corr}	0.107674	0.090049	0.012339
G_{corr}	0.067591	0.056467	-0.014949
$\epsilon_0 + \epsilon_{ZPE}$	-436.80699	-231.53994	-205.161912
$\epsilon_0 + E_{tot}$	-436.799967	-231.53542	-205.158969
$\epsilon_0 + H_{corr}$	-436.799022	-231.53448	-205.158025
$\epsilon_0 + G_{corr}$	-436.839105	-231.56806	-205.185314
S_{tot}	0.13444017	0.112636391	0.091527426

Using the raw data from Table D7, the enthalpy, Gibbs energy and entropy of reaction were calculated below and results converted from Hartree to kcal mol⁻¹ and kJ mol⁻¹,¹⁵⁷ useful unit conversion factors are shown in Table D8.

Table D8: Conversion factors.

1 Hartree	627.5059 kcal mol ⁻¹
1 kcal mol ⁻¹	4.1868 kJ mol ⁻¹
1 kJ mol ⁻¹	0.239005736 kcal mol ⁻¹

To calculate enthalpy of reaction appropriate sums and differences of heats of formation are taken:

$$\Delta_r H^\circ(298K) = \sum \Delta_f H^\circ_{prod}(298K) - \sum \Delta_f H^\circ_{react}(298K) \quad \text{Equation D.1}$$

Using Gaussian sum of electronic and thermal enthalpies calculating difference for the products and reactants:

$$\Delta_r H^\circ(298K) = \sum (\epsilon_0 + H_{corr})_{prod} - \sum (\epsilon_0 + H_{corr})_{react} \quad \text{Equation D.2}$$

$$\begin{aligned} \Delta_r H^\circ(298K) = & -66.842312 \quad \text{kcal mol}^{-1} \\ & -279.855392 \quad \text{kJ mol}^{-1} \end{aligned}$$

The predicted $\Delta_r H^\circ$ value for formation of nitrobenzene was approximately -279.9 ± 3.4 kJ mol⁻¹, the mean absolute deviation was calculated for BPV86/6-311(d,p) in method development section.

The next calculated value was Gibbs energy:

$$\Delta_r G^\ominus(298K) = \sum(\epsilon_0 + G_{corr})_{prod} - \sum(\epsilon_0 + G_{corr})_{react} \quad \text{Equation D.3}$$

$$\begin{aligned} \Delta_r G^\ominus(298K) = & -53.797017 \quad kcal \, mol^{-1} \\ & -225.237351 \quad kJ \, mol^{-1} \end{aligned}$$

The Gibbs energy value for the formation of nitrobenzene was negative, $-53.8 \pm 3.4 \text{ kJ mol}^{-1}$, that suggested that this reaction proceeds spontaneously at 1 bar and 298 K.

The standard entropy change for a reaction at 298K and 1bar ($\Delta_r S^\ominus$) is defined as a difference between standard entropies of the reactants and products:

$$\Delta_r S^\ominus(298K) = \sum S^\ominus_{prod}(298K) - \sum S^\ominus_{react}(298K) \quad \text{Equation D.4}$$

The standard entropy change ($\Delta_r S^\ominus$) for the formation of nitrobenzene was calculated using Gaussian's values of Total entropies (S_{tot}) for product and reactants, which are the sums of the individual components of the third law entropy of a mole of identical molecules at 298K and 1 bar pressure. The Total entropy is represented by a sum of entropy due to translation, entropy due to rotational motion, entropy due to vibrational motion and entropy due to electronic motion.

$$\begin{aligned} \Delta_r S^\ominus(298K) = & -44.295 \quad cal \, mol^{-1} K^{-1} \\ & -185.454 \quad J \, mol^{-1} K^{-1} \end{aligned}$$

Based on calculated thermochemical values of $\Delta_r H^\ominus$, $\Delta_r G^\ominus$ and $\Delta_r S^\ominus$ the reaction kinetics could be explain and the dependence of formation of particular products.

Table D9: Thermochemical values form Gaussian calculated for reactants and product of BHT–NO₂ formation, using BPV86/6-311G (d,p) method, units Hartees. [This work]

	BHT-NO ₂	BHT [*]	NO ₂
ϵ_0	-866.043787	-660.843285	-205.170364
ϵ_{ZPF}	0.347347	0.333425	0.008452
E_{tot}	0.368597	0.351922	0.011395
H_{corr}	0.369541	0.352866	0.012339
G_{corr}	0.298737	0.287678	-0.014949
$\epsilon_0 + \epsilon_{ZPE}$	-865.69644	-660.50986	-205.161912
$\epsilon_0 + E_{tot}$	-865.675189	-660.49136	-205.158969
$\epsilon_0 + H_{corr}$	-865.674245	-660.49042	-205.158025
$\epsilon_0 + G_{corr}$	-865.745049	-660.55561	-205.185314
S_{tot}	0.237479838	0.218641768	0.091527426

Table D10: Thermochemical values form Gaussian calculated for reactants and product for BHT–ONO formation using BPV86/6-311G (d,p) method, units Hartees. [This work]

	BHT-ONO	BHT [*]	NO ₂
ϵ_0	-866.035779	-660.843285	-205.170364
ϵ_{ZPF}	0.344956	0.333425	0.008452
E_{tot}	0.366773	0.351922	0.011395
H_{corr}	0.367717	0.352866	0.012339
G_{corr}	0.296144	0.287678	-0.014949
$\epsilon_0 + \epsilon_{ZPE}$	-865.690823	-660.50986	-205.161912
$\epsilon_0 + E_{tot}$	-865.669007	-660.49136	-205.158969
$\epsilon_0 + H_{corr}$	-865.668063	-660.49042	-205.158025
$\epsilon_0 + G_{corr}$	-865.739635	-660.55561	-205.185314
S_{tot}	0.240055113	0.218641768	0.091527426

Table D11: Thermochemical values form Gaussian calculated for reactants and product for TTBP–NO₂ formation, using BPV86/6-311G (d,p) method, units Hartees. [This work]

	TTBP-NO ₂	TTBP [•]	NO ₂ [•]
ϵ_0	-984.007546	-778.802907	-205.170364
ϵ_{ZPF}	0.429304	0.415417	0.008452
E_{tot}	0.454592	0.437964	0.011395
H_{corr}	0.455537	0.438908	0.012339
G_{corr}	0.376972	0.364813	-0.014949
$\epsilon_0 + \epsilon_{ZPE}$	-983.578242	-778.38749	-205.161912
$\epsilon_0 + E_{tot}$	-983.552953	-778.36494	-205.158969
$\epsilon_0 + H_{corr}$	-983.552009	-778.36399	-205.158025
$\epsilon_0 + G_{corr}$	-983.630574	-778.43809	-205.185314
S_{tot}	0.429304	0.415417	0.008452

Table D12: Thermochemical values form Gaussian calculated for reactants and product of EthPh–NO₂ formation, using BPV86/6-311G (d,p) method, units Hartees. [This work]

	EthPh-NO ₂	EthPh [•]	NO ₂
ϵ_0	-905.366438	-700.166453	-205.170364
ϵ_{ZPF}	0.375015	0.361457	0.008452
E_{tot}	0.39773	0.381163	0.011395
H_{corr}	0.398674	0.382107	0.012339
G_{corr}	0.324426	0.314636	-0.014949
$\epsilon_0 + \epsilon_{ZPE}$	-904.991423	-699.805996	-205.161912
$\epsilon_0 + E_{tot}$	-904.968708	-699.78529	-205.158969
$\epsilon_0 + H_{corr}$	-904.967764	-699.78435	-205.158025
$\epsilon_0 + G_{corr}$	-905.042012	-699.85182	-205.185314
S_{tot}	0.249031921	0.226302254	0.091527426

Table D13: Thermochemical values form Gaussian calculated for reactants and product for analogue OHPP–NO₂ formation, using BPV86/6-311G (d,p) method, units Hartees. [This work]

	OHPP-NO₂	OHPP[•]	NO₂[•]
ϵ_0	-1172.647943	-967.447386	-205.170364
ϵ_{ZPF}	0.4437	0.430912	0.008452
E_{tot}	0.472461	0.456363	0.011395
H_{corr}	0.473405	0.457307	0.012339
G_{corr}	0.381405	0.373782	-0.014949
$\epsilon_0 + \epsilon_{ZPE}$	-1172.204243	-967.016474	-205.161912
$\epsilon_0 + E_{tot}$	-1172.175482	-966.991023	-205.158969
$\epsilon_0 + H_{corr}$	-1172.174538	-966.990079	-205.158025
$\epsilon_0 + G_{corr}$	-1172.266538	-967.073604	-205.185314
S_{tot}	0.30856921	0.280145573	0.091527426

Table D14: Thermochemical values form Gaussian calculated for reactants and product of EthPh–QM formation, using BPV86/6-311G (d,p) method, units Hartees. [This work]

	EthPh-QM	EthPh[•]	NO₂	HONO
ϵ_0	-699.566691	-700.166453	-205.170364	-205.794754
ϵ_{ZPF}	0.350549	0.361457	0.008452	0.019211
E_{tot}	0.370026	0.381163	0.011395	0.022436
H_{corr}	0.37097	0.382107	0.012339	0.02338
G_{corr}	0.305039	0.314636	-0.014949	-0.004843
$\epsilon_0 + \epsilon_{ZPE}$	-699.216142	-699.804996	-205.161912	-205.775543
$\epsilon_0 + E_{tot}$	-699.196666	-699.78529	-205.158969	-205.772319
$\epsilon_0 + H_{corr}$	-699.195721	-699.78435	-205.158025	-205.771375
$\epsilon_0 + G_{corr}$	-699.261652	-699.85182	-205.185314	-205.799598
S_{tot}	0.221132582	0.226302254	0.091527426	0.094660464

Table D15: Thermochemical values form Gaussian calculated for reactants and product for ODTBHPP–QM formation, using BPV86/6-311G (d,p) method, units Hartees. [This work]

	Quinone Methide	L107 [*]	NO ₂ [*]	HONO
ϵ_0	-966.846359	-967.447386	-205.170364	-205.794754
ϵ_{ZPF}	0.420189	0.430912	0.008452	0.019211
E_{tot}	0.445304	0.456363	0.011395	0.022436
H_{corr}	0.446249	0.457307	0.012339	0.02338
G_{corr}	0.364229	0.373782	-0.014949	-0.004843
$\epsilon_0 + \epsilon_{ZPE}$	-966.42617	-967.016474	-205.161912	-205.775543
$\epsilon_0 + E_{tot}$	-966.401055	-966.991023	-205.158969	-205.772319
$\epsilon_0 + H_{corr}$	-966.400111	-966.990079	-205.158025	-205.771375
$\epsilon_0 + G_{corr}$	-966.48213	-967.073604	-205.185314	-205.799598
	0.275095421	0.280145573	0.091527426	0.094660464

Table D16: O–H Bond Dissociation Energies of different phenolics calculated using BPV86/6-311G (d,p) method.[This work]

Phenolic	BDE [kJ mol ⁻¹]	
	Calculated (this work)	Experimental
BHT(O–H)	338.1 ± 3.4	342 ± 8 ^a
EthPh(O–H)	338.7 ± 3.4	not known
OHPP(O–H)	341.3 ± 3.4	339.7 ± 0.4 ^b

*Ref.162, ^a Ref.164, ^b

E. Appendix to chapter 6.

Identification of seven products from interaction of aminic antioxidant (DODPA) with NO₂ detected by TOF/GC MS (EI)

Peak assignments were undertaken using mass spectrum data with GC retention times as the library spectra were unavailable. Primarily characteristic signals for DODPA were assigned to show similarity with identified intermediate products.

Aminic antioxidant (DODPA)

Peak at 48.0 min.: 4-(1,1,3,3-tetramethylbutyl)-N-[4-(1,1,3,3 tetramethylbutyl)phenyl]aniline

Assignment

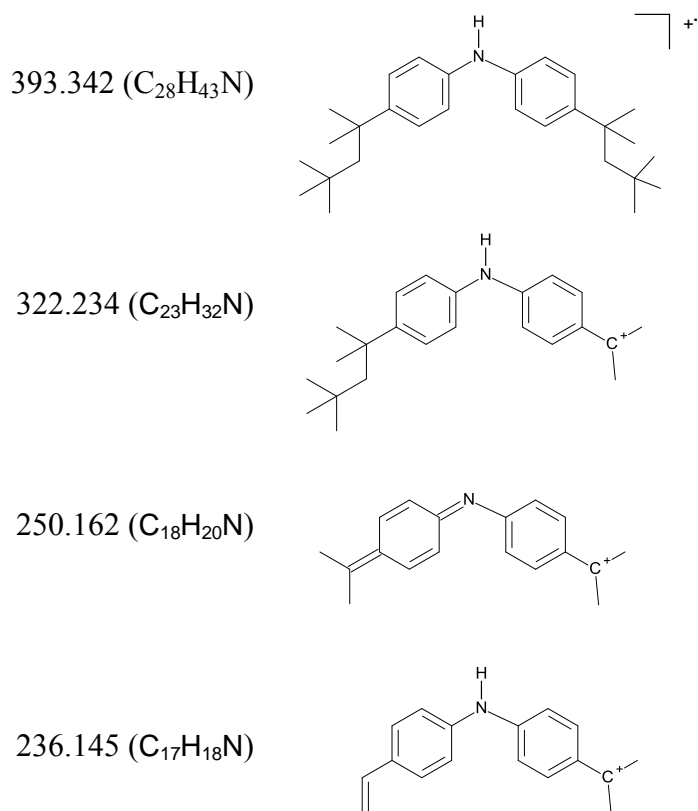


Figure E1: TOF/GC MS (EI) aminic antioxidant (DODPA).

The main fragments were formed by loss of alkyl groups. The same fragmentation pattern was characteristic for all products.

Product A

Peak at 50.8 min.: (6E)-3-(1,1,3,3-tetramethylbutyl)-6-[4-(1,1,3,3-tetramethylbutyl)phenyl] imino-cyclohexa-2,4-dien-1-one

Assignment

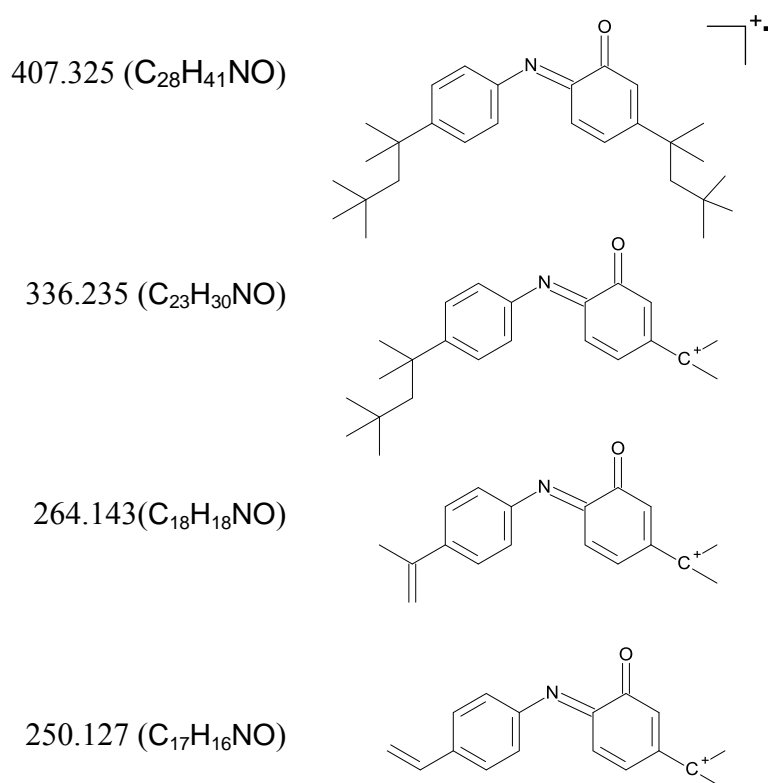


Figure E2: TOF/GC MS (EI) Product A.

Product B was identified as a nitrated amine with a characteristic fragment m/z 333, which possibly forms by hydrogen transfer to the oxygen atom of nitro group, then elimination of an OH radical and then elimination of another OH radical.

Product B

Peak at 52.0 min.: 6-nitro-4-(1,1,3,3-tetramethylbutyl)-N-[4-(1,1,3,3-tetramethylbutyl)phenyl]cyclohexa-2,4-dien-1-imine

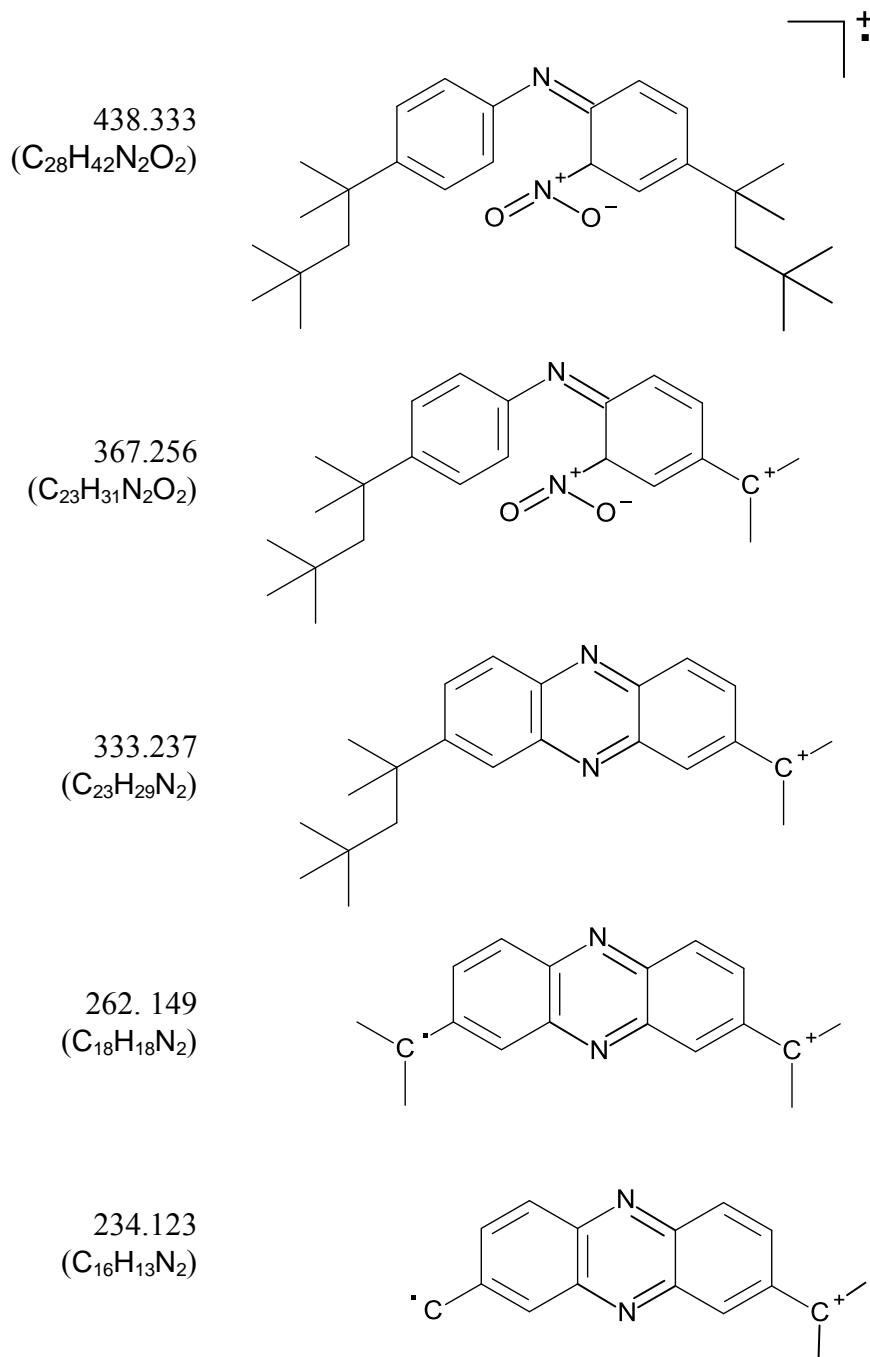
Assignment

Figure E3: TOF/GC MS (EI) Product B.

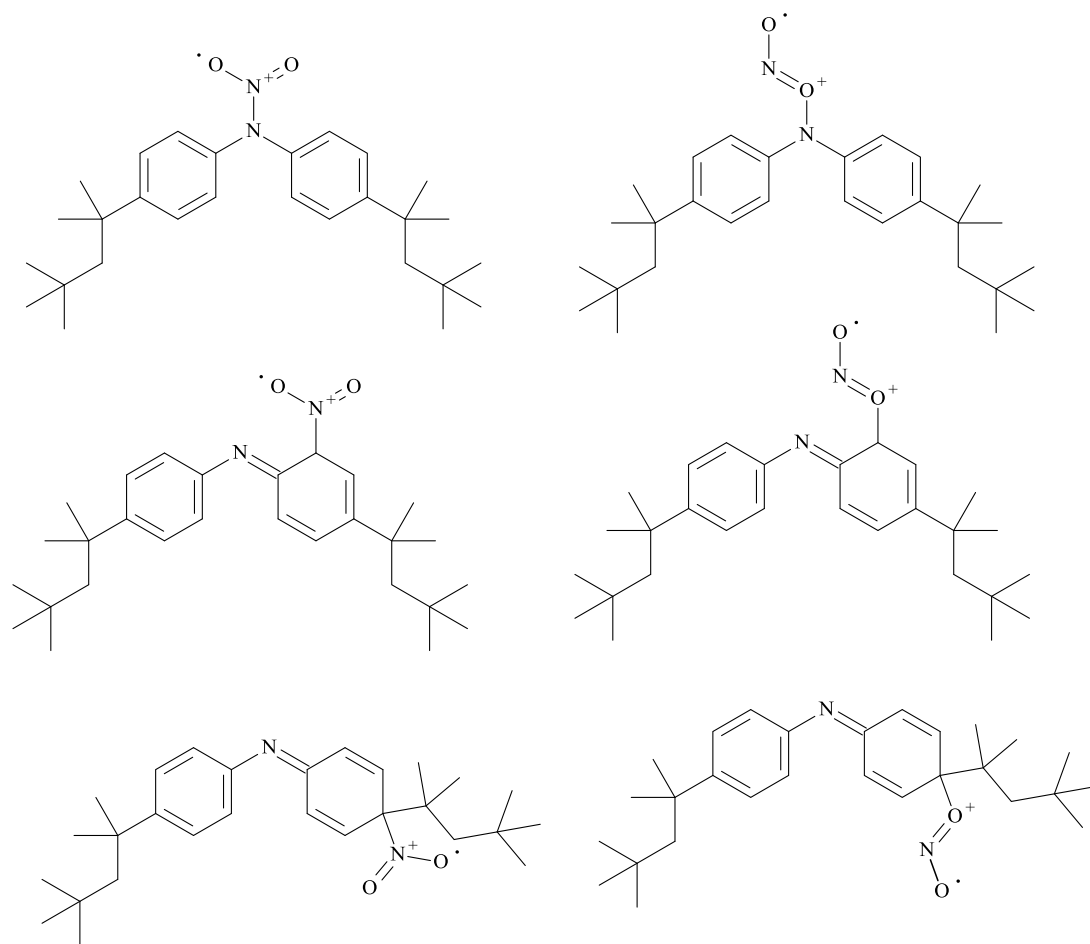


Figure E4: Possible structures of product B.

Product 1

Peak at 69.7 min.: 4-(1,1,3,3-tetramethylbutyl)-N-[4-(1,1,3,3-tetramethylbutyl)phenyl]-6-[(6E)-3-(1,1,3,3-tetramethylbutyl)-6-[4-(1,1,3,3-tetramethylbutyl)phenyl]imino-cyclohexa-2,4-dien-1-yl]cyclohexa-2,4-dien-1-imine

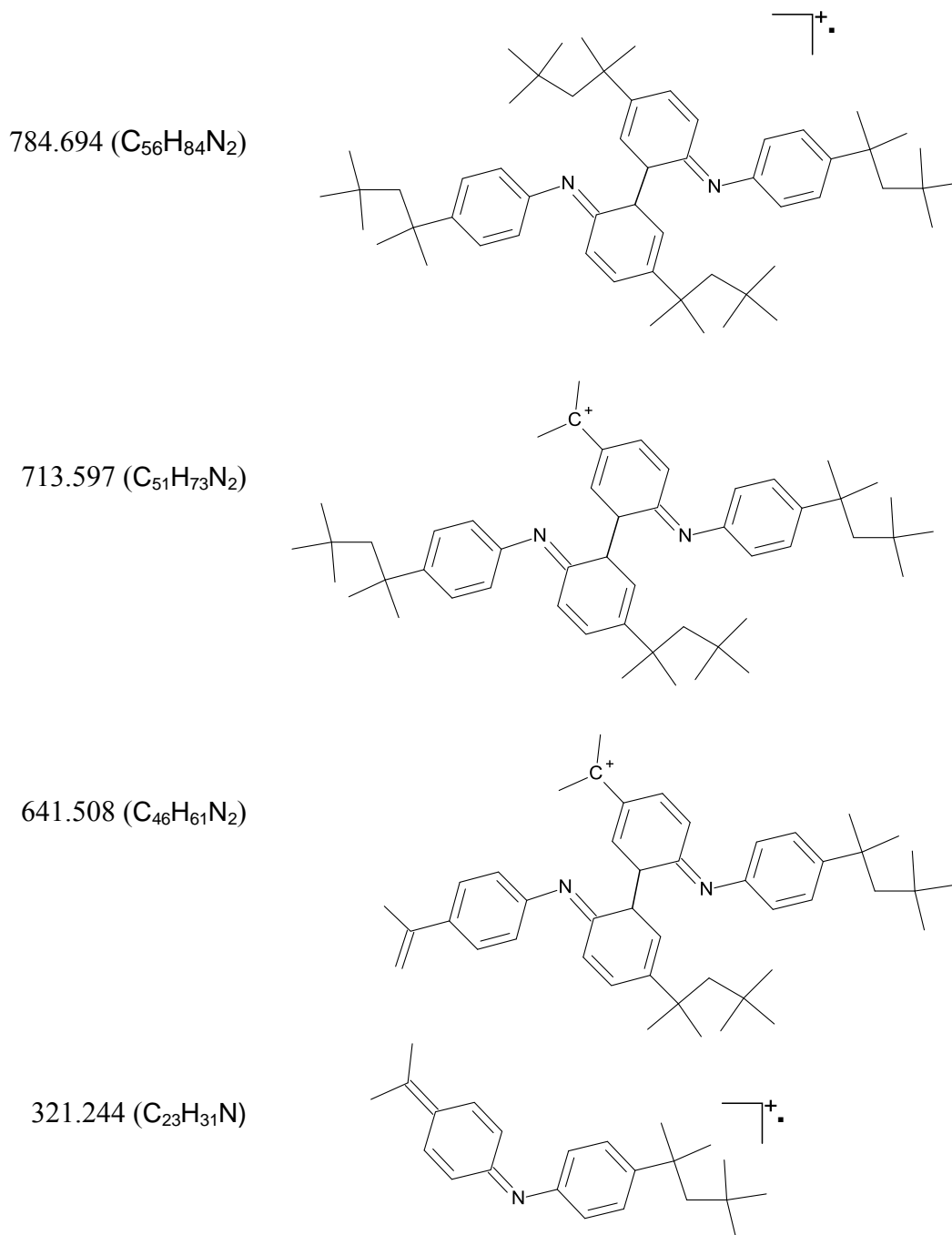
Assignment

Figure E5: TOF/GC MS (EI) Product 1.

Product 1 or 2, fragmentation follows the same pattern as for an antioxidant, by loss of alkyl groups, where the signal m/z 321.244 suggesting its fragmentation into two

monomers, possible structures below. The same fragmentation rules for product 2 as for product 1.

Product 2

Peak at 70.8 min.: 1,1,2,2-tetrakis[4-(1,1,3,3-tetramethylbutyl)phenyl]hydrazine

Assignment

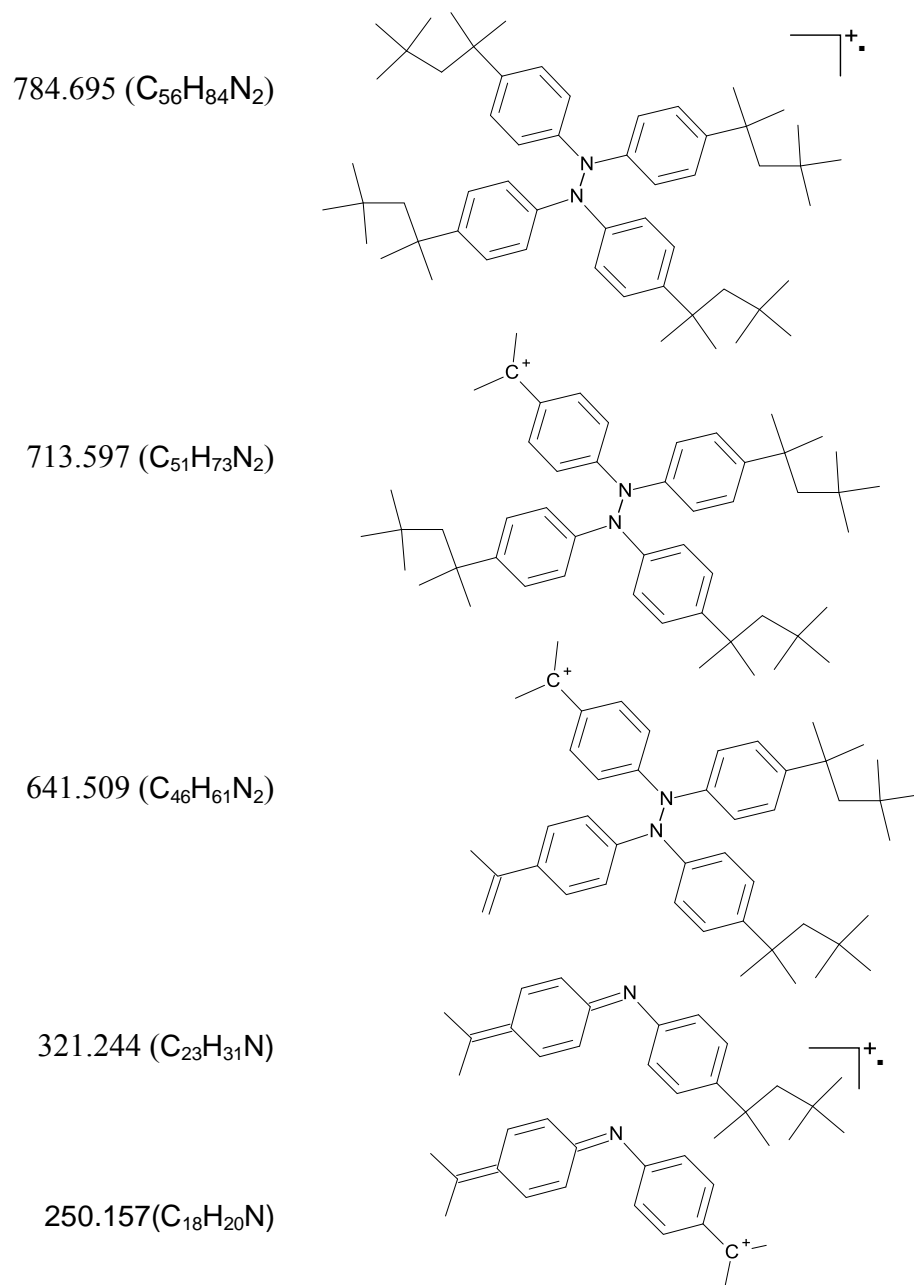


Figure E6: TOF/GC MS (EI) Product 2.

Product 3

Peak at 69.7 min.: 4-(1,1,3,3-tetramethylbutyl)-N-[4-(1,1,3,3-tetramethylbutyl)phenyl]-6-[(6E)-3-(1,1,3,3-tetramethylbutyl)-6-[4-(1,1,3,3-tetramethylbutyl)phenyl]imino-cyclohexa-2,4-dien-1-yl]cyclohexa-2,4-dien-1-imine

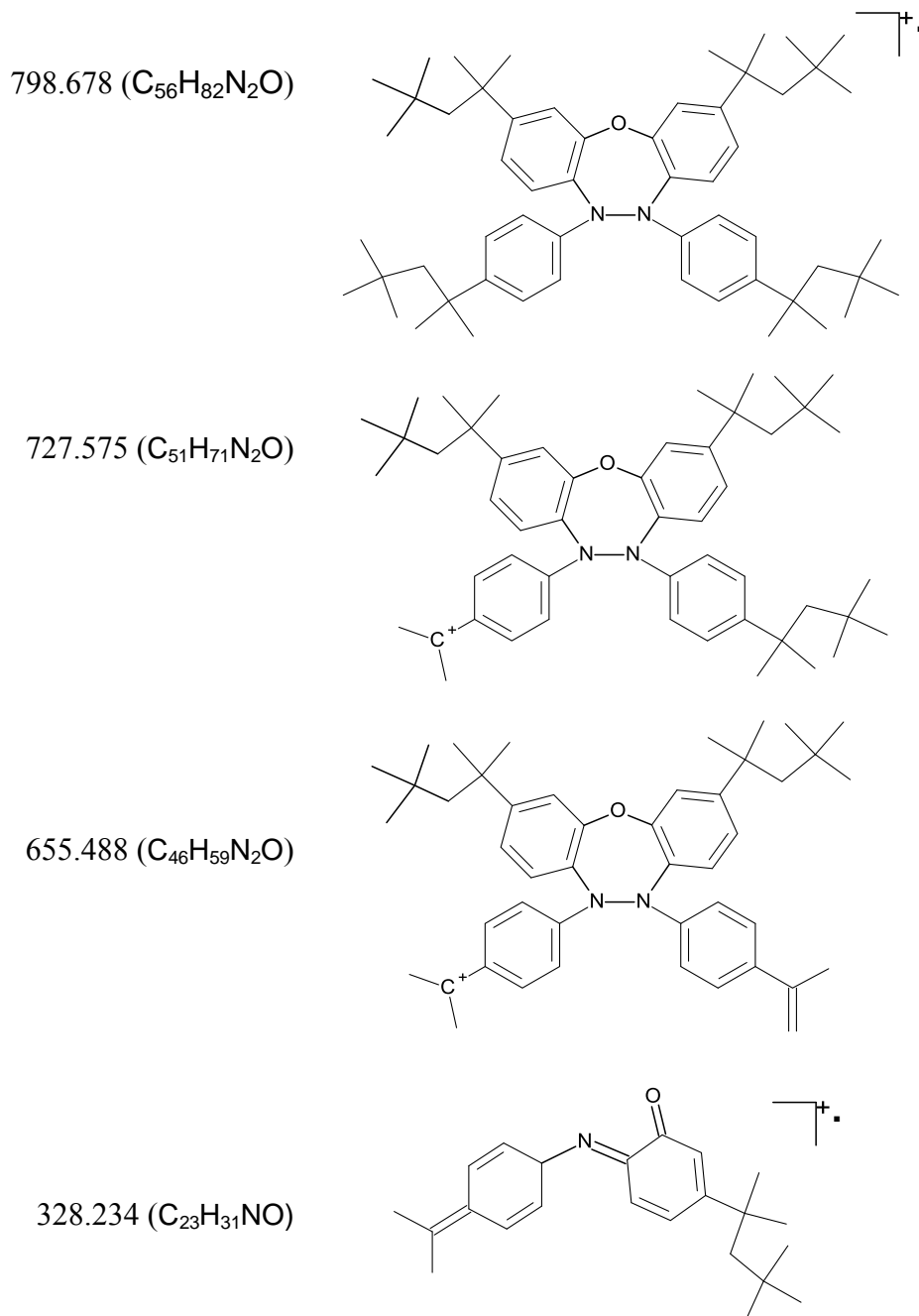
Assignment

Figure E7: TOF/GC MS (EI) Product 3.

Product 4

Peak at 75.4 min.: (6E)-4-(1,1,3,3-tetramethylbutyl)-N-[4-(1,1,3,3-tetramethylbutyl)phenyl]-6-[(6E)-3-(1,1,3,3-tetramethylbutyl)-6-[4-(1,1,3,3-tetramethylbutyl)phenyl]imino-cyclohexa-2,4-dien-1-ylidene]cyclohexa-2,4-dien-1-imine

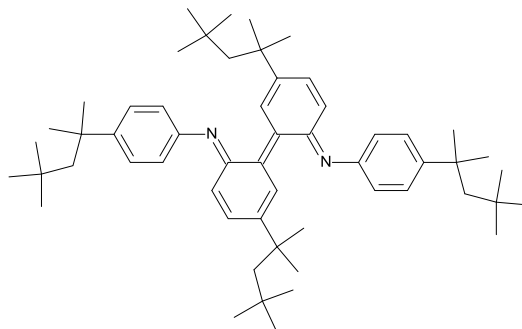
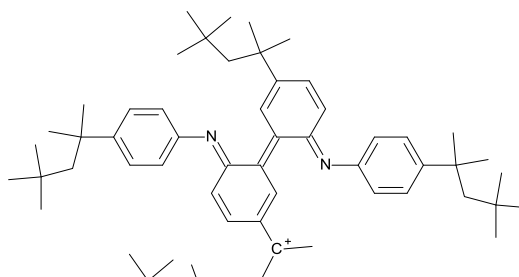
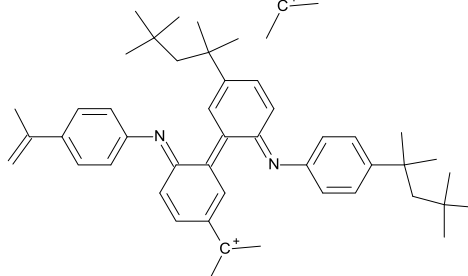
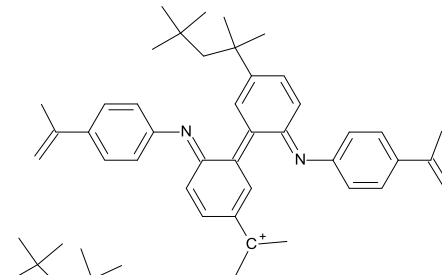
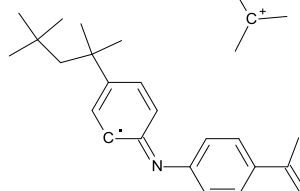
Assignment782.681 (C₅₆H₈₂N₂)711.586 (C₅₁H₇₁N₂)639.490 (C₄₆H₅₉N₂)567.394 (C₄₁H₄₇N₂)320.235 (C₂₃H₃₀N)

Figure E8: TOF/GC MS (EI) Product 4 and 5.

Product 5 (the same as 4)

Peak at 76.1 min.: (6Z)-4-(1,1,3,3-tetramethylbutyl)-N-[4-(1,1,3,3-tetramethylbutyl)phenyl]-6-[(6E)-3-(1,1,3,3-tetramethylbutyl)-6-[4-(1,1,3,3-tetramethylbutyl)phenyl]imino-cyclohexa-2,4-dien-1-ylidene]cyclohexa-2,4-dien-1-imine

List of References

1. C. Berggren and T. Magnusson, *Energy Policy*, **2012**, *41*, 636-643.
2. A. M. K. P. Taylor, *Energy Policy*, **2008**, *36*(12), 4657-4667.
3. W. Knecht, *Energy*, **2008**, *33*, 264-271.
4. W. M. Studzinski, P. M. Liiva, P. J. Choate, W. P. Acker, T. Litzinger, S. Bower, M. Smooke and K. Brezinsky, *SAE Paper No. 932815*, **1993**.
5. J. Wang, Z. Huang, B. Liu and X. Wang, *Front. Energy Power Eng. China*, **2009**, *3*(2), 204-211.
6. S. R. Turns, *Prog. Energy. Combust. Sci.*, **1995**, *21*, 361-385.
7. Y. Mukarami and H. Aihara, *SAE Paper No. 910747*, **1991**.
8. K. Iwakata, Y. Onodera, K. Mihara and S. Ohkawa, *SAE Paper No. 932839*, **1993**.
9. M. Kawamura, H. Moritani, M. Nakada and M. Oohori, *SAE Paper No. 892105*, **1989**.
10. M. J. Piphio, D. B. Kittelson and D. D. Zarling, *SAE Paper No. 910231*, **1991**.
11. R. R. Rain, C. R. Stone and J. Gould, *Combust. Flame*, **1995**, *102*, 241-255.
12. A. K. Brewer and P. D. Kueck, *J. Phys. Chem.*, **1933**, *37*, 889-896.
13. Y. Qingjiang, and G. A. Hongxia, *J. Chem. Edu.* **1997**, *74*, 233-234.
14. W. S. Epling, J. E. Parks, G. C. Campbell, A. Yezeretsb, N. W. Currier and L. E. Campbell, *Catal. Today*, **2004**, *96*, 21-30.
15. J. B. Heywood, "Internal Combustion Engine Fundamentals", International ed., McGraw-Hill Publishing, Singapore, **1988**.
16. E. A. Bardosz and G. D. Lamb in "Lubricant Additive Chemistry and Applications", 2nd ed.; L. E. Rudnik, CRC Press, CRC Taylor & Francis: Boca Raton, **2009**, 457-492.

-
17. R. I. Taylor, R. Mainwaring and R. M. Mortier, *Proc. I. Mech. Eng. Part J, J. Eng. Trib.* **2005**, 219,1-16.
 18. G. H. Guither, M. T. Devlin, T. C. Jao and G. P. Anderson, *Patent No. 20080269091*, Tysons Corner, VA, US, **2008**.
 19. R. Gligorijevic, J. Jevtic, and D. J. Borak, *J. Syn. Lub.*, **2006**, 23, 27-38.
 20. M. Corradi, *Base Stocks - Seminar Papers*, Milton Hill, UK, June **2007**, 1-7.
 21. M. Rasberger in “Chemistry and Technology of Lubricants”, eds. R.M. Mortier, and S. T. Orszulik, 2nd ed., Blackie Academic, London, **1997**, p. 98-14.
 22. A. R. Lansdown, “Lubrication and Lubricant Selection”, Professional Engineering Publishing **2004**.
 23. A. J. Caines, and R. F. Haycock, “Automotive Lubricants Reference Book”, Mech. Eng. Pub., UK, **1996**.
 24. L. E. Rudnik, “Lubricant Additive Chemistry and Applications”, CRC Press, CRC Taylor & Francis: Boca Raton, **2009**.
 25. M. S. Stark, R. J. Gamble, C. J. Hammond, H. M. Gillespie, J. R. Lindsay Smith, E. Nagatomi, N. Priest, C. M. Taylor, R. I. Taylor and D. J. Waddington, *Trib. Lett.*, **2005**, 19(3), 163-168.
 26. R. J. Gamble, M. Priest and C. M. Taylor, *Trib. Lett.*, **2003**, 14(2), 147-156.
 27. H. Moritani and Y. Nozawa, *R & D Rev. Toyota CRDL*, **2003**, 38, 36-43.
 28. R. I. Taylor and P. G. Evans, *Proc. Inst. Mech. Eng., Part J*, **2004**, 218, 185-200.
 29. C. S. Kang, *PhD Thesis*, School of Science at Nottingham Trent University, **2003**.
 30. Z. Qian, H. Liu, G. Zhang and D. J. Brown, Temperature Field Estimation for Piston of Diesel Engine., *Lecture Notes in Computer Science*, **2006**, 1198-1205.
 31. M. Diaby, M. Sablier, A. Le Negrate, M. El Fassi and J. Bocquet, *Carbon*, **2007**, 47, 355-366.

-
32. B. D. Vineyard and A. Y. Coran, Gasoline Engine Deposition: 1. Blowby collection and the identification of deposit precursors. *Symposium on Deposit, Wear, and Emission Control by Lubricant and Fuel Additives*, New York, **1969**.
33. K. Kannan and M. Udayakuma, *Am. J. Applied Sci.*, **2009**, 6 (7), 1313-1320.
34. M. A. Hess, M. J. Haas, T. A. Foglia and W. N. Marmer, *Energy & Fuels*, **2005**, 19, 1749-1754.
35. C. D. Rakopoulos and C. N. Michos, *Eng. Conv. Manag.*, **2008**, 29, 2924-2938.
36. C.P. Fenimore, *Thirteenth Symposium (International) on Combustion. The Combustion Institute*. **1970**, p.313.
37. J. Hartung, *Chem. Rev.*, **2009**, 109, 4500-4517.
38. J. A. Miller, and C. T. Bowman, *Prog. Energ. Combust. Sci.*, **1989**, 15, 287-338.
39. J. Kones, *Int. Combust. Eng.*, **2003**, 10, 1-2.
40. R. E. Huie, *Toxicology*, **1994**, 89, 193-216.
41. D. L. Baulch, C. T. Bowman, C. J. Cobos, R. A. Cox, Th. Just, J. A. Kerr, M. J. Pilling, D. Stocker, J. Troe, W. Tsang, R. W. Walker, J. Warnats, *J. Phys. Chem. Ref. Data*, **2005**, 34 (3), 757-1397.
42. C. D. Cooper and F. C Alley, "Air Pollution Control: A Design Approach", 2nd ed., Waveland Press, **1994**.
43. Z. Huang, S. Shiga, T. Ueda, H. Nakamura, and T. Ishima, *J. Automobile Engineering, Proc. Inst. Mech. Eng.*, **2003**, 217(D), p.938.
44. V. Knop, A. Benkenida, S. Jay and Olivier Colin, *Int. J. Hydrogen Energy*, **2008**, 33(19), 5083-5097.
45. K. Cupial, and A. Jamrozik, J. Kones, *Int. Combust. Engines*, **2002**, 3-4, 1231-4005.

-
46. I. M. Kennedy, R. Milhacea, J. Kostka, M. Cramer, R. Pasek, and D. P. Y. Chang, *Combust. Sci. and Tech.* **1997**, *123*, 63-82.
47. W. G. Bessler, *Proc. Combust. Inst.*, **2005**, *30*, 2667-2674.
48. M. D. Johnson and S. Korcek, *Lubric. Sci.*, **1991**, *4*, 95-118.
49. E. Ya. Davydov, S. Korcek, R. K. Jensen and G. E. Zaikov, *Int. J. Polymeric Mater.*, **1997**, *37*, 201-216.
50. M. E. Jenkin, S. M. Sunders and M. J. Pilling, *Atmos. Env.* **1997**, *31*(1), 81-104
51. M. S. Stark, C. Anastasi and J. T. H. Harrison, *J. Geog. Res.* **1996**, *101*(D3), 6963-6969.
52. H. K. Roscoe and A. K. Hind, *J. Atmos. Chem.*, **1993**, *16*, 257-276.
53. F. Murad, *Angew. Chem. Int. Ed.*, **1999**, *38*, 1856-1868.
54. R. F. Furchgott, *Angew. Chem. Int. Ed.*, **1999**, *38*, 1871-1880.
55. L. J. Ignarro, *Angew. Chem. Int. Ed.*, **1999**, *38*, 1882-1892.
56. G. I. Borodkin and V. G. Shubin *Russ. Chem. Rev.*, **2001**, *70*, 211-230.
57. M. Shiri, *Synlett.* **2006**, 1789-1790.
58. M. Shiri, M. A. Zolfigol, H. G. Kruger and Z. Tanbakouchian, *Tetrahedron*, **2010**, *66*, 9077-9106.
59. M. N. Hughes and H.G. Nicklin, *J. Chem. Soc. A*, **1971**, p.164.
60. Q. Yu and H. Gao, *J. Chem. Educ.*, **1997**, *74*(2), p.233.
61. G. N. Lewis, *J. Am. Chem. Soc.* **1916**, *38*(4), 762-785.
62. L. Pauling, *J. Am. Chem. Soc.* **1931**, *53*, 1367-1400.
63. H. L. Johnston and W. F. Giaque, *J. Am. Chem. Soc.*, **1929**, *51*, 2300-3194.
64. W. J. Sulmage, E. A. Meyers and W. N. Lipscomb, *Acta Crystallogr.* **1953**, *6*, 753-760.

-
65. W. N. Lipscomb, F. E. Wang, W. R. May and E. L. Jr. Lippert, *Acta Crystallogr.* **1961**, *14*, p.1100.
66. H. E. Watson, G. G. Rao, K. L. Ramaswamy, *Proc. R. Soc.*, **1934**, *A134*, 558-588.
67. A. W. Shaw, A. J. Vosper, *J. Chem. Soc.*, **1929**, *51*, 3194-3214.
68. J. Mason, *J. Chem. Edu.*, **1975**, *52*, 445-447.
69. A. L. Smith, "The Coblenz Society Desk Book of Infrared Spectra", 2nd Ed., The Coblenz Society: Kirkwood, MO, **1982**. [IR spectrum in the gas phase at: <http://webbook.nist.gov>]
70. E. E. van Faassen, A. F. Vanin, "Radicals for life: The various forms of Nitric Oxide", Elsevier, Amsterdam, **2007**.
71. K. Jug, *J. Am. Chem. Soc.* **1978**, *100*, p.6581.
72. B. G. Gowenlock and G. B. Richter-Addo, *Chem. Rev.*, **2004**, *104*, 3315-3340.
73. E. A. Arden, L. Phillips and R. Shaw, *J. Chem. Soc.*, **1964**, 982,5126-5129.
74. W. Deng, C. Wang, D. R. Katz, G. R. Gawinski, A. J. Davis and T. S. Dibble, *Chem. Phys. Lett.*, **2000**, *330*, 541-546.
75. J. Hartung, T. Gottwald and K. S. Pehar in "Organic Radical Reactions Associated with Nitrogen Monoxide". Hartung, J., *Chem. Rev.*, **2009**, *109*, p.4508.
76. E. G. Janzen, J. L. Jr. Meyer and C. L. Ayers, *J. Phys. Chem.*, **1967**, *71*, p3108.
77. A. L. Wilcox and E. G. Janzen, *J. Chem. Soc., Chem. Commun.*, **1993**, 1377-1379.
78. E. G. Janzen, A. L. Wilcox and V. Manoharan, *J. Org. Chem.*, **1993**, *58*, 3598-3599.
79. W. A. Prutz, H. Monig, J. Butler and E. J. Land, *Arch. Biochem. Biophys.*, **1985**, *243*, 125-134.
80. L. Batt, *Int. Rev. Phys. Chem.* **1987**, *6*, 53-90.
81. T. Logager and K. Sehested, *J. Phys. Chem.*, **1993**, *97*, 10047- 10052.

-
82. A. I. Titov, *Tetrahedron*, **1963**, *19*, 557-580.
83. G. Brunton, H. W. Cruse, K. M. Riches and A. Whittle, *Tetrahedron Lett.*, **1979**, *12*, 1093-1094.
84. R. J. Singh, S. P. A. Gross, J. Joseph and B. Kalyanaraman, *Proc. Natl. Acad. Sci. USA*, **1998**, *95*, 12912-12917.
85. K. Kikugawa, K. Hiramoto, Y. Okamoto and Y. K. Hasegawa, *Free Radical Res.*, **1994**, *21*, 399-408.
86. S. Jaffe, *Chem. React. Urban Atmos. Proc.*, **1971**, 103-109.
87. W. A. Pryor and J. W. Lightsey, *Science*, **1981**, *214*, 435-437.
88. W. A. Pryor, W. Lightsey and D. F. Church, *J. Am. Chem. Soc.*, **1982**, *104*, 6685-6692.
89. H. Jiang, N. Kruger, D. R. Lahiri, J.-M. Vatele and M. Balazy, *J. Biol. Chem.*, **1999**, *274*, 16235-16241.
90. R. E. Huie and P. Neta, *J. Phys. Chem.*, **1986**, *90*, 1193-1198.
91. Z. B. Alfassi, R. E. Huie and P. Neta, *J. Phys. Chem.*, **1986**, *90*, 4156-4158.
92. Z. B. Alfassi, *Int. J. Radiat. Appl. Instrum., Part C: Radiat. Phys. Chem.*, **1987**, *29*, 405-406.
93. A. I. Titov, *Zh. Obshch. Khim*, **1940**, *10*, p.1878.
94. P. Astolfi, M. Panagiotaki and L. Greci, *Eur. J. Org. Chem.*, **2005**, 3052-3059.
95. E. Y. Davydov, I. S. Gaponova and G. B. Pariiskii, *J. Chem. Soc., Perkin Trans. 2*, **2002**, 1359-1363.
96. P. Astolfi, M. Panagiotaki, C. Rizzoli and L. Greci, *Org. Biomol. Chem.*, **2006**, *4*, 3282-3290.
97. H. Suzuki and N. Nonoyama, *Tetrahedron Lett.*, **1998**, *39*, 4533-4536.
98. T. G. Bonner and R. A. Hancock, *J. Chem. Soc.*, **1970**, B, 519-524.

-
99. B. G. Gowenlock, J. Pfab, V. M. Young, *J. Chem. Soc.*, **1997**, 2, 1793-1798.
 100. S. Blaine and P. E. Savage, *Ind. Eng. Chem. Res.*, **1991**, 30(9), 2185-2191.
 101. S. Blaine and P. E. Savage, *Ind. Eng. Chem. Res.*, **1992**, 31(1), 69-75.
 102. R. K. Jensen, S. Korcek, L. R. Mahoney and M. Zinbo, *J. Am. Chem. Soc.*, **1979**, 101, 7574-7584.
 103. R. K. Jensen, S. Korcek, L. R. Mahoney and M. Zinbo, *J. Am. Chem. Soc.*, **1981**, 103, 1742-1749.
 104. M. S. Stark, J. J. Wilkinson, J. R. Lindsay Smith, A. Alfahad and B. A. Pochopien, *Ind. Eng. Chem. Res.*, **2011**, 50, 817-823.
 105. N. M. Emanuel, E. T. Denisov and Z. K. Maizus, "Liquid-Phase Oxidation of Hydrocarbons", *Plenum Press*, New York, **1967**, 223-281.
 106. I. V. Berezin, E. T. Denisov, and N. M. Emanuel, "The Oxidation of Cycloalkanes", *Pergamon Press*, Oxford, **1966**, p.89.
 107. E.T. Denisov and I. B. Afanas'ev Oxidation and Antioxidants in Organic Chemistry and Biology. CRC Press of Taylor and Francis, Florida, **2005**.
 108. M. Lundback, M. S. Hedenqvist, A. Mattozzi and U. W. Gedde, *Polym. Deg. and Stab.* **2006**, 91(7), 1571-1580.
 109. N. Balasundram, K. Sundram and S. Samman, *Food Chem.*, **2006**, 99(1), 191-203.
 110. C. Migdal, Antioxidants. In: L. Rudnick, (Ed.), *Lubricant Additives: Chemistry and Applications*. Marcel Dekker, Inc., New York, pp. 1-28. **2003**.
 111. J. Pfaendtner and L. J. Broadbelt, *Ind. Eng. Chem. Res.*, **2008**, 47, 2890-2900.
 112. L. F. Wang, Y. G. Song, X. Zhang and Y. Liu, *Bioorg. & Medicinal Chem. Lett.*, **2006**, 16(12), 3241-3244.

-
113. J. Pospisil, W. D. Habicher, J. Pilar, S. Nespurek, J. Kuthan, G. O. Pringer and H. Zweifel, *Polym. Deg. and Stab.* **2002**, *77*, 531-538.
114. M. R. Naimi-Jamal, H. Hamzeali, J. Mokhtari, J. Boy and G. Kaupp, *Chem. Sus.Chem.*, **2009**, *2*, 83-88.
115. A. Alfadhl, *Ph.D. Thesis*, University of York, York; **2008**, p. 225.
116. Aldrich-Sigma ($\geq 99.5\%$) NO₂ MSDS, accessed on www.sigmaaldrich.com, MSDS No. 295582.
117. Aldrich-Sigma ($\geq 98.5\%$) NO MSDS, accessed on www.sigmaaldrich.com, MSDS No. 295566.
118. J. Scanlon and D. Willis, *J. Chrom. Sci.*, **1985**, *23*, 333-340.
119. K. Miyamoto and S. U. Fujimaki, *R. Com. Mass Spect. J.*, **2009**, *20* (23), 3350-3354.
120. T.-TL. Hwang and A. J. Shaka, *J. Magn. Reson.*, **1995**, Series A, *112*, 275-279.
121. M. W. Dong, "Modern HPLC for Practicing Scientists", John Wiley & Sons Inc., **2006**, p. 175.
122. D. Mao, H. Van De Weghe, R. Lookman, G. Vanermen, N. De Brucker and L. Diels, *Fuel*, **2009**, *88*, 312-318.
123. M. A. Ghouti and L. Al-Atoum, *J. Env. Manag.*, **2009**, *90*, 187-195.
124. J. Mihalcova, *Chem. Pap.* **2003**, *57* (3), 211-215.
125. D. H. Williams and I. Fleming, "Spectroscopic methods in Organic Chemistry", 5th Edition, McGraw-Hill, London, **1995**, 46-54.
126. C. D. Cook and B. E. Norcross, *J. Am. Chem. Soc.*, **1958**, *81*, 1176-1118.
127. S. Blaine and P. E. Savage; *Ind. Eng. Chem. Res.*, **1991**, *30*, 792.
128. S. McKenna, M. Casserino, and K. Ratliff; *STLE Annual Meeting*, Huston, **2002**.

-
129. Aldrich-Sigma Squalane MSDS, accessed on www.sigmaaldrich.com, MSDS No. 234311.
130. B. Maillard, K. Ingold, and J. Scaiano; *J. Am. Chem. Soc.*, **1983**, *105* (15), 5095-5099.
131. J. A. Howard; in “Peroxyl and related radicals”, eds. H. Fischer, 18 (d2), Springer, London, **1997**, p. 291.
132. D. E. Van Sickle; *J. Org. Chem.* **1972**, *37*, 755.
133. A. B. Mathur, V. Kumar and G. N. Mathur; *Polym. Photochem.*, **1982**, *2*, 161.
134. M. Diaby, M. Sablier, A. Le Negrate and M. E. Fassi; *J. Eng. Gas Turbines Power* **2010**, *132*, 032805.
135. J. J. Wilkinson; *PhD. Thesis, University of York*, **2006**, 36.
136. Y. Ogata and Y. Sawaki; *J. Org. Chem.* **1969**, *34*, 3985-3990.
137. Z. P. Prisyazhnyuk, S. S. Levush and V. U. Shevchuk; *Kinet Katal*, **1975**, **16**, 1397.
138. C. J. Hammond, J. R. L.; Smith, E. Nagatomi, M. S. Stark and D. J. Waddington; *New J. Chem.* **2006**, *30*, 741-750.
139. Z. Yuan, Y. Ni and A. R. P. Van Heiningen; *Can. J. Chem. Eng.* **1997**, *75*, 37-41.
140. A. Goosen and S. Kindermans; *S. Afr. J. Chem.* **1997**, *50*, 9.
141. Y. N. Belenkov; *Theor. Exp. Chem.* **1989**, *25*, 345.
142. R. N. Hazlett, M. J. Hall, and M. Matson; *Ind. Eng. Chem. Prod. Res. Dev.* **1977**, *16*, 171.
143. E. A. Bardosz and G. D. Lamb, “Additives for Crankcase Lubricant Applications”, in *Lubricant Additive, Chemistry and Applications*. 2nd Edition, L. E. Rudnik, CRC Press, CRC Taylor & Francis: Boca Raton, **2009**.

-
144. R. Taylor, R. Mainwaring and R. Mortier, *Proc .In. Mech. Eng;J. Eng.Trib.* **2005**, *219*, 1-16.
145. G. H. Guither, M. T. Devlin, T. C. Jao and G. P. Anderson, *Patent No.* *20080269091*, Tysons Corner VA US, **2008**.
146. M. D. Johnson and S. Korcek, *Lubric. Sci.*, **1991**, *4*, 95-118.
147. R. G. Coombes and A.W. Diggle, *Tetra. Lett.*, **1993**, *34*, 8557-8560.
148. E. Ya. Davydov, S. Korcek , R. K. Jensen and G. E. Zaikov, *Int. J. Polymeric Mater.*, **1997**, *37*, 201-216.
149. P. P. Klemchuk and P. L. Horng, *Polym. Deg. and Stab.* **1991**, *34*, 333-346.
150. F. W. McLafferty, *Appl. Spectrosc.*, **1957**, *11*, 148.
151. J. Pospisil, S. Nespurek and H. Zweifel, *Polym. Deg. and Stab.* **1996**, *54*, 15-21.
152. W. Steglich and B. Neises, *Chem. Int. Ed.* **1978**, *17*, 522-524.
153. P. J. Hore, J. A. Jones and S. Wimperis “NMR: The Toolkit”, Oxford University Press Inc., New York, **2000**, 28-30.
154. D. H. Williams and I. Fleming, “Spectroscopic methods in Organic Chemistry”, 5th Edition, McGraw-Hill, London, **1995**, 46-54.
155. M. L. Meyerson, *Spectrochimica Acta*, **1985**, *41A(11)*, 1263-1267.
156. P. Atkins and J. de Paula, “Physical Chemistry”, 8th Edition, W. H. Freeman and Company, NY, **2006**.
157. J. B. Foresman and E. Frisch, “Exploring Chemistry with Electronic Structure Methods”, 2nd Edition, Gaussian Inc., Pittsburgh, PA, **1993**.
158. J. Shao, X. Cheng and X. Yang, *Struct. Chem.*, **2006**, *17*, 547-550.
159. J. Shao, X. Cheng and X. J. Yang, *Molec. Struct.*, **2005**, *755*, 127-130.
160. J. Shao, X. Cheng, X. Yang and B. He, *Chin. Phys. Soc.*, **2006**, *15* (2), 329-333.
161. A. K. Chandra and T. Uchimaru, *Int. J. Mol. Sci.*, **2002**, *3*, 407-422.

-
162. B. S. Jursic and R. M. Martin, *Int. J. Quant. Chem.*, **1996**, *59*, 495-501.
163. S. J. Blanksby and G. B. Ellison, *Acc. Chem. Res.*, **2003**, *36*, 255-263.
164. Y. R. Luo, "Handbook of BDE in organic compounds", CRC Press, Boca Raton, FL, **2003**.
165. P. Mulder, H. - G. Korth, D. A. Pratt, G. A. DiLabio, L. Valgimigli, G. F. Pedulli and K. U. Ingold, *J. Phys. Chem. A*, **2005**, *109* (11), 2647-2655.
166. B. Ruscic, R. E. Pinzon, M. L. Morton, N. K. Srinivasan, M. - C. Su, J. W. Sutherland and J. V. Michael, *J. Phys. Chem. A*, **2006**, *110*, 6592-6601.
167. J. D. Cox, D. D. Wagman, V. A. Medvedev, "CODATA Key Values for Thermodynamics", Hemisphere, New York, **1989**.
168. L. V. Gurvich, I. V. Veyts, C. B. Alcock, "Thermodynamic Properties of Individual Substances", 4th Edition, Hemisphere Pub. Co., New York, **1989**.
169. Gaussian 09, Revision B.01, M. J. Frisch, G. W. Trucks, H. B. Schlegel, G. E. Scuseria, M. A. Robb, J. R. Cheeseman, G. Scalmani, V. Barone, B. Mennucci, G. A. Petersson, H. Nakatsuji, M. Caricato, X. Li, H. P. Hratchian, A. F. Izmaylov, J. Bloino, G. Zheng, J. L. Sonnenberg, M. Hada, M. Ehara, K. Toyota, R. Fukuda, J. Hasegawa, M. Ishida, T. Nakajima, Y. Honda, O. Kitao, H. Nakai, T. Vreven, J. A. Montgomery, Jr., J. E. Peralta, F. Ogliaro, M. Bearpark, J. J. Heyd, E. Brothers, K. N. Kudin, V. N. Staroverov, T. Keith, R. Kobayashi, J. Normand, K. Raghavachari, A. Rendell, J. C. Burant, S. S. Iyengar, J. Tomasi, M. Cossi, N. Rega, J. M. Millam, M. Klene, J. E. Knox, J. B. Cross, V. Bakken, C. Adamo, J. Jaramillo, R. Gomperts, R. E. Stratmann, O. Yazyev, A. J. Austin, R. Cammi, C. Pomelli, J. W. Ochterski, R. L. Martin, K. Morokuma, V. G. Zakrzewski, G. A. Voth, P. Salvador, J. J. Dannenberg, S. Dapprich, A. D. Daniels, O. Farkas, J. B.

-
- Foresman, J. V. Ortiz, J. Cioslowski, and D. J. Fox, Gaussian, Inc., Wallingford CT, **2010**. Gaussian 09: IA32W-G09RevB.01 12-Aug-2010, 08-Sep-2011.
170. J. W. Ochterski, "Thermochemistry in Gaussian", Gaussian Inc., Pittsburgh, PA, **2000**, gaussian.com.
171. E. T. Denisov, *Kinet. Catal.*, **1995**, 36 (3), 351-355.
172. S. W. Benson, *J. Am. Chem. Soc.*, **1965**, 87 (5), 972-979.
173. G. Aguilar, G. Mazzamaro and M. Rasberger, "Inhibition of Oxidative Degradation of Lubricants: Radical Scavengers", in Chemistry and Technology of Lubricants. Blackie Academic. 3rd Edition, R. M. Mortier, M. F. Fox and S. T. Orszulik, Springer, London, **2010**, 118-126.
174. E. A. Bardosz and G. D. Lamb, "Mechanism of Primary antioxidants: Aromatic Amines", in Lubricant Additives, Chemistry and Applications. 2nd Edition, L. E. Rudnik, CRC Press, CRC Taylor & Francis: Boca Raton, **2009**, 24-28.
175. F. W. McLafferty and F. Turecek, "Basic Mechanism of Ion Fragmentation", in Interpretation of Mass Spectra. 4th Edition, University Science Books, Sausalito, **1993**.
176. M. Bernabei, R. Secli and G. Bocchinfuso, *J. Microcol. Sep.*, **2000**, 12, 585-592.
177. M. Jonsson, D. D. Wayner and J. Luszyk, *J. Phys. Chem.* **1996**, 100, 17539-17543.
178. W. Dankiewicz, *Eur. Mass Spectrom.*, **1998**, 4, 167-179.
179. S. F. Nelsen, H. Q. Tran, R. F. Ismagilov, M. T Ramm, L. - J. Chen and D. R. Powell, *J. Org. Chem.*, **1998**, 63, 2536-2543.
180. A. T. Nielsen and G. W. Lawrence, *J. Org. Chem.* **1977**, 42(17), 2900-2902
181. P. Purkayastha and N. Chattopadhyay, *J. Molec. Struct.*, **2002**, 604, 87-99.
182. F. G. Bordwell and X.-M. Zhang, *J. Org. Chem.* **1993**, 58, 6410-6416.

-
183. V. T. Varlamov and E. Denisov, *Bull Acad Sci USSR* **1987**, *36*, 1607-1612.
184. E. T. Denisov, T. G. Denisova and T. S. Pokidova, "Products of Radical Pair Combination", in Handbook of Free Radical Initiators. John Wiley and Sons, Inc., Hoboken, NJ, **2003**.
185. F. Sánchez-Viesca, M. Berros and J. Pérez-Flores, *Rapid Commun. Mass Spectrom.* **2008**, *28*, 253-256.
186. E. A. Bardosz and G. D. Lamb, "Antioxidant Synergism", in Lubricant Additives, Chemistry and Applications. 2nd Edition, L. E. Rudnik, CRC Press, CRC Taylor & Francis: Boca Raton, **2009**, 29-30.
187. G. Aguilar, G. Mazzamaro and M. Rasberger, "Oxidative Degradation and stabilisation of Lubricants", in Chemistry and Technology of Lubricants. Blackie Academic. 3rd Edition, R. M. Mortier, M. F. Fox and S. T. Orszulik, Springer, London, **2010**, 107-152.
188. J. Pospisil, *Adv. Polym. Sci.*, **1995**, *124*, 87-190.
189. V. T. Varlamov and E. Denisov, *Bull Acad Sci USSR*, **1987**, *36*, 1607-1612.
190. G. Silva, C. C. Chen and J. W. Bozzelli, *Chem. Phys. Lett.*, **2006**, *424*, 42-45.